FATIGUE CHARACTERISATION OF FRP STRUCTURAL TEE JOINTS

by

Paul John Charles Lewis Read

of the

DEPARTMENT OF SHIP SCIENCE,

FACULTY OF ENGINEERING AND APPLIED SCIENCE,

UNIVERSITY OF SOUTHAMPTON

England.

Thesis submitted for the degree of

Doctor of Philosophy

March 1997

UNIVERSITY OF SOUTHAMPTON

ABSTRACT

FACULTY OF ENGINEERING AND APPLIED SCIENCE

DEPARTMENT OF SHIP SCIENCE

Doctor of Philosophy

FATIGUE CHARACTERISATION OF FRP STRUCTURAL TEE JOINTS

by **Paul John Charles Lewis Read**

Joints are a necessity in the construction of large structures such as ships. In the context of Fibre Reinforced Plastics (FRP), joints present a site of potential weakness due to material and geometric discontinuities. This problem is most significant in out-of-plane joints were stresses can occur in the materials weaker through-thickness direction. It is important therefore that the behaviour of these type of joints is fully understood. A substantial body of literature exists concerning their static behaviour but very little exits concerned with their long term fatigue behaviour. The aim of this thesis is to present an understanding of the long term fatigue behaviour of a particular out-of-plane joint, the single skin tee joint.

Initially a review is presented of the current knowledge concerning the load transfer mechanisms of tee joints. This highlights the substantial knowledge available on tee joint static behaviour and also establishes what is still not clearly understood. A review is then presented of the fatigue damage mechanisms of FRP materials including what is known currently of in-plane joints and out-of-plane tee joints. This highlights the lack of understanding surrounding the long term behaviour of FRP tee joints and establishes possible damage and failure processes which could occur in these joints.

As a first step in understanding the fatigue behaviour of tee joints, further static experimentation of four different joint configurations is presented. This helps fill the gaps in the knowledge of static load transfer mechanisms using thermoelastic and photoelastic techniques to produce novel full field pictures of through-thickness stress and strain distributions. The static experimental results also provide a first point on the fatigue load-life curve for each joint configuration. Extensive fatigue experimentation is then presented for

the same four tee joint configurations. Uniquely, load-life curves and stiffness degradation, residual strength degradation and energy dissipation through life results are presented for the tee joints subjected both to constant loading and two-step loading fatigue. Damage processes and failure mechanisms are also highlighted in detail, as never before.

Theoretical analysis of the tee joints is presented in two parts as internal behaviour predictions and global behaviour predictions. Internal behaviour is modelled using Finite Element Analysis (FEA). The results are used in a novel manner for tee joints to provide a means of understanding and predicting the damage processes and failure mechanisms seen during experimentation. Global behaviour is modelled using a new method based on energy dissipation as a damage indicator. This method gives relatively good predictions of two step load fatigue lives compared to existing theoretical approaches. Further more a second new method of global fatigue behaviour prediction is proposed for use as a design tool. This approach gives a means of producing a design envelope of tee joint design solutions for a given application. Within the bounds of this investigation the method gives very good predictions of constant load fatigue lives.

Acknowledgements

I am indebted to many people for the help and guidance they provided whilst I was producing the work described in this thesis. With out them this work would not have been possible.

My most profound thanks go to my supervisor, Dr R. Ajit Shenoi, for all his advice and support through-out my period of study.

I would also like to thank Prof W. G. Price and all the staff of the Department of Ship Science for providing such a friendly enjoyable atmosphere in which to work, and especially Guy Hawkins and Simon Clarke for their ideas and thoughts along the way.

Thanks also go to Vosper Thornycroft UK Ltd for providing the test specimens, particularly Alan Dodkins and John Holness and especially Les Wallin who provided his time and his expertise in measurement.

Further thanks must go to all the technicians involved in the experimental work for there invaluable help. Especially, Mike Bartlett and Colin (Workshop), Bob Stansbridge and Graham King (Electronics) and Dave Edwards (Lab Technician).

Last, but by no means least, thanks go to my wife Fran for all her help with preparing this thesis and for all the tolerance and support she has shown me.

CONTENTS LIST

1.0 Introduction

Today's trend in the marine industry is for faster, lighter vessels, carrying larger payloads with greater longevity. This has led to an increasing interest by Naval Architects in more unconventional materials for the construction of vessel structures. A particular material which is in growing use by both high performance naval and commercial ships is fibre reinforced plastics (FRP). This has the unique potential of allowing designers to tailor material properties to optimise their structural designs.

To afford flexibility in the construction of large structures, such as ships, requires the inclusion of joints. When FRP materials are being used their low specific stiffness can require the inclusion of further joints for the addition of structural reinforcements.

Bonded or laminated joints between two structural members represent a zone of potential weakness in context of FRP materials. The weakness in this case is caused by the absence of load bearing fibres across bonded surfaces and through the occurrence of stress concentrations associated with joint geometry and production considerations. It is important then that their behaviour when subjected to typical in-service loads is completely understood.

FRP joints can be split into two general groups, either in-plane or out-of-plane joints. The primary function of an in-plane joint is to transfer tensile loads between two in-plane panels. In the marine industry these types of joints have generally been used to join prefabricated modules and to carry out repairs. The coverage of in-plane joints in the literature is fairly exhaustive, addressing their behaviour when subjected to static and impact loads and long term fatigue. See for example Matthew *et al.* (1982). The primary function of an out-of-plane joint is to transmit flexural, tensile and shear loads between two out-of-plane panels. In the marine industry these types of joints are very common and have generally been used to join bulkheads or stiffeners to the hull of a ship. There has been an emergence of a wide body of literature concerning the static behaviour of out-of-plane joints. See for example Junhou and Shenoi (1996). There is however, a conspicuous lack of work concerning the long term behaviour of these joints.

The long term behaviour of joints is currently of particular importance as the oldest FRP ships reach their design lives and new ships are designed for minimum weight with the requirement of longer design lives and lower through-life repair bills. Consequently the aim of this investigation is to understand the long term fatigue behaviour of a particular out-of-plane joint, the single skin tee joint. The main objectives are to understand the physical characteristics of FRP under fatigue, to extend this to the performance of tee joints in an experimental context and to identify failure mechanisms, to develop modelling techniques to characterise their long term cyclic behaviour and to propose an approach for incorporating

fatigue characteristics in tee joint design.

A typical single skin tee joint is shown in figure 1.1. The joint itself is formed by hand laminating strips of reinforcing cloth (or overlaminates) either side of the joint to form a double (or boundary) angle connection. The load transmission is done entirely through the cloth-resin plies and any filleting resin within the boundary angle.

To establish what is known at present about the load transfer mechanisms of tee joints and to identify any shortcomings in that knowledge, current design guidelines, experimental investigations and theoretical modelling concerning these joints are examined. Any shortcomings are addressed in a programme of static experimentation. This experimentation is also used in understanding the fatigue behaviour of the tee joints in terms of damage initiation and mechanisms.

To understand the fatigue mechanisms and behaviour of FRP materials and joints, there is a progressive examination of fatigue behaviour; from continuous fibre laminates through to marine type laminates, on to in-plane lap joints and then finally to the current understanding of out-of-plane tee joints. This highlights the lack of knowledge concerning single skin tee joint fatigue behaviour.

As an initial step in the derivation of a method for defining fatigue damage accumulation in tee joints, the various theoretical techniques currently available for laminates are examined. This includes methods based on stiffness and strength degradation and energy dissipation. An assessment is made as to the applicability of the various techniques to tee joints in light of the current understanding of their behaviour.

Experimental evaluation of static stress and strain distributions utilising novel techniques, combined with theoretical investigations of the internal behaviour of various tee joint configurations using finite element analysis (FEA), highlight in detail joint behaviour and damage mechanisms. Extensive experimental evaluation of the fatigue performance of the same tee joint configurations then produces load-life data, stiffness and strength degradation and energy dissipation data. From this data it is possible to determine the influences of geometric configuration on fatigue strength and damage mechanisms.

The data produced from the experimental programme is combined with currently available theoretical techniques and a novel theoretical approach to produce a damage accumulation method for use in the fatigue assessment of tee joints. The data is also combined with data from other sources, to produce a set of novel design curves that allow preliminary predictions of static and fatigue strength for a large range of tee joint configurations.

2.0 Tee Joints

2.1 Background

2.1.1 Marine Applications

A typical stiffened single skin ship structure is shown in figure 2.1. The structure comprises a large number of different out-of-plane connections including frame to shell, bulkhead to shell, stiffener ends, stiffener intersections, deck edges and so on. These connections can be split into two main types. The first is the laminated tee joint where two orthogonally placed pre-fabricated panels are connected and there is access to both sides of the joint. The second is the top-hat stiffener joint where a pre-fabricated stiffener is connected to a panel and there is only access to one side of the joint.

The two joint types are required to transmit direct and shear forces and bending moments caused by normal hydrostatic and wave loads together with hydrostatic pressure loads under damage conditions.

The construction of the tee joint and top-hat joint is similar. Typically a joint is formed with a pure resin fillet over-laminated with strips of reinforcing cloth to form boundary angles. The geometry of the joints results in an out-of-plane loading being applied to the curved boundary angles which in turn causes interlaminar stresses. FRP materials have an inherently low interlaminar strength due to the lack of reinforcing fibres orientated normal to the laminae. As a result these joints are susceptible to delamination within the curved overlaminate at relatively low loads, when compared to the in-plane strength of the material.

2.1.2 Design Guidelines

Various sources of design guidelines are available to help in the design of out-of-plane joints. One of the earliest sources is the "Marine Design Manual for Fibreglass Reinforced Plastics" by Gibbs and Cox (1960). This manual covers both tee joints and stiffener joints and gives recommended arrangements and design examples. It recommends that a low density fillet be inserted between the members being joined to reduce the rigidity of the connection. It also suggests that the dimensions of the overlaminates should be "minimum consistent with strength requirements" to be "determined by test", although a minimum overlap of 50mm is recommended.

Early work on FRP marine structures in the U.K. centred around the design of the Royal Navy Minehunters. The extensive analysis conducted by the Ministry of Defence in support of its minehunter programme formed the impetus to the drawing up of naval engineering

standards. Standard NES140 gives detailed guidelines on the design of structural intersections. It specifies that the thickness of the overlaminate, t, is to be at least half, and preferably two-thirds, the thickness of the thinnest member being joined. The length of the overlaminate overlap should be at least 100mm, and preferably 150mm. The radius of the fillet is specified as t + 20mm and the gap between the members being joined is specified as less than t, except over short lengths. In addition guidelines are also given on lay-up and stacking sequence. It states that the overlaminates are to be made up of two layers of CSM plus one layer of woven fabric reinforcement, repeated as necessary such that, with the addition of at least two layers of woven reinforcement to the outside of the joint, the desired thickness is achieved.

Probably the most usual source of design guidelines utilised by designers in the marine field are the Classification Society Rules.

Lloyd's Register of Shipping (LRS) rules (1983) state that for vessels greater than 30m in length "the scantlings are to be determined by direct calculation ". For shorter vessels guidance is given on the design of both top-hat stiffener joints and tee joints. For tee joints it is stated that the overlaminate should overlap onto the members being joined by a minimum of "50mm + 25mm per 600 g/m^2 of reinforcement". In addition the weight of the laminate forming each angle should be at least 50% of the weight of the lightest member being joined, or 900g/m^2 of chopped strand mat (CSM) or equivalent, whichever is greater. Explicit guidance on the resin fillet radius is not given, however it is stated that in bonded joints, polyester or epoxide resins should be used and that "the contact area is to be as large as practicable". Guidance is also provided with regard general lay-up and stacking sequence, in particular that the first layer laminated onto a pre-cured surface should be chopped strand mat (CSM).

The American Bureau of Shipping (ABS) rules (1978) are applicable to GRP vessels under 61m in length. Both top-hat stiffener joint and tee joint design guidance is given. For tee joints it is stated that the overlaminate thickness should be one-half the thickness of the thinner of the two laminates being joined, provided it exceeds a certain minimum value governed by the length of the vessel. The overlaminate overlap is specified as being not less than 15 times its thickness. As with the LRS rules guidance on the lay-up and stacking sequence suggests that the first layer laminated onto a pre-cured surface be CSM.

The Det Norske Veritas (DNV) rules (1991) utilise a unique approach in that no formulae is given for the direct derivation of scantlings. The rules offer instead tables of loadings, allowable material properties and maximum limiting stresses from which the overlaminate details are to be determined. The method by which this is to be achieved is left to the designer to determine, although certain minimum requirements are specified. The resulting

calculations and derived scantlings are then to be submitted for approval.

2.2 Characterisation of Behaviour Through Experimentation

Until recently there has been little work concerned with the characterisation of the behaviour of tee joints. The work has been predominantly application specific, in that a particular design of joint has been modified in one direction only to enable it to achieve the necessary level of performance required by the particular application being considered.

Early work was conducted by the structure manufacturers to overcome particular problems within their own products. In the marine field this experience was collated and used as the basis for the Marine Design Manual from Gibbs and Cox (1960).

A large experimental programme was conducted prior to the construction of the first of the Royal Navy's minehunters, HMS Wilton, with regard to many aspects of FRP construction, Dixon *et al.* (1972), Smith (1972), Harrhy (1972). This highlighted the weakness of out-of-plane joints as frames were found to debond from the shell under shock loading tests. The solution adopted to overcome this problem was to through-bolt the connections. Following the development of the larger Hunt Class MCMV's it was decided that improvements should be made to the joints performance, Chalmers *et al.* (1984), Pitts and Dorey (1984), Green and Bowyer (1981), Dodkins (1989). This involved disposing of the bolts and replacing the filled polyester fillet with a flexible urethane acrylate fillet. Tee joint test specimens were subjected to 45° pull-off tests (the 45° loading represented a tank under hydrostatic pressure) and then the joints were tested in full scale tank structure tests subjected to explosive loading. These tests resulted in a bonded joint with a similar ultimate static strength to that of the bolted joints. Initial failure however, was still by delamination of the overlaminate. The inclusion of these joints in the Sandown class of SRMH's highlighted problems with premature delaminations in the tee joints in certain areas of the ships. A further experimental programme was undertaken with the aim of delaying the delaminations, detailed in Vosper Thorneycroft (UK) Ltd Report No. D/89-452 and Report No. D/89-455. Modification of the overlaminate resin system from pure polyester to a polyester/urethane acrylate mix was found to be the solution. The resin improved the toughness and flexibility of the overlaminates and hence was found to delay the onset of delamination. The mode of failure remained the same, however, with delamination occurring well before the final failure of the joint.

Work in the aeronautical field has been mainly directed towards bonded tee joints incorporated in wing structures. A comprehensive study of the behaviour of a spar-wingskin joint has been carried out by Cope and Pipes (1978). The investigation involved developing the correct size and shape of epoxy insert around which the spar was laid. The test method

used to assess the tee joints was a vertical pull-off. The results showed that radiused inserts were much better than triangular ones, and the larger the radius, the stronger the joint.

Arguably, the most rigorous investigation into the behaviour of tee joints up to now, was performed by Hawkins (1995). This work followed on from the experimentation undertaken within the UK minehunter programmes. The 45° pull-off was again used to simulate the loading patterns experienced by the tee joints. A radial test method was adopted allowing geometric and material variables to be investigated within a limited programme of testing. This method produced test specimen types where each type varied from the "common" type by one feature only. The joint chosen to be the hub of the variants featured a pure fillet only, with no overlaminate and was designated sample C. Variations from this sample were made by changing either the fillet radius, the gap between the members being joined, the preparation of the tee-piece or by the addition of an overlaminate. In addition to these variants the joint designs in current use were also tested.

The details of each specimen type tested are given in table 2.1. All the base plates to be joined were the same polyester resin with E-glass woven fabric reinforcement and all fillets were produced from urethane acrylate resin. Samples A, L and M had overlaminates based on polyester resins, whilst samples B, F, J and K used a urethane acrylate/polyester resin mix in the overlaminate.

The thick overlaminate joints were seen to be prone to premature failure by delamination. This progressed through the laminate as load was increased until final failure occurred when the overlaminate detached from the fillet, and the fillet failed. Premature delamination was not seen in the thin overlaminate joints and hence final failure was catastrophic with no clear order of failure. The pure resin samples all failed within the fillet, sometimes preceded by detachment of the fillet from the web or flange. In all cases final failure initiated from the tension side of the fillet on the outer face.

It was observed from the test results that the fillet radius and overlaminate thickness were very significant joint variables, with all others being considerably less significant. Increasing fillet radius was seen to increase the ultimate strength, failure deflection and joint stiffness. The incorporation of a thin overlaminate was seen to produce similar effects to increasing fillet radius with an increase in stiffness, strength and failure deflection. Increasing the overlaminate thickness was seen to increase joint stiffness, but no concrete conclusions could be reached as to its effects on joint strength and failure deflection. Increase in gap size and modification of the end of the tee-piece seemed to have little effect on joint stiffness, but increased joint strength and failure deflection. These changes also appeared to increase scatter in the failure values making the improvements in performance unreliable. Finally, modification of the overlaminate resin was seen to cause a delay in initial delamination and

hence an increase in strength and also failure deflection, but little change to joint stiffness.

In addition it was noted that there was a relationship between the quality of construction and the design of the joints. Large radius and thin overlaminate joints tended to lend themselves to more consistent production and hence a more consistent performance. This was reflected in their narrow band of experimental scatter. Furthermore it was pointed out how joint flexibility enhanced joint performance. This was contrary to the design guidelines which promote the use of stiff joints through the use of excessively thick overlaminates.

2.3 Theoretical Modelling of Mechanical Behaviour

As with the experimental work, very little theoretical work had been concerned with tee joints behaviour and performance, until recently. The complex geometries associated with tee joints lend themselves to numerical techniques, hence all the theoretical analyses have been performed using finite element methods.

Smith (1972) and (1990), performed a two dimensional plane strain finite element idealization of a bulkhead/shell connection incorporating a single boundary angle. The joint was subjected to a vertical pull-off load and a 90° bend simulating flooding loads. Distributions of tensile and shear stresses were computed across the bonded interfaces of the joint. These showed high stresses were likely to be present at the ends of the boundary angle overlaps.

In their study of aircraft spar-wingskin joints Cope and Pipes (1978) used two dimensional finite elements for their idealization. Verification of the model was achieved by comparing applied load to experimental strain measurements taken from the wingskin. A reasonable correlation was found to exist. The mode of failure was predicted to be debond of the fillet from the overlaminate. This mode could not be confirmed by experiment, however, due to the catastrophic nature of failure, which made the determination of the location of failure initiation difficult.

Gillespie and Pipes (1978) also investigated aircraft spar-wingskin joints. They too used two dimensional finite elements in a plane stress idealization. Three types of joint were studied, a joint with no-insert, with a titanium insert and a graphite-epoxy insert between wingskin and spar. The joints were subjected to a pull-off load applied as a pressure load to the wingskin. Verification of the models was achieved by comparing predicted load-deflection response and strength with experimentally determined results. Relatively good agreement was found to exist, although the finite element analysis was unable to predict the bilinear load-deflection response of the joints containing inserts. The joint strength predictions were

based on interlaminar failure at the base of the spar.

In the most recent investigation into tee joint behaviour, Hawkins (1995) used three dimensional non-linear finite element idealization to illustrate the internal behaviour the joints types detailed in table 2.1 and hence determine their load transfer mechanisms. In addition he performed a parametric study showing the effects of critical design variables on joint performance. The joints were all subjected to a 45° pull-off load. Verification of the models was achieved by a comparison between the predicted load-deflection responses and experimental results. Furthermore a comparison was made between predicted stress levels, material strength values and experimentally determined joint strengths. Reasonable correlation was found to exist.

Comparison of the stress distributions for the different joint types at a constant load, showed that in the thick overlaminate joints in-plane stresses in the overlaminate were approximately 50% of the ultimate strength of the laminate, whilst the stresses in the fillet were around 65%. The interlaminar stresses in the overlaminate however, were found to be 100%, indicating possible failure by delamination. Fillet stresses in the pure fillet samples were found to be between 80% and 90% of ultimate. In the thin overlaminate joints overlaminate in-plane stresses were found to have increased slightly compared to the thick overlaminate joints, and the fillet stresses were similar to the pure fillet joints. The interlaminar stresses in the overlaminate however, were found to have reduced by 60%.

The parametric study was based on the variation of the fillet radius, the overlaminate thickness and the gap size, as these were deemed to be the variables having the most influence on joint performance. The results are given as a series of design curves in terms of overall deflection, maximum stress in the fillet, maximum overlaminate in-plane stress, and maximum overlaminate interlaminar stress, for a constant load of 12.5 kN. Figure 2.2 shows the results for the variation in overlaminate thickness and fillet radius. The gap size is constant at 20mm. It was found that increasing overlaminate thickness and fillet radius caused overall deflections and in-plane stresses in the overlaminate to decrease. In addition the increase in overlaminate thickness also caused a decrease in fillet stresses and increase in overlaminate interlaminar stresses. Investigations into the variation of gap size found it to have no significant effect on overall deflections or stresses in the overlaminate. The stresses in the fillet however, increased with increasing gap size, but this effect was reduced by the increase in fillet radius.

2.4 Discussion

A substantial amount of work has been directed towards understanding the load transfer

mechanisms of tee joints. From the aeronautical field to the marine field, whether through experimentation or theoretical modelling, the knowledge gained up to now has been extensive. Unfortunately, at present, the design guidelines available do not reflect this. Most guidelines are based on experience and give no guidance on some important design variables such as fillet radius. Infact if the base plates to be joined are the same thickness and material as the overlaminate, which tends to be the case, the majority of the guidelines could be reduced to two simple rules; use CSM as the first overlaminate layer and construct the overlaminate so that its thickness is half that of the base plates being joined. This guidance may actually be detrimental to the joints behaviour because it produces an inherently stiff joint. As Gibbs and Cox (1960) first advised and further investigations have agreed, the aim of the joint design should be to "reduce the rigidity of the connection".

All the experimental investigations into tee joints are in general agreement with each other, they show that thick overlaminates lead to delaminations well before final failure of the joint. Furthermore they show that the overlaminate thickness and fillet radius are crucial geometric variables governing joint performance. All the data available relate to load-deflection or just ultimate failure load. Much has been learnt from these investigations about the influence of geometric variables on joint performance, however there is little experimental knowledge of the actual load transfer mechanisms, particularly load paths and internal stress and strain distributions.

Theoretical modelling of tee joints has been restricted to finite element analysis (FEA) only. This is due to the complicated nature of tee joint geometry and construction. The finite element approach has allowed a detailed understanding of the stress distributions within tee joints. Importantly, Hawkins (1995) has shown that relative interlaminar stresses in the overlaminates can be extremely high. These stresses have been taken to be the most likely cause for the delaminations observed in the experimental investigations.

Computational limitations at the time of each FEA investigation, have meant that the mesh of the FEA models tend to be rather coarse, hence there is not an element per layer of laminate and elements have had to be used in a deformed shape around the curved boundary angles. This will have caused approximations to be made during solving and averaging of the results. In addition, in some cases there was a significant lack of accurate material property data available, which would have caused approximations in the modelling and hence further approximations in the results. There also tended to be little substantial model verification, with the assumption that if a single point measurement of deflection or strain is similar to the FEA result then the rest of the stress and strain results should be correct. These shortcomings in the way the FEA models have been produced has meant that although the relative stress values and distributions predicted are likely to be correct, the actual magnitudes of stress predicted may be unreliable.

3.0 Fatigue Processes in Fibre Reinforced Plastics

3.1 Continuous Fibre Laminates

3.1.1 Unidirectional Laminates

The simplest form of composite material is one with all the reinforcing fibres aligned in a single direction. Curtis (1989) points out that the application of such composites is limited, due to the poorer mechanical properties in directions other than normal to the fibres.

Damage mechanisms, produced by tensile fatigue loading of unidirectional laminates, have been extensively investigated by Talreja (1987). For loads applied parallel to the fibres he divides the damage mechanisms into three types as shown in Figure 3.1. Firstly, at stresses exceeding the strength of the weakest fibre in the laminate, fibre breakage occurs (Figure 3.1a). This causes shear stress concentrations at the fibre matrix interface close to the broken fibre. The interface may then fail, leading to debonding of the fibre from the surrounding matrix. This debonded area acts as a stress concentration site for longitudinal tensile stress. If the stresses in this area exceed the fracture stress of the matrix a transverse crack will form in the matrix. The second and third damage mechanisms involve cracks initiated from flaws in the matrix which grow until they encounter an interface. The matrix damage is controlled by applied strain due to the constraint provided by the fibres. At sufficiently low strains cracks are confined to the matrix alone, increasing only in numbers (Figure 3.1b). At higher applied strains the stress at a crack tip might exceed the fracture stress of fibres, leading to fibre failure and allowing matrix cracks to grow. If a crack is long enough, the shear stress at its tip may become sufficient to cause a fibre matrix interface to fail bringing about a diversion of the crack into the fibre direction (Figure 3.1c).

As the numbers of fatigue cycles increases initiated matrix cracks will propagate. Isolated fibres are rendered ineffective load carriers, causing fibres to become locally overloaded and static failures occur. Close to failure, matrix and interfacial damage cause extensive longitudinal splitting parallel to the fibres, leading to a characteristic brush-like failure.

Dharan (1975) investigated the fatigue mechanisms of a unidirectional glass fibre-epoxy material. He concluded that the fatigue response could be divided into three distinct life ranges. In the first region (less than 200 cycles), there was a small dependence of the fatigue life on cycling. Observation of the specimen during the first cycle showed that in addition to a progressive increase in matrix cracks with stress, the peak stress was high enough to precipitate large numbers of fibre failures within the material. Failure occurred by the coalescence of local fibre breaks which then propagated in a few cycles to connect other such regions until the specimen failed catastrophically. In the second region (200 to 10^6 cycles),

matrix cracks were still formed in the first cycle. Several random fibre breaks were also observed, but not in large numbers. As cycling progressed, one (or more) surface crack was seen to propagate perpendicular to the tensile axis breaking fibres in its path until it was large enough to satisfy the criterion for fibre matrix interfacial shear failure. When this occurred, delamination began, leading to eventual failure. In the third region (greater than 10^6 cycles), the applied stress was below the matrix crack initiation stress and none of the few specimens tested failed.

Loading inclined to the fibres has been assessed by Talreja (1987). For off-axis angles between 0° and 90°, the tip of a crack initiated in the matrix will be subject to two displacement components, i.e. an opening normal to the fibres and a sliding parallel to the fibres. This will lead to mixed mode crack growth parallel to the fibres. At an off-axis angle of 90°, the crack growth will occur in the opening mode only. This will lead to debonding of the fibre matrix interface, referred to as 'transverse fibre debonding'.

3.1.2 Cross-Ply Laminates

More useful composite materials are formed by the combination of several laminae (or plies) in various directions, with a lay-up based on the design load requirements. The damage development in such composites under tensile fatigue loading has been discussed by Reifsnider and Talug (1980). The initial damage consists of matrix cracking along the fibre direction in the off-axis plies. These cracks form through the thickness of the plies by transverse fibre debonding. The cyclic stress level controls which plies will form cracks and the number of loading cycles influences the number of cracks formed. The cracking process continues until each off-axis ply has attained an equilibrium or saturation crack spacing consistent with the development of, what Reifsnider and Jamison (1982) term the Characteristic Damage State (CDS). When the CDS has formed no new transverse cracks form independently in the off-axis plies. The existing cracks in a particular ply act to reduce the stress locally, to the extent that the material between adjacent cracks cannot be subjected to a stress sufficient to cause the formation of another intermediate crack. The regular crack spacing is characteristic of the material and the laminate's stacking sequence, but independent of the load history.

As transverse cracks form they initiate short microcracks observed running perpendicular to the primary transverse cracks. These microcracks are caused by tensile stresses ahead of the transverse cracks. They are located at or near the ply interfaces and tend to cluster in zones centred around the transverse cracks.

The interlaminar shear and normal stresses which vanish in regions remote from the edges

of undamaged laminates are observed to take on non-zero values in damaged regions, Reifsnider and Talug (1980). As the fatigue cycles increase delamination occurs. This is caused by the growth of interlaminar cracks driven by the interlaminar stresses in regions where transverse and microcracks cross. Delamination can contribute to crack growth by allowing cracks in adjacent plies to connect up with one another by climbing along the ply interfaces. This type of crack growth is also greatly enhanced by the through-the-thickness tensile stresses which tend to pull the ply interfaces apart.

Continued cycling results in regions of high crack connectivity and high crack density developing. One of these regions is generally the final fracture site. The terminal event of separation usually consists of large scale fibre breakage and debonding in the plies aligned with the principal tensile stress, Talreja (1987).

3.2 Marine Type Laminates

3.2.1 Chopped Strand Mat Laminates

Owen and Dukes (1967) examined the tensile fatigue behaviour of laminates of E-glass CSM and a general purpose polyester resin. They observed a series of damage events similar to those of continuous fibre laminates. The first type of damage was debonding of the fibres lying at 90° to the direction of load caused by a breakdown in the fibre matrix interfacial region (transverse fibre debonding). With continued loading damage spread to fibres aligned at progressively smaller angles to the applied load. It was seen that damage could be initiated at any point along a fibre and did not seem to be particularly associated with fibre ends. Further damage involved intensive resin cracking which occurred in the resin rich zones of the material. Cracks were predominantly perpendicular to the applied load and appeared to originate from some of the debonds. These transverse resin cracks in turn caused debonding of fibres aligned with the applied load wherever these were intersected by the transverse cracks.

Owen and Howe (1972) observed that the number of resin cracks tended to become saturated at some point during the fatigue life. This then initiated the development of debonds which spread among the aligned fibres, increasing in number sharply before failure. Bourban et al. (1989) found a similar sequence of damage events when testing glass CSM set within three different epoxy resins.

An early investigation was made by Owen and Smith (1968) into the effects of varying glass content and test frequency when fatigue loading CSM. They found that at short life times increasing the glass content increased the fatigue strength, but at longer life times the glass

content became less important. The long-life behaviour was found to be dependant primarily on the resin. Increasing the test frequency was found to considerably change the fatigue strength of CSM. This Owen and Smith associated with a significant increase in internal temperature rise at each applied stress amplitude which caused a change in the damage process within the material.

3.2.2 Woven Fabric Laminates

Woven fabric reinforcement consists of two sets of interlaced yarns where the longitudinal direction of the fabric is termed the warp and the transverse direction is referred to as the weft. The yarn crossovers are commonly referred to as undulations.

In fabric-reinforced laminates the earliest signs of damage take the form of transverse fibre debonding and among the weft fibre strands and resin cracking in the resin-rich zones of the material, Beaumont (1990). Continued cycling leads to the development of intensive damage in the form of delamination located at the undulations.

Tanimoto and Amijima (1975) performed tensile fatigue tests on a series of satin woven glass reinforced polyester laminates loaded in the warp fibre direction. They divided the fatigue process into three stages; stage one involved the initiation of transverse cracks in the resin phase of the laminates at the centre of the undulations (see figure 3.2a). During this stage the transverse crack density was seen to gradually reach a constant value. The second stage involved the propagation of the transverse cracks through the weft fibre strands up to the adjacent longitudinal fibres where they initiated longitudinal cracks (see figure 3.2b). The third stage involved the longitudinal crack density also becoming constant up until the fatigue life was reached at which stage the specimen failed suddenly.

Schultz *et al.* (1987) performed tensile fatigue tests on a fabric-reinforced laminate loaded in the weft fibre direction. As would be expected, during early fatigue cracks were initiated and developed along the transverse threads, in this case in the warp direction. These cracks were considered to initiate at the centre of the undulations. Cracks are seen to initiate in the undulated region because there is a lower stiffness than in the surrounding regions where straight fibres are present. The lower stiffness causes a maximum strain to appear at the centre of the undulation, Ishikawa and Chou (1983). Further damage involved the development of longitudinal cracks which increased both in length and density. At the undulation of warp and weft threads delamination developed being initiated at cross sections of transverse and longitudinal cracks. As soon as delamination occurred the stiffness of the laminate decreased considerably leading to final failure.

3.3 Loading Effects

3.3.1 Loading Configuration

Compressive fatigue of composites is not thoroughly understood, Curtis (1989). Less information is available mainly because the compressive testing of these materials presents many problems, such as the need to support the specimens from undergoing global macrobuckling. An experimental study of compression-compression fatigue has been undertaken by Grimes (1981).

In compression, the fibres remain the principal load bearing elements, Curtis (1989). They must, however be supported from becoming locally unstable and undergoing a microbuckling type of failure by the matrix and fibre matrix interface. Matrix and interfacial damage develops for much the same reasons as for tensile loading, but the greater demand on the matrix and interface causes greater strength degradation during compressive fatigue. In addition, local matrix and interfacial damage leads to fibre instability in compressive loading which is more severe than the fibre isolation mode which occurs in tensile loading.

The worst fatigue loading condition for composite materials is tension-compression loading. The poorer behaviour that is observed, is because many of the laminate off-axis plies develop intra-ply damage which causes local layer delamination at relatively short lifetimes. In the compression half cycle tensile induced damage can lead to local layer instability and layer buckling, before resin and interfacial damage within the layers has initiated fibre microbuckling. Thus fatigue lives in tension-compression loading are usually shorter than for other loading configurations.

Flexural bending fatigue of composites is another subject where little information is available. The main reason for this is that designers tend to use inplane properties to predict fatigue lifetimes of materials subjected to flexure. Scholte (1993) points out however, that flexural fatigue can produce poorer behaviour than inplane fatigue. This is due to the large stress gradient through the thickness of a laminate, which causes significant shear stresses to occur at the interface between fibres and resin.

3.3.2 Stress Ratio

The stress ratio R, is defined as the ratio of minimum applied stress to maximum applied stress. Mandell and Meier (1983) studied the effect of varying this ratio for glass reinforced epoxy laminates under tensile fatigue. They found that as the stress ratio increased towards R = 1 the fatigue lifetimes of the laminates increased.

Poppen and Bach (1996) present constant life diagrams for three different glass fibre reinforced laminates (see figures 3.3a, 3.3b and 3.3c). Lines originating from the origin represent a constant stress ratio. The y-axis represents a stress ratio of R = -1 (symmetric tensile/compressive loading) the intersection with the x-axis is the static strength value of the laminate. It can be clearly seen that for each of these laminates an increase in stress ratio again leads to an increase in fatigue lifetimes.

3.3.3 Frequency

The effect of load frequency during the fatigue of composites has been investigated by various authors, Mandell and Meier (1983), Saff (1983), Sun and Chan (1979), Reifsnider *et al.* (1977). They have all indicated that the frequency of cyclic loading has a significant effect on the fatigue life of fibre reinforced composite materials. In general they have found that decreasing load frequency decreases the fatigue life of a laminate due to damage developing more rapidly at lower frequencies. Saff (1983) concludes that matrix-dominated lay-ups are more sensitive to load frequency than are fibre-dominated lay-ups. He relates the sensitivity of given lay-ups to the stress state in the matrix. Curtis (1989) discusses the hysteresis heating effects related to fatigue frequency. He states that laminates dominated by mainly continuous fibres in the test direction develop small strains and there is little hysteresis heating. However, resin dominated laminates, with few or any fibres in the test direction, show larger strains and thus marked hysteresis heating. He concludes that the effect of fatigue loading rate is negligible for most continuous fibre composites tested in the fibre direction, as long as hysteresis heating is also negligible. The main exception is glass-reinforced plastic (GRP) in which there is a significant loading rate effect, believed to be due to the environmental sensitivity of the glass fibres.

3.3.4 Environment

One concern in the incorporation of GRP into marine construction programs is the long term durability of the material in a salt water environment. Penetration of fibre reinforced plastics by water occurs both by diffusion through the matrix and by capillary flow through defects and along imperfect fibre matrix interfaces, Smith (1990). Higher absorbtion levels will occur if the laminate contains damage in the form of matrix cracking and fibre debonding. More detrimental than environment alone is the combined effect of stress and environment. Tensile stress coupled with salt water immersion can result in stress corrosion of the glass fibres. This results in the growth of microscopic cracks in individual fibres which leads to catastrophic fracture of the laminate.

Hofer and Skaper (1985) studied the effect on the fatigue endurance of a GRP laminate when submerged in salt water. They examined two glass fibre/polyester laminates and two glass

fibre/epoxy laminates. The results of the tests undertaken showed that for the polyester laminates there was an initial gradual degradation in residual strength followed by a sharp loss in residual strength. The loss was so severe that most specimens failed during the subsequent stress cycling phase. The drop off in residual strength of the epoxy laminates was seen to be much less abrupt.

3.4 Material Effects

3.4.1 Resin Type

Several investigations, Surendra (1987), Owen and Rose (1970), have been made concerning the contribution of matrix properties to the fatigue of fibre-reinforced composites. These have shown that the mixing of flexible resin with a general purpose polyester resin has little effect on the fatigue life of a laminate. In addition, resin cracking in fatigue is not suppressed by increased flexibility, although the onset of cracking and fibre matrix debonding is delayed.

Echtermeyer *et al.* (1995) compared the tension-compression fatigue behaviour of glass reinforced laminates made with polyester and phenolic resins. they concluded that the two resin systems exhibited similar fatigue characteristics. However, as opposed to the polyester laminates, the phenolic laminates were found to develop some damage during the compressive part of the fatigue cycle. This was attributed to the presence of micropores in the resin which are often created during curing of phenolic resin. It was argued that the pores could collapse under compression and allow some microbuckling of adjacent glass fibres.

3.4.2 Fibre Type

The use of aramid fibres instead of, and combined with glass fibres has lead to significant increases in fatigue life compared with traditional glass fibre laminates, Howson *et al.* (1992). This has also been seen to be true for carbon fibre and hybrid carbon/ glass fibre laminates, Bach (1996). The glass fibre laminates tend to be more susceptible to damage, this may be due to the fact that the greater stiffness of the carbon fibres reduces the strains within the laminate resin delaying resin cracking. Within the hybrid carbon/ glass fibre laminates the carbon fibres carry more of the applied load reducing the stress in the glass fibres.

3.4.3 Stacking Sequence

The stacking sequence of a laminate indicates the lay-up of the individual plies forming the laminate. For continuous fibre composites this will be a combination of plies with different fibre orientations to the direction of applied load. For marine type laminates it will possibly be a combination of woven fabric plies at various orientations and chopped strand mat plies.

Echtermeyer *et al.* (1996) studied the influence of different fabric stacking sequences by performing fatigue tests on a glass stitch bonded combination mat and four laminates of inlaid construction having straight glass fibres held together by polyester yarns. All the laminates were produced using polyester resin. They found that fibre orientation and fabric type affected fatigue strength, but the fatigue strain to failure was very similar for all the glass laminates, as long as some fibres ran in the load direction. Laminates with no fibres in the load direction failed much earlier than fabrics with some fibres in the load direction.

3.5 Bonded Joints

3.5.1 Lap Joints

In-plane joints are commonly used by the aerospace industry in the construction of aircraft structures. In the marine industry their use is limited to applications such as, providing a connection between prefabricated hull units and the repair of damaged laminate.

An insight into the behaviour of these type of joints was given by Smith (1972) using finite element analysis of a butt-strap connection. Figure 3.4 shows the connection and the calculated distributions of direct and shear stresses acting across the bonded interfaces for the joint statically loaded in bending and also in tension. As can be seen both types of loading induce tensile (peeling) and shear stresses which reach their maximum values near the lap ends.

Imanaka *et al.* (1988) investigated the importance of the complex stress distributions found within in-plane connections with relation to their fatigue strength. This was achieved by conducting fatigue tests on standard single lap joints with different lap length and adhesive layer thickness. Figures 3.5a and 3.5b show the tensile and shear stress distributions in the adhesive layer of the lap joint with adhesive thickness t = 0.1mm. The results indicated that the fatigue strength of adhesively bonded lap joints can be well characterized by the maximum tensile stress in the adhesive layer. Furthermore, maximum tensile and shear stress increase with the increase in lap length and the decrease of adhesive layer thickness.

Johnson and Mall (1985) and Tiu and Sage (1986) investigated the effect of joint geometry on fatigue strength. Tiu and Sage conducted fatigue tests on three different double lap joint configurations, the standard square-ended joint, the inverse taper joint and the radiused joint (a customized taper joint). The standard joint's fatigue strength was low. The mode of failure was a crack which started in the adhesive fillet at the end of the lap and then continued down into the composite for a short distance before propagating along the fibre direction until final failure occurred, see Figure 3.6a. The radiused joint configuration was intended to relieve the stress concentration by a gradual change in cross-section. It was found to be effective because the fatigue strength was improved by some 50%. The mode of failure was different from the standard joint, being entirely interlaminar failure of the composite in the lap initiating at the radiused surface, see Figure 3.6b. The inverse taper joint retained the gradual change in section of the lap whilst increasing the glue-line thickness to relieve the shear stress in the adhesive. The joint showed only a slight increase in fatigue strength over the standard joint. Failure occurred by the initiation of a tensile crack in the fillet which propagated down into and then along the base plate, finally delaminating the composite, see Figure 3.6c. It was therefore concluded that the radiused joint appeared to be the best configuration for fatigue applications. A similar conclusion was drawn by Johnson and Mall who conducted tests on single lap joints with varying angles of lap taper. They found that a taper of 5° resulted in a 50% improvement in the debond resistance of the joint compared with no taper.

3.5.2 Tee Joints

Out-of-plane connections are used extensively in marine construction, whether it be for the attachment of stiffeners or bonding of decks and bulkheads to the hull shell. The study of the fatigue behaviour of these types of joints has however been fairly limited.

One of the earliest investigations was presented by Dixon, Ramsey and Usher (1972) and was part of the design development work for the construction of the Royal Navy's first GRP minehunter HMS Wilton. Tests were performed on various bolted and unbolted bonded connections including frame to shell, frame to keel, deck to shell and bulkhead to shell joints. Figure 3.7 shows the bulkhead to shell joint test specimen details. Two test configurations were employed and these consisted of a compression load applied to the top of the web with the flange clamped and a bending load applied at 90° to the top of the web also with the flange clamped. Although the test results were very limited a number of conclusions could still be made. Firstly, the fatigue lives of the connections were considered adequate, this was in relation to the minesweeper requirement that structural connections should be able to withstand 10^4 cycles at 50% and 10^6 cycles at 25% of their ultimate static failure load, Smith (1972). Secondly, fatigue had no significant effect on the subsequent static strength of the connections. This was apparently true even in those cases where resin crazing and/or

delamination had occurred in the joint overlaminates during the fatigue loading. Thirdly, some of the connections experienced a significant and progressive loss of stiffness during the fatigue loading.

In a study by Scholte and van-Leeuwan (1977) a single type of bulkhead to shell connection was subjected to a series of fatigue tests. Figure 3.8 shows the test specimen details. Two specimens were tested statically and a further eleven specimens were tested at different applied fatigue loads. The loading was tensile-compressive with minimum to maximum load ratios of R = -0.5 and R = -1. Due to hydraulic limitations the cycle frequency used was varied from 0.6 Hz at high loads to 1.15 Hz at lower loads. Figure 3.9 shows the results of the fatigue tests in terms of double amplitude load vs number of cycles to failure. The damage mechanisms were similar for static and fatigue loading with delamination of the overlaminates and disbonding of the glass pins during static loading and fatigue cycling. Near final failure a disbond occured at the fillet/flange interface leading to peeling of the overlaminate from the flange and separation of the joint. For specimen no. 11 fatigue loading was only continued up to 10^7 cycles at which point the specimen was subjected to a static test. From the results of this test it was concluded that fatigue did not cause a significant reduction in joint strength even though the joint had developed a number of large cracks during fatigue loading. In addition to this a number of other conclusions were made. Firstly, fatigue loading caused a substantial loss of overall joint stiffness. In one case a 30% loss of stiffness was noted at only half the fatigue life of the specimen. Secondly, delamination and crack formation started at a very early stage of the fatigue life. In eight of the specimens cracks were initiated on the first cycle. Thirdly, some specimens had small defects prior to testing but these did not seem to significantly influence the results.

In a very recent study by the Defence Research Agency (DRA) Dunfermline, into defect tolerence of FRP structures, Defence Research Agency Report No. DRA/SMC/CR963033 (1996), included in it an investigation into the fatigue of tee joints, Defence Research Agency Report No. DRA/SMC/TR963012 (1996). The main aim of this work was to evaluate whether damage in the form of overlaminate root whitening, had any effect on the fatigue performance of tee joints representative of those found in the Royal Navy's Single Role Mine Hunters. The joint test specimens were constructed entirely using polyester resin, with overlaminates of 11 plies having the lay-up of 2 Chopped Strand Mat (CSM), 1 Woven Roving (WR), 2 CSM, 1 WR, 2 CSM, 3 WR. A typical specimen is shown in figure 3.10. The joints were loaded at 45° in compression, with a stress ratio of R=0 and a frequency of 1 Hz. Figure 3.11 shows the results of the tests in terms of stress at the overlaminate root versus number of cycles to failure. The stress at the root was derived from a strain gauge positioned at the surface of the overlaminate on the tension side of the joint. It was concluded from the S-N results that root whitening damage had little effect upon the fatigue performance of these tee joints. Defence Research Agency Report No. DRA/SMC/TR963013

(1996) evaluated the failure mechanisms induced by the fatigue testing and concluded that the principal failure mechanism was severe delamination occurring along the interface between the fillet and first CSM overlaminate ply on the tension side.

3.6 Discussion

It is obvious from the large number of variables associated with all composite material that the variation of anyone of these variables whether fibre, resin, loading or lay-up can have a significant effect on the behaviour of the material during fatigue loading. A general underlying behaviour can be identified, however, for most laminate types. In general damage is initiated on the first loading cycle and cracks form perpendicular to the direction of loading. The crack formation then progressively changes direction until cracks are formed parallel to the applied load, at which point final failure begins. Increasing frequency and stress ratio in general increases fatigue lives. Generally stiffer laminate lay-ups, i.e fibre dominated laminates are less susceptible to damage and hence less fatigue sensitive.

The knowledge concerning fatigue of laminates is extensive. The knowledge surrounding the fatigue behaviour of joints, particularly tee joints is however, very limited.

The understanding of lap joint fatigue behaviour is mainly confined to failure mechanisms for various joint designs. Although it is known that the stresses have maximum values at the end of the laps and designing to reduce these stresses, whether with radii or tapers can result in significantly improved joint performance.

The understanding of tee joint fatigue behaviour is based on a very small number of fatigue test results. Surprisingly it has been found in two separate studies that fatigue loading does not cause a significant reduction in joint strength, but it does cause a significant loss of stiffness. These conclusions have however, been based on only one or two test specimen results with no detailed analysis of how the strength or stiffness varies over the lifetime of the joint configurations. There is no quantification of the scatter present in the results and no calculation as to the percentage of fatigue life that the joints have experienced before they are statically loaded. Unfortunately this makes the conclusions unreliable.

The work up to now on fatigue behaviour of tee joints has been limited to application specific investigations and little understanding of the behaviour of these joints has been established. Load-life data is very limited, the understanding of the fatigue mechanisms and processes is inadequate and the understanding of the effect of geometric variables on fatigue performance is practically non-existent.

4.0 Fatigue Modelling of Fibre Reinforced Plastics

4.1 Load-Life Representation

4.1.1 S-N Equations

An important first step in modelling the fatigue behaviour of a material is to characterise its constant stress or strain fatigue life. A large number of models exist in the literature with various approaches, but each has a similar purpose and that is to fit a curve to experimental fatigue life data. The models available can be sorted into three general types; straight line fits, power law fits and inverse power law fits.

Metal fatigue has been studied for many years and several empirical fatigue models have been established for describing S-N curves, these include the Basquin law, the conventional straight line in S-N and the Manson-Coffin law.

The Manson-Coffin law is a power law based on plastic strain amplitude,

$$\varepsilon_{ap} = \varepsilon_f (2N)^c \tag{4.1}$$

where ε_{ap} is the plastic strain amplitude, 2N is the reversals to failure, ε_f is the fatigue ductility coefficient and c is the fatigue ductility exponent.

Basquin's relation is a power law based on applied stress,

$$\sigma_a = \sigma_f (2N)^b \tag{4.2}$$

where σ_a is the applied stress, σ_f is the fatigue strength coefficient and b is the Basquin's exponent.

The conventional S-N curve, straight line fit is,

$$s = k \log(N) + d \tag{4.3}$$

where s is the applied stress normalised withrespect to the ultimate static stress, k is the slope of the S-N curve and d is the s-intercept of the S-N curve.

There has been some success in applying the Basquin relation and the conventional S-N model to composite materials. The application of the Manson-Coffin model directly would however, be difficult due to the complexity of defining plastic strain for this type of material.

Models relating specifically to composite materials have been proposed by Hahn and Kim (1976) and Hwang and Han (1986).

Hahn and Kim proposed the power law,

$$K\sigma_a{}^d N = 1 \tag{4.4}$$

where σ_a is the applied stress, N is the number of cycles to failure and K and d are model parameters or 'material constants'. This model is similar to the Basquin's relation.

Hwang and Han proposed the inverse power law,

$$N = [B(1-s)]^{1/c} \tag{4.5}$$

where B and c are the model parameters. This equation was derived using the concept of fatigue modulus combined with a strain failure criterion.

Appendix A gives a comparison of the application of these models to various composite data.

4.1.2 Statistical Characterisation of Scatter

Variability of testing, material characteristics and specimen preparation results in a large degree of scatter in the basic fatigue data.

It has been found that scatter in fatigue life can be statistically explained using a log-normal distribution, as with regression analysis, or a Weibull distribution. Whitney (1981) put forward a procedure which allows the generation of an S-N curve using a distribution of this type. Firstly, a classical empirical power law was used to model the S-N curve of the material under investigation, the model having a set of unknown parameters. The fatigue life data, N, at each stress level was then fitted to a two-parameter Weibull distribution. The distribution was of the form,

$$R(N) = \exp\left[-\left(\frac{N}{N_0}\right)^{\alpha}\right] \tag{4.6}$$

where, R(N) is the reliability of N (probability of survival), N_0 is the Weibull location or scale parameter (Characteristic life) and α is the Weibull shape parameter. The maximum likelihood estimator (MLE) method combined with a data pooling scheme was used to determine the shape parameter, α, and characteristic life, N_0. Finally, a straight line was fit to the log S versus log N_0 data to determine the power law model parameters. Whitney went

on to estimate the effect of sample size on the Weibull parameters. He found that the values of N_0 where not radically effected by sample size, but the shape parameter α was very sensitive. From his comparisons of sample size it would seem that sample numbers of 20 per stress level are desirable for reasonable results. This approach enables a family of S-N curves to be found each corresponding to a particular level of reliability. These are known as P-S-N (probability-stress-life) curves.

Sendeckyj (1981), proposed a method again using the Weibull distribution. As with Whitney's method an assumed fatigue model was used to describe the S-N curve. An assumption of strength life equal rank was made which states that in a group of experimental specimens the strongest specimen will have the longest fatigue life. This was used to allow the transformation of the fatigue data into equivalent static strength data. A Weibull distribution was then fit to this data and the MLE method was used to estimate the shape and location parameters. These parameters then allowed the unknown parameters in the fatigue model to be obtained. As the Weibull distribution was fit to all the data at once, less samples were required per stress level than for Whitney's method. However, only one S-N curve is produced using Sendeckyj's method.

Barnard *et al.* (1988) also assumed strength life equal rank and showed that the fatigue scatter was a direct consequence of the variation in the static strengths of individual test specimens. They also showed that the scatter was a function of applied stress and an inverse function of the slope of the S-N curve. They propose that the static and fatigue distributions are two-parameter Wiebull distributions and that the correlation between the two distributions is the S-N curve. They go on to show how it is possible to generate P-S-N curves from only a limited amount of fatigue test data.

4.2 Stiffness Degradation

In chapter 3.0 it was shown that numerous defects within a composite laminate may contribute to the eventual failure of the material. This progressive build-up of damage causes a degradation in the mechanical response of the material which is manifested as a reduction of stiffness. Estimation of the change in stiffness therefore, can be a useful measure of damage development and residual life.

Highsmith and Reifsnider (1982) used an analytical shear lag model to estimate the degradation in stiffness for a specified crack density in glass/epoxy cross-ply laminates. The shear lag model involved introducing a transverse crack into the off-axis ply of a laminate. At the crack surface the stress in the ply is zero, but away from the crack the stress becomes non-zero; load was assumed to be transferred back into the cracked ply via shear transfer

across the resin-rich boundaries of the un-cracked plies. With a specified crack density in the off-axis ply of a laminate the shear lag model could be used to calculate the contribution to the overall load carried by that ply and hence its degraded stiffness could be determined. The overall laminate stiffness could then be modelled using the reduced stiffness value of the cracked ply and a laminate analysis. They found that for the [0,90] laminates agreement between theory and experiment was reasonably good, however the analysis was somewhat conservative in that it overestimated the stiffness change. In the case of the [0, 45] laminate agreement between theory and experiment was not good. This was believed to be due to other damage modes that were observed, which the analysis did not account for.

Talreja (1985) also proposed a modelling technique based on the association between stiffness degradation and crack density. He used a continuum damage mechanics approach to modify the stiffness matrix of a composite laminate to account for damage. His method allowed residual stiffness of a laminate to be calculated given the crack density and certain material constants. For orthotropic laminates these constants were determined from measured values of Youngs moduli, Poisson's ratio and shear moduli for the undamaged and damaged state at a known crack density. Talreja suggests that a cross-ply laminate is the most suitable configuration for determining these constants. Comparison of his theory with experimental observations for glass/epoxy and carbon/epoxy laminates demonstrated good accuracy.

Yang *et al.* (1990) approached the problem of stiffness degradation from a more practical view point. They put forward an approach that predicts the residual stiffness degradation of specimens in service from base-line laboratory data and in service measurements. The assumption was made that the residual stiffness degradation rate was a power function of the number of fatigue load cycles, such that

$$\frac{dE(n)}{dn} = -E(0)Qvn^{v-1} \tag{4.7}$$

where, n is the number of cycles, E(0) is the initial stiffness and Q and v are random variables that depend on applied stress level, loading frequency, stress ratio and the environment. From experimental investigation they found that Q and v were strongly correlated and v was a function of applied stress level. Integration of equation (4.7) and substitution of relationships for the random variables, based on stress independent parameters, led to,

$$E(n) = E(0)[1-(a_1+a_2a_3+a_2B\sigma)(n)^{a_3+B\sigma}] \tag{4.8}$$

where, a_1,a_2 and a_3 are the stress independent parameters, σ is the applied stress level, and B is a random variable. Experimental data indicated that the distribution of both E(0) and B could be represented reasonably well by a lognormal distribution. Residual stiffness

degradation for a specimen was then predicted using either a linear regression analysis or Bayesian approach. Agreement between experimental and theoretical results was found to be reasonable.

Hwang and Han (1986,1989) proposed the concept of fatigue modulus to predict fatigue life. This concept is shown schematically in figure 4.1. Elastic modulus at the nth cycle is obtained from a line nm. Fatigue modulus, F, at the nth cycle is obtained from the slope of the line on'. Therefore

$$F(n) = \frac{\sigma_a}{\varepsilon(n)} \tag{4.9}$$

where σ_a is the applied stress and $\varepsilon(n)$ is the resultant strain at the nth loading cycle. They suggest that the fatigue modulus and conventional secant modulus will differ considerably for matrix dominated composites, such as CSM laminates, but for unidirectional composites, differences will be small.

Hwang and Han assumed that the fatigue modulus degradation rate, dF/dn, was a power function of the number of fatigue load cycles, such that

$$\frac{dF}{dn} = -Acn^{c-1} \tag{4.10}$$

where, A and c are constants. This was integrated and a strain failure criterion was adopted, such that final failure was assumed to occur when the fatigue resultant strain reached the static ultimate strain. This resulted in the fatigue life equation, equation (4.5) given in section 4.1.1. The power function was further generalised to create seven different fatigue life equations.

Yang *et al.* (1992) combined the residual stiffness degradation model of Yang *et al.* (1990) and the fatigue modulus concept to produce a fatigue modulus degradation model suited to matrix dominated composites. The model was therefore,

$$F(n) = F(0)[1-(a_1+a_2a_3+a_2B\sigma)n^{a_3+B\sigma}] \tag{4.11}$$

where F(0) is the initial fatigue modulus at n = 0. They go on to suggest that for matrix dominated composites the stress-strain relation will tend to be nonlinear, thus the initial fatigue modulus will be a function of the applied stress and static secant modulus. The stress-strain relation is assumed to be modelled by,

$$\sigma = \beta(1-e^{-re}) \tag{4.12}$$

where β and r are model parameters. This then leads to an expression for initial fatigue modulus, such that

$$F(0) = \frac{\sigma_a}{\beta \ln\left(\frac{\beta}{\beta-\sigma_a}\right)} E(0) \tag{4.13}$$

The residual fatigue modulus degradation for a specimen was then predicted using either a linear regression analysis or Bayesian approach. Agreement between experimental and theoretical results was found to be reasonable. This theory is taken further by Lee *et al.* (1993), and a fatigue life prediction equation is developed using a fatigue modulus failure criterion.

4.3 Strength Degradation

The build-up of damage within a composite laminate not only changes stiffness but also changes the strength of the laminate. Knowledge of the strength of a structure in service is very important as it can dictate the frequency of inspections and component maintenance or replacement. Prediction of the change in strength of a composite subjected to fatigue has therefore been investigated extensively.

One of the earliest studies of strength degradation in composite materials was by Halpin *et al.* (1973). They proposed a degradation equation based on the crack propagation of homogeneous materials and introduced the 'Wearout' type residual strength degradation model. Hahn and Kim (1975) followed on from this work and introduced the concept of rate of change of residual strength, with no reference to any crack growth. They used a rate-type equation which assumed that residual strength decreases monotonically with increasing fatigue life, so that,

$$\frac{d\sigma_r}{dn} = -A\sigma_r^{-m} \tag{4.14}$$

where σ_r is residual strength, A is a parameter which is a function of applied stress and m is a constant. This equation was integrated and a residual strength failure criterion was introduced. This stated that fatigue failure occurs when the residual strength reduces to the applied stress. From this a relation was developed between the static strength, σ_s, and the fatigue life, N, such that,

$$N = (\sigma_s^{m+1} - \sigma_a^{m+1})/(m+1)D \tag{4.15}$$

where D is a parameter which is a function of applied stress, σ_a. This relation implied that the strength life equal rank assumption was valid. Equation (4.15) was then used to develop a fatigue life distribution based upon a truncated static strength distribution.

Yang and Liu (1976) used a similar approach to Hahn and Kim (1975) to develop a residual strength degradation model for cyclic fatigue. They assumed the static strength distribution followed a two parameter Weibull distribution and then developed the fatigue life distribution. With this distribution and a S-N curve relation (equation (4.4)) they established an equation for the stress dependent function, equivalent to Hahn and Kim's parameter D. This then led to the residual strength degradation model,

$$\sigma_r^{\,c} = \sigma_s^{\,c} - \beta^c K \sigma_a^{\,d} n \tag{4.16}$$

where K, d and c are constants and β is the characteristic ultimate strength derived from the static strength distribution. Constants K and d are derived from the S-N relation and constant c is equivalent to m+1 in Hahn and Kim's model. Application of the residual strength degradation model to a limited number of carbon/epoxy cross-ply laminates gave reasonable results.

Yang (1978) expanded the theory of Yang and Liu (1976) to account for stress ratio. In this case the model parameter equivalent to Hahn and Kim's parameter D, was assumed to be a function of applied stress and stress ratio. The equation defining this parameter was derived, which then led to a residual strength degradation model. This model was similar to equation (16) except the parameters K and d were implicit functions of stress ratio.

Chou and Croman (1978) introduced the 'Sudden-Death' model as a limiting case of residual strength degradation. The model was based on the assumption that the strength of the specimen does not change with each fatigue load cycle. Only when the cycles are close to the fatigue life will the strength then drop drastically in a short number of cycles. As with Wearout models an assumption was made of strength life equal rank. The sudden-death model was then established by replacing the residual strength degradation model suggested by Yang and Liu (1975) with,

$$\sigma_r = \sigma_s \tag{4.17}$$

They suggested that this model may be useful for describing the behaviour of unidirectional composites where the decrease in residual strength is less than for composites of general lay-

up.

Chou and Croman (1978) went on to identify a number of limitations of the degradation model of Hahn and Kim and Yang and Liu. They suggested it was overly restrictive and introduced a degradation model with an open parameter which could accomodate different residual strength distributions. Initially they assumed the static strength and fatigue life distributions followed the two parameter Weibull distribution. A degradation model was then introduced of the form,

$$\left(\frac{\sigma_r}{\beta}\right)^{\alpha} = \left(\frac{\sigma_s}{\beta}\right)^{\alpha} - \left(\frac{N}{N_0}\right)^{\alpha_1} \left(\frac{n}{N}\right)^{i\alpha_1} \qquad (4.18)$$

where α and α_1 are the static strength and fatigue life shape parameters, respectively and β and N_0 are the static strength and fatigue life scale parameters, respectively. The parameter i allows the model to be fit to various experimental residual strength results. A value of i $= \infty$ was shown to produce the sudden-death model. They point out that the model is unable to accommodate an increase in residual strength, a behaviour which has been observed in a few composite materials.

4.4 Energy Approaches

The application of a load to a material produces strains. The effect of these strains is to increase the energy level of the material itself. Strain energy, U, is defined as the energy absorbed by the material during the loading process. The work done, W, on the material by the applied load is defined by the area under the load-deflection curve. According to the law of energy conservation the strain energy will be equivalent to the work done.

Removal of the applied load will cause the material to either partially or fully return to its original shape. Thus, during unloading, some or all of the strain energy of the structure may be recovered in the form of work. In an ideal material below the elastic limit all of the stored strain energy will be recovered as work done in resuming the structure to its original shape. In a real material some of the strain energy will be dissipated in driving damage processes and as heat. This dissipated energy will create a hysteresis loop in the load deflection curve.

Due to its non-homogeneous nature, damage in fibre reinforced composite materials is characterised by complex damage zones involving cracks in many directions formed by matrix micro-cracking, fibre fracture, fibre/matrix debonding and fibre pull-out (see chapter 3.0). Other damage may include localized yielding and viscoelastic behaviour (creep). Each of these damage processes will require energy and this must be supplied through the work

done by the external forces. Beaumont (1989) noted that the failure mechanism which contributes most to the total work to fracture the composite will depend on the material properties of the matrix and fibres.

Wu (1974) studied the global energy balance of a composite material under load. He suggested that for composite materials the global energy balance should account for the energy dissipation due to all the various damage processes. He separated the incremental strain energy into reversible and irreversible parts. The two parts accounted for the incremental elastic strain energy and the plastic or viscoelastic strain energy. The irreversible strain energy was further partitioned into the dissipation local to the crack tip and global dissipation. The energy dissipated due to the crack propagation was also partitioned. As has been established in chapter 3.0, for a crack in a heterogeneous solid such as a composite, the crack growth can be entirely confined in the fibre or in the matrix. In these cases the propagation energy will be equivalent to the cohesive energy of the fibre or the cohesive energy of the matrix. For the case where the crack growth is in the interface between the fibre and matrix, the propagation energy will be equivalent to the adhesive energy between the fibre and matrix. In general, the energy required to propagate the crack can consist of one or more of these quantities. The global energy balance due to the incremental growth of one crack from length A to A+dA was therefore expressed as,

$$dW - d\bar{U} = d\tilde{U}_c + d\tilde{U}_g + (d\gamma^f + d\gamma^m + d\gamma^{fm}) \qquad (4.19)$$

where U_c is the dissipation local to the crack tip, U_g is the global dissipation, γ_c^f and γ_c^m are the cohesive energies of the fibre and the matrix, respectively and γ_a^{fm} is the adhesive energy between the fibre and matrix. The bar denotes reversibility and the tilde denotes irreversibility. The total energy dissipated by all the damage was then the summation of all the incremental dissipation energies.

Wu pointed out that the LHS (left-hand-side) of the global energy balance can be determined simply by geometric interpretation of the load displacement diagram, specifically from the area bounded by the hysteresis loop. The determination of the terms on the RHS (right-hand-side) however, would be rather more complex. A possibility suggested by Wu (1974) and Beaumont (1989) was to solve for the RHS by performing independent experiments, where there is a systematic variation of fibre volume, adhesion strength and laminate geometry. If the sensitivity to fracture of these variables was identified then the RHS could conceivably be solved as a system of simultaneous equations.

In the study of metal fatigue hysteresis energy has been used extensively to characterise fatigue behaviour and predict fatigue life, Feltner and Morrow (1961), Halford (1966), Chang *et al.* (1967), Stowell (1965). The assumption is made that the hysteresis energy per cycle,

Δw, is constant for the majority of the fatigue life and that the hysteresis energy accumulates until it reaches a critical value W_f at which point fatigue failure occurs. The value of Δw can be measured directly but it is more convenient to estimate this energy by calculation. Halford (1966) showed that the area bounded by a hysteresis loop could be estimated from,

$$\Delta w = \left(\frac{1-n'}{1+n'}\right) \Delta\sigma_a \, \Delta\varepsilon_p \tag{4.20}$$

where $\Delta\sigma_a$ and $\Delta\varepsilon_p$ are defined in figure 4.2 and n' is a stress dependent parameter obtained from a plot of log $\Delta\sigma_a$ versus log $\Delta\varepsilon_p$.

Originally it was believed that the amount of total dissipated energy to failure was a constant, but later it was recognised that W_f increases as the load amplitude decreases. This relation was found to be linear in the log σ_a-log W_f plane, Bily (1993).

Treshenko and Khamaza (in Bily (1993)) proposed that Δw and W_f be evaluated from,

$$\frac{\sigma_{uts}}{\sigma_a} = \left(\frac{W_f}{W_{fs}}\right)^k \tag{4.21}$$

and,

$$\Delta w = 2\, W_{fs} \left(\frac{\sigma_a}{\sigma_{uts}}\right)^{\alpha} \tag{4.22}$$

where W_{fs} is the energy dissipated during static loading, k is a parameter characterising the increase in total dissipated energy with decreasing stress amplitude σ_a and α is a parameter characterising the intensity of increasing Δw versus the stress amplitude σ_a. They found that the parameter k could be considered a constant for a given material and that it was closely related to material plasticity. The parameter α however, was generally found to be a linear function of applied stress level.

Opp *et al.* (1969) proposed a combined energy model to estimate the hysterisis energy per cycle for a polymer. They proposed the hysteresis energy was in two parts such that,

$$\Delta w = \Delta w_M + \Delta w_T \tag{4.23}$$

where Δw_M is the mechanical hysteresis energy per cycle and Δw_T is the thermal hysteresis energy per cycle. They assumed the total mechanical hysteresis energy to failure was equivalent to the area under the stress strain curve, and derived the thermal hysteresis energy

by solving the thermodynamic energy balance equation for a rectangular cross-section specimen under uniaxial strain. The expression for hysteresis energy per cycle was then given as,

$$\Delta w = \frac{W_{fs}}{2N} + \frac{\Delta w_l}{1-e^{-\gamma N}} \tag{4.24}$$

where

$$\gamma = \frac{4}{\rho C a}\sqrt{\frac{2K\ \Delta w_l}{T_g}} \tag{4.25}$$

Δw_l is the limiting energy below which the temperature will never reach the glass transition temperature, Tg, ρ is the density, C is the specific heat and K is the thermal conductivity of the polymer and a is the width of the specimen. The coefficient Δw_l was obtained by plotting total hysteresis energy and thermal energy against strain. The intersection of the two lines gave the limiting energy. The total hysteresis energy was calculated by using the stress-strain curve as the loading curve and the elastic modulus to give the unloading curve. The thermal energy was assumed to be given by elementary viscoelasticity as,

$$\Delta w_T = 2\pi E'' \varepsilon^2 \tag{4.26}$$

where E'' is the loss modulus.

Ellyin and El-Kadi (1990) studied composite laminae using an approach based on the assumption that the damage in a lamina due to cyclic loading was proportional to the work done by the applied load. Where the work done was defined as,

$$\Delta W = \frac{1}{2}(\sigma_{max}\varepsilon_{max} - \sigma_{min}\varepsilon_{min}) \tag{4.27}$$

They suggested that the relation between work done and number of cycles to failure was a power law such that,

$$\frac{\Delta W}{k} = N^{\alpha} \tag{4.28}$$

where for unidirectional lamina, α is a material constant and k is a parameter dependent on fibre orientation angle. The application of this model to three different types of unidirectional composite gave good results and showed that the parameter k could be represented by the equation,

$$\log k = \log k_0 + b\theta^{\beta} \tag{4.29}$$

where θ is fibre orientation angle and b and β are constants. El-Kadi and Ellyin (1994) took this method further and studied the effect of variation in stress ratio on the model parameters k and α. They found that the values of k, for the same fibre orientation angle but different values of stress ratio, were about the same as the work done to failure under static tensile load, W_s. To take account of negative stress ratios they introduced a compressive work done term into their method. Their model thus became,

$$\left(\frac{\Delta W}{W_s(\theta)}\right)_T + \left(\frac{\Delta W}{W_s(\theta)}\right)_c = N^{\alpha} \tag{4.30}$$

where the subscripts T and C indicate the tensile and compressive parts of the work done, respectively. Kadi and Ellyin note that their model would not apply to laminates in its present form.

4.5 Cumulative Damage

Cumulative damage theory is concerned with the lifetime prediction of materials through an assessment of damage accumulation. The complicated damage regions produced in composites means that defining fatigue damage is not a simple problem. There are a number of variables that could be used for its definition such as crack density, number of debonded fibres, delamination, stiffness degradation, strength degradation or energy dissipation.

The general cumulative damage approaches involve fatigue damage due to cyclic loading being represented by a damage function, D, of the form,

$$D = F(n,\sigma_a,f,T,M,...) \tag{4.31}$$

where n is number of fatigue cycles, σ_a is applied stress level, f is frequency, T is temperature and M is moisture content.

It is generally assumed that frequency and environmental conditions are constant. This reduces the damage function to,

With a second assumption that there is no initial damage (D=0 when n=0), the damage

$$D = F(n,\sigma) \tag{4.32}$$

function for a sequence loading should satisfy the following property when failure occurs,

$$D = \sum_{i=1}^{m} \Delta D_i = 1 \tag{4.33}$$

where m is the number of load sequences until final failure, D_i is the amount of damage accumulation during fatigue at stress level s_i.

The simplest assumption for the functional form of D is,

$$D = F(n/N) \tag{4.34}$$

The dependency on applied stress is implicit in the equation, with N being defined by the S-N curve. Taking this assumed function results in the well known Palmgren-Miner's linear damage rule, Miner (1945),

$$D = \sum_{i=1}^{m} n_i/N_i \tag{4.35}$$

In many cases a non-linear damage model is more appropriate. A non-linear form of the Palmgren-Miner rule is generally referred to as the modified Palmgren-Miner rule. The damage function in this case is defined as,

$$D = \left(\frac{n}{N}\right)^c \tag{4.36}$$

where c is a constant.

When Owen and Howe (1972) investigated damage accumulation in glass CSM/polyester laminates, they found that curves of resin crack damage versus cycle ratio and residual strength versus cycle ratio were similar and that they could be represented by the quadratic equation,

$$D = A + B\sum_{i=1}^{m}\left(\frac{n}{N}\right) + C\sum_{i=1}^{m}\left(\frac{n}{N}\right)^2 \tag{4.37}$$

A, B and C are constants, where A is zero and C is negative.

Hashin (1985) proposed that since fatigue damage varies more nearly logarithmically with the number of cycles, a better assumption for the damage function would be,

$$D = F[\log(n/N_e)/\log(N/N_e)] \tag{4.38}$$

For two-stage loading this assumption leads to the Hashin-Rotem theory,

$$\left(\frac{n_1}{N_1}\right)^{\log(N_2/N_e)/\log(N_1/N_e)} + \frac{n_2}{N_2} = 1 \tag{4.39}$$

where N_e is a parameter. This can be associated with damage curves linear in (s,log n) or (log s,log n) that converge into the fatigue limit defined by e and number of cycles Ne. In the case where $N_e = 1$, the damage curves converge into the ultimate static strength at log n = 0.

Hashin also proposed a damage function based on residual strength. The function is of the form,

$$D = F(s,s_r) \tag{4.40a}$$

$$s_r = \sigma_r/\sigma_0 \qquad s = \sigma/\sigma_0 \tag{4.40b}$$

He used an approach based on the residual strength degradation model proposed by Hahn and Kim (1975) and Yang and Liu (1977) to develop a series of equations for two-stage loading, which predict the residual life, n_{2r}, of composites. If the composite is firstly loaded for n_1 cycles at stress level s_1 then the residual life is defined as the number of cycles required to fail the composite at the second applied stress level, s_2. The equations are as follows,

$$s_{r1}^c = 1 - (1-s_1^c)\frac{n_1}{N_1} \tag{4.41a}$$

$$s_{r2} = 1 - (1-s_{r1})\frac{1-s_2}{1-s_1} \tag{4.41b}$$

$$n_{12} = N_2 \frac{1-s_{r2}^c}{1-s_2^c} \tag{4.41c}$$

$$n_{2r} = N_2 - n_{12} \tag{4.41d}$$

where c is a constant defining the rate of residual strength degradation (see Section 4.3).

Hwang and Han (1986) proposed three different damage models based on the fatigue modulus concept and material strain. The application of the models to a woven glass/epoxy composite suggested a model of the form,

$$D = \left[\frac{s}{(1-s)}\right]\left[\frac{n^c}{(B-n^c)}\right] \tag{4.42}$$

where the parameters B and c were calculated by fitting the S-N data to the S-N characterisation model given in equation (4.5) Section 4.1.1. Hwang and Han (1989) proposed four further damage functions also based on fatigue modulus and material strain. They introduced seven different S-N curve characterisation models which were then applied to the damage functions, to produce twenty-three cumulative damage models. They have applied all these models to two-stage loading data for the low cycle fatigue of a short glass and carbon fibre-reinforced thermoplastic. Their results pointed towards a cumulative damage model of the form,

$$D = \frac{s}{1-s}\left[\left(\frac{1}{1-\frac{1}{B}n^c}\right)^{1/d} - 1\right] \tag{4.43}$$

where the parameters B,c and d were calculated using a non-linear least squares method fitting the S-N data to the S-N characterisation model,

For two-stage loading the residual life, n_{2r}, is calculated by finding n_{12}, the cycle at the stress

$$N = [B(1-s^{d})]^{1/c} \tag{4.44}$$

level s_2, which has equivalent damage under the stress s_1 and cycle n_1. This is achieved by equating,

$$D_1 = D_{12} \tag{4.45}$$

The residual life is then predicted as follows,

$$n_{2r} = N_2 - n_{12} \tag{4.46}$$

Plumtree and Shen (1991) identified that the damage accumulation in some composites was in two parts. Initially a decelerating damage accumulation stage followed by a second stage of accelerating damage accumulation. They subsequently proposed the two part damage function,

$$D = D^{(1)} + D^{(2)} \tag{4.47}$$

where D(1) is the decelerating part and D(2) is the accelerating part. For the decelerating part they suggested a model based on a two parameter Weibull distribution and for the accelerating part they suggested a model based on a crack growth rate power law. The damage model thus developed was,

$$D = D_c\left[1-\exp\left[-\left(\frac{n}{\alpha N}\right)^{\beta}\right]\right] + D_a\left[1-\left(1-\frac{n}{N}\right)^{\gamma}\right] \tag{4.48}$$

where α, β and γ are parameters that can be obtained by a least squares fit on experimental damage accumulation data. The coefficient D_c accounts for the damage at the characteristic damage state (CDS) (see Chapter 3). The coefficient D_a accounts for prior damage and allows control of the critical value of D at fracture.

Appendix A gives a comparison of the application of some of these cumulative damage models to various composite data.

4.6 Discussion

As has been established, there are many theoretical models concerning the fatigue behaviour

of materials and structures. The models given in this chapter are by no means exhaustive but are intended to give a broad spectrum of models which may or may not be applicable to tee joints.

The applicability of any model to the tee joint problem can only be assessed when the true characteristics of tee joint fatigue are known. In all cases the theoretical models assume certain fatigue characteristics; for example, in the case of the characterisation of the S-N curve, the choice of model is reliant on the curve shape conforming to either a linear or power law form. Any other shape of curve will require an additional curve fit model is used. In the case of residual strength modelling, if contemporary residual strength models are to be used, then the residual strength must decrease monotonically with increasing number of fatigue cycles. In the case of the cumulative damage approaches it must be known whether the damage accumulates linearly or non-linearly through the life of the joints and whether it is stress dependent or stress independent.

A further important point in deciding what type of modelling is to be used for tee joints, concerns what is required with regard predictions. As the joints are derived from a marine structure and no significant work has been directed towards them on the fatigue side, up to now, prediction of fatigue life under constant and varying fatigue loads is the primary requirement. Models predicting stiffness and strength distributions would therefore, not be applicable at this stage. The most relevant modelling technique would therefore be cumulative damage, which allows fatigue life predictions to be made for spectrum loading cases. This approach could possibly be combined with energy methods, which are applicable to any material and structure, to produce a tee joint fatigue life prediction model.

The most promising energy method seems to be that proposed by Treshenko and Khamaza (in Bily (1993)), although this requires that the relation between total energy dissipated to failure and applied load is a power law. The tee joint may not exhibit this relation.

In terms of contemporary cumulative damage models the most promising models for laminates, identified in appendix A, are the Hashin-Rotem model (equation 4.38) due to its prediction accuracy or the Palmgren-Miner rule (equation 4.34) due to its ease of use. As has been stated previously, these models may not give good predictions of fatigue life for tee joints unless the damage accumulation characteristics of the joints is similar to that of laminates.

5.0 Tee Joint Experimental Characterisation - Static

5.1 Experimental Design

5.1.1 Test Programme

The aim of the static test programme was to establish the ultimate strengths of the different tee joint types to allow the load levels to be chosen for the fatigue test programme. In composite materials the ultimate strength can vary depending on the strain or load rate applied to the material: therefore the ASTM standards D 3479 (1982) recommend that the ultimate strength be established by static testing at a rate approximating the load rate that is to be used in the fatigue test. The static loading of the joints, in the work of Hawkins (1995), was undertaken at very low load rates. This was done in order to identify the various failure mechanisms that occurred. In this investigation static tests were carried out at a variety of load rates in order to identify any rate sensitivity. Measurements of load and deflection were made for each specimen tested.

During all the tests a visual examination was made of each specimen to establish their failure modes and characteristics when subjected to each particular loading.

In addition to the basic static tests, experiments were carried out on the B type joint involving photoelastic and thermoelastic analysis. The main aim of this work was to identify the load paths through the joint and create experimental data to validate theoretical predictions of internal stress and strain distributions. Appendix C gives a brief outline of photoelastic and thermoelastic theory and measurement techniques. The thermoelastic analysis was performed at a cyclic load level of 1.7 ± 0.7 kN and a frequency of 8Hz. Both sides of the joint were scanned. To check the linearity of the thermoelastic data, point readings were taken from six points on the tee joint and compared with results at a second load level of 1.3 ± 0.41 kN. To produce comparable results to that of the thermoelastic analysis, the photoelastic analysis measurements were taken at a constant load of 1.4 kN, which is equivalent to the load range used for the thermoelastic analysis. In addition a thermoelastic analysis was performed on the tee joint with the photoelastic coating bonded in place.

To produce quantitative data from the thermoelastic analysis required that two constants A' and α be experimentally determined. Where A' is a calibration constant and α is the ratio of the coefficients of thermal expansion of the principal material directions. A series of calibration experiments were therefore performed on sections of the tee joint overlaminate material, these are detailed in Appendix C.

Further strain measurements were made on one of the B type joints using strain gauges. The aim of this part of the programme was again to validate theoretical predictions of overlaminate strains.

5.1.2 Test Apparatus

In the Course of Previous work on the static behaviour of tee joints, it was identified that simulation of the combined moments and forces experienced by the tee joints in-service, could be achieved by fully clamping the flange close to the fillet on both sides of the web and applying a 'pull off' at 45° to the top of the web (see Chapter 2.0).

All the tee joint tests were performed in the heavy structures test facility, FORTReSS. Appendix B gives an outline of the FORTReSS test facility. Figure 5.1a illustrates the test rig set-up for the tee joint test programme. The rig consisted of a steel beam, held in FORTReSS at an angle of 45° , to which the tee joint specimens were clamped. The spacing of the 50mm clamps was 240mm centre to centre, these dimensions were based on the work of Hawkins (1995). A hydraulic ram was then positioned on the FORTReSS structure so as to apply a pull off load in the horizontal plane. The ram was connected to the tee joint specimen using a specially designed connection rod and an eye plate bolted to the web of the specimen. The eye plate was positioned so as to apply a load at 230mm above the flange inner surface. Joint deflection was measured by a linear potentiometer attached to the joint using a screw which was positioned on the side of the web at the same height as the loading eye plate. The applied load was measured using a load cell located at the very end of each ram rod. The calibration methods used for these transducers are explained in Appendix B.

Four Measurement Group UK Ltd strain gauges, type CEA-06-375UW-350 were bonded to the overlaminate using M-Bond AE-10 epoxy adhesive. The gauges had a resistance of 350 Ω and a gauge factor of 2.100. All the gauges were positioned along the centreline of the joint, two gauges on each overlaminate located at the top and at the root of the fillet radius. The gauges were calibrated using a shunt resistance technique described in detail in Appendix B.

The thermoelastic analysis was performed using a SPATE (Stress Pattern Analysis by Thermal Emissions) 9000 system with the detector tilted at an angle of 10° and set at a working distance of 380mm from the test specimen. The approximate SPATE scan area is shown in figure 5.1a. Prior to the analysis, the tee joint specimen was coated with two passes of RS matt black paint to increase the emissivity of the surface to be scanned.

The photoelastic analysis was performed with a Measurements Group UK Ltd Reflection Polariscope, model 031 and the fractional fringe orders were measured using a Manual Null-

Balance Compensator, model 232. The photoelastic coating utilised was type PS-1D with a thickness of 0.5mm and a fringe value of 3790 μstrain per fringe. The coating was bonded to both sides of the tee joint specimen using a reflective epoxy adhesive type PC-1.

Three different test control programs were employed to produce the correct loading conditions for the measurement of the load-deflection and strain and the implementation of the photoelastic and thermoelastic analyses.

For the load-deflection and strain gauge measurements a general static test was performed. A set voltage was sent to the servo-hydraulic control valve. This opened the valve slightly and allowed the hydraulic pressure to increase and hence a force to be applied to the specimen, via the ram. The load rate was controlled by varying the set voltage and adjusting the hydraulic pump compensator.

Thermoelastic analysis required that the specimen be cycled over a chosen load range at a frequency of 8Hz. To produce a sinusoidally varying load required closed loop control of the FORTReSS hydraulic system. This method of control involves the comparison of a required input signal with a system output, the difference or error signal produced is then used as a system input. In the case of the thermoelastic analysis the input signal was the required sinusoidal pattern and the system output was the signal from the load cell. The PC and software performed the task of signal comparison and supplied the system input to the servo-hydraulic control valves.

The basic layout of the control program was as follows: An input file produced a sine wave varying from -1 to 1. This was immediately scaled and offset to give the load range and magnitude (in kN) required. At this point the load cell signal was read and calibrated also into kN. The difference between the required load and actual load was then found. This error value, in kN, was then changed into an appropriate voltage signal to control the servo valve. To achieve this the error value was divided by a scaling factor and then offset by a voltage equivalent to zero flow through the servo valve. The magnitudes of the scaling factor and offset voltage were found by an initial calibration of the control loop (see Appendix B).

Photoelastic analysis could be performed under the general static test conditions if only full field qualitative data was required. As quantitative data were required at certain applied loads however, the control program was modified to allow the specimen to be held at a chosen load while measurements were taken. To achieve this loading pattern a closed loop control program was utilised. In this case the input signal was a load ramp up to a chosen load magnitude at which point it became constant. This was achieved in the control program with an input file which produced a ramp varying from 0 to 1 which then became constant

at 1. This was immediately scaled and offset to give the load magnitude (in kN) at which photoelastic measurements were to be made.

5.1.3 Test Specimen Construction

The tee joint test specimens comprised of a 560mm flange and 260mm web cut into 100mm wide sections. Connection was achieved with pure resin, injected between the plates on both sides of the web to form a fillet. The fillet was then overlaminated to form boundary angles. The joints were post cured for 16 hours at 40°C to simulate a full in service cure. Four types of joint were investigated. In each joint type the flange and web were constructed from 17 plies of woven roving (WR) set in Scott Bader Crystic 489 Polyester resin. The fillet in all four specimens was constructed of Crestomer 1152 Urethane Acrylate resin, with specimens designated B and K having a nominal 50mm fillet radius, the specimen designated N having a nominal 30mm fillet radius and the specimen designated F having a nominal 75mm fillet radius. The boundary angles of the specimen types B and N had 12 plies and there lay-up was 2x600g Chopped Strand Mat (CSM), 1x780g WR, 2xCSM, 1xWR, 2xCSM, 1xWR, 1xCSM, 2xWR, with Crestomer 1200 resin, which is a 50-50 mix of polyester and urethane acrylate resins. The boundary angles of the specimen types F and K had 2 plies and there lay-up was 2x780g WR again with Crestomer 1200 resin. Figure 5.1b shows the tee joint test specimen details.

5.2 Load-Deflection Characterisation

5.2.1 Load vs Deflection

The results of the static tests are presented in two forms. Firstly, figure 5.2 shows typical load deflection (P-δ) curves for each joint type at low load rates. There are two curves for the F type joint, the continuous curve is taken from the previous static work and the curve which does not continue up to failure, is taken from the present work and illustrates the agreement between the two sets of experimental data. Secondly, table 5.1 lists the results of the rate sensitivity tests, giving the load and deflection at failure for each applied load rate. The results show that for each joint type, there is a reduction in failure strength and deflection corresponding to an increase in the load rate.

The P-δ curves of the type B and N joints both display discontinuities and changes in stiffness which relate to the delamination of the overlaminate. In the case of the type B joint the delamination was at ply 6 and in the type N joint at ply 6 and ply 9. As was established in the previous work and can also be seen here, the strength and stiffness of the joints has been little affected by the delaminations.

The P-δ curves for the F type joint show its approximate constant stiffness up until failure. The curve of the K type joint however shows a knee at approximately 18% of its ultimate strength.

5.2.2 Load-Rate Effects

To emphasise the static load rate sensitivity of each joint type, the results of the tests were plotted in the form of energy absorbed versus load rate applied, see figure 5.3. The energy absorbed was calculated by measuring the area under each load deflection curve. As was established above, the F and K type joints are very sensitive to the load rate applied, this is especially so in the low load rate region. The drop in energy absorbed can be attributed to the reduction in ultimate strength of the joints and the increase in their stiffness, as indicated by the results in table 5.1. The N type joint on the other hand, has been seen to be fairly insensitive to load rate.

5.2.3 Damage and Failure

From visual examinations of each joint, failure mechanisms were observed. For all the static tests the mechanisms were the same as those observed in the previous static experimentation. Specimens B and N failed initially by delamination within the boundary angle corner on the side in tension (see Figure 5.4a and 5.4c). This delamination occurred initially within the ninth or sixth ply of the overlaminate. If ply 9 had delaminated first then the application of further load would lead to the delamination of ply 6 this could then be followed by an additional delamination at ply 3 and or final failure of the joint. Final failure occurred when the remaining boundary angle plies delaminated and the fillet failed. Specimens F and K both failed in a similar manner to each other. Failure was catastrophic and was characterised by delamination of the overlaminate on the face in tension and splitting of the fillet (see Figure 5.4b and 5.4d). These two mechanisms occurred too rapidly to distinguish their order.

5.3 Stress-Strain Characterisation

5.3.1 Load vs Strain

The load vs strain plots for the tee joint are shown in figure 5.5. The joint was loaded to approximately one third of its ultimate failure load (5 kN for a B type joint). Strain 1 and strain 3 relate to data from the strain gauges positioned on the compression side of the joint at the top of and the root of the radius, respectively. Strain 2 and strain 4 relate to data from the strain gauges positioned on the tension side of the joint at the top of and the root of the radius, respectively. The results indicate that a larger strain is experienced on the tension

side of the joint, with the largest strain occurring at the root of the radius. On the compression side however the strain gauges seem to indicate that the strain is effectively the same at the top and at the root of the joint radius. At 5 kN the strain on the compression side both at the top and at the root of the radius is -1495 μstrain, on the tension side at the top of the radius the strain is 1688 μstrain and at the root of the radius it is 2594 μstrain.

5.3.2 Thermoelastic Stress Analysis

Figures 5.6a and 5.6b give SPATE contour plots from both side faces of the tee joint; the slight distortion of the plots is due to the 10° tilt of the detector. The signal levels given in each plot have been calibrated using an A' value of 9.78×10^{-3} MPa/U, derived in Appendix C. It should be noted that the value of A' is valid for the boundary angle only. The signal levels from the fillet and the web are therefore, only qualitative indications of the stress distribution therein. The signal levels from both sides of the specimen show good agreement. The laminated construction of the boundary angles can be clearly seen, especially on the tension side of face 2 (figure 5.6b) where the individual woven roving lamina can be identified from the location of the maximum signal values. The transition between the boundary angle material and the fillet is well defined with the signal being at least three times greater in the boundary angle. An interesting feature is the small area of positive signals in the compressed section of the fillet on face 1 (figure 5.4a), this was found to be the location of a surface void.

Figures 5.7 and 5.8 show line plots through the SPATE data along the lines marked in figures 5.6a and 5.6b respectively. (The distances represented on the abscissa of figures 5.7 and 5.8 are measured from the tension side of the joint for lines 1 and 2 and from the outer edge of the joint for lines 3 and 4.). Peak signal values are sometimes seen at the edge of specimens, these can be attributed to the scan continuing off the edge of the specimen. Figures 5.7a and 5.8a show data along line 1 cut through the overlaminate and web material at the top of the joint radius. The average signal in both cases is seen to decrease from around 5MPa to -3MPa crossing from positive to negative between 22 and 25 mm. The change in material from the boundary angle to the web material is apparent in the central region of both plots. Figures 5.7b and 5.8b show data along line 2 cut through the overlaminate, fillet and web material close to the root of the joint radius. Figure 5.7b shows the average signal in the boundary angle in tension as being nominally constant at 6MPa. The boundary angle in compression is seen to have a signal that decreases from -2.5MPa to -4MPa. The "spike" that occurs at 50 mm may be caused by damage or a void in the material. Figure 5.8b shows the average signal in the boundary angle in tension decrease from 6.5MPa to 3MPa. In compression the signal is seen to be nominally constant at -3MPa. The transition from one material to another is easy to see in both plots, with the fillet material being quite distinct in the positive signal region between 15 and 20 mm.

Figures 5.7c, 5.7d, 5.8c and 5.8d show data along lines 3 and 4 cut through the overlaminate material perpendicular to the edge of the joint close to the root of the joint radius. Figures 5.7c and 5.8c show data from the compression side of the joint the average maximum signal being around -3MPa. Figures 5.7d and 5.8d show data from the tension side of the joint the average maximum signal being significantly greater than the compression side at around 10MPa. The transition between boundary angle and fillet material is quite distinct in each case.

Figure 5.9 shows data along line 2 on face 1 for the tee joint with a photoelastic coating bonded in place. For comparative purposes the coated joint data was calibrated using the same values used for the uncoated joint. The values shown are therefore only qualitative. These results can be directly compared with figure 5.7b, which shows the SPATE data along the same line without the coating. It can be seen that the form of figure 5.9 is practically identical to figure 5.7b, except that the data in figure 5.9 seems to be 'smoothed'. An example of this is the spike observed in figure 5.7b at around 50 mm which is considerably less pronounced in figure 5.9.

The linearity check on the SPATE data gave the average ratio of high load signal to low load signal to be 1.75. The average ratio of high load range to low load range was calculated from load cell measurements to be 1.68. The 4% difference in these values can easily be accounted for in experimental errors, with a possible 5% error in the load data and a possible 10 % error in the SPATE data at these load levels.

5.3.3 Photoelastic Strain Analysis

A full field picture of the strain distribution within the tee joint at a load of 5 kN, is shown in figure 5.10. This is a photograph of the fringe patterns produced by the photoelastic coating bonded on face 2. The fringes indicate contours of equal principal strain difference (or maximum shear strain). They suggest relatively high strains occur in the fillet material compared to the overlaminate material, with peak strains occurring at the interface between the overlaminate and fillet. The low sensitivity of the coating material means the strain distribution in the overlaminate is difficult to visualize. The distribution can however, be measured. Figure 5.11 shows a full field picture of the strain distribution at zero load. The small number of fringes indicate some initial strain is present within the joint before loading. This strain is induced by the test rig clamps acting on small amounts of distortion within the joint, which derive from manufacture.

Point measurements of strain were made at intervals along four lines approximately in the same position as the SPATE lines described in section 5.3.1. Measurements were made at full load (1.4 kN) and zero load. The difference between full load and zero load for each

line is shown in figure 5.12 presented in the same format as figure 5.7 and 5.8 (i.e. The distances represented on the abscissa of figure 5.12 are measured from the tension side of the joint for lines 1 and 2 and from the outer surface of the joint for lines 3 and 4).

Figure 5.12a shows the photoelastic measurements along line 1. There is a steady decrease in strain from 1200 μstrain through the overlaminate, on the tension side, becoming negative at 8 mm. The strain then rapidly increases becoming positive at 11 mm, and close to the interface with the fillet it is seen to peak. There is a slight drop in strain in the fillet and then between 15 mm and 30 mm the web is encountered where the strain remains constant. There is then a peak maximum strain of 2500 μstrain in the fillet on the compression side, which drops away across the interface of the fillet and overlaminate. The strain then decreases through the overlaminate until close to the outer surface where it begins to increase again, increasing to 1000 μstrain.

Figure 5.12b shows the photoelastic measurements along line 2. There is a rapid decrease in strain from 840 μstrain through the overlaminate, on the tension side, becoming negative at 4 mm. There is then a steady decrease in strain until at 10 mm the strain begins to increase again becoming positive at 11 mm, and close to the interface with the fillet it is seen to peak. The strain drops across the fillet and then between 23 mm and 38 mm the web is encountered where the strain increases linearly. There is then a peak maximum strain of 1540 μstrain in the fillet on the compression side, which drops away across the interface of the fillet and overlaminate. The strain then remains approximately constant through the overlaminate until close to the outer surface it begins to decrease again, decreasing to 200 μstrain.

Figure 5.12c shows the photoelastic measurements along line 3. With an initial strain of 200 μstrain, the strain through the overlaminate on the compression side steadily increases to approximately 400 μstrain at approximately 5mm. The strain then becomes fairly constant until close to the interface between fillet and overlaminate where there is maximum peak strain of 820 μstrain. The strain then drops steadily through the fillet.

Figure 5.12d shows the photoelastic measurements along line 4. With an initial strain of 1200 μstrain, the strain through the overlaminate on the tension side steadily decreases to 200 μstrain at approximately 6mm. The strain then steadily increases again up to 1900 μstrain at the interface between the overlaminate and fillet. It then remains fairly constant through the fillet.

5.4 Discussion

The P-δ data in table 5.1 can be used to assess the dependence of joint strength on geometric variations, namely fillet radius and overlaminate thickness. For a given number of plies in the overlaminate and hence a given overlaminate thickness, the static strengths are seen to increase with an increase in fillet radius. Conversely, for a given fillet radius the static strengths are seen to increase with an increase in the number of plies in the overlaminate. In addition to this the test results show that as the number of plies increases the overall joint stiffness also increases, but the overall energy absorption of the particular joint decreases. This decrease is also apparent with a reduction in fillet radius. These results are in agreement with those of Hawkins (1995), detailed in chapter 2.0.

As was established above, the F and K type joints are very sensitive to the load rate applied, this is especially so in the low load rate region. The drop in energy absorbed can be attributed to the reduction in ultimate strength of the joints and the increase in their stiffness, as indicated by the results in table 5.1. The N type joint on the other hand, has been seen to be fairly insensitive to load rate. It could be argued that the material in each joint most sensitive to load rate, is the fillet resin. The N joint is therefore insensitive to load rate because of the dominance of the thick overlaminate in its behaviour, whereas the F and K type joints are dominated to a greater extent by the fillet.

The measurement of strains on the joints using strain gauges was fraught with a number of difficulties. Bonding the gauges was not straight forward onto a woven roving undulating surface. Furthermore the tight radius of the B type joint meant that the gauges could not be guaranteed to have completely bonded into the root of the radius. Due to the irregular surface of the material it is advisable to use gauges with large gauge lengths, hence the strain measured is not a point strain. The large size of the gauges also meant only a few measurements could be taken, so a full picture of strain distribution would not be possible. These difficulties suggested full field techniques such as thermoelastic and photoelastic analyses should be more applicable to the joint problem.

The thermoelastic analysis using SPATE gave a good understanding of the load paths through the joint, even showing the high stress paths along the woven roving layers in the overlaminate material. A comparison between lines 1 and 2 (figures 5.7a and 5.8a and 5.7b and 5.8b respectively) gives some insight into the overall joint load paths. In line 1 the signal can be seen to decrease monotonically through the thickness of both boundary angles and web indicating all the material is carrying the applied load. In line 2 however, there is a step change in the signal levels at the interface of the boundary angles and the fillet with the signal being much greater in the boundary angles than the fillet or web. This indicates that at the root of the radius the majority of the load is being carried by the boundary angles.

A high degree of signal noise was apparent in all the SPATE data plots. The minimum resolvable temperature difference of the SPATE equipment is 1 mK which is equivalent to a $\sigma_p + \alpha \sigma_t$ value of 0.9MPa. As the maximum signal measured was around 10MPa (see figures 5.7 and 5.8) the noise will at best account for 10% of the signal, with increasingly higher noise contributions as the signal decreases. This high noise contribution is due to the low load level used for the analysis. This was chosen to reduce the risk of joint failure through fatigue from the 8Hz vibration applied for the analysis. The analysis often had a duration of the order of 2 hours.

The photoelastic theory shows good qualitative agreement with the results of the strain gauges. The photoelastic measurements show that at the surface of the joint overlaminate on the compression side that the strain is similar at the top and root of the radius. For the overlaminate on the tension side the measurements show a substantial increase in strain at the root of the radius compared to the top of the radius.

6.0 Tee Joint Experimental Characterisation - Fatigue

6.1 Experimental Design

6.1.1 Test Programme

Constant fatigue load versus life data for each joint type were produced using load control fatigue tests performed at various constant maximum applied loads. These loads were; 90%, 70%, 50% and 30% of the ultimate static strength (USS) for each joint type. The cyclic loading pattern chosen for the fatigue experiments was a sinusoidal wave with a stress ratio of R=0 and a frequency of 1 Hz (60 cycles/min). At this frequency it was expected that heating within the joints would be negligible and that testing would be relatively quick. A one off measurement was made of the frequency using a spectral analyser and this is detailed in appendix B. Throughout each experiment maximum and minimum values of load and deflection were recorded for each fatigue cycle. In addition, complete load deflection data for selected individual cycles were recorded at intervals.

To gain some understanding of the behaviour of the joints when subjected to varying maximum applied fatigue loads, two-stage step loadings were performed. These involved first applying a chosen constant maximum load for a set number of cycles, then changing the load and continuing testing until failure occurred. These tests could take two formats, either an initial high load followed by a low load to failure (High-Low test) or an initial low load followed by a high load to failure (Low-High test). For each specimen type, both load formats were used and the loads applied were 70% and 50% of the USS. To allow correlation of results the wave form, stress ratio and frequency were the same as for the constant load tests. The measurements recorded were also the same as for the constant load fatigue tests.

A small number of residual strength tests were undertaken on the F and N specimen types. These involved applying a constant load for a set number of cycles and then immediately static testing the specimens to establish there ultimate strength. The static loads were performed at a load rate equivalent to the load rate of fatigue. The fatigue loads were 70%, 60% and 50% of the USS of the 'virgin' joints, and the wave form, stress ratio and frequency were again the same as for the other fatigue tests. For each specimen tested, maximum and minimum values of load and deflection were recorded during fatigue loading and complete load deflection data during static loading.

During all the tests a visual examination was made of each specimen to establish their failure modes and characteristics when subjected to each particular loading.

6.1.2 Test Apparatus

A set of three identical test rigs was designed for the purpose of applying the required boundary conditions and load configuration, these were located within FORTReSS. The provision of three test rigs allowed two tests to be performed in parallel and therefore to produce data quickly. The two rigs acted independently, but used a common hydraulic pressure supply. The third rig was used to rotate the use of each rig for maintenance.

The test rigs were identical to the rig used for the static experimentation detailed in chapter 5. The life of each T-joint was measured by counting each fatigue cycle up to failure.

As with the thermoelastic analysis in chapter 5, closed loop control was used to produce the sinusoidally varying load. In the case of the fatigue experiments the input signal was the required sinusoidal wave and the system output was the signal from the load cell. The PC and software performed the task of signal comparison and supplied the system input via the servo-hydraulic control valves.

The programs used for control and measurement were designated TEST1 and TEST2. Program TEST1 contained control information for only one test rig and TEST2 contained the information for two test rigs. This gave the flexibility needed for maintenance while still allowing at least one experiment to be performed.

The basic layout of the control program for each rig was as follows: An input file produced a sine wave varying from -1 to 1. This was immediately scaled and offset to give the loading format and magnitude (in kN) required. at this point the load cell signal was read and calibrated also into kN. The difference between the required load and actual load was then found. This error value, in kN, was then changed into an appropriate voltage signal to control the servo valve. To achieve this the error value was divided by a scaling factor and then offset by a voltage equivalent to zero flow through the servo valve. The magnitudes of the scaling factor and offset voltage were found by an initial calibration of the control loop (see appendix B).

All the measurement data were stored directly on to the PC hard disc. Two forms of data file were created for each control program. The first recorded continuously throughout an experiment. The data stored took the form of maximum and minimum values of load and displacement for each fatigue cycle. It was identified that if a power failure was to occur during the storage of data then all the data for an experiment could be lost. Hence, the file was part stored every two hours and a new file was named to store the data in. In the case of a power failure it was therefore only possible to loose the last two hours of data. The second file was created to record complete load deflection data for selected individual cycles

at intervals throughout an experiment.

For safety reasons the data stored in the first file was also monitored by two alarm systems within the control program. The two alarms were designated the 'outer limits alarm' and the 'inner limits alarm'. They involved the monitoring of the maximum and minimum load applied during each cycle. If the load values monitored exceeded the defined outer load limits or came within the inner load limits then the experiment was shut down.

The amount of data stored during an experiment was found to be extremely large. This was due to fact that six data points were recorded every cycle. The size of data files produced were such that transfer to floppy disc or edit programs, in there 'raw' state, was impossible. For easier handling and storage the raw data was processed after each experiment using a data processor program written exclusively for the purpose. The processor designated DATSPLIT was designed to perform two tasks. Firstly it divided the data into two files one containing the maximum load and displacement data and the other minimum load and displacement data. It would then go on to reduce the size of each file by only storing that data identified by the user. For example the user may decide to store only data relating to every 100th cycle. From these processed data files test results could then be plotted directly on to the appropriate graphs.

6.1.3 Test Specimen Construction

The tee joint specimen construction was as for the static tests. The details of the construction of each joint type are given in chapter 5.0. Each specimen fillet radius was measured prior to testing. Observations were also made of any inconsistencies concerning the overlaminates. The results of these examinations are given in table 6.1.

6.2 Constant Load-Life Characterisation

6.2.1 Load vs Life

The P-N data for the various joint types are given in tables 6.2, 6.3, 6.4 and 6.5 and are presented graphically in figures 6.1 and 6.2. Figure 6.1a and 6.1b show the data for the joint types with 12 ply overlaminates (B & N joints) plotted together and 2 ply overlaminates (F & K joints) plotted together, respectively. All the curves seem to exhibit the familiar inverse S-shape commonly seen when glass reinforced plastics are fatigue. It should also be noted that the larger fillet radius joints, types F and B, display a greater static and fatigue strength compared to their smaller counterparts, K and N. Figure 6.2a and 6.2b show the same data, but with the two large radius joints (B & F joints) plotted together and the two

small radius joints (K & N joints) plotted together, respectively. In figure 6.2a joint type F with 2 ply overlaminates is seen initially to have a steeper curve than joint type B. At this stage joint F has a substantially higher fatigue strength. However at a load of approximately 14 kN the P-N curves of the F joint and B joint appear to merge together and the fatigue strengths of the two joints become very similar. The two curves continue together, down to approximately 5 kN where they seem to flatten out. In figure 6.2b joint type N with 12 ply overlaminates is seen initially to have a higher fatigue strength than joint type K. As before with a reduction in applied load the two curves come together. In this case however, the similarity between both curves seems to be less. This was difficult to confirm with the small amount of data available.

6.2.2 Deflections

During fatigue cycling the maximum and minimum deflections followed a similar pattern for each joint type. Figures 6.3a through 6.3d show typical deflections versus the number of cycles for the joints type B, F, K and N respectively. It can be seen, that as cycling continues the maximum and minimum deflections increase steadily, and approximately linearly, up to a point just before failure, where there is a sudden large increase in deflection.

6.2.3 Stiffness Degradation

From the intermittent measurements of the joint load and deflection during constant load fatigue experimentation, the change in the slope of the load-deflection (P-δ) curve could be established and therefore any global stiffness degradation could be identified. The slope of the curves was defined as the initial slope of the loading curve. The slope of the P-δ curve versus the life of the specimen normalised with respect to the number of cycles to failure, for joints type F and N, are shown in figures 6.4a and 6.4b, respectively. The figures show that the 'stiffness' drops away quite quickly for about the first 20% of the joints life. The degradation is then approximately linear up until 80% of the life, at which point the degradation rate increases again and joint failure occurs. In the case of the N type joints the curves exhibit discontinuities. These correspond to the delamination of the overlaminate material. For the higher load, delamination occurred at 10% life and involved the delamination of ply 3. For the lower load, two delaminations occurred at 0.1% and 1% life and involved the delamination of ply 9 and ply 6 respectively.

6.2.4 Energy Dissipation

Due to energy dissipation processes within the material of the joints, the intermittent measurements of the joint load and deflection exhibited hysteresis. When the results were plotted as load deflection curves they formed hysteresis loops. The area within each of these

loops could then be calculated to give the energy dissipated during one cycle at a particular point in the life of a joint specimen. Typical hysteresis loops are shown in figure 6.5 at increasing number of cycles, for a joint type F subjected to a load of 70% USS.

Figure 6.6a and 6.6b show plots of the energy dissipated against normalised life (cycle number,n / number of cycles to failure, N) for joint types F and N at loads of 70% USS and 50% USS. In the cases of the F joints the energy dissipation characteristics are similar, an initial maximum which steadily decreases to about 50% life before increasing again up to final failure. In the case of the N joints the energy dissipation exhibits an initial minimum from which there is a sharp increase up to a maximum. The characteristics of the dissipation then follow a similar pattern as the F joints. The position of the maximum dissipation seems to coincide with the point where delamination occurred in the overlaminate material. This occurred at approximately 1% life for the higher load and at 10% life for the lower load.

6.2.5 Residual Strength

The results of the residual strength tests are shown in figures 6.7, 6.8 and 6.9. Figure 6.7 shows the N type joint fatigued at 60% USS. The residual strength decreases monotonically with increasing number of cycles. Figures 6.8 and 6.9 show the results for the joint types F and K respectively, loaded at approximately 70% and 50% USS. In the case of these two joints, the residual strength seems to increase with an increase in number of cycles up to a point near failure where the strength drops away rapidly. This is most noticeable in the joint type K.

The residual strength tests were performed on a very limited number of specimens. The lack of data meant that the degree of scatter and any trends in the data were difficult to ascertain. Scatter bars were therefore plotted on each plot (figures 6.7,6.8 and 6.9) derived from the static test data.

6.2.6 Damage and Failure

For the type B and N specimens, the failure mode was found to be extremely similar to the mode observed during static loading. Firstly, at a very limited number of cycles the overlaminate on the tension side of the joint delaminated across the width of the specimen. The number of cycles to cause delamination was loosely dependant on the applied load. As the load increased the number of cycles tended to decrease. The delamination was limited to the root of the radius and was located either at ply 3, ply 6 or ply 9 counted from the inside (in a 12 ply overlamination). For the B type joint the delamination occurred initially at ply 9 then the next failure event was the delamination of ply 6. For the N type joint the initial delamination was generally located at ply 3. With continued cycling the

delaminations were not observed to grow and no further damage was apparent up to final failure. Final failure involved the delamination of the overlaminate from the resin fillet and the propagation of a crack through the fillet. The failure events were instantaneous and therefore observing their sequence with the naked eye was impossible.

With the type F specimens the final failure mode was again found to be similar to the static failure mode. However, in most cases, additional fatigue damage was observed. On loading the joint the overlaminate resin, on the tension side, exhibited whitening. This was noticed initially on the first cycle. When the load returned to zero, however, the whitening was observed to disappear. It was only after a large number of cycles that permanent whitening of the overlaminate was induced. A few specimens also sustained a small crack in the fillet between the web and the overlaminate near the top of the fillet on the tension side. This crack propagated slowly delaminating the overlaminate slightly and causing a small disbond between the web and the fillet. In all the cases the crack seemed to be limited to the edge of the specimen. A further form of fatigue damage was noticed, located on the compression side of the joint; this occurred in the overlaminate and was seen as a thin white line at the top of the radius. This phenomenon was limited to those specimens loaded at 70% USS of the joint. The damage seemed to occur at the same height as the small crack found in the tension side of the fillet. When this was noticed it was usually across the entire width of the specimen and extended through the entire thickness of the overlaminate. The damage was characterised by localised resin cracking, fibre fracture and delamination. This laminate failure occasionally induced a small crack in the fillet which extended to the web of the joint. None of the observed fatigue damages were identified as direct initiation points for final failure. Final failure was consistent and occurred remote from these smaller damages. As with the static tests, final failure was similar to the type B failure mode, involving delamination of the overlaminate from the fillet and a crack in the fillet itself. During the fatigue of some of the joints a significant rise in temperature was noticed in way of the fillet.

As was seen in the static tests the K type joints exhibited failure mechanisms very similar to those of the F type joints. In fatigue the same was true, although the additional damage sustained during loading of the K joint was limited to the whitening of the overlaminate and in some cases, a disbond of the web from the top of the fillet on the tension side. No compression damage was observed during any test. As with the F type joints a rise in temperature was also noticed in way of the fillet, on some of the joints.

6.3 Step Load-Life Characterisation

6.3.1 Two-Stage Load vs Life

The results of the two stage load step fatigue tests are given in table 6.6 and table 6.7 for joint types N and F respectively. P_1 and P_2 are the applied loads for stages 1 and 2, and n_1 and n_2 are the number of cycles at load 1 and the number of cycles to failure at load 2, respectively. Two load levels 70% and 50% USS were chosen as the loads to be used for the tests and the loading formats were designated high-low and low-high.

6.3.2 Deflections

Figure 6.10 shows typical maximum and minimum deflections versus number of cycles for joint type N subjected to a high-low loading format. A delamination occurs in the overlaminate during load 1 and this is characterised by a step in the deflection data. With the exception of this discontinuity the deflections follow a similar pattern to that of the constant fatigue load deflections; i.e. within each load stage they increase steadily, and approximately linearly, up to a point just before failure, where there is a sudden large increase in deflection.

Figures 6.11 shows typical maximum and minimum deflections versus number of cycles for joint type F subjected to a low-high loading format. In the case of this joint type no discontinuities are observed within either of the two load stages. the deflections within each load stage follow a similar pattern to that of the constant fatigue load deflections.

6.3.3 Stiffness Degradation

As with the constant load fatigue intermittent measurements of the joint load and deflection during experimentation allowed the change in the slope of the load-deflection (P-δ) curve to be established and therefore any global stiffness degradation to be identified. The slope of the P-δ curves was defined as the initial slope of the loading curve. The joint stiffness versus normalised life, for joints type F and N, are shown in figures 6.12 and 6.13, respectively. (In the case of two stage loading life was normalised with respect to the sum of the number of cycles at loads 1 and 2) The figures show that the degradation characteristics of the joints under two stage loading are very similar to that of the constant fatigue loading. Figure 6.12 shows low-high loading of the N type joint. As with the constant load the curve exhibits a discontinuity which corresponds to the delamination of the overlaminate material. This occurred at 50% life and involved the delamination of ply 3. Figures 6.13a and 6.13b show the high-low and low-high loading, respectively, of the F type joint. The low-high loading shows an initial drop in the stiffness for the first 20% of life

similar to the constant load results. The high-low loading, however shows the drop in stiffness occurring over only approximately 2% of the life of the joint. This effect could be due to the normalisation process. Interestingly, the point of load level change does not cause a discontinuity for either of the joint types.

6.3.4 Energy Dissipation

Figure 6.14 and 6.15 show plots of the energy dissipated against normalised life (cycle number,n / the sum of the number of cycles at load 1 and 2) for joint types F and N respectively. In the cases of the N type joint subjected to low-high loading (figure 6.14) the energy dissipation follows the characteristics of the dissipation under constant load. While at 50% USS load the joint has an initial minimum followed shortly by a maximum energy dissipation. The dissipation then decreases steadily to approximately 50% life where it increases again until at 99% life the load level changes to 70% USS load. The dissipation then follows the constant load pattern for this load and increases to failure. Figures 6.15a and 6.15b show the energy dissipation for the F joint subjected to high-low and low-high loading respectively. In the case of the high-low loading (figure 6.15a) the energy dissipation follows a similar pattern to the constant load energy dissipation except that the dissipation during load 1 (70% USS) seems compressed into the first 2% of life. Under constant load this amount of dissipation was seen over 20% of life. This effect could be due to the normalisation process. The dissipation at load 2 (50% USS) then follows a similar pattern to that of the constant load dissipation with an initial maximum, then a steady decrease to 50% life, followed by a steady increase to failure. In the case of low-high loading (figure 6.15b) the energy dissipation at load 1 (50% USS) also follows this pattern of dissipation until at between 90% to 95% life the load level changes. At load 2 the data is quite scattered and so it is difficult to establish any patterns of dissipation. It seems however, that there is possibly an initial peak in the energy dissipation which decreases and then possibly increases again close to failure. The level of dissipation at this load is difficult to establish but is in the region of the constant load dissipation level.

6.3.5 Damage and Failure

The damage observed in the N type joints during two stage loading, was found to be similar to the damage observed during constant fatigue loading. All the joints tested experienced damage during load 1 in the form of delaminations within the overlaminate on the tension side of the joint. With continued cycling at load 2 the delaminations were not observed to grow and no further damage was apparent up to final failure. As with the constant loading final failure involved the delamination of the overlaminate from the resin fillet and the propagation of a crack through the fillet. The failure events were instantaneous and therefore observing their sequence with the naked eye was impossible.

The damage observed in the F type joints during two stage loading was found to be similar to the damage observed during constant loading, however not all of the different possible types of damage were observed to occur. The joints subjected to the high-low loading format did not experience any damage during load 1. During load 2 whitening was observed, in the overlaminate on the tension side and localised whitening of the overlaminate at the top of the radius on the compression side, similar to the damage observed during constant fatigue loading. The joints subjected to the low-high loading format experienced whitening of the overlaminate and cracking of the fillet/overlaminate interface at the top of the radius on the tension side. None of the joints tested exhibited the localised tension overlaminate damage that was observed during constant fatigue loading. Final failure was as for the constant loading.

6.4 Discussion

The P-N data in figures 6.1 and 6.2 can be used to assess the dependence of joint fatigue strength on geometric variations, namely fillet radius and overlaminate thickness. For a given number of plies in the overlaminate and hence a given overlaminate thickness, the fatigue strengths are seen to increase with an increase in fillet radius. Conversely, for a given fillet radius the fatigue strengths are seen to increase with an increase in the number of plies in the overlaminate.

The amount of scatter in the load-life data associated with each joint type varies considerably. The B type joint has a substantially larger amount of scatter compared to the F type joint. This can be clearly seen in the P-N diagrams for both joints, figure 6.2a. It can be argued that the scatter relates to the consistency of specimen manufacture. The fact that joint type F has less scatter than joint type B, would suggest that joint F is less production sensitive. From a practical view point the tight radius of joint B coupled with the very thick overlaminate means that production of a consistently good joint is difficult. This is highlighted in table 6.1 which notes the 'squashing' of the thick overlaminate at the mid radius of some of the N and B type joints.

Stiffness degradation and energy dissipation mechanisms have been shown to be possible indicators of damage within composites, see chapters 2 and 3. These two mechanisms in the case of the tee joints under constant load, suggest that the rates of damage accumulation within the joints are similar in form to the rates of accumulation in a laminate; i.e. there is an initial decreasing rate of accumulation followed by an approximately constant rate and then finally an increasing rate up to failure.

The curves of stiffness degradation for two-stage loading showed no discontinuity when the

load level was changed. For linear materials this may be an expected result, but for materials such as the flexible resin fillet of the tee joints, change of load level could change the material properties dramatically. What these results seem to suggest is that the joint stiffness degradation is independent of load level within the limited range of 50% to 70% USS.

The energy dissipation for two-stage loading showed similar characteristics to the constant load dissipation, with the energy dissipation magnitudes and the pattern of dissipation being approximately the same. This would indicate that for two-stage loading, the energy dissipation is independent of loading history.

The data shown in figure 6.7 for the N type joint implies that the relationship between residual strength and number of cycles is approximately linear, with the residual strength decreasing with increased number of cycles. In complete contrast to this, the other two types of tee joint (F and K) in figures 6.8 and 6.9 show a nonlinear relationship where the residual strength seems to increase. This curious phenomenon could be attributed to two possible mechanisms. Firstly, it was observed that during the fatigue of the F and K joints there was a significant rise in the temperature of the fillet. The fillet resin material has been seen to have a substantial affect on the overall behaviour of the these joints. The temperature dependence of this material is uncertain, but it is known that with relatively small temperature rises above ambient the material becomes substantially more compliant. The observed temperature rises could therefore have been enough to have caused a change in the fillet material properties. Therefore when the joints were static tested immediately after being fatigued, higher strains could be sustained by the fillet and hence the ultimate strengths of the joints increased. Secondly, the overlaminate material of the F and K joints was observed to sustain a substantial amount of matrix resin cracking, characterised by whitening. This cracking would have degraded the stiffness of the material. It is known from previous work (see chapter 2) that the stiffness of tee joints is governed primarily by the overlaminates forming the boundary angles. The degradation of the overlaminates could therefore have been to such an extent that the overall joint flexibility increased. Subsequently this would then cause the ultimate static strengths of the joints to increase. An increase in joint flexibility during fatigue is shown by the curves of stiffness degradation in figures 6.4, 6.12 and 6.13 and by the increases in the deflections of the joints shown in figures 6.3 and 6.11.

7.0 Theoretical Modelling of Tee Joints - Internal Behaviour

7.1 Finite Element Models

Numerical modelling was implemented to identify possible damage locations and fatigue mechanisms in joint types B and F. The analysis was performed using the ANSYS finite element analysis (FEA) package, Swanson Analysis Systems (1992). Two dimensional (2-D) and three dimensional (3-D) models were constructed. For the 3-D models guidance was sort from Hawkins (1995) in terms of mesh density and choice of element. In 3-D the ANSYS package has a composite capability in that it provides three types of layered elements, comprising two eight-nodded shell elements and one eight-nodded solid. The geometry of the boundary angle problem precluded the use of shell elements as some stacking was required. The solid element assumes a linear variation of stresses through the element thickness; so several elements were required through the thickness of a laminate to illustrate the stress distributions within it. In the case of the joint type B, two models were generated. One of these pertained to the "perfect" specimen without any disbonds or delaminations. Additionally, a second model was generated to account for the delamination observed in the experimentation. In this model gap elements were inserted between the inner and outer laminates around the radius on the tension side of the joint.

The flexible resin fillet was represented using an isoparametric three-dimensional solid element with large deflection and plasticity capabilities. The model was made up of two elements across the width of the joint with one element through the thickness of the base plates and two elements through the thickness of the boundary angles. This particular scheme was found by Hawkins (1995) to give a good representation of the stress distributions through the thickness of the boundary angle without excessive processing. The material properties used for the analyses are given in Table 7.1. The non-linear stress-strain characteristics of the fillet resin are shown in figure 7.1.

A Two dimensional model was also constructed of the B type joint to allow the inclusion of an element per layer in the overlaminate. This was to give better resolution and accuracy of the stresses within the overlaminate. The elements used were 2-D plane elasticity structural solid elements. The model was made up of one element through the thickness of the flange and web and twelve elements through the thickness of the boundary angles. The flexible resin was represented using the same 2-D solid elements but with non-linear material characteristics.

In each case the model was restrained to represent the clamping arrangement used during experimentation and force vectors were applied near to the top of the web to simulate the 45° pull-off load.

7.2 Verification of Analyses

7.2.1 Load-Deflection

Initial verification of the results of the FEA models was made by plotting the derived load-deflection curves against the results obtained from the experimentation. Figures 7.2a and 7.2b show the load-deflection results of the FEA against experimental results for the joints type B and F respectively.

Figure 7.2a (B type joint) shows two FEA load-deflection curves, relating to analyses with and without gap elements inserted in the overlaminate, and an experimentally derived curve. The discontinuity in the experimental curve indicates the point at which a delamination occurred in the overlaminate. The FEA curve produced without gap elements (i.e. the solid line) predicts the experimental curve before delamination and the FEA curve produced with gap elements (i.e. the dotted line) predicts the experimental curve after delamination.

The FEA predicts the load deflection curves for the two joint types fairly well. In each case however, the predicted overall stiffness of the joints is less than the experimental stiffness. This indicates that the stress and strain magnitudes predicted by the FEA may not be entirely correct. The distributions and relative stress and strain values would however, be expected to be fairly accurate.

7.2.2 Load-Strain

Additional verification of the FEA modelling procedure was made by comparing the experimental strain gauge results, for the B type joint, against the predicted surface strains. Figures 7.3 shows the load-strain results of the 3-D FEA. These can be compared with the experimental load-strain results detailed in chapter 5 (figure 5.5). It is immediately obvious that the FEA is over predicting the magnitudes of the strain. The relative magnitudes of the predicted strains are however, similar to the experimental strains. On the tension side the FEA predicts higher strains occur at the root of the radius than at the top. On the compression side the FEA predicts that the strains will be similar at the top and root of the radius. These characteristics agree with the experimental results. These results support the expectation that the FEA gives fairly accurate qualitative results.

7.2.3 Stress and Strain Distributions

To give a further benchmark as to the accuracy of the FEA modelling and computations, comparisons were made between the experimental stress and strain results, of the thermoelastic and photoelastic analyses (detailed in chapter 5), and the FEA results. For the

purpose of benchmarking, the experimental result line plots of line 2 (defined in chapter 5), were chosen to be compared with the 2-D FEA. Location line 2 was chosen because it allowed comparisons to be made within all material components of the joint. The line cuts horizontally through the joint close to the root of the radius, cutting through both overlaminates, the fillet material and the web.

The FEA provided stresses and strains at nodal positions. To make a direct comparison with the experimental data obtained along line 2 it was necessary to determine stress and strain values at the positions were the line crossed the mesh. Since the elements used to model the overlaminate material had first order shape functions it was possible to do this by linear interpolation.

Figures 7.4 and 7.5 show the FEA line plots along line 2. Figure 7.4 shows the stress results in the same format as the SPATE line plots detailed in chapter 5 (figure 5.7b and 5.8b). The stress values were derived from the thermoelastic equation $\sigma_p + \alpha\sigma_t$ (derived in Appendix C) using the experimentally determined α value of 3.1. Details of the experimental derivation of α are given in Appendix D. The directions p, parallel to the fibre direction and t, transverse to the fibre direction represent the FEA element local coordinate directions x and y, respectively. Comparison of figure 7.4 with the SPATE line plots of line 2 in chapter 5 seem to show good qualitative and quantitative correlation between the predicted and measured stresses. A slight difference however, in the stress distribution across the overlaminates is apparent. In the experimental results, the average stress across the overlaminates seems to be nominally constant, however the FEA prediction shows them monotonically decreasing.

Figure 7.5 shows the strain results in the same format as the photelastic line plots detailed in chapter 5 (figure 5.12). The strain values for an isotropic material are derived from the photoelastic equation $\varepsilon_1 - \varepsilon_2$ (detailed in Appendix C). The plot of this principal strain difference for the B type tee joint, was found to exhibit extremely different characteristics to the photoelastic results. A good quantitative correlation between the FEA and experimental results could be achieved however, if the strain values were derived from the equation $\varepsilon_p - \varepsilon_t$, where p and t are directions parallel and transverse to the fibre direction and represent the FEA element local coordinate directions x and y, respectively.

7.3 Predicted Failure Mechanisms

Figures 7.6a, 7.6b and 7.6c show the through-thickness stresses and inplane stresses in the overlaminate and the principal stresses in the fillet respectively, for the joint type B at a relatively high applied load of 11.44 KN (70% USS). The maximum through-thickness stress

occurs at mid-radius, with a value of 6.32 MPa. The maximum stress in the fillet is 7.71 MPa. Since the fillet would be expected to withstand more than twice the stress compared with the laminate in the through-thickness direction (see table 7.1), it can be deduced that failure would initially occur within the overlaminate. Experimental data relating to the ultimate strength of the overlaminate material in the through-thickness direction was unavailable, but it would be expected to be slightly less than that for polyester laminates. The previous work had established the value to be approximately 8 MPa [1-3].

To model the behaviour of the B type joint after an initial delamination, gap elements with suitable properties were inserted between the inner and outer laminates around the radius on the tension side of the joint. Figures 7.7a, 7.7b and 7.7c show the stresses in the joint (in the same format as figure 7.6). The result was increased stresses in the fillet, up to a maximum of 12.14 MPa, illustrating the transfer of load from overlaminate to fillet as delamination proceeds. It can therefore be argued that as loading continues, the through-thickness stresses in the remaining overlaminate will increase to a point where a further delamination occurs leading ultimately to a disbonding of the overlaminate from the fillet. When this happens the stresses in the fillet will increase to a level where instantaneous failure of the resin occurs.

Joint type F is similar to joint B except the fillet radius is increased and the thickness of the overlaminate is substantially reduced. Figures 7.8a, 7.8b and 7.8c show the stresses in the joint (again in the same format as figure 7.6) for the joint at a load of 10.30 KN (50% USS). The maximum tensile through-thickness stress in the laminate is shown as 2.62 MPa and the maximum stress in the fillet as 18.60 MPa. This indicates that failure would tend to occur within the resin fillet and not by delamination. A better balance of stresses within both elements of the joint has also been achieved. This is consistent with the experimental observations where fillet and overlaminate failure mechanisms were indiscernible.

7.4 Discussion

It was assumed that any significant fatigue damage would occur initially at locations of high relative stress, that is, where the ratio of stress to ultimate strength of a component material was the greatest. The three separate component materials were the fillet resin, the overlaminate and the base laminate. With this in mind an attempt was made to correlate the FEA stress contours and the experimentally observed fatigue damage.

It was shown that the verification results that the FEA model may not have been producing completely accurate stress magnitudes. The FEA was however producing good qualitative results and therefore the relative stress magnitudes, material to material, could be relied upon.

In joint type B, the highest relative stresses are seen to occur within the thick overlaminate on the tension side, in the through-thickness direction (see figure 7.6 and 7.7). Hence, although other components in the joint would experience fatigue damage, causing a loss in strength and stiffness, the dominating failure process would be expected to follow static failure. Initially the stresses in the overlaminate cause fatigue damage in the form of a delamination at ply 6, as cycling continues the overlaminate/fillet bond weakens until disbonding occurs. At this instant the stresses in the fillet increase substantially and due to its loss of strength through increased strain rate and fatigue damage, static failure of the fillet resin occurs. Experimental observations follow this failure process.

In joint type F, the highest relative stresses are in the fillet resin (see figure 7.8). The maximum and minimum stresses occur near the top of the fillet and coincide with the observed cracks. It is likely that the occurrence of these cracks will redistribute the stresses in the fillet. Fairly high relative stresses occur within the overlaminate, in the inplane direction. The location of the highest inplane stresses matches the position of the observed whitening of the overlaminate during fatigue. The whitening is most likely to be due to matrix cracking, which will cause a loss of strength and stiffness in the laminate, leading to increased stresses in the fillet. This cracking could induce final failure of the joint by initiating a disbond of the overlaminate from the fillet. Then, as with the joint type B, instantaneous static failure of the fillet resin would occur, intensified by a loss of strength due to accumulated fatigue damage and increased strain rate. However, as was mentioned in the previous section, the sequence of final failure events could not be clearly discerned. It is therefore plausible that final failure of the joint could be due solely to the increased stresses in the fillet, without an initial disbond occurring at the overlaminate/ fillet interface.

8.0 Theoretical Modelling of Tee Joints - Global Behaviour

8.1 Fatigue Life Characterisation

In chapter 4 several empirical fatigue models were presented for composite materials. The models were shown to be one of three general curve fitting types, either a straight line fit, a power law fit or an inverse power law fit. It was found that these basic models were unable to characterise fully the double curvature, inverse-s-shape of the glass reinforced plastic (GRP) laminate S-N curves. A possible way to model this characteristic would be with a polynomial fit of the form,

$$\log(N) = C_0 + C_1 S + C_2 S^2 + C_3 S^3 + \ldots\ldots C_n S^n \qquad (8.1)$$

where C_0, C_1, ...C_n are all model parameters. Although more complicated, the model should be able to define the inverse-s-shape of the fatigue life distributions. This type of model would be particularly suited to a system of materials where so called 'material constants' are unimportant, such as in the case of the tee joints.

The polynomial model was applied to the tee joint experimental data along with the Hwang and Hahn model (equation 4.5), the Han and Kim model (equation 4.4) and the straight line model (equation 4.3), to assess which model would be most appropriate to tee joints. The model parameters in each case were derived using least squares methods. Correlation coefficients were calculated in each case to allow a comparison of goodness of fit.

Figure 8.1 shows the P-N data for the B type tee joint. The best overall fit was given by the 3rd order polynomial,

$$\log(N) = 22.0199 - 4.9228\ P_a + 0.4547\ P_a^2 - 0.0143\ P_a^3 \qquad (8.2)$$

The Hwang and Han model gave a fair fit to the low cycle data whereas the Hahn and Kim model gave a fair fit to the high cycle data. The large scatter in this data meant a good fit could not be established.

Figure 8.2 shows the P-N data for the F type tee joint. The best overall fit was given by the 3rd order polynomial,

$$\log(N) = 15.6167 - 2.1895\ P_a + 0.1395\ P_a^2 - 0.0034\ P_a^3 \qquad (8.3)$$

The Hwang and Han and Hahn and kim models gave good fits to the low and high cycles fatigue data respectively.

Figure 8.3 shows the P-N data for the K type tee joint. The paucity of data for this type of joint meant the shape of the curve was not well defined and hence any fit to the data was questionable. The best apparent overall fit seemed to be given by the Hwang and Han inverse power law,

$$N = [\ 10.982(1-s)]^{1/0.1575} \tag{8.4}$$

It is expected that a more appropriate fit may be given by a 3rd order polynomial if more data were available.

Figure 8.4 shows the P-N data for the N type tee joint. As with the K type joint the paucity of data meant no reliable fit could be established. A polynomial fit could not be attempted due to the lack of data. The best apparent overall fit seemed to be given by the Hahn and Kim power law,

$$1.9807e{-}15\ P_a^{13.6277}\ N = 1 \tag{8.5}$$

as with the K type joint, it is expected that a more appropriate fit would be given by a 3rd order polynomial if more data were available.

Quantifying the scatter seen in the tee joint experimental data using confidence limits was found to be impractical. This was due mainly to the large magnitude of scatter and the low number of data points which produced extremely large and divergent confidence intervals. The definition of scatter bands was found to be a more useful approach. The bands were established by assessing the variation in the number of cycles to failure at each load level and then relating this to an approximately constant variation in applied load about the mean. In the case of the F type joint all the scatter came within approximately ± 2.3 KN of the mean and for the B joint, within approximately ± 3.1 KN of the mean. The mean line was taken to be the best model fit for each set of data. The paucity of data for the N and K type tee joints made it very difficult to define scatter bands for these joints.

8.2 Multi-load Level Fatigue Life Prediction

The investigation into currently available life prediction models for composites, in chapter 4, showed that the most appropriate way to model multi-load level tee joint fatigue would be with a cumulative damage approach were fatigue damage was defined by energy dissipation.

Due to energy dissipation processes within a material, its load displacement relationship for a single cycle, will exhibit a hysterisis loop. The area enclosed by the hysterisis loop is equivalent to the strain energy dissipated. The remaining area under the load displacement

curve is equivalent to the stored energy or reversible strain energy within the material. It was shown in chapter 4 that it has be assumed by various researchers that the energy dissipated per unit cycle is related to the increase in damage per unit cycle. The summation of the dissipated energy over the life of a particular material is then proportional to the accumulated damage within that material.

The majority of the energy methods described in chapter 4 were originally proposed for metal fatigue and assume that the energy dissipated per cycle is constant over the life of the metal. It is obvious from experimental data that this is not true for GRP and imparticular for the tee joints (see chapter 6).

As was shown in chapter 3, the specific form of damage sustained by a composite depends on the stacking sequence, type of reinforcement and matrix used in the material. Poursartip et al. (1982) pointed out however, that the general rates of damage accumulation in GRP tend to be similar and can be broadly split into three parts; first an initial growth phase at decreasing rate followed by an intermeadiate phase at constant rate and then a final phase at increasing rate. If the energy dissipation characteristics of the tee joints are considered (see chapter 6) it can be seen that the energy dissipation per cycle follows the same trend as this general rate of damage accumulation for GRP. Initially there is a large amount of energy dissipated this drops away during mid life and then increases again up to failure. It is proposed that this behaviour could be modelled with a sine function of the form

$$-A \sin(b\, n_i) \tag{8.6}$$

Where the subscript i denotes the load level number for multi-load level fatigue.

It is first assumed that the average energy per cycle Δw_{av} is given by

$$\Delta w_{av} = \frac{W_{fi}}{N_i} \tag{8.7}$$

where W_{fi} is the total energy dissipated to failure. The energy dissipated per cycle Δw_i, can then be written as

$$\Delta w_i = \frac{W_{fi}}{N_i} + A_o \left(\frac{2}{\pi} - \sin(\pi \frac{n_i}{N_i}) \right) \tag{8.8}$$

the parameter A_o defines the variation of Δw_i about Δw_{av}. To quantify this parameter measured tee joint data and various other composite material experimental data were examined. The other materials chosen were all glass/polyester composites and included a woven glass laminate and a sheet moulding compound (SMC) from Renz et al. (1990) and

a unidirectional pultruded rod from Jessen and Plumtree (1991). For each material the difference between the maximum and minimum Δw_i was established at each stress level and then this difference was normalised with respect to the maximum Δw_i. Table 8.1 shows the values obtained for the different materials at given fatigue load levels. The fatigue loads have been normalised with respect to the ultimate static load of the material in each case. The average of these results is 0.2205 with a standard deviation of 0.0295. This average value was used to derive the parameter A_o such that,

$$A_o = \frac{0.2205\ W_{fi}}{N_i\ (1-0.4410/\pi)} \tag{8.9}$$

Subsequently the energy dissipated per cycle becomes

$$\Delta w_i = \frac{W_{fi}}{N_i} + \frac{W_{fi}}{N_i}\ \frac{0.2205}{(1-0.4410/\pi)}\left(\frac{2}{\pi} - \sin(\pi\ \frac{n_i}{N_i})\right) \tag{8.10}$$

to establish the energy dissipated w_i over the life of the tee joint or the energy accumulation, equation (8.10) must be integrated,so that

$$w_i = \frac{W_{fi}}{N_i}\ n_i + \frac{W_{fi}}{N_i}\ \frac{0.2205}{(1-0.4410/\pi)}\left(\frac{2n_i}{\pi} + \frac{N_i}{\pi}\cos(\pi\ \frac{n_i}{N_i})\right) + C \tag{8.11}$$

With the assumption that $w_i=0$ at $n_i= 0$ this gives

$$w_i = \frac{W_{fi}}{N_i}\ n_i + \frac{W_{fi}}{N_i}\ \frac{0.2205}{(1-0.4410/\pi)}\left(\frac{2n_i}{\pi} + \frac{N_i}{\pi}\ \cos(\pi\ \frac{n_i}{N_i})\right) - \frac{W_{fi}}{N_i}\ \frac{0.2205}{(1-0.4410/\pi)}\ \frac{N_i}{\pi} \tag{8.12}$$

The chosen definition of the parameter A_o assumes that the variation of Δw_i about Δw_{av} is independent of applied fatigue load. This may not be the case in all situations. The variation of Δw_i may be a function of applied fatigue load, in which case the model parameter must be modified so that,

$$A_o(P_a) = \frac{f(P_a)\ W_{fi}}{N_i\ (1\ -\ 2.f(P_a)/\pi)} \tag{8.13}$$

A comparison of the stress independent model, given in equation (8.12), with the experimental data for the F and N type joint are shown in figures 8.5 and 8.6 respectively. It can be seen that there is a good correlation between the experimental variation in dissipated energy and the sine model.

The prediction of multi-load level fatigue lives using the sine model is accomplished using linear summation, as used in the Palmgren-Miner rule. The prediction is made by the summation of the energy dissipated at each load level, until the total energy dissipated is equal to the total energy dissipated to failure for constant load fatigue. This requires that the relationship between load level and total energy to failure for constant load fatigue be known. In the case of the tee joints this was achieved using the experimental dissipation energy data given in chapter 6. It could be argued that the load-energy relationship should be of a similar form to that of the P-N curve and hence, in the case of the F type joints a 3rd order polynomial was fit to the data so that,

$$\log(W_F) = 22.646 - 84.981\ P + 129.650\ P^2 - 64.969\ P^3 \qquad (8.14)$$

where P is the applied fatigue load normalised with respect to the ultimate static load. In the case of the N type joint a power law fit was made to the data so that,

$$W_f = 97\ P^{-1/0.1082} \qquad (8.15)$$

Due to the lack of data the accuracy of this fit is questionable. It is likely that if more data were available a 3rd order polynomial fit would be more appropriate. Figure 8.7 shows the comparison of the experimental total energy dissipation with the curve fits for the two joint types.

A comparison of the predictions of the sine model with the experimental two-stage fatigue lives of the F and N type joints (detailed in chapter 6) is given in tables 8.2 and 8.3, along with predictions made by the Palmgren-Miner rule (equation 4.35), the Hashin-Rotem theory (equation 4.39) and the Treshenko-Khamaza model (equations 4.21 & 4.22). These three models having been identified in chapter 4 as being the most likely models to give good predictions for tee joint fatigue. Each model was used to predict the residual number of cycles to failure, n_r, at load level P_2 after an initial loading period of n_1 cycles at load level P_1. Where a negative number of residual cycles to failure was predicted by any of the models, it was assumed to indicate a failure in the first cycle of the second load stage.

Application of the Treshenko-Khamaza model required the derivation of the model parameters K and α. Parameter k was derived using equation (4.21) applied to experimental data of the total energy absorbed to failure for both joints. A value of k=0.1186 was established for the F type joint and a value of k=0.1082 was established for the N type joint. A plot of equation (4.21) versus the experimental total energy dissipated for both joints is shown in figure 8.8. The parameter α is known to be dependent on stress level and as stated in chapter 4 tends to be a linear relationship in metals. To derive this relationship for the tee joints, equation (4.22) was applied to experimental data of the average energy dissipated per cycle for both joints. The parameter was found to follow a power law relationship of the form,

$$\alpha = 49.75\ N^{-0.2269} \tag{8.16}$$

for the F type joint and,

$$\alpha = 31.61\ N^{-0.1479} \tag{8.17}$$

for the N type joint.

For the F type joint, table 8.2, the best overall performance was given by the Sine model with an average percentage error of 4%. The Palmgren-Miner rule and Hashin-Rotem relationship both gave similar accuracies of prediction as each other with 39% and 34% average errors respectively. The Treshenko-Khamaza theory gave the least accurate prediction with a -46% average error. A negative percentage error indicates an average underestimate of the residual lives where as a positive percentage error indicates an average overestimate.

For the N type joint table 8.3, the best overall performance was again given by the Sine model with an average percentage error of -29%. The Palmgren-Miner rule and Hashin-Rotem theory produced overall percentage errors of 37% and 53% respectively. The Treshenko-Khamaza theory again gave the least accurate prediction with a 684% average error.

8.3 Design Envelope

An important preliminary step in the design of a structure is to establish basic geometric properties of structural elements given the required design loads. A widely used tool which helps designers accomplish this is the design envelope. The design envelope produces a series of possible design solutions given various design constraints. The boundaries of the envelope are based on these constraints combined with design curves.

Given the extensive experimental data available for single skin tee joints presented in this thesis and the thesis of Hawkins (1995), it was considered possible that design curves could be produced for a large range of joint geometries. These curves could then be used to help designers produce useful design envelopes for tee joints, given amoung other constraints, the likely static and fatigue loadings to be carried by a particular joint.

It has been shown in chapter 2 that the most significant geometric variables for a tee joint are the fillet radius and the overlaminate thickness. The design curves have therefore been drawn up based on these two variables.

The static strength design curves are presented in figure 8.9. The curves have been derived from experimental results for various joint configurations assuming the relation between number of overlaminate plies and strength is linear over the range of 2 to 12 plies. The curve for zero plies has been derived from the experimental data of Hawkins (1995) and Wolfson Unit MTIA Report No. 1231 (1995).

The fatigue strength curves are presented in figure 8.10 through 8.13. The curves are given at 10^3, 10^4, 10^5 and 10^6 fatigue cycles and have been derived from the P-N data presented in chapter 6 assuming that, as for the static strength, the relationship between number of overalminate plies and fatigue strength is linear. Due to the limited amount of fatigue data it was assumed that the relationship between fillet radius and fatigue strength was also linear over the majority of joint geometries. For the curves at 10^3 and 10^4 cycles, the relationship at the lower radii was distorted so as to produce positive fatigue strengths for the joints with small numbers of overlaminates. The linear regions of the data were found to be between 2 and 12 plies over the range of 30mm to 100mm radii. The equation used to define this region was,

$$P_a = m_1(radius) + m_2(plies) - c \qquad (8.18)$$

where m1, m2 and c are constants. Table 8.4 gives the value of these constants for the fatigue strength curves.

The fatigue strength design curves give an average fatigue strength. To give an account of the scatter in strength values seen in the experimental data, a scatter design curve was formulated. It was established in chapter 6 that the scatter could be related to ease of manufacture of each joint type, with thick overlaminated joints being more difficult to manufacture than thin overlaminates. It seemed sensible therefore to assume a relationship existed between scatter and the number of overlaminate plies. When comparing the scatter in the data for the two joints with 12 overlaminate plies (B and N), it was found that the scatter normalised with respect to the ultimate static strength was the same. This was also found to be true for the two joints with 2 overlaminate plies (F and K). The two normalised scatter values were used as the basis for a design curve and a linear relationship was assumed to hold between them, such that,

$$\frac{Scatter}{USS} = 0.0156(plies) + 0.1918 \qquad (8.19)$$

Predictions of the static and fatigue strengths made by the design curves, for the four joint types investigated in this thesis (joints B,F,K and N), are shown in figure 8.14. For each joint the predicted strength and scatter bands are shown plotted against the experimental fatigue

data. It can be seen that there is good correlation between the predictions of the design curves and the experimental data.

The proceedure that could be adopted to design a particular tee connection would need to follow a series of steps. Initially the design constraints would need to be defined, e.g. maximum practical radius and number of overlaminate plies, required fatigue strength, etc. The next step would be to produce a design envelope. From this envelope of design solutions a particular combination of radius and number of plies would then be chosen. A fatigue curve, including strength scatter, could then be produced for the chosen joint.

A possible design envelope is shown in figure 8.15. The fatigue strength boundary has been drawn from the design curves given in this chapter. The boundaries for fillet failure and overlaminate inplane failure and delamination have been drawn from the data given in the parametric study of Hawkins (1995), detailed in chapter 2 (figure 2.2). Additional boundaries could be included based on manufacturing cost and joint weight. In this way detailed design envelopes could be constructed to give a designer a 'first shot' at the design solution.

8.4 Discussion

Characterisation of the tee joint P-N data using a 3rd order polynomial fit was found to be the best approach in the case of the F and B type joints. The lack of data points in the cases of the K and N type joint meant no positive conclusions could be drawn as to which method would give a best fit. It is believed however, that these joints would exhibit similar characteristics to the F and B type joints and that a 3rd order polynomial would ultimately give the best fit in each case.

Prediction of two stage fatigue lives of the F and N type tee joints was acheived with most accuracy using the proposed Sine model. The worst predictions seemed to be made by the Treshenko-Khamaza theory, underestimating for the F type joint and overestimating considerably for the N type joint. The Palmgren-Miner rule and Hashin-Rotem method both tended to give similar predictions, overestimating for the F type joint and underestimating for the N type joint. This similarity is not surprising as the Hashin-Rotem method was derived from the Palmgren-Miner rule (see chapter 4).

The percentage error of prediction for the N type joint seemed to be significantly greater in the cases of the Sine model and the Treshenko-Khamaza method. It was believed that this could be due to the greater amount of scatter in the P-N data and the total energy dissipated data for this joint type. It could also be due to a poor fit to the two sets of data caused by the low number of data points.

To bring the percentage prediction errors for each fatigue model into context, they must be compared with the percentage scatter in the experimental P-N data. The F type joint was chosen for this comparison because it had the narrowest scatter band and would therefore show the minimum effect on the prediction errors due to scatter. The P-N data were considered at the two load levels used in the two stage fatigue work, which were 50% and 70% USS. The mean fatigue life and standard deviation of the P-N data at these load levels was calculated using the data in table 6.3 (see chapter 6). The percentage scatter was then taken to be two standard deviations about the mean life. For 50% USS the percentage scatter was found to be ±104% about the mean and for 70% USS the percentage scatter was found to be ±80% about the mean. The error in the two stage fatigue lives is an addition of these two errors and could therefore be as much as 184%. With such a great possible percentage error in the life predictions of each model, due to scatter in the P-N data. It could be argued that any of the four fatigue models will give reasonable life predictions.

In terms of design, the four fatigue life prediction models would need to be combined with statistical proceedures to give upper and lower bounds of the life predictions calculated. This would be achieved with statistically dependent variables.

An important point to note is that the Hashin-Rotem, Treshenko-Khamaza and Sine model methods have only been applied to two stage loading fatigue. For practical applications, spectrum loading of a structure is more likely to be the case.

The design curves in the design envelope proceedure showed good predictions of the static and fatigue strength and scatter of the strengths for the four joint types studied in this thesis (joint types B, F, K and N). This indicates that the assumed linear relationships for the design curves are good approximations within the range of number of plies and radii chosen. This therefore gives some confidence in the prediction of the static and fatigue strengths of other joint configurations.

It must be remembered that the design curves relate to joints were the lay-up of plies follows NES 140 in a 50/50 mix urethane acrylate/ polyester resin with a urethane acrylate fillet, subjected to a 45° pull-off loading applied to the web of the tee at 230mm above the flange. A more general set of curves could be produced by using the basic material properties of the overlaminates in conjunction with the number of plies and using bending moment and component forces at the joint instead of the combined 45° pull-off strength.

9.0 Discussion and Further Work

9.1 Discussion

Reviews of the current literature on the load transfer mechanisms of tee joints, fatigue characteristics of FRP materials and possible modelling approaches that could be used to predict fatigue behaviour, show clearly an avenue of study to be taken. Initial conventional static experimentation provides a check with previous work on the validity of the current experimental method and gives a first point on the load-life curve of the tee joints. Application of experimental techniques never used before on tee joints, then allows an insight into the internal static stress and strain distributions of the joints and provides new methods for Finite Element Analysis (FEA) model verification and a new detailed understanding of load transfer mechanisms. FEA calculations enhance the understanding of static load transfer mechanisms and used in a novel way for tee joints, establish failure initiation sights and damage mechanisms. Constant load fatigue tests produce more extensive load-life characteristics and stiffness and strength degradation characteristics than ever before and introduce the concept of energy dissipation characteristics for the first time for tee joints. These tests also give a new understanding of fatigue damage processes and failure mechanisms. Two-stage loading never applied previously to tee joints, produces new information on fatigue life, stiffness degradation and energy dissipation characteristics. The results provide a basis for the novel modelling of the energy dissipation of the joints to produce a new method of fatigue life prediction. The results also provide a basis for a new tee joint design approach based on newly derived design curves which can produce load-life characteristics for a large number of possible tee joint designs.

It is clear that present conventional design guidelines are inadequate in helping structural designers to understand the load transfer mechanisms within composite tee connections. This impedes their ability to optimise designs in terms of weight and cost. Recent experimental and theoretical work has contributed substantially to the understanding of tee joints under static loading. This has highlighted the importance of overlaminate thickness and fillet radius and shown how high tensile interlaminar stresses in the boundary angles of joints with thick overlaminates could cause the initiation of joint failure through delamination. Furthermore it has shown how increased joint flexibility using thin overlaminates could lead to higher overall joint strengths.

The static experimental work carried out in this investigation increases the current understanding of tee joint load transfer mechanisms. This is achieved with two new approaches to the investigation of tee joint static behaviour. The first is load rate sensitivity tests, which add a pseudo-dynamic angle to the static investigations. These show that the more flexible joints, whose behaviour is more dependent on the resin fillet, exhibit a

significant drop off in strength as the rate of load application increases. The gain in strength seen during low load rate static testing is therefore countermanded with an increase in applied load rate. The second approach is an investigation into the internal stress and strain distributions within a tee joint using two full field experimental techniques. The two techniques, thermoelastic stress analysis and photoelastic strain analysis, show how the overlaminates carry a large proportion of the applied load, in particular how the highest stresses occur in the woven roving layers. Furthermore the two experimental techniques give results which can easily be used to benchmark finite element analysis (FEA). Benchmarking the FEA in this investigation shows how manufacturing inconsistencies that are not included in the FEA modelling, can effect the stress values and distributions within the joints. See also Dulieu-Smith, Shenoi, Read, Quinn and Moy (in press).

Modelling of the internal behaviour of tee joints must be performed with numerical methods such as FEA. A number of shortcomings are highlighted with the way previous FEA models of tee joints have been constructed, so to address these, further modelling is carried out. To address the problem of a coarse mesh definition, the tee joints are modelled in two dimensions, which allows a more detailed finer FEA mesh to be utilised. This means an element per layer/ply can be used through the thickness of the overlaminates, which gives a more detailed prediction of the internal stress and strain patterns. Furthermore, to address the problem of inadequate model verification, the results of the FEA models are experimentally verified through four techniques; load-displacement comparison, strain gauge measurement, photoelastic strain measurement and thermoelastic stress analysis. The FEA stress and strain distributions calculated are then used to help establish possible fatigue damage processes and failure mechanisms. As with static loading the relatively high normal interlaminar stresses in the thick overlaminates, seem most likely to be responsible for overall failure initiation through delamination. In the joints with thin overlaminates the inplane stresses seem most likely to be responsible for failure initiation, through matrix resin cracking. See also Shenoi, Read and Hawkins (1993).

It is obvious from the limited amount of previous work that there is a significant lack of understanding, compared to FRP laminates, of the fatigue behaviour of FRP tee joints, in particular load-life characteristics, and stiffness and strength degradation. This is addressed in this investigation with an examination of stiffness and strength through-out the fatigue lives of the four tee joint types. It is shown that as the joints are fatigued their stiffness decreases. In the case of the thick overlaminate joints their residual strength also decreases. In the case of the thin overlaminate joints however the residual strength of the joints seems to initially increase. Furthermore, to address the lack of understanding concerning load-life characteristics, an examination of the constant and multiple fatigue loading of the four joints is carried out. This produces a considerable amount of load-life data and allows an overview of the influence of geometric variables on fatigue performance. It is found that fatigue

strength seems to increase with an increase in fillet radius and the number of overlaminate plies. The work also highlights the importance of manufacturing consistency and shows that fatigue strength can vary to a large extent for joints with inconsistencies. Inconsistencies have been seen to occur easily in difficult to manufacture joint geometries, which highlights an important design consideration.

The two-stage fatigue loading work establishes how load history affects the joints fatigue lives, specifically how stiffness degradation and energy dissipation seem to be independent of load history. This implies that the two physical phenomena can be used as damage indicators in theoretical fatigue life prediction techniques similar to those used for FRP laminates.

A review of fatigue life prediction methods for FRP materials, shows that in many cases the approaches are applicable to lamina or laminates only and can not be adapted easily to tee joints, see Read and Shenoi (1995). The application of conventional strength degradation methods to tee joints is also found to be difficult. This is due to the thin overlaminate joints not exhibiting monotonically decreasing residual strength. It is discovered however, that cumulative damage methods combined with modified energy methods can be applied to tee joints and in fact to any other structural element. The prerequisite however is that the tee joint damage accumulation needs to be similar to that of FRP laminate damage accumulation. This is found to be the case in the fatigue experimentation. It is observed that the energy dissipation characteristics, shown to be related to damage accumulation, are similar to the rate of damage accumulation in FRP laminates, see Shenoi, Read and Hawkins (1995).

Global modelling of the fatigue behaviour of tee joints is split into two main areas, characterisation of load-life and multiple load fatigue life prediction. Characterisation of the constant load-life data is carried out using empirical methods. It is shown that a third order polynomial formulation gives the best fit to the load-life data of the tee joints, when compared with established models. To predict the multiple load fatigue life of the joints, a novel sine based model is proposed modelling the energy dissipation characteristics of the tee joints. It is applied to the two-stage fatigue loading results. When compared with established models the sine model seems to give the most accurate predictions overall. See Read and Shenoi (under Preparation). With scatter in the data so pronounced however, it is difficult to draw accurate conclusions as to the best theoretical method.

To incorporate the new knowledge of tee joint fatigue behaviour into an approach for tee joint design, a novel design envelope procedure is proposed. It is based on design curves derived from the experimental data of this and previous investigations. The procedure allows the correct geometric configuration of a tee joint to be chosen for a given application. It produces an envelope of design solutions from which a particular solution can be chosen and

then a full load-life curve produced. Comparison of the procedure predictions with the experimental results for the four tee joint types of this investigation shows good correlation. See also Read and Shenoi (under Preparation).

9.2 Further Work

Experimental thermoelastic and photoelastic analysis of the tee joints, gives a unique insight into the stress and strain distributions within these joints. The two experimental techniques have the potential to become powerful tools in the quantifying of stress and strain distributions within FRP structural elements. See Read, Dulieu-Smith and Shenoi (1996). At present the techniques can only easily give the sum of the stresses and the difference of the strains. A programme therefore needs to be established to develop and implement procedures for developing these techniques and combining them to produce full field separation of stress and strain.

The more detailed FEA modelling of the internal stress and strain distributions gives more reliable predictions than previous work, however shortcomings in the construction of the model are still evident. In particular the curved boundary angles still have to be modelled with straight sided elements. An element formulation is currently under development that will model curved surfaces more accurately. See Hawkins and Shenoi (1995). This needs to be implemented in further modelling of tee joints to achieve more accurate stress and strain predictions.

Although the fatigue experimentation is extensive, it is by no means exhaustive and further fatigue testing of other joint geometries is needed to expand and enhance the knowledge gained in this investigation. In particular further study into the phenomenon of increasing residual strength in thin overlaminate joints is needed. Further study is required to confirm the observations made concerning stiffness degradation and energy dissipation and to investigate whether they hold for higher numbers of loading stages and eventually load spectrums. Further work is also needed to produce more data to prove the predictive capabilities of the new sine model. The new model also needs to be applied to a higher number of load stages and to load spectrums to assess its true usefulness.

The fatigue design curves used in the design envelope procedure are developed from the data available in this current investigation only. Further corroborative data is therefore needed to assess the validity of the curves. In addition, all the design curves need to be generalised in terms of forces and bending moments and material properties so that designers can apply them in a wider range of applications.

10.0 Concluding Remarks

The use of FRP in marine structures is increasing and joints in these structures present a potential problem as a site of potential structural weakness. Tee joints in FRP structures are particularly problematic due to the out-of-plane loading that the FRP will be subjected to. A large amount of knowledge has been accumulated from previous work, mainly through the use of finite element analysis (FEA), on the effect of geometric variables on static performance and the possible stress distributions within certain tee joints. Most notably the understanding that increased joint flexibility can lead to higher overall static strengths. There has been an obvious lack of knowledge relating to actual stress and strain distributions within these types of joints and their long term fatigue behaviour. This is addressed in this investigation through an extensive experimental programme and through theoretical modelling.

Internal stress and strain distributions are studied using two full field experimental techniques. These show how, for joints with thick overlaminates, the load is transferred mainly through the boundary angle. The results of these techniques are also found to be useful for benchmarking the FEA. This highlights how manufacturing inconsistencies in the test specimens could produce results quite dissimilar to the perfect FEA model.

The experimental programme highlights a large number of dynamic and fatigue behaviour characteristics. High load rate static tests reveal that the flexible joints, more dependent on filleting resin, although stronger at low load rates, exhibit a significant strength reduction as the load rate is increased. The fatigue testing of four different joint types under constant and two-stage cyclic loading, show how the joints strength, stiffness and energy absorption vary through-out their fatigue lives. It is found that all the joints exhibit a loss of stiffness but only the stiffer joints also exhibited a loss of strength, the more flexible joints seem to retain their strength until close to failure. For all the joint types the energy dissipation is seen to follow similar patterns to that of laminate damage accumulation. Load-life data for each joint type is presented and allows an understanding of the effects of joint geometry on fatigue strength. It shows that fatigue strength seems to increase with an increase in fillet radius and number of overlaminate plies.

FEA stress and strain distribution results increase the understanding of the fatigue behaviour of tee joints. They allow the areas of likely fatigue damage and failure initiation to be located and give some understanding as to the sequence of failure events. For the more flexible joints with thin overlaminates, the inplane overlaminate stresses are seen as the most likely cause of failure initiation. For the stiffer joints with thick overlaminates, the normal interlaminar stresses are seen as the most likely cause.

A damage accumulation method is proposed for use in the fatigue assessment of tee joint designs. The method is compared with various theoretical methods currently available and seems to perform well. Further evaluation of the method is required.

A preliminary tee joint design proceedure is proposed utilizing design curves to produce a design envelope. The design curves are shown to give good predictions for the joint configurations of this investigation, but further evaluation of the method is required.

References

"Calibration of Photoelastic Coatings", **Measurement Group Technical Note TN-701,** Measurement Group UK Ltd, 1989.

"Introduction to Stress Analysis by the PhotoStress Method", **Measurement Group Technical Note TN-702,** Measurement Group UK Ltd, 1989.

"Final Review of Project Support Tasking DNA1217 - Damage Tolerance in FRP Ship's Structures",**Defence Research Agency,** Report No. DRA/SMC/CR963033, May 1996.

"Fatigue Performance of Damaged and Undamaged GRP T Joints", **Defence Research Agency,** Report No. DRA/SMC/TR963012, March 1996.

"Microstructural Analysis of Fatigue and Shock Damaged T Joints", **Defence Research Agency,** Report No. DRA/SMC/TR963013, March 1996.

"GRP Boundary Angle Strength Tests", **Vosper Thornycroft (UK) Ltd,** Report No. D/89-452, 1989.

"Full Scale Tests on GRP Boundary Angles", **Vosper Thornycroft (UK) Ltd,** Report No. D/89-455, 1989.

"Experimental Characterisation of the Strength of Plywood-GRP Bonded T-Section Joints", **Wolfson Unit for Marine Technology and Industrial Aerodynamics,** Report No. 1231, July 1995.

"Standard Test Methods for Tension-Tension Fatigue of Orientated Fibre, Resin Matrix Composites", **ASTM Standard D 3479,** 1982.

"GRP Ship Design", **Naval Engineering Standards,** NES140, Issue 2, Undated.

"Rules for Building and Classing Reinforced Plastic Vessels", **American Bureau of Shipping,** New York, 1978.

"Rules for Classification of High Speed and Light Craft", **Det Norske Veritas,** Hovik, 1991.

"Rules for Yachts and Small Craft", **Lloyds Register of Shipping,** London, 1983.

Bach, P. W. 'Glass and Hybrid Fibre Performance', in Design of Composite Structures Against Fatigue - Applications to Wind Turbine Blades, Ed. Mayer, R. M., Mechanical Engineering Publications Ltd, 1996.

Beaumont, W.R. 'Damage and Fracture of Fibre Composites' in Design with Advanced Composite Materials, Ed Philips, L.N., The Design Council, 1989.

Beaumont, P.W.R. 'Failure Analysis of Composite Materials' Delaware Composite Design Encyclopedia, Vol. 4, Technomic Publishing Company, 1990.

Bily, M. 'Cyclic Deformation and Fatigue of Metals', Material Science Monographs 78, Elsevier, 1993.

Boller, K.H. 'Effect of Pre-Cyclic Stresses on Fatigue Life of RP Laminates', Modern Plastics, Vol 42,April 1965, pp162-173.

Bourban, P.E., Cantwell, W.J., Kausch, H.H. and Youd, S.J. 'Damage Initiation and

Development in Chopped Strand Mat Composites' ICCM 5, Honolulu, Hawaii, 1989.
Bream, R.G., Gasper, B.C., Lloyd, B.E. and Page, S.W.I. "The SPATE 8000 thermoelastic camera for dynamic stress measurement on nuclear plant components", Proc. 2nd Int. Conf. on Stress Analysis by Thermoelastic Techniques, 1987, SPIE Vol 931, London, pp132-148.
Chalmers, D.W., Osborn, R.J. and Bunney, A. "Hull Construction of MCMV's in the United Kingdom", RINA Symposium on Mine Warfare Vessels and Systems, June 1984.
Chang, C.S., Pimbley, W.T. and Conway, H.D. 'An Analysis of Metal Fatigue Based on Hysteresis Energy' IBM Technical Report, TR 01.1047, Sept. 25, 1967.
Chou, P.C. and Croman, R. 'Degradation and Sudden-Death Models of Fatigue of Graphite/Epoxy Composites', in Composite Materials: Testing and Design (Fifth Conference), ASTM STP 674, 1978, pp431-454.
Chou, P.C. and Croman, R. 'Residual Strength in Fatigue Based on the Strength-Life Equal Rank Assumption', Journal of Composite Materials, Vol 12, April 1978, pp177-194.
Cope, R.D. and Pipes, R.B. "Design of the Spar Wingskin Joint", Proceedings of the Fourth Conference on Fibrous Composites in Structural Design, edited by Lenoe, E.M., Oplinger, D.W. and Burke, J.J., San Diego, California, November 14-17, 1978, pp603-618.
Curtis, P.T. 'The Fatigue Behaviour of Fibrous Composite Materials' Journal of Strain Analysis 24 (4) 1989 pp47-56.
Curtis, P.T. 'Theoretical Predictions of Failure Mechanisms and Strength', in 'Composite Materials in Maritime Structures, Vol 1: Fundamental Aspect's', Shenoi, R.A. and Wellicome, J.F. (ed), Cambridge Ocean Technology Series 4, Cambridge University Press, 1993, pp280-307.
Dharan, C.K.H. 'Fatigue Failure Mechanisms in a Unidirectionally Reinforced Composite Material', in Fatigue of Composite Materials, ASTM STP 569, 1975 pp171-188.
Dixon, R.H., Ramsey, B.W. and Usher, P.J. "Design and Build of the GRP Hull of HMS Wilton", Proceedings of the Symposium on GRP Ship Construction, The Royal Institution of Naval Architects, London, October, 1972, pp1-32.
Dodkins, A.R. "The Structural Design of the SRMH", RINA Symposium on Mine Warfare Vessels and Systems-2, May 1989.
Dulieu-Smith, J.M. "Alternative calibration techniques for quantitive thermoelastic stress analysis", Strain, Journal of the British Society for Strain Measurement, February 1995, pp9-16.
Dulieu-Smith, J.M., Shenoi, R.A., Read, P.J.C.L., Quinn, S. and Moy, S.S.J. "Thermoelastic stress analysis of a GRP tee joint" Journal of Composite Materials, (in press).
Dulieu-Smith, J.M. and Stanley, P. "Developments in the interpretation of the thermoelastic response of composite materials", Proc. 2nd Int. Seminar on Exp. Techniques and Design in Composite Matls., Sheffield, 1994, pp120-139.
Echtermeyer, A.T., Engh, B. and Buene, L. 'Lifetime and Young's Modulus Changes of

Glass/Phenolic and Glass/Polyester Composites under Fatigue' in Composites, Vol. 26(1), 1995, pp10-16.

Echtermeyer, A. T., Engh, B. and Buene, L. 'Influence of Matrix and Fabric' in Design of Composite Structures Against Fatigue - Applications to Wind Turbine Blades, Ed. Mayer, R. M., Mechanical Engineering Publications Ltd, 1996.

El-Kadi, H. and Ellyin, F. 'Effect of Stress Ratio on the Fatigue of Unidirectional Glass Fibre/ Epoxy Composite Laminae', Composites, Vol 25(10), 1994, pp917-924.

Ellyin, F. and El-Kadi, H. 'A Fatigue Failure Criterion for Fibre Reinforced Composite Laminae', Composite Structures, Vol 15, 1990, pp61-74.

Feltner, C.E. and Morrow, J.D. 'Microplastic Strain Hysteresis Energy as a Criterion for Fatigue Fracture', Transactions of ASME,Journal of Basic Engineering, March, 1961, pp15-22.

Gibbs and Cox "Marine Design Manual for GRP", McGraw Hill Book Company, New York, 1960.

Gillespie, J.W. and Pipes, R.B., "Behaviour of Integral Composite Joints - Finite Element and Experimental Evaluation", Journal of Composite Materials, Volume 12, October 1978.

Green, A.K. and Bowyer, W.H. "The Development of Improved Attachment Methods for Stiffening Frames on Large GRP Panels", Composites 12, January 1981.

Grimes, G.C. 'Experimental Study of Compression-Compression Fatigue of Graphite/Epoxy Composites' in Test Methods and Design Allowables for Fibrous Composites, ASTM STP 734, 1981, pp281-337.

Hahn, H.T. and Kim, R.Y. 'Proof Testing of Composite Materials' Journal of Composite Materials, Vol 9, July 1975, pp297-311.

Hahn, H.T. and Kim, R.Y. 'Fatigue Behaviour of Composite Laminate', Journal of Composite Materials, Vol 10, April 1976, pp156-180.

Halford, G.R. 'The Energy Required for Fatigue', Journal of Materials, Vol 1(1), March, 1966, pp3-18.

Halpin, J.C., Jerina, K.L. and Johnson, T.A. 'Characterisation of Composites for the Purpose of Reliability Prediction', in Analysis of Test Methods for High Modulus Fibres and Composites, ASTM STP 521, 1973, pp5-64.

Harrhy, J. "Structural Design of Single Skin Glass Reinforced Plastic Ships", Proceedings of the Symposium on GRP Ship Construction, The Royal Institution of Naval Architects, London, October 1972, pp57-68.

Harwood, N and Cummings, W.M. (eds), Thermoelastic Stress Analysis, IOP Publishing Ltd, Bristol, 1991.

Hashin, Z. 'Cumulative Damage Theory for Composite Materials: Residual Life and Residual Strength Methods', Composites Science and Technology, 23, 1985, pp1-19.

Hawkins, G.L. "The Behaviour of Bonded Out-of Plane Joints in Fibre Reinforced Plastic

Structures" PhD Thesis, Department of Ship Science, University of Southampton, Southampton, April 1995.

Hawkins, G.L., Holness, J.W., Dodkins, A.R. and Shenoi, R.A. 'The Strength of Bonded Tee-Joints in FRP Ships', Plastics Rubber and Composites Processing and Applications, 19(5), 1993, pp279-284.

Hawkins, G.L. and Shenoi, R.A. 'A Parametric Study to Determine the Influence of Geometric Variations on the Performance of a Bulkhead to Shell Plating Joint', Proceedings of the 9th International Conference on Composite Materials, ICCM/9, Madrid, 12-16 July 1993, Vol IV, pp97-104.

Highsmith, A.L. and Reifsnider, K.L. 'Stiffness-Reduction Mechanisms in Composite Laminates', in Damage in Composite Materials, ASTM STP 775, 1982, pp103-117.

Hofer, K.E. and Skaper, G. 'Fatigue Endurance of Glass Reinforced Plastic Laminate Material in a Marine Environment' 40th Annual Conference, Reinforced Plastics/ Composites Institute, The Society of the Plastics Industry, 1985.

Howson, J.C., Rymill, R.J. and Pinzelli, R.F. 'Fatigue Performance of Marine Laminates Reinforced with Kevlar Aramid Fibre' Journées Européennes des Composites, International Conference and Exhibition, Paris, April 1992.

Hwang, W and Han, K.S. 'Cumulative Damage Models and Multi-Stress Fatigue Life Prediction', Journal of Composite Materials, Vol 20, March 1986, pp125-153.

Hwang, W and Han, K.S. 'Fatigue of Composites - Fatigue Modulus Concept and Life Prediction', Journal of Composite Materials, Vol 20, March 1986, pp154-165.

Hwang, W and Han, K.S. 'Fatigue of Composite Materials - Damage Model and Life Prediction', in Composite Materials: Fatigue and Fracture, Vol 2, ASTM STP 1012, 1989, pp87-102.

Imanaka, M. ***et al.*** 'Fatigue Life Estimation of Adhesively Bonded Lap Joints' Transactions of the ASME, Vol. 110, Oct. 1988, pp350-354.

Ishikawa, T. and Chou, T.W. 'Nonlinear Behaviour of Woven Fabric Composites' Journal of Composite Materials, Vol. 17, September 1983, pp399-413.

Jessen, S.M. and Plumtree, A. 'Continuum Damage Mechanics Applied to Cyclic Behaviour of a Glass Fibre Composite Pultrusion', Composites, Vol. 22, No. 3, May 1991, pp181-190.

Johnson, W.S. and Mall, S. 'A Fracture Mechanics Approach for Designing Adhesively Bonded Joints', in Delamination and Debonding of materials, ASTM STP 876, 1985, pp189-199.

Junhou, P. and Shenoi, R.A. 'An examination of Key Aspects Defining the Performance Characteristics of Out-of-Plane Joints in FRP Marine Structures', Composites, Vol. 27A, No. 2, 1996, pp89-103.

Lee, L.J., Yang, J.N. and Sheu, D.Y. 'Prediction of Fatigue Life for Matrix Dominated Composite Laminates', Composite Science and Technology, Vol 46, 1993, pp21-28.

Mandell, J.F. and Meier, U. 'Effects of Stress Ratio, Frequency, and Loading Time on the Tensile Fatigue of Glass-Reinforced Epoxy', in Long-Term Behaviour of Composites, ASTM STP 813, 1983, pp55-77.

Matthews, F.L., Kilty, P.F. and Godwin, E.W. 'A Review of the Strength of Joints in Fibre Reinforced Plastics, Pt 2 - Adhesively Bonded Joints', Composites, Vol. 13, No. 1, 1982, pp29-37.

Miner, M.A. 'Cumulative Damage in Fatigue', Journal of Applied Mechanics, September, 1945, pp159-164.

Opp, D.A., Skinner, D.W. and Wiktorek, R.J. 'A Model for Polymer Fatigue', Polymer Engineering and Science, Vol 9(2), March, 1969, pp121-130.

Owen, M.J. and Dukes, R. 'Failure of Glass-Reinforced Plastics Under Single and Repeated Loading' in Journal of Strain Analysis, Vol. 2 (4), 1967, pp272-279.

Owen, M.J. and Howe, R.J. 'Cumulative Damage in Chopped Strand Mat/Polyester Resin Laminates' Proc. of 8th Int. Reinforced Plastics Congress, BPF, London, 1972.

Owen, M.J. and Rose, R.G. 'Polyester Flexibility Versus Fatigue Behaviour of RP' Modern Plastics, vol. 47 (11), November 1970, pp130-138.

Owen, M.J. and Smith, T.R. 'Some Fatigue properties of Chopped Strand Mat/Polyester Resin Laminates' in Plastics and Polymers, February 1968, pp33-44.

Pitts, E.C. and Dorey, A.L. "Experience with the Design of GRP MCM Vessels", RINA Symposium on Mine Warfare Vessels and Systems, June 1984.

Plumtree, A. and Shen, G. 'Fatigue Damage Evolution and Life Prediction', International Conference on Composite Materials VIII, Honolulu, Hawaii, 1991.

Poppen, M. and Bach, P. 'Influence of Spectral Loading' in Design of Composite Structures Against Fatigue - Applications to Wind Turbine Blades, Ed. Mayer, R. M., Mechanical Engineering Publications Ltd, 1996.

Poursartip, A., Ashby, M.F. and Beaumont, P.W.R. 'Damage Accumulation in Composites During Fatigue' in Fatigue & Creep of Composite Materials, Ed Talreja, R. and Lilholt, H., RISO National Laboratory, Roskilde, Denmark 1982, pp279-284.

Read, P.J.C.L., Dulieu-Smith, J. and Shenoi, R.A. 'Thermoelastic and Photoelastic Analysis to Characterise Stresses in FRP Connections', Proc. 1st. Int. Conf. on Composite Science and Technology, Durban, 18-20 June, 1996, pp415-420.

Read, P.J.C.L. and Shenoi, R.A. 'A Review of Fatigue Damage Modelling in the Context of Marine FRP Laminates', Marine Structures, Vol. 8, 1995, pp257-278.

Read, P.J.C.L. and Shenoi, R.A., 'A Design Procedure for FRP Tee Joints Subjected to Fatigue', Int Jnl of Fatigue, (under preparation).

Read, P.J.C.L. and Shenoi, R.A., 'Experimental and Theoretical Characterisation of FRP Tee Joints', Composite Structures, (under preparation).

Reifsnider, K.L. and Jamison, R. 'Fracture of Fatigue-Loaded Composite Laminates'

International Journal of Fatigue, October 1982, pp187-197.
Reifsnider, K. L., Stinchcomb, W. W. and O'Brien, T. K. 'Frequency Effects on a Stiffness-Based Fatigue Failure Criterion in Flawed Composite Specimens' Fatigue of Filamentary Composite Materials, ASTM STP 636, 1977,pp171-184.
Reifsnider, K.L. and Talug, A. 'Analysis of Fatigue Damage in Composite Laminates' International Journal of Fatigue, January 1980, pp3-11.
Renz, R., Altstadt, V. and Ehrenstein, G.L. 'Fatigue Behaviour of RP Described by Hysteresis Measurements' 45th Annual conference, Composites Institute, SPI, Session 19-B, February 1990, pp1-9.
Saff, C.R. 'Effect of Load Frequency and Lay-up on Fatigue Life of Composites', in Long-Term Behaviour of Composites, ASTM STP 813, 1983, pp78-91.
Scholte, H.G. 'Fatigue Characteristics' in Composite Materials in Maritime Structures, Vol. 2, Ed. Shenoi, R.A. & Wellicome, J.F., Cambridge Ocean Technology Series 5, 1993.
Scholte, H. G. and van-Leeuwen, R. T. 'Investigation on the Behaviour Under Fatigue Loading of Orthogonally Placed Plates of Glass Reinforced Polyester', Technical University of Delft Report No. 211, November 1977.
Sendeckyj, G.P. 'Fitting Models to Composite Materials Fatigue Data', in Test Methods and Design Allowables for Fibrous Composites, ASTM STP 734, 1981, pp245- 260.
Schultz, K., Reese, E. and Chou, T.W. 'Fatigue Behaviour and Damage Development in Woven Fabric and Hybrid Fabric Composites' ICCM VI and ECCM 2, Proceedings of Sixth Int. Conf. and Second European Conf. on Composite Materials, 1987, Elsevier Applied Science, London, Vol. 4, pp89-99.
Schutz, D. and Gerharz, J.J. 'Fatigue Strength of a Fibre-Reinforced Material', Composites, Oct. 1977, pp245-250.
Shenoi, R.A. and Hawkins, G.L. 'Influence of Material and Geometry Variations on the Behaviour of Bonded Tee Connections in FRP Ships', Composites, 23(5), September, 1992, pp335-345.
Shenoi, R.A. and Hawkins, G.L. 'The formulation of a Curved Composite Brick Finite Element Using a Layer-Wise Theory', ICCM-10, Proceedings of the 10th Int. Conf. on Composite Materials, 1995, Woodhead Publishing, Cambridge, Vol. 5, p149
Shenoi, R.A., Read, P.J.C.L. and Hawkins, G.L. 'Damage Characterisation of FRP Single-Skin Tee Joints' RINA Small Craft Group Conference on Advanced Materials for Ships and Small Craft, RINA, London, 1993.
Shenoi, R.A., Read, P.J.C.L. and Hawkins, G.L. 'Fatigue Failure Mechanisms in Fibre-Reinforced Plastic Laminated Tee Joints' Int. Jnl. of Fatigue, 17(6), 1995, pp415-426.
Shenoi, R.A., Read, P.J.C.L., Walters, C.L. and Thelu,S.C.M. 'The Development of a Flexible, Multi-Configuration structural Test Facility', Int. Jnl. of Fatigue, 15(4), July, 1993, pp317-323.

Smith, C.S. 'Structural Problems in the Design of GRP Ships' Proceedings of the Symposium on GRP Ship Construction, RINA, London, 1972, pp33-52.

Smith, C.S. 'Design of Marine Structures in Composite Materials' Elsevier Applied Science, London 1990.

Stanley, P. "Stress separation from SPATE data for a rotationally symmetrical pressure vessel", Proc. Int. Conf. on Stress and Vibration (Incorporating 3rd Int. Conf. on Stress Analysis by Thermoelastic Techniques), SPIE Vol. 1084, London, 1989, pp72-83.

Stanley, P and Chan, W.K. "Stress studies in composite cylinders based on the measurement of infra-red emissions due to cyclic loading", Proc. Int. Symp. on Mechanical Properties of Composites, Prague, 1986, pp266-273.

Stanley, P. and Dulieu-Smith, J.M. "A thermoelastic study of the stresses in pinloaded lugs", Proc. of 6th Nat. Symp. on Exp. Mech., Craiova, 1992, pp160-169.

Stanley, P. and Dulieu-Smith, J.M. "Progress in thermoelastic evaluation of mixed-mode stress intensity factors", Proc. of S.E.M. Spring Conf. on Exp. Mech., Dearbom, 1993, pp617-629.

Stowell, E.Z. 'A Study of the Energy Criterion for Fatigue', Nuclear Engineering and Design, Vol 3, 1966, pp32-40.

Sun, C.T. and Chan, W.S. 'Frequency Effect on the Fatigue Life of a Laminated Composite', in Composite Materials: Testing and Design, ASTM STP 674, 1979, pp418-430.

Surendra, K.J. 'Matrix Contribution to Fatigue Behaviour of Glass Reinforced Polyester Composites' Journal of Reinforced Plastics and Composites, Vol. 6, October 1987, pp343-357.

'Users Manual for ANSYS', **Swanson Analysis Systems**, Houston, PA, USA, 1992.

Tanimoto, T. and Amijima, S. 'Progressive Nature of Fatigue Damage of Glass Fibre Reinforced Plastics', Journal of Composite Materials, Vol. 9, October 1975, pp380-390.

Talreja, R. 'Transverse Cracking and Stiffness Reduction in Composite Laminates', Journal of Composite Materials, Vol 19, July 1985, pp355-375.

Talreja, R. 'Fatigue of Composite Materials' Technomic Publishing Company, Pennsylvania 1987.

Thompson, W. (Lord Kelvin) "On the dynamical theory of heat", Trans. Royal Society, Vol. 20, 1853, pp261-283.

Tiu, W.P. and Sage, G.N. 'Fatigue Strength of Bonded Joints in Carbon Fibre Reinforced Plastics', in Structural Adhesives in Engineering, Proceedings of the Institution of Mechanical Engineers, Mechanical Engineering Publications Ltd, London, 1986, pp77-82.

Whitney, J.M. 'Fatigue Characterisation of Composite Materials', in Fatigue of Fibrous Composite Materials, ASTM STP 723, 1981, pp133-151.

Wu, E.M. 'Strength and Fracture of Composites' in Composite Materials: Fracture and Fatigue, Vol 5, Ed Broutman, L.J., Academic Press, 1974.

Yang, J.N. 'Fatigue and Residual Strength Degradation for Graphite/Epoxy Composites Under Tension-Compression Cyclic Loadings' Journal of Composite Materials, Vol 12, January 1978, pp19-39.

Yang, J.N., Jones, D.L., Yang, S.H. and Meskini, A. 'A Stiffness Degradation Model for Graphite/Epoxy Laminates', Journal of Composite Materials, Vol 24, July 1990, pp753-769.

Yang, J.N. and Liu, M.D. 'Residual Strength Degradation Model and Theory of Periodic Proof Tests for Graphite/Epoxy Laminates' Journal of Composite Materials, Vol 11, April 1977, pp176-203.

Yang, J.N., Lee, L.J. and Sheu, D.Y. 'Modulus Reduction and Fatigue Damage of Matrix Dominated Composite Laminates', Composite Structures, Vol 21, 1992, pp91-100.

Yang, J.N. and Shanyi, D. 'An Exploratory Study into the Fatigue of Composites Under Spectrum Loading', Journal of Composite Materials, Vol 17, Nov. 1983, pp511-527.

Appendix A - Application of Theoretical Modelling Techniques

A1 Characterisation of S-N Curves

To assess the applicability the theories given in chapter 4 to marine applications, fatigue data has been gathered for various laminates from Hwang and Han (1986), Howsen *et al.* (1992) and Owen and Smith (1968). There is a paucity of data relating to representative marine lay-ups; hence, some data pertaining to laminates more commonly found in the aerospace industry have also been used. The experimental data points shown in each figure are mean values of the life data at each load/ stress level. The number of these points shown relates to the amount of data provided by each literature source.

The straight line model, Hahn and Kim's model and one of Hwang and Han's models have been applied to the collected S-N data. In each case the individual model parameters and material constants have been calculated using linear least squares methods. The figures A.1 to A.4 show the results of this exercise. Correlation coefficients, r, for each fit have also been indicated.

Figure A.1a shows the S-N curve of a 100% glass fabric/ polyester resin lay-up termed Rovimat loaded in bending. This laminate is a marine laminate incorporating a gel coat. As can easily be seen the best overall fit was obtained with the log-linear straight line theory. However the fit at the extreme ends of the data, for low and high cycle fatigue, was very poor. A similar observation was made for the S-N curve of the glass/aramid hybrid termed Aramat shown in figure A.2. This again was a marine laminate incorporating a gel coating.

For low-cycle fatigue data, pertaining to the glass fibre cloth/ epoxy resin laminate loaded inplane, the best fit was made using the theory proposed by Hwang and Han (see figure A.3). However the straight line S-N curve still gave a good approximation to the data.

Figure A.4 shows the high-cycle fatigue S-N curve for a glass CSM/ polyester resin laminate loaded inplane. The best fit for this data was again made using the straight line S-N curve. The Hwang and Han theory was also observed to correlate fairly closely to the data and could possibly give a "best fit" for the complete S-N data.

Figure A.1b shows only the low-cycle fatigue part of the Rovimat S-N curve. In this case the best fit was made using Han and Kim's power law. This is an obvious result when the shape of the complete curve is examined, and it can be seen that a similar result could be obtained using the Hwang and Han theory for the high-cycle fatigue part of this curve. Hence the reason for an established characterisation technique can be understood. That is, the type of approach chosen to characterise the S-N curve data should depend on what part of the curve is most relevant. Therefore the general shape of the chosen S-N curve should

firstly be assessed and then a curve fit chosen appropriately.

A2 Application of Cumulative Damage Theories

In a similar way to the procedure adopted for the characterisation of S-N curves, a number of cumulative damage theories were applied to experimental data collected from the literature. Experimental data relating to cumulative damage for any type of laminate was found to be extremely rare and, although a wide literature search was made, no data representative of marine laminates was found to exist. The majority of the data available was for two-stage loading cases, although Yang and Shanyi (1983) and Schutz and Gerharz (1977) have both dealt with spectrum loading of a carbon fibre / epoxy laminate representative of a fighter aircraft's wing.

The laminates chosen for the theoretical comparison were all glass fibre / epoxy resin laminates. These were chosen because they were seen to have some relevance for marine structural applications. The most applicable data obtained was for a woven glass cloth / epoxy laminate (Hwang and Han (1986)). Also obtained were a further three sets of data relating to glass cross-ply / epoxy laminates, each having different stacking sequences, fibre volume fractions and epoxy resin systems (Hashin (1985), Boller (1965)). It must be remembered that these laminates were drawn from literature in the aerospace field and therefore have higher fibre volume fractions and different stacking sequences compared to those that might be found in marine structures.

The S-N curves for the four chosen laminates are shown in figure A.5. The curves are drawn direct from the literature as experimental data and are not regression curve fits. The shape of the curve for the woven glass cloth laminate is similar to those curves for the marine laminates in figures A.1 and A.2. It could therefore be argued that any conclusions drawn from the woven cloth laminate could apply to these marine laminates and therefore be extended to other marine structures. All three curves for the cross-ply laminates exhibit the familiar inverse S-shape and thus their fatigue life characteristics should be of a similar nature.

Application of four cumulative damage approaches was made to the two-stage loading data of the four chosen laminates. The approaches were, Hashin's residual strength method - equation (15), Hwang and Han's fatigue modulus method - equations(18-20), the Palmgren-Miner rule - equation(10) and the Hashin-Rotem method - equation(13). The results of the calculated predictions can be seen in tables A.1 to A.4. The initial stress level and number of cycles are represented by s_1 and n_1 respectively. The final stress level and residual life (number of cycles to failure) are represented by s_2 and n_{2r}.

Table A.1 contains the residual life results for the glass/ epoxy cross-ply laminate used by

Hashin (1985). The residual lives shown are average lives for each particular loading pattern. The table is split into two halves, the top half being high-low loading data and the bottom half low-high loading data. In the top half of the table the Hashin theory and the Palmgren-Miner rule both gave the closest predictions with average errors of 20% and 21% respectively. It should also be noted that the Hashin-Rotem theory also gave reasonable results with an average error of 32%. The Hashin residual strength theory relies upon a parameter α which, for this data, was taken to be 7. This value was given by Hashin for the data and it was confirmed for the purpose of this comparison by a parametric study assessing the accuracy of the theoretical predictions with change in α. It should be noted that when α=1 the residual life predictions are equal to those produced by the Palmgren-Miner rule. It can be seen that where a close prediction of the residual life has been made, the prediction is generally an overestimate. From the practical point of view it would be better for the theoretical predictions to be underestimates. In the bottom half of the table the closest predictions were given using the Hashin-Rotem method with an average error of 80%. Over the complete table the average errors for the Hashin Residual strength Method, the Palmgren-Miner rule and the Hashin-Rotem method were 72%, 64%and 56% respectively. The theory that gave the most number of inaccurate predictions was found to be Hwang and Han's fatigue modulus theory. This was not a surprising result, as the Hwang and Han theory relies heavily upon the assumption that the S-N curve can be characterised by the power law given previously, and it can easily be seen that this is not true. If one of the other cumulative damage approaches proposed by Hwang and Han was used, one based on a model which would characterise the S-N curve of this material well, then better results would be expected.

Table A.2 contains the residual life results for the woven glass cloth / epoxy laminate used by Hwang and Han (1986). Unfortunately the experimental data is extremely limited and this questions any conclusions drawn from it. The closest theoretical predictions were made by the Hashin-Rotem theory and Hwang and Han's theory with average errors of 2% and 3% respectively. Hwang and Han's S-N curve power law assumption can be said to be true in this case. The least accurate theory was found to be the Palmgren-Miner rule with an average error of 9%. Again the table was in two halves with high-low and low-high loading data, and again the closest predictions were generally overestimates of the experimental values. Note here that the Hashin residual strength method gave the best fit to the data when α=-4, (as opposed to α =7 for the cross-ply laminate). Both laminates are epoxy based, therefore the reason for the large difference in the parameter values could be related to the differing fatigue failure mechanisms of woven and unwoven composite materials, as previously explained. This difference can be seen in the shapes of the S-N curves of the two types of laminate as shown in figure A.5.

Tables A.3 and A.4 contain data for the two other glass cross-ply epoxy laminates investigated. To assess the possibility that the parameter α was a 'material constant', it was

given the established value of 7 in both cases. Table A.3, containing the residual life results for the glass cross-ply with epoxy 1009 resin (Boller (1965)), exhibits the same trends as those observed in table A.1. Again the most number of closest predictions was made by the Palmgren-Miner and Hashin's residual strength theories with average errors of 32% each. It should be noted that, as before, the Hashin-Rotem method also gave reasonable results with an average error of 34%. Yet again the most number of inaccurate predictions was made by Hwang and Han's theory which as before does not characterise the S-N curve shape very well. The good result obtained from Hashin's residual strength method seems to suggest that the parameter α can be assumed to be a material constant.

Table A.4 contains the residual life results for the glass cross-ply with the epoxy 1002 resin (Boller (1965)). It can be seen from the S-N curves (see figure A.5) that this laminate has very similar fatigue characteristics to the laminate whose results are contained in table 1. However the cumulative damage results for this final laminate show that in two of the loading cases, the theoretical predictions made by each of the methods are extremely inaccurate. The reason for this apparent collapse of all the theoretical predictive methods can be established if the experimental residual lives are compared with the S-N curve for this laminate. For example, at the stress level s=0.386 the fatigue life obtained from the S-N curve is N=89,580 cycles. Comparing this with the result for two stage loading where s_1=0.802 for n_1=3 cycles and s_2=0.386 it is found that the experimental residual life is 42 times greater than the single stress level life, that is n_{2r}=3,767,860 cycles. From this it could be concluded that certain loading patterns actually increase the fatigue life of these types of laminates. This would mean that any theory describing the damage accumulation within these laminates could not be based on the usual damage laws. This phenomenon however, has not been found again in any subsequent literature.

For the data given in the tables A.1-A.4 the most consistently accurate predictive method seems to be the Hashin-Rotem method - equation(13). However if one looks at the overall average errors for each method, ignoring the Hwang and Han theory, then it can be seen that the Hashin residual strength theory - equation(15) and the Palmgren-Miner rule - equation(10) also give reasonably accurate predictions. In fact the percentage errors are very similar for all three cases. If the experimental errors could be quantified for each particular test, then it may be found that it is difficult to establish which theoretical method is the most accurate.

A further observation is that the original Palmgren-Miner rule seems to be no worse in its predictions than any of the other 'newer' theories. This coupled with its ease of use and simple implementation in a practical situation compared to the relative complexity of the other predictive methods questions whether they are really more useful. Of course it must always be borne in mind that if the Palmgren-Miner rule is used it is likely to give an unconservative estimate of the fatigue life (Curtis (1993), Yang and Shanyi (1983)) and

therefore should be used with extreme caution.

Appendix B - Heavy Structures Test Rig FORTReSS

B1 Flexible Orthoginal Rig For Testing Real Ship Structures

The Ship Science heavy structures test rig, dubbed FORTReSS, was designed by an undergraduate team for the purpose of testing large marine structures constructed from composite materials. See Shenoi *et al.* (1993). This is by no means its test limitation. The rig is extremely flexible and adaptable and any kind of structural element, whether it be an aerospace structure, automotive structure or part of a building, can be tested, on the condition that it conforms to the loading and space limitations of the test rig itself.

The test rig is comprised of three main components. A large adjustable reaction frame, a hydraulic load delivery system and a computer control and data acquisition system. The 7.5 Tonne steel reaction frame can be adjusted to give a test area from 1000mm x 1000mm to 2440mm x 2440mm with a maximum depth of 1720mm. It is possible to test in the horizontal plane up to a load of 50 Tonnes and loads applied in the vertical plane can be up to 16 Tonnes. Three hydraulic pressure mains ring the outside of the test frame with four plug in points available for flexible hose attachment. The maximum flow rate delivered by a hydraulic power pack is 19.55 ltr/min at a maximum pressure of 240bar. Computer control is performed by a 33MHz PC-486 with a data acquisition interface supporting 32 measurement input channels and 4 control output channels.

For a typical test the basic test facility must be adapted by the addition of further structure, to either produce the correct loading configuration or, hold the test specimen and apply the correct boundary conditions. Hydraulic actuators can be positioned anywhere within the reaction frame as required and plugged into one of the three hydraulic ring mains. Hydraulic pressure or the applied load, and hydraulic flow rate or loading rate, can then be controlled using electro-hydraulic servo valves via the computer to suit the specific test loading requirements. Test measurements are also performed by the computer and a large variety of different measurements can be made. The management of the measurement data, calculations using the data to produce the correct control output and the measurement display format on the computer screen are all defined for each different test using the computer control and data acquisition software.

The computer software used to control FORTReSS is Labtech Notebook. This is a general control and data acquisition package which provides a means of creating individual experimental control programs based around an icon block environment. The icon blocks represent input and output devices and also perform data calculation and storage. They are arranged as required and data links are established between them simply by joining them together with arrows. The user has complete control over all the necessary variables within each block and can even organise the layout of the VDU screen, for experimental

measurement display.

The test procedure followed will vary from test to test but in general there are four main steps. (1) The computer control and measurement program is started. (2) A manual bypass valve on the hydraulic power pack is turned to the on position allowing pressure into the ring mains. (3) The computer performs the experiment and continues until it encounters a defined situation causing it to stop, such as specimen failure. (4) The manual bypass valve is turned to the bypass position isolating the hydraulic power pack from the experiment. A manual bypass valve is used as opposed to an electronic bypass valve so as to incorporate a fail safe isolation device into the experimentation procedure.

Tests that have been undertaken using FORTReSS include, the evaluation of the ultimate strength of various foam sandwich beams, static and fatigue five point bending of single skin FRP deck sections, evaluation of the ultimate strength of an aircraft wing spar and static four point bending of aluminium deck sections.

B2 Calibration of Transducers

The transducers used within the FORTReSS rig can be of any type. The prerequisite is that, for it to be used, a transducer must produce a voltage output. The transducers most commonly used are load cells, displacement transducers and strain gauges.

The displacement transducers used in the FORTReSS are linear potentiometers. Their output voltage varies from a nominal 0 volts when the potentiometers are fully retracted to a nominal 5 volts when they are fully extended. Calibration is therefore very simple; a potentiometer is fully retracted and a voltage reading is taken, this voltage becomes the zero offset. The voltage is then zeroed with this offset and the potentiometer is fully extended. A voltage reading is again taken and a scale factor is calculated from,

$$Scale\ factor = \frac{Stroke\ (mm)}{Voltage\ Reading}$$

the scale factor can then be used within the data acquisition program (Labtech Notebook) to produce displacement measurements in milimeters.

The load cells used in the FORTReSS are a basic rod type, consisting of a steel rod with a full strain gauge Wheatstone bridge bonded around its circumference. Calibration is performed by placing each load cell in a calibrated loading machine, the desired calibration load is then applied and the output voltage is measured. A decade resistance box, which is a readable variable resistor, is then applied across one arm of the load cell's strain gauge bridge and the resistance is changed until the voltage output from the load cell returns to zero. The load is then removed from the load cell and the 'shunt' resistance is recorded.

The load cell can then be put back into the FORTReSS and as with the linear potentiometers a zero voltage reading is taken. The shunt resistance is then applied to one arm of the load cell strain gauge bridge and a voltage reading is taken. This voltage is equivalent to the voltage that will be output if the load cell is loaded to the calibration load. A calibration table is then created within the data acquisition program (Labtech Notebook) giving voltage output at zero load and voltage output at calibration load. Any load in between these two values can be found by linear interpolation and any load above the calibration load can be found by linear extrapolation, which is performed within Labtech Notebook.

Calibration of the strain gauges was performed in a similar manner to the calibration of the load cells, with a shunt resistance. The shunt resistor value in this case is calculated using the following,

$$R_{SH} = \frac{R_g \, x \, 10^6}{GF.\varepsilon_c.AA} - R_g$$

where ε_c is the calibration strain value, R_g is the gauge resistance, GF is the gauge factor and AA is the number of active arms. A zero voltage reading is taken and the gauge is zeroed. The shunt resistance is then applied across the strain gauge using a decade resistance box and a voltage reading is taken. This voltage reading is equivalent to the voltage output from the gauge when it is subjected to the calibration strain value. A scale factor can then be calculated from,

$$Scale\ Factor = \frac{Calibration\ Strain}{Voltage\ Reading}$$

the scale factor can then be used within the data acquisition program (Labtech Notebook) to produce strain measurements directly.

B3 Calibration of Fatigue Control Program

Initial calibration of the closed loop control program was performed to obtain two constants referred to as the offset constant and scale factor. These constants controlled how the error signal, derived from the comparator part of the program, was converted into an input signal for the servo hydraulic control valves. The values of the two constants was established for each load magnitude by an iterative process. Initially the values were set using the following,

$$Offset\ Constant = 2.5$$

The overall system pressure is also initially set at a value calculated from,

$$Scale\ Factor = \frac{Max\ Load - Min\ Load}{2.5}$$

$$Pressure = \frac{Max\ Load}{Area\ of\ Ram}$$

this pressure is set at the hydraulic power pack pump. The control program is now run with a specimen in place and the wave form is observed. If the wave form is overdamped then the scale factor must be reduced. If the wave form is unstable or underdamped then the scale factor must be increased. When the correct scale factor is achieved, that is when the wave form is a regular sine wave, then the overall system pressure can be adjusted to achieve the correct maximum load. The offset constant can also be adjusted at this point to achieve the correct minimum load.

B4 Frequency Verification

The FORTReSS uses electro-hydraulic servovalves to control the hydraulic flow and pressure during testing. These valves can be nonlinear in their behaviour during dynamic applications. In the case where the valves are being used in a cyclic manner, such as in fatigue control, erroneous frequencies can be produced.

To check for erroneous frequencies in the fatigue control setup of the tee joints, a spectral analysis was made of the frequency produced by the FORTReSS control system. This was achieved by running a tee joint in the fatigue setup at the required frequency of 1Hz. The output from the control loop loadcell was then amplified using the FORTReSS amplfiers and fed directly into a Hewlett-Packard HP3566A Digital Signal Analyser. The analyser was controlled using a PC running the Hewlett-Packard Analyser Software. The frequencies combining to produce the waveform seen by the tee joints could then be isolated and any anomalies could be identified.

Figure B.1 shows the spectral analysis of the loadcell signal at a fairly low applied load of 0.4 kN. A low applied load was chosen for two reasons; firstly, the spectral analyser could not deal with any signal larger than that produced at this load and secondly, at lower loads the loadcells resolution introduces more inaccuracies and hence a worst case measurement can be made of the applied frequency. The figure shows that the primary frequency is 1Hz, with a small interference from 2Hz and 3Hz frequencies. The fact that as detailed in chapter 2, higher frequencies lead to longer fatigue lives seems to indicate that the small amplitude 2 and 3Hz frequencies are insignificant.

Appendix C - Thermoelastic and Photoelastic Theory

C1 Thermoelastic Analysis using SPATE

When a material is subjected to an elastic cyclic stress a small temperature change is induced which is proportional to the sum of the principal stress changes in the material. This is the thermoelastic effect which was first formulated by Lord Kelvin in 1853, Thompson (1853). The standard equipment for thermoelastic stress analysis is the SPATE (Stress Pattern Analysis by Thermal Emissions) system. The conventional SPATE system incorporates a highly sensitive single-cell infra-red detector which operates in a scanning mode over a pre-defined area. A point-by-point surface stress map is developed within the SPATE system computer and over a period of 1 to 2 hours a full field stress image is available for analysis. A full SPATE system description and the underlying theory are presented by Harwood and Cummings (1991).

Thermoelastic stress analysis is a well established technique for measuring the stresses in linear elastic, isotropic, homogeneous materials such as metals, for example, Bream *et al.* (1987), Stanley (1989), Stanley and Dulieu-Smith (1992) and (1993). Kelvin's formulation shows that a small temperature change is directly related to the change in the sum of the principal surface stresses by,

$$\Delta T = KT(\sigma_1 + \sigma_2) \qquad \text{(C1)}$$

where ΔT is the small temperature change due to the thermoelastic effect, T is the absolute temperature of the surface body, σ_1 and σ_2 are the changes in the principal surface stresses and K is the thermoelastic constant which is directly related to the material properties of the body in the form,

$$K = \frac{\alpha}{\rho C_p} \qquad \text{(C2)}$$

where α is the coefficient of thermal expansion of the body, ρ is the density and C_p is the specific heat at constant pressure.

When the small surface temperature change, ΔT, is measured using an infra-red detector such as the SPATE detector, equation (C1) can be simply restated as,

$$\sigma_1 + \sigma_2 = AS \qquad \text{(C3)}$$

where S is the thermoelastic signal and A is a calibration constant.

The use of the thermoelastic technique for the analysis of composite materials is a more recent development. A review of developments in the understanding of the nature of the

thermoelastic response of composites is given by Dulieu-Smith and Stanley (1994). In the case of orthotropic composites Stanley and Chan (1986) showed that equation (C1) should be modified so that,

$$\Delta T = \frac{T}{\rho C}(\alpha_p \sigma_p + \alpha_t \sigma_t) \qquad \text{(C4)}$$

where α_p and α_t are the two principal coefficients of thermal expansion of the material and σ_p and σ_t are the normal stress changes in the directions of the material axes.

The SPATE relationship between the thermoelastic signal and the stress changes can then be expressed as,

$$\sigma_p + \alpha \sigma_t = A'S \qquad \text{(C5)}$$

where α is the ratio of the principal coefficients of thermal expansion, i.e. α_t/α_p, and A' is a calibration constant. It may be possible to derive A' and α using material property values given in the literature. Unfortunately for many materials these values are unreliable due to variations in the materials used for constructing the composite and differences in the manufacturing process. A better approach is to determine A' and alpha experimentally using a calibration procedure. Details of various calibration techniques are presented by Dulieu-Smith (1995) and Dulieu-Smith *et al.* (to appear).

C2 Photoelastic Analysis using the Reflection Method

Photoelasticity is a widely used full-field technique for accurately measuring surface strains in structures during static or dynamic testing.

The reflection photoelastic method involves a birefringent plastic coating being bonded to the surface of the structure to be analysed. The plastic coating is bonded in place with an adhesive containing reflective particles. Then, as a load is applied to the structure, the coating is illuminated by polarized light from the polariser of a reflection polariscope. When viewed through the analyser of the polariscope, the coating displays strains as contours of colour which reveal the overall strain distribution and pinpoints highly strained regions. With an optical transducer attached to the polariscope, quantitative strain analysis can then be performed. Permanent records of overall strain distribution can be made by photography or through video.

Photoelasticity relies on the phenomenon that plastics behave isotropically when unstressed but become optically anisotropic when stressed, Measurement Group Technical Note TN-702 (1989). When a polarized beam of light propagates through a transparent plastic of thickness t, the light vector splits and two polarized beams are propagated in planes parallel to the directions of the principal strains. If the strain intensity in these two planes is ε_1 and ε_2, and

the speed of light vibrating in these directions is V_x and V_y, respectively, the time necessary to cross the plate for each of them will be t/V, and the relative retardation, δ, between the two beams is,

$$\delta = C\left(\frac{t}{V_x} - \frac{t}{V_y}\right) = t(n_x - n_y) \qquad \text{(C6)}$$

where C is the speed of light (3×10^{10} cm/sec) and n_x and n_y are the indices of refraction in the principal directions.

Brewster's law established that; "the relative change in index of refraction is proportional to the difference of the principal strains", so that,

$$(n_x - n_y) = K(\varepsilon_x - \varepsilon_y) \qquad \text{(C7)}$$

The constant K is the strain-optical coefficient and is material specific. The basic relation

$$\varepsilon_x - \varepsilon_y = \frac{\delta}{2tK} \qquad \text{(C8)}$$

for strain measurement using the reflection photoelasticity technique is therefore,
Due to the relative retardation δ , the two polarized light beams emerging from the plastic are no longer in phase. The beams interfere and the resulting light intensity is a function of the retardation and direction of the principal strains. With a plane polariscope set up the light intensity becomes zero when the polarizer or analyzer is parallel to the direction of principal strains. Adding optical filters in the light path produces circularly polarized light and the image observed is not influenced by direction. It can be shown that with a circular polariscope set up the light intensity becomes zero when,

$$\delta = N\lambda \qquad \text{(C9)}$$

where N is 1,2,3, etc. The number N is the fringe order and expresses the size of δ. The wave length λ is chosen to be 575nm because of its distictiveness and resolution. The relation for strain measurement can then be expressed as,

$$\varepsilon_x - \varepsilon_y = N\frac{\lambda}{2tK} = Nf \qquad \text{(C10)}$$

where f is the fringe value and N is the result of measurements. The value of f is obtained for a particular photoelastic coating by calibration. Details of the calibration procedure are given in Measurement Group Technical Note TN-701.

Appendix D - Calibration of Thermoelastic Constants

The thermoelastic equation governing SPATE measurement of composite materials is,

$$\sigma_p + \alpha\sigma_t = A'S \tag{D1}$$

Under certain loading conditions σ_p or σ_t can be eliminated from the thermoelastic equation making it possible to uniquely determine the constants A' or α. Of particular interest is the quantification of stresses in the boundary angles of the B type joint. This is because it is delamination of the boundary angles, due to normal interlaminar stresses, that is the initial failure mechanism in this type of joint.

Although the tee joint boundary angle material consists of layers of woven roving and chopped strand mat, in the through-thickness plane the material can be approximated to a unidirectional material. If a unidirectional material is loaded parallel to the fibre direction then the principal directions of the material are aligned with the principal stress directions and $\sigma_t = 0$. The principal stress σ_t can therefore be eliminated from equation (D1) by loading the boundary angle material in pure tension, so that,

$$\sigma_p = \sigma_{ten} = S_{ten}A' \tag{D2}$$

where S_{ten} is the thermoelastic signal obtained from the boundary angle material loaded in pure tension.

The principal stress σ_p can be eliminated from equation (D1) by loading the boundary angle material in compression perpendicular to the fibre direction, so that,

$$\sigma_t = \sigma_{comp} = \frac{S_{comp}A'}{\alpha} \tag{D3}$$

where S_{comp} is the thermoelastic signal obtained from the boundary angle material loaded in pure compression.

The constant A' can be determined directly from equation (D2). The constant α can be determined by combining equations (D2) and (D3) so that,

$$\alpha = \frac{\sigma_{ten}}{\sigma_{comp}} \frac{G_{comp}S_{comp}}{G_{ten}S_{ten}} \tag{D4}$$

where G is the SPATE system sensitivity setting (a signal amplification factor).

The tensile test specimens, shown in figure D.1, were constructed from four strips of boundary angle material cut away from a tee joint specimen. The length of each specimen

was 87.5 mm by 50.4 mm wide. The thickness of each specimen was measured at three positions on each specimen (see figure D.1); these measurements are provided in table D.1. To ensure that the specimens were loaded uniformly a filler was used to fill any gaps between the loading jig and the specimens.

The compressive test specimens, shown in figure D.2, were constructed from 38mm squares cut from the boundary angle material of a tee joint specimen and layered to form two specimens. The layers of boundary angle material were bonded together using an epoxy adhesive. The edges of the specimens were trimmed flat using a diamond tipped saw to produce specimens with finished dimensions of 31 mm square by 85 mm deep. Steel end-pieces were attached to both ends of each specimen using epoxy adhesive, to facilitate loading. Locating pips were machined in the end-pieces to ensure that the load was applied through the central axis of each specimen.

Prior to testing each specimen was coated with two passes of matt black paint. The specimens were cyclically loaded using an Instron 8501 servo-hydraulic test machine at a frequency of 8 Hz. The tensile specimens were loaded at levels of 6 ± 2 kN and 6 ± 4 kN and the compression specimens were loaded at levels of -8 ± 3.25 kN and -8 ± 6.5 kN. the SPATE detector was set at a working distance of 400 mm for all tests. SPATE scans were made over the areas shown in figures D1 and D2 on both sides of each tensile specimen and on all four faces of the compression specimens.

For the tensile specimens average thermoelastic signal readings were obtained from horizontal line plots taken at the three positions shown in figure D.1. The signal readings from both sides of each specimen and under both load levels are given in table D.2. The applied stress range was calculated using the cross-sectional area at each position. The calibration constants A' were derived from the signal and the applied stress at each position using equation (D1). The mean A' value is 10.50×10^{-3} MPa/U with a standard deviation of 1.81 MPa/U giving a coefficient of variation of 17.2%. The A' values determined from specimen 1 are somewhat greater than the values determined from the other three specimens. this could be due to variations in the boundary angle material. If the A' values from specimen 1 are neglected then the average A' value is 9.78 x 10-3 MPa/U with a standard devation of 0.97 MPa/U giving a coefficient of variation of 10.0%. Comparisons of the A' at the two loads, in the main show very good agreement.

For the compressive specimens thermoelastic signal readings were taken at three positions in each layer. The average of these for each face of the specimens is given in table D3 along with the applied stress range, for both load levels. The readings from the top and bottom layers were consistently low. This was attributed to edge effects and these readings were neglected. The average of the signal readings for the lower stress is 475.6 U with a standard deviation of 46.8 U giving a coefficient of variation of 9.8%. The signal values obtained

from specimen 1 face 3 and specimen 2 face 2 are however, very low. Neglecting these gives a mean signal of -501.7 U with a standard deviation of 12.8 U giving a coefficient of variation of 2.5% and for the high stress amean signal of -974.4 U with a standard deviation of 44.8 U giving a coefficient of variation of 4.5%.

The constant alpha was determined using equation (D4) with the average signal values for both stress levels, obtained from the compression specimens (i.e. S_{comp} = -501.7 U and -974.4 U and σ_{comp} = -6.26 MPa and -12.52 MPa). For the compression tests the SPATE sensitivity setting, G_{comp}, was 20 mV. These values were used with each of the tensile signal and stress values in table D2 (for these tests the sensitivity, G_{ten}, was 5 mV) to derive an average α value of 3.33 with a standard deviation of 0.55 and a coefficient of variation of 16%. Neglecting the values from tensile specimen 1 gives an α value of 3.1 with a standard deviation of 0.30 giving a coefficient of variation of 9%.

Table 2.1 Tee Joint Test Specimen Details. (Hawkins (1995))

Sample	Boundary Angle Thickness (mm)	Fillet Radius (mm)	Resin for Boundary Angle	Edge Gap (mm)	Edge Detail
A	10	30	Polyester	20	Plain
B	14.5	30	CR1200	20	Plain
C	–	75	–	15	Plain
D	–	75	–	25	Plain
E	–	75	–	15	6mm Bevel
F	2	75	CR1200	15	Plain
G	–	100	–	15	Plain
J	3	75	CR1200	15	Plain
K	2	50	CR1200	15	Plain
L	3	75	Polyester	15	Plain
M	2	50	Polyester	15	Plain

Table 5.1 Failure Load - Deflection Results for Rate Sensitivity Tests.

N Type Joint			F Type Joint			K Type Joint		
Load Rate (KN/s)	Failure Load (KN)	Failure Defln. (mm)	Load Rate (KN/s)	Failure Load (KN)	Failure Defln. (mm)	Load Rate (KN/s)	Failure Load (KN)	Failure Defln. (mm)
1.29	14.08	11.42	0.29	24.57	20.03	0.02	11.03	18.77
1.41	10.63	8.88	19.62	20.69	19.30	1.23	10.33	17.46
7.30	9.50	4.075	39.24	20.76	19.37	13.82	6.10	15.94
10.34	12.94	9.68	39.24	20.53	19.51	22.45	5.20	16.74
84.27	9.26	6.89	39.24	19.70	17.01			
			78.48	17.59	16.21			

Table 6.1 Visual Examination of Each Joint Type Prior to Testing.

Joint Type	Fillet Radius (mm)	Overlaminate Condition
B	50	Small amount of squashing of overlaminate at mid-radius
F	75	good
N	30-35	Very tight radius, substantial squashing of overlaminate at mid-radius
K	45-50	good

Table 6.2 Load - Life Results for Joint Type B Subjected to Constant Fatigue Loading.

Joint No.	Nom. Load (Kg)	Actual Load (kN)	No. Cycles	Initial Max. Defln.	Final Max. Defln.	Final Min. Defln.	Delam. Ply No.	Fail.† Mech.
B1	1500	-	181	-	-	-	3 6	1
B2	1500	-	207	-	-	-	3	1
B3	1500	14.38	3344	-	-	-	6	1
B4	1500	14.23	3236	6.27	9.83	4.52	6	1
B5	1500	14.28	9503	4.45	9.98	4.30	6	1
B6	1200	11.84	140	4.01	4.52	0.08	None	2
B7	1200	11.28	14385R	4.08	6.48	1.31	6	-
B8	500	5.131	3585007R	1.00	1.42	0.40	3 6	-
B9	850	8.172	220645	2.95	4.94	1.11	3 6	1
B10	850	8.231	60552	3.24	4.79	1.33	6	1
B11	850	8.397	5614	2.50	3.09	0.51	3	1
B12	1200	11.74	2583	3.16	4.05	0.44	3 6	1
B13	1200	10.83	7350	4.94	6.04	0.81	6	1

†**Final Failure Mechanism**
Type 1. Overlaminate delamination at fillet/overlaminate interface and single crack across fillet.
Type 2. Single crack across fillet and delamination of flange at flange/fillet interface.

Table 6.3 Load - Life Results for Joint Type F Subjected to Constant Fatigue Loading.

Joint No.	Nom. Load (Kg)	Actual Load (kN)	No. Cycles	Initial Max. Defln.	Final Max. Defln.	Final Min. Defln.	Fat.* Damage	Fail.† Mech.
F1	750	7.191	1538976	4.56	11.34	7.66	a,d	3
F2	1890	17.74	42	10.61	11.27	0.00	None	3
F3	1890	-	1	-	-	-	None	3
F4	1890	-	1	-	-	-	None	3
F5	1890	16.72	173	12.89	14.00	0.59	d	3
F6	1470	13.71	1446	8.69	11.12	2.14	b,d	3
F7	1470	14.17	2384	9.13	11.04	1.17	b,c,d	3
F8	1470	-	-	-	-	-	b,c,d	3
F9	1470	13.74	2274	8.10	11.49	1.48	b,d	3
F10	1050	10.44	5580	6.99	8.32	1.77	d	3
F11	1050	10.43	17294	8.03	-	-	c,d	3
F12	1050	10.45	26322	7.51	9.57	1.84	d	3
F13	1050	9.79	14041	9.43	-	-	d	3
CDF1	1890	-	9	-	-	-	None	3
CDF2	1890	-	1	-	-	-	None	3
CDF3	1050	10.22	19432	10.48	11.21	0.83	d	3
RSF190	1470	14.37	892	14.26	17.68	3.34	d	3
RSF260	1050	9.77	7502	12.15	28.52	16.88	d	3
RSF290	1050	9.80	9223	11.20	29.98	21.39	d	3

†**Final Failure Mechanisms**

Type 3. Catastrophic failure of the fillet and delamination of the overlaminate at the fillet/overlaminate interface.

***Fatigue Damage Sustained During Loading**

Type a. Small amount of cracking in fillet at web corner on compression side of web.

Type b. Crack through thickness of overlaminate across width of joint on compression side of web at top of radius.

Type c. Crack in fillet/overlaminate interface at edge of joint on tension side of web at top of radius.

Type d. Whitening/ resin cracking in overlaminate on tension side of radius

Table 6.5 Load - Life Results for Joint Type K Subjected to Constant Fatigue Loading.

Joint No.	Nom. Load (Kg)	Actual Load (kN)	No. Cycles	Initial Max. Defln.	Final Max. Defln.	Final Min. Defln.	Fat.* Damage	Fail.† Mech.
K1	545	5.58	1403	9.82	15.64	2.98	d	1
K2	545	4.79	4887	8.00	14.70	6.69	a,d	1
K3	650	5.85	59	10.7	11.65	0.95	None	1
K4	650	5.89	7	-	-	-	None	1
K5	330	3.36	78561	5.67	21.90	16.30	a,d	1
K6	330	3.32	181755R	5.9	15.36	9.1	a,d	-
K7	330	3.07	24156	5.67	15.06	8.95	a,d	1

†Final Failure Mechanisms

Type 1. Overlaminate delamination at fillet/overlaminate interface and single crack across fillet.

***Fatigue Damage Sustained During Loading**

Type a. Small amount of cracking in fillet at web corner on loading side of web.

Type d. Whitening/ resin cracking in overlaminate on tension side of radius

Table 6.6 Load - Life Results for Joint Type F Subjected to Two-Stage Fatigue Loading.

Joint No.	Nom. Load 1 (Kg)	Nom. Load 2 (Kg)	Act. Load 1 (kN)	Act. Load 2 (kN)	No. Cycles @ Load 1	No. Cycles @ Load 2	Fat.* Damage	Failure† Mech.
CDF1(b1)	630	1050	6.867	9.673	5415	15758	d	3
CDF4	1470	1050	14.421	9.83	60	7814	b,d	3
CDF5	1470	1050	14.293	9.967	58	8111	b,c,d	3
CDF6	1050	1470	9.761	14.166	14912	132	d	3
CDF7	1050	1470	10.212	14.028	15288	328	a,d	3
CDF8	1470	1050	14.234	10.556	57	12709	None	3
CDF9	1050	1470	10.457	14.146	15381	1217	a,c	3

†Final Failure Mechanisms

Type 3. Catastrophic failure of the fillet and delamination of the overlaminate at the fillet/overlaminate interface.

***Fatigue Damage Sustained During Loading**

Type a. Small amount of cracking in fillet at web corner on compression side of web.

Type b. Crack through thickness of overlaminate across width of joint on compression side of web at top of radius.

Type c. Crack in fillet/overlaminate interface at edge of joint on tension side of web at top of radius.

Type d. Whitening/ resin cracking in overlaminate on tension side of radius

Table 6.7 Load - Life Results for Joint Type N Subjected to Two-Stage Fatigue Loading.

Joint No.	Nom. Load 1 (Kg)	Nom. Load 2 (Kg)	Act. Load 1 (kN)	Act. Load 2 (kN)	No. Cycles @ Load 1	No. Cycles @ Load 2	Delam.* Ply No.	Failure† Mech.
CDN1	810	580	7.799	5.454	324	37117	3 9	1
CDN2	810	580	7.976	5.602	337	53739	9	1
CDN7	580	810	5.778	7.730	10719	108	12	1
CDN8	580	810	5.131	-	11747	1	3	1

†Final Failure Mechanism

Type 1. Overlaminate delamination at fillet/overlaminate interface and single crack across fillet.

Table 7.1 Material Properties used in the Finite Element Analysis.

Material	Modulus of Elasticity (GPa)	Poisson's Ratio	Shear Modulus (GPa)	Ultimate Static Strength (MPa)	Failure Strain (%)
Resin alone					
Polyester	3.2	-	-	58	6
CR1152[+]	1.5	-	-	20	80
CR1200[*]	0.7	-	-	32	27
Polyester/WR					
Warp	14.68	0.123	3.09	207	1.4
Weft	13.06	0.139	3.09	207	1.4
Interlaminar	-	-	-	12.2	-
Polyester/CSM					
In-plane	6.89	0.13	3.45	-	-
Interlaminar	-	-	-	11.2	-
CR1200/WR					
Warp	6.375	-	-	183.3	2.8
Weft	3.926	-	-	188.9	4.8
CR1200/CSM					
In-plane	3.023	-	-	110.4	3.6

[+] Urethane-acrylate resin
[*] Polyester/urethane-acrylate mix

Table 8.1 Variation of Δw_i about Δw_{av} for Various Fibre Reinforced Polyester Structures

Material / Structure	P_a/P_u	$(1 - \Delta w_{min}/\Delta w_{max})$
SMC	0.78	0.21
	0.67	0.25
	0.56	0.29
Pultruded Rod	0.88	0.173
	0.76	0.21
	0.64	0.23
	0.51	0.189
WR	0.28	0.21
T-Joint Type F	0.7	0.21
	0.5	0.219
T-Joint Type N	0.7	0.224
	0.5	0.231
Av.		0.2205
Std. Dev.		0.0295

Table 8.2 Residual Number of Cycles to Failure for Joint Type F.

Expt. Results	Palmgren-Miner	Hashin-Rotem	Trashenko-Khamaza	Sine Model
15758	25870	25467	11025	18755
7814	20355	21682	10235	20996
8111	17970	18985	9567	18266
132	320	230	1	39
328	4.78	3.4	1	1
12709	10487	10992	7085	10585
1219	1	1	1	1
Average Error	38.96	33.57	-46.32	3.78

Table 8.3 Residual Number of Cycles to Failure for Joint Type N.

Expt. Results	Palmgren-Miner	Hashin-Rotem	Trashenko-Khamaza	Sine Model
37117	3825	6768	50749	45228
53739	1	1	38490	33459
108	108	131	2316	1
1	242	179	1930	1
Average Error	-36.99	-53.49	684.42	-28.74

Table 8.4 Equation Constants for the Fatigue Strength Design Curves.

N	m_1	m_2	c
10^3	0.300	0.571	8.952
10^4	0.220	0.461	6.598
10^5	0.180	0.376	5.831
10^6	0.156	0.317	5.361

Table A.1 Cumulative Damage Prediction Results for a Glass / Epoxy Cross-Ply.

s_1	s_2	n_1	Expt. n_{2r}	$n_{2r}1^*$	$n_{2r}2^*$	$n_{2r}3^*$	$n_{2r}4^*$
0.855	0.641	250	6454	6727	6816	9863	12652
0.855	0.641	100	13354	12673	18112	14529	16427
0.855	0.748	250	1534	1248	1394	1481	1691
0.855	0.748	100	1899	2051	3520	2181	2342
0.748	0.534	1000	142348	95821	72628	128578	161041
0.748	0.534	250	179546	175795	92703	187057	201263
0.748	0.641	1000	10373	9584	22118	10981	12372
0.748	0.641	250	9511	15517	26999	15976	16697
0.641	0.534	10000	103694	72035	.60890	89465	105049
0.641	0.534	2000	139047	177563	92441	183133	193010
0.534	0.641	49940	5280	14155	16593	13375	11966
0.534	0.641	19975	12847	16269	24641	15934	14912
0.534	0.748	49940	484	2234	3250	2008	1587
0.534	0.748	19975	1169	2488	4604	2392	2060
0.534	0.855	19975	209	540	324	512	397
0.641	0.748	10000	339	1380	3665	1147	972
0.641	0.748	2000	1469	2414	4943	2348	2190
0.641	0.855	2000	428	528	343	503	428
0.748	0.855	1000	360	395	300	353	308
0.748	0.855	250	543	526	344	513	482

*1. Hashin Residual Strength Method ($\alpha = 7$) [17]
2. Hwang and Han Fatigue Modulus Method [12]
3. Palmgren-Miner Rule
4. Hashin and Rotem Method ($N_e = 1$) [17]

Table A.2 Cumulative Damage Prediction Results for a Glass Fibre Cloth/ Epoxy Laminate.

s_1	s_2	n_1	Expt. n_{2r}	$n_{2r}1^*$	$n_{2r}2^*$	$n_{2r}3^*$	$n_{2r}4^*$
0.600	0.700	10000	2125	2002	2009	2408	2145
0.700	0.600	300	20740	20102	20999	19630	20162

*1. Hashin Residual Strength Method (α = -4) [17]
2. Hwang and Han Fatigue Modulus Method [12]
3. Palmgren-Miner Rule
4. Hashin and Rotem Method (N_e = 1) [17]

Table A.3 Cumulative Damage Prediction Results for a Glass Cross-Ply/ Epoxy 1009 Laminate.

s_1	s_2	n_1	Expt. n_{2r}	$n_{2r}1^*$	$n_{2r}2^*$	$n_{2r}3^*$	$n_{2r}4^*$
0.705	0.528	1	700	1479	3934	1485	1499
0.705	0.311	1	188200	184856	96014	186837	188599
0.705	0.528	3	1461	1438	3724	1457	1494
0.705	0.311	3	145900	177481	85262	183312	188582
0.311	0.528	600	1927	1496	4076	1495	1452

*1. Hashin Residual Strength Method (α = 7) [17]
2. Hwang and Han Fatigue Modulus Method [12]
3. Palmgren-Miner Rule
4. Hashin and Rotem Method (N_e = 1) [17]

Table A.4 Cumulative Damage Prediction Results for a Glass Cross-Ply/ Epoxy 1002 Laminate.

s_1	s_2	n_1	Expt. n_{2r}	$n_{2r}1^*$	$n_{2r}2^*$	$n_{2r}3^*$	$n_{2r}4^*$
0.802	0.594	1	1480	1718	6259	1721	1724
0.802	0.386	1	572620	89067	38114	89370	89579
0.802	0.594	3	2055	1705	6159	1712	1721
0.802	0.386	3	3767860	88047	36653	88949	89572
0.386	0.594	600	3002	1717	6291	1713	1659

*1. Hashin Residual Strength Method ($\alpha = 7$) [17]
2. Hwang and Han Fatigue Modulus Method [12]
3. Palmgren-Miner Rule
4. Hashin and Rotem Method ($N_e = 1$) [17]

Table D.1 Thickness Measurements for Tensile Specimens.

Specimen	Location	Width (mm)	Thickness (mm)
1	1	50.05	13.00
	2	49.85	13.74
	3	49.90	14.48
2	1	50.70	13.06
	2	50.85	13.75
	3	50.95	14.33
3	1	49.40	11.60
	2	50.40	11.57
	3	49.75	11.50
4	1	50.45	11.26
	2	50.50	11.52
	3	50.45	11.55

Table D.2 Signal Readings from the Tensile Specimens.

Specimen	Face	Location	Load range = 4 kN			Load range = 8 kN		
			Applied stress range (MPa)	Signal (U)	A′ x 10^{-3} (MPa/U)	Applied stress range (MPa)	Signal (U)	A′ x 10^{-3} (MPa/U)
1	1	1	6.15	463	13.28	12.30	839	14.65
		2	5.84	432	13.52	11.68	817	14.30
		3	5.54	451	12.27	11.08	970	11.41
	2	1	6.15	401	15.33	12.30	818	15.03
		2	5.84	525	11.12	11.68	1027	11.37
		3	5.54	561	9.87	11.08	1226	9.03
2	1	1	6.04	574	10.52	12.08	1087	11.11
		2	5.72	649	8.81	11.44	1241	9.22
		3	5.48	626	8.75	10.96	1233	8.89
	2	1	6.04	573	10.54	11.08	1146	10.54
		2	5.72	580	9.86	11.44	1107	10.34
		3	5.48	584	9.38	10.96	1225	8.94
3	1	1	6.84	702	9.75	13.68	1411	9.70
		2	6.86	790	8.68	13.72	1584	8.66
		3	6.99	715	9.78	13.98	1608	8.70
	2	1	6.84	710	9.64	13.68	1395	9.81
		2	6.86	589	11.65	13.72	1167	11.76
		3	6.99	604	11.58	13.98	1268	11.03
4	1	1	7.04	797	8.83	14.08	1199	11.75
		2	6.88	689	9.98	13.76	1234	11.14
		3	6.86	692	9.92	13.72	1264	10.86
	2	1	7.04	747	9.43	14.08	1521	9.26
		2	6.88	793	8.67	13.76	1473	9.34
		3	6.86	756	9.08	13.72	1535	8.94

U = Uncalibrated signal unit

Table D.3 Average Signal Readings from the Compressive Specimens.

Specimen	Applied Stress (MPa)	Face	Signal (U)
1	-6.26	1	-511.7
		2	-496.9
		3	-406.2
		4	-476.5
	-12.56	1	-988.6
		2	-948.3
		3	-563.0
		4	-951.8
2	-6.26	1	-516.1
		2	-388.1
		3	-502.0
		4	-506.9
	-12.52	1	-943.1
		2	-738.5
		3	-853.9
		4	-906.2

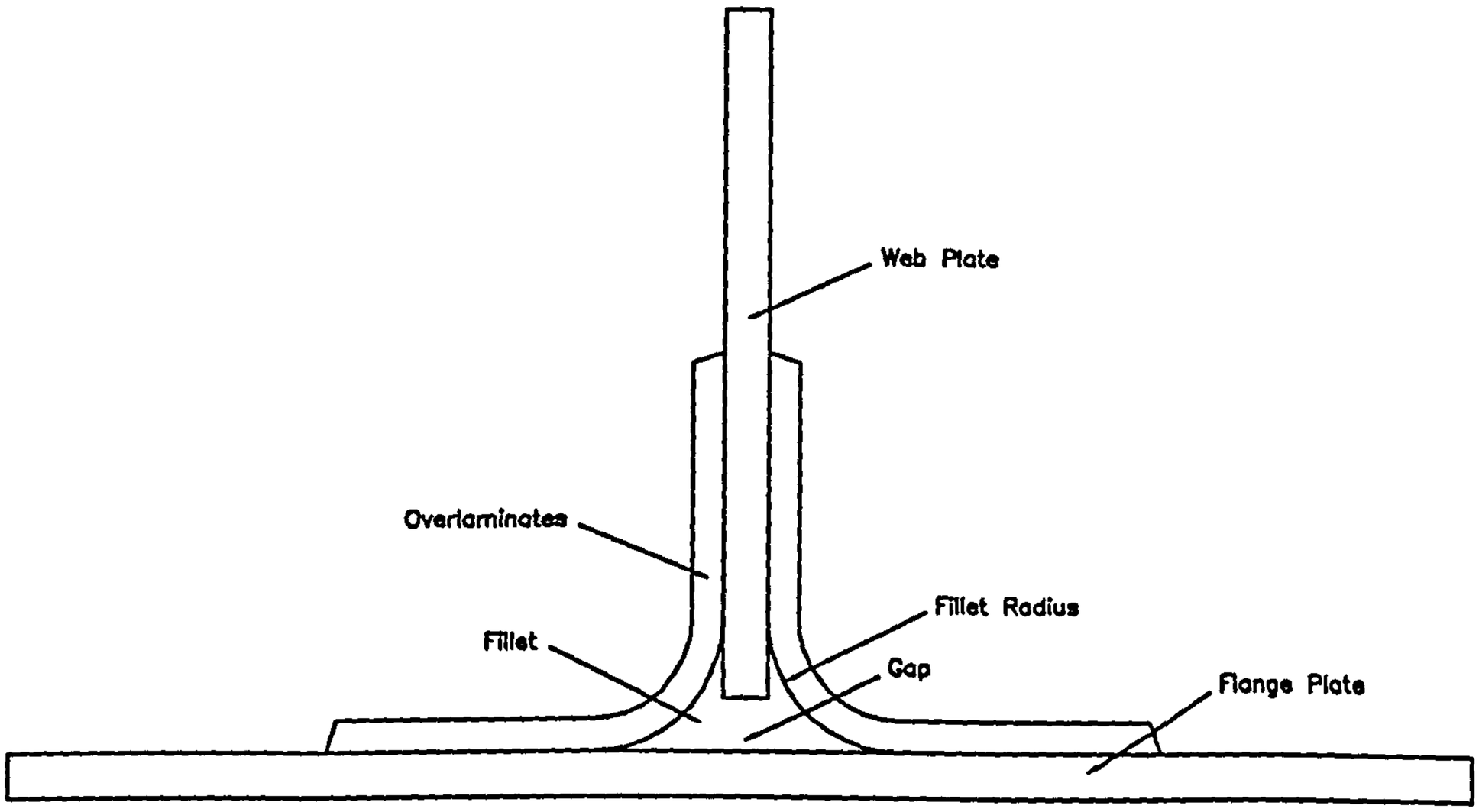

Figure 1.1 Detail of a Typical Tee Joint.

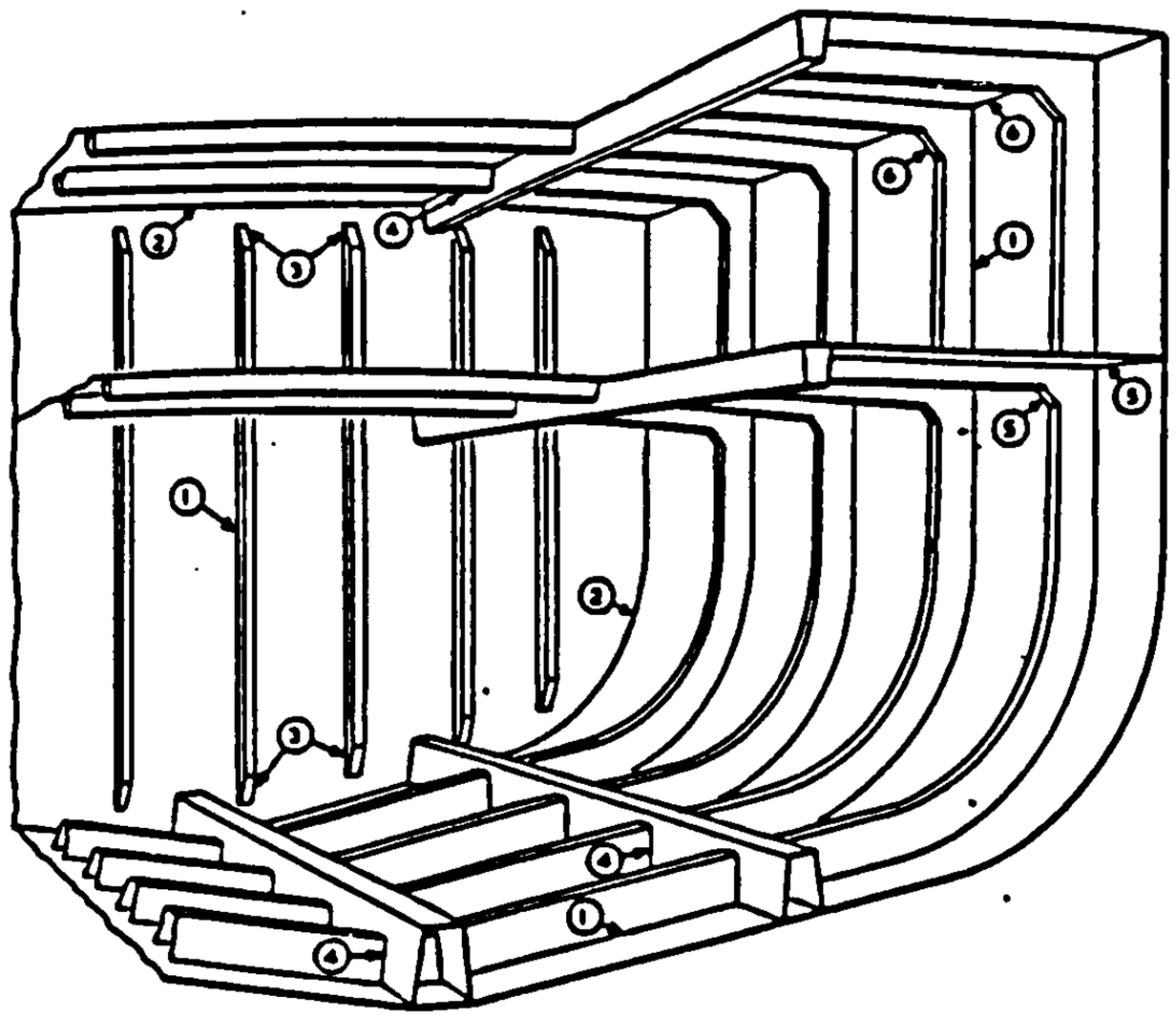

(1) Frame/shell
(2) Bulkhead/shell
(3) Stiffener ending
(4) Stiffener intersection
(5) Deck-edge (tee)
(6) Deck-edge (knee)

Figure 2.1 Typical Stiffened Single Skin Composite Ship Structure.(Smith (1990))

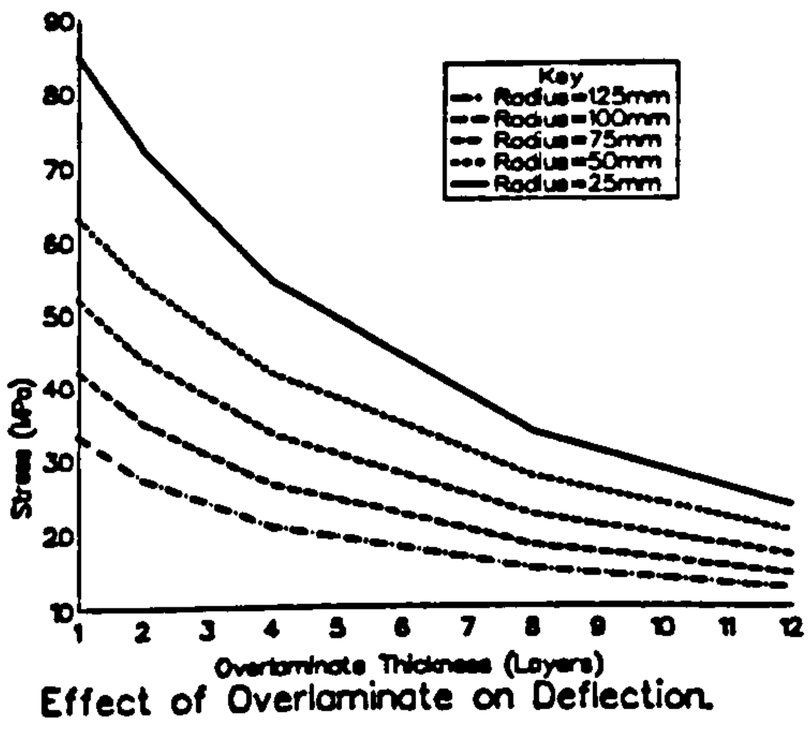

Effect of Overlaminate on Deflection.

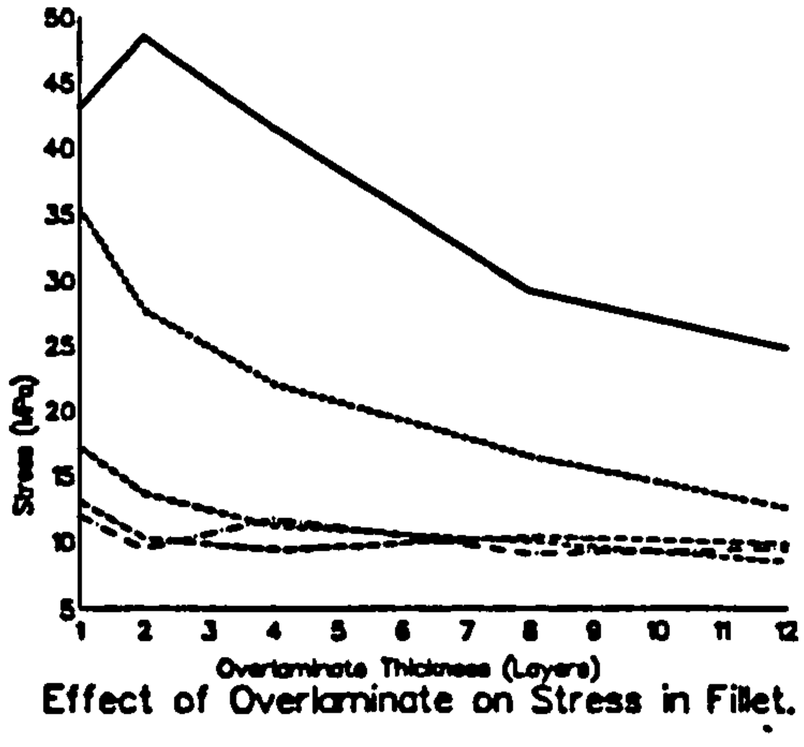

Effect of Overlaminate on Stress in Fillet.

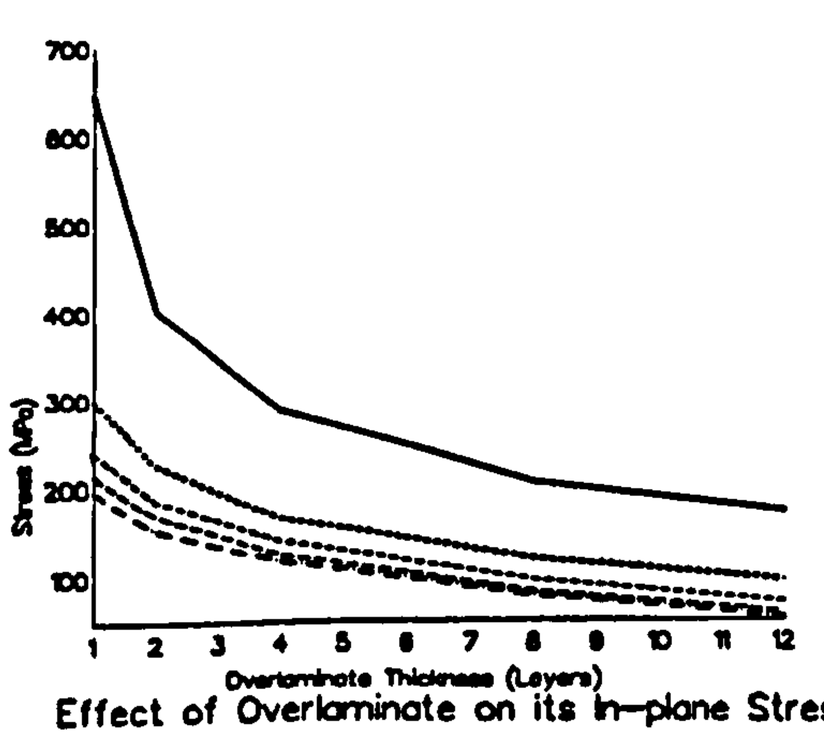

Effect of Overlaminate on its In-plane Stress

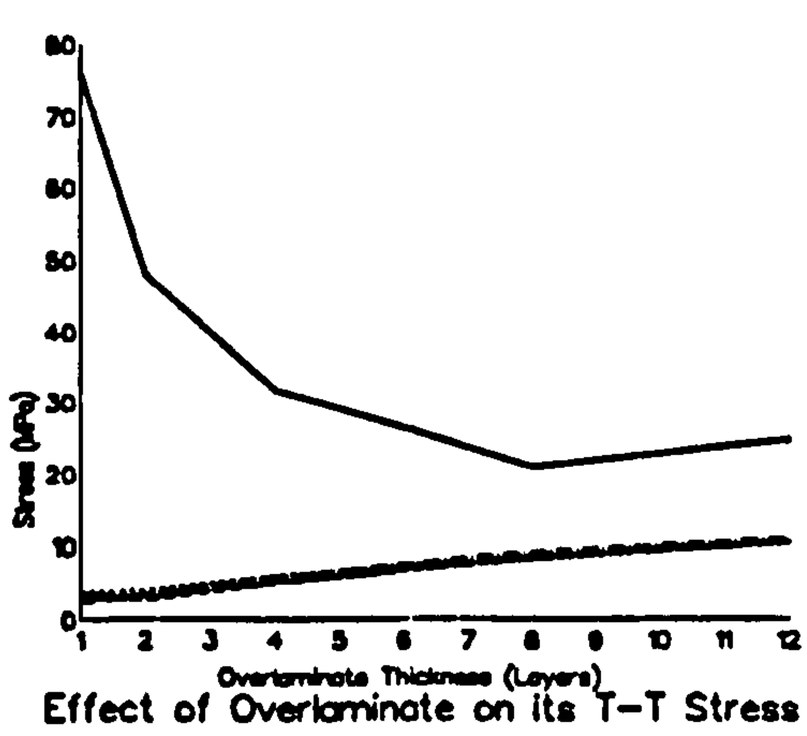

Effect of Overlaminate on its T-T Stress

Figure 2.2 Parametric Study Results for the Variations in Overlaminate Thickness and Fillet Radius.(Hawkins (1995))

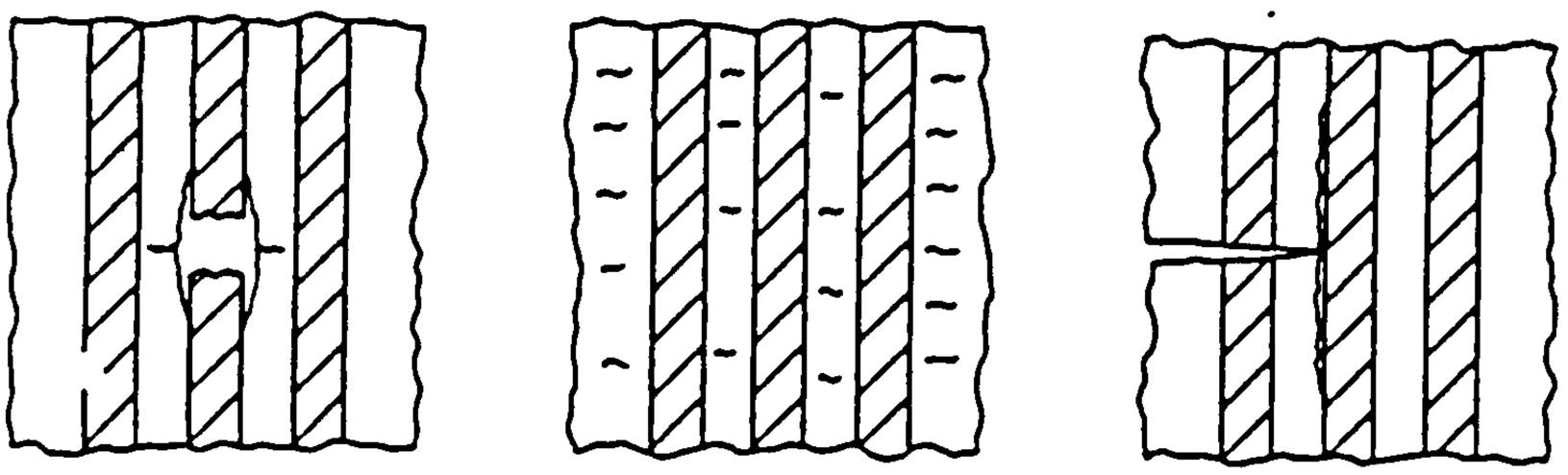

(a) (b) (c)

Figure 3.1 Fatigue Damage Mechanisms in Unidirectional Composites; (a) Fibre Breakage, Interfacial Debonding; (b) Matrix cracking; (c) Interfacial Shear Failure.(Talreja (1987))

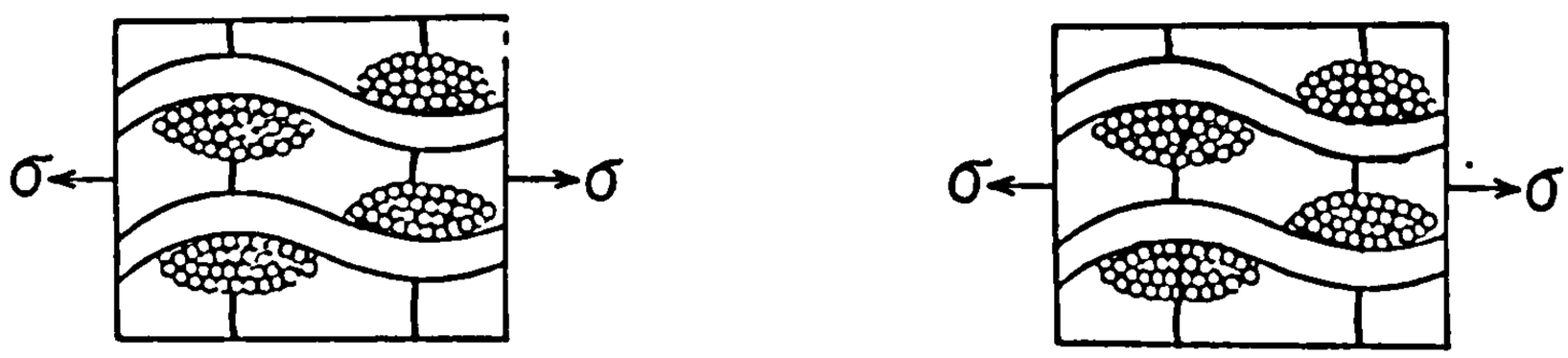

(a) (b)

Figure 3.2 Fatigue Damage Mechanisms in Woven Fabric Composites; (a) First Stage, Matrix Cracks; (b) Second Stage, Interfacial Debonding. (Tanimoto and Amijima (1975))

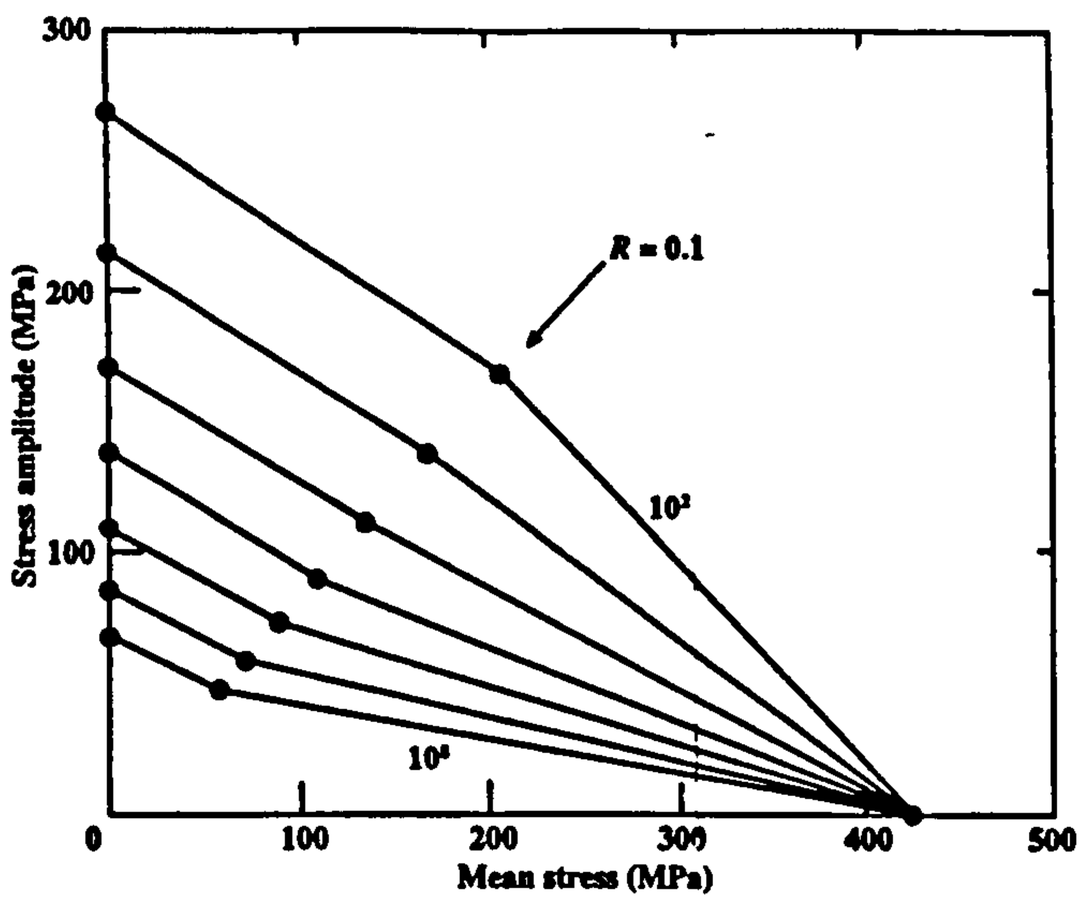

Figure 3.3a Constant Life Diagram for a Glass Fibre 0/±45 Polyester Composite.(Poppen and Bach (1996))

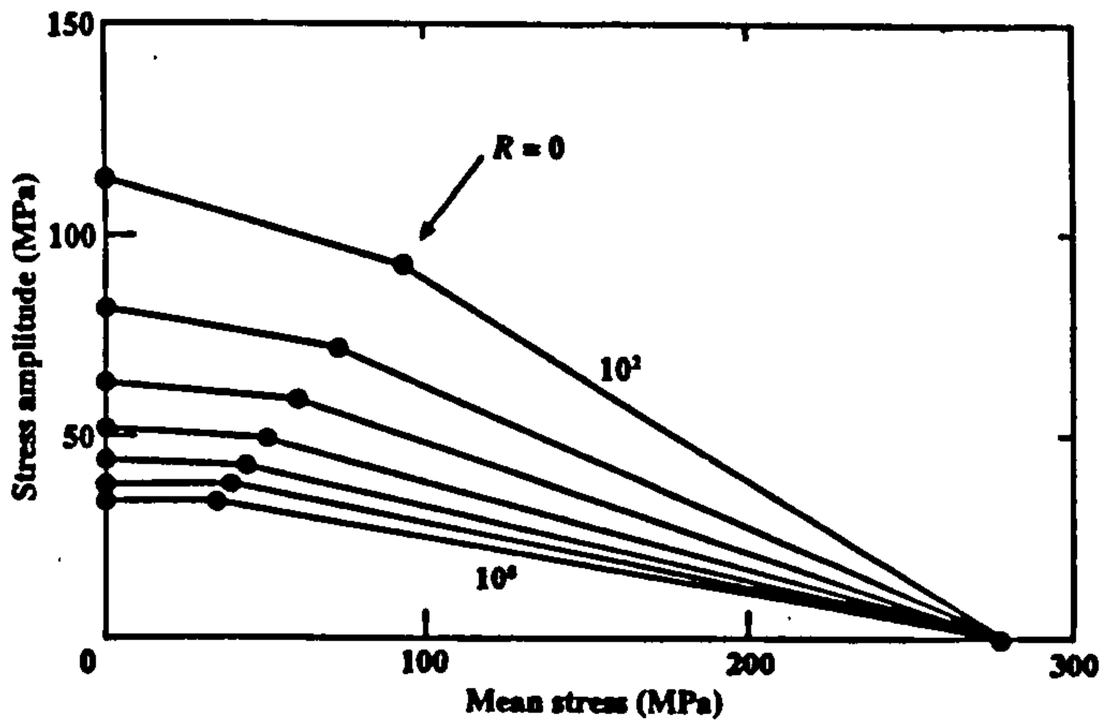

Figure 3.3b Constant Life Diagram for a Glass Fibre ±30 Epoxy Composite. (Poppen and Bach (1996))

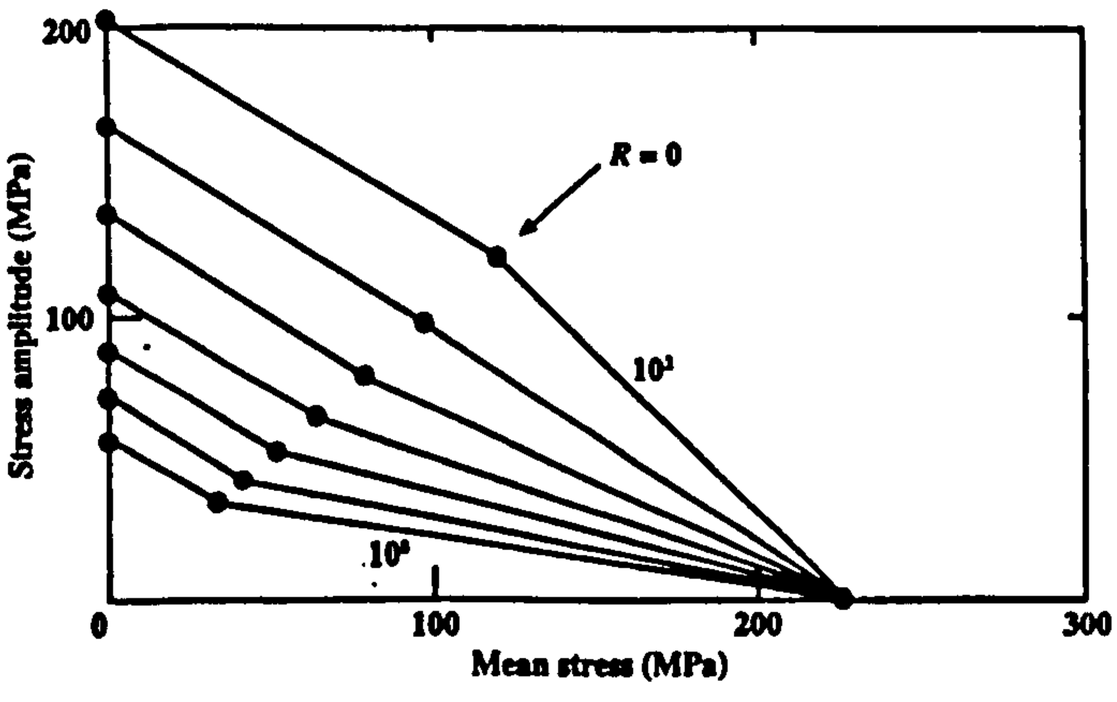

Figure 3.3c Constant Life Diagram for a Glass Fibre CSM 0/90 Vinyl Ester Composite.(Poppen and Bach (1996))

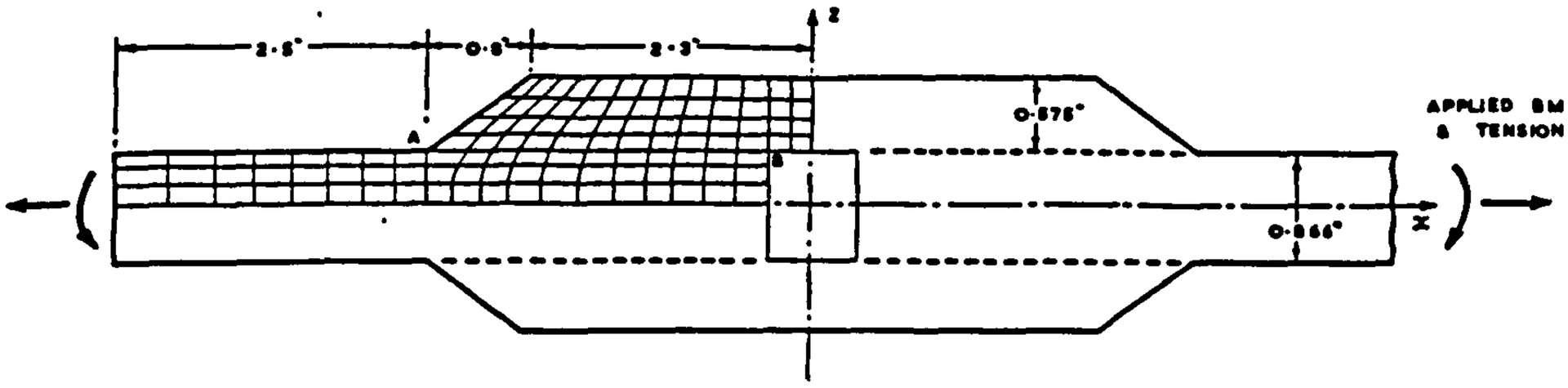

Figure 3.4 Direct Tensile and Shear Stresses in the Adhesive Layer of a Butt-Strap Connection. (Smith (1972))

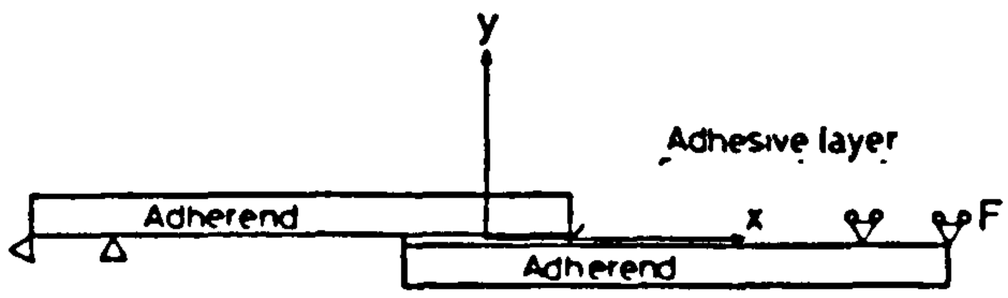

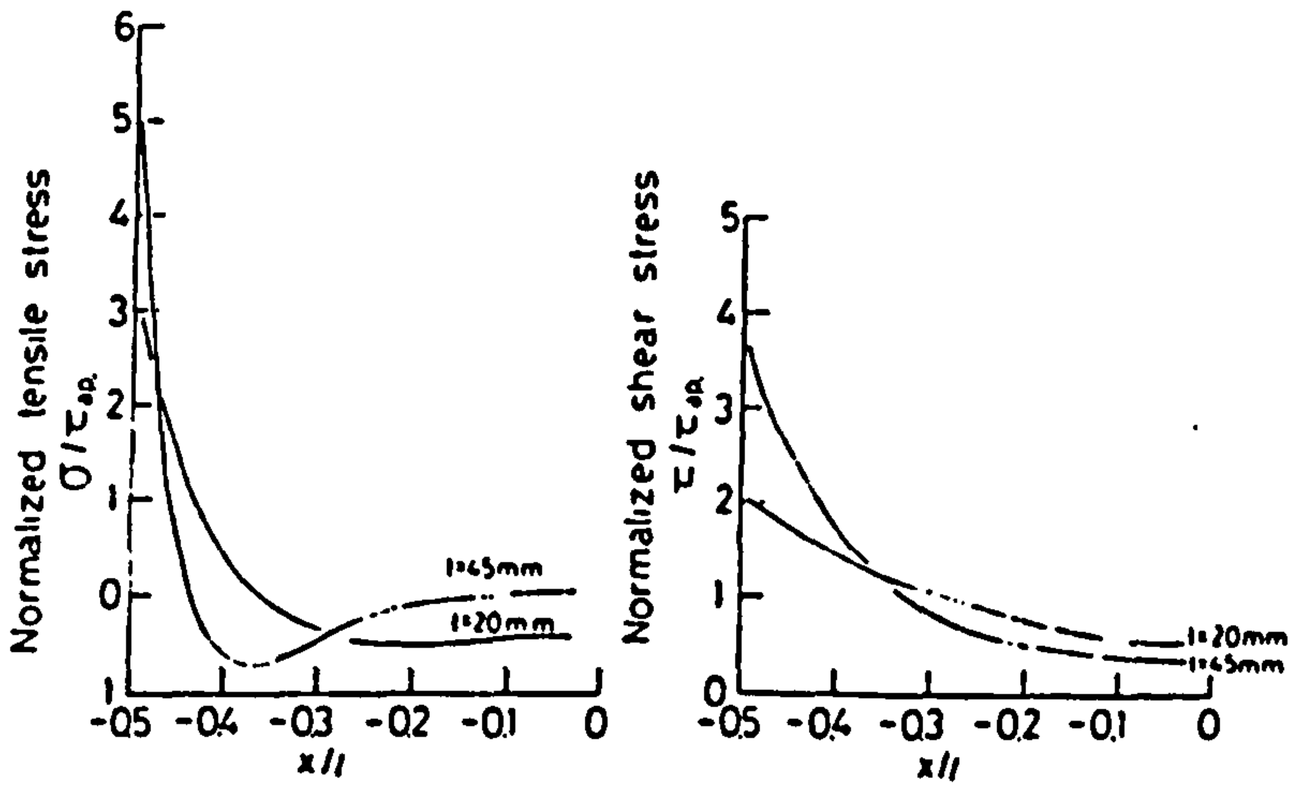

Figure 3.5 Direct Tensile and Shear Stresses in the Ashesive Layer of a Lap Joint. (Imanaka (1988))

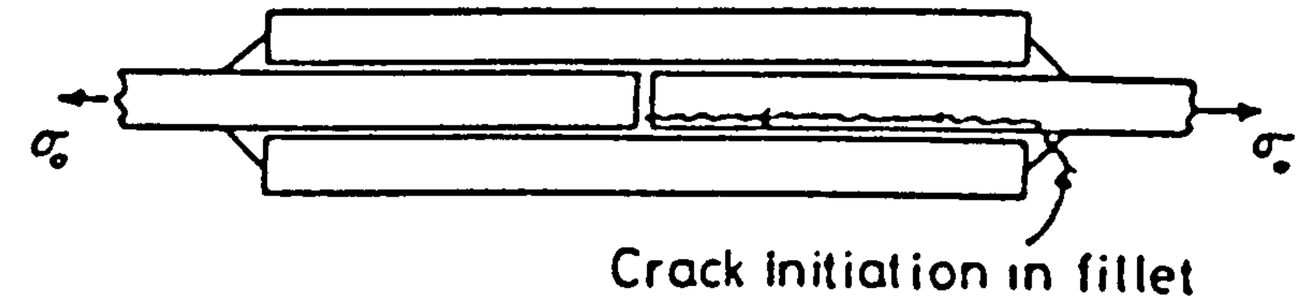

(a) Failure mode of square-ended joint

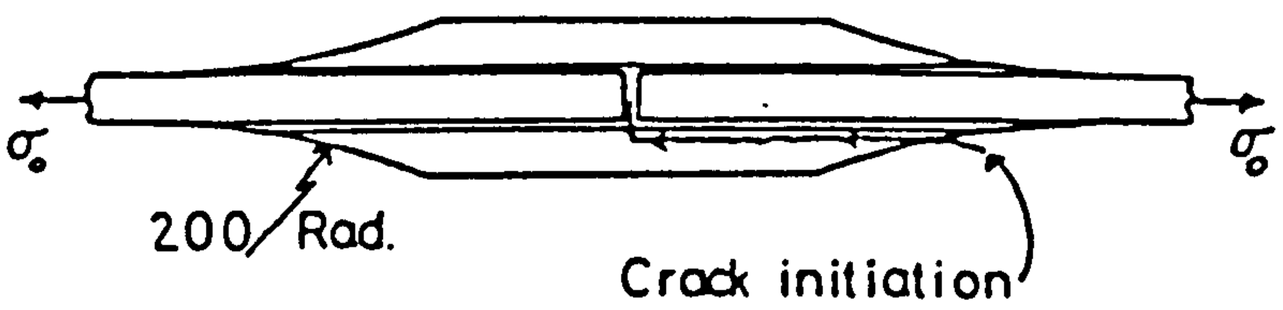

(b) Failure mode of radiused joint

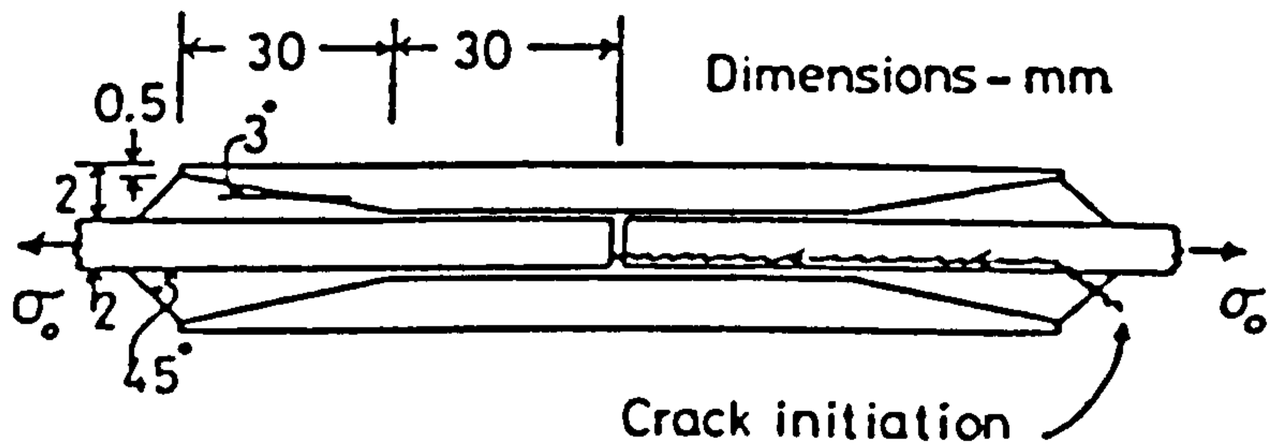

(c) Failure mode of inverse taper joint

Figure 3.6 Failure Modes of Three Inplane Joint Configurations. (Tiu and Sage (1986))

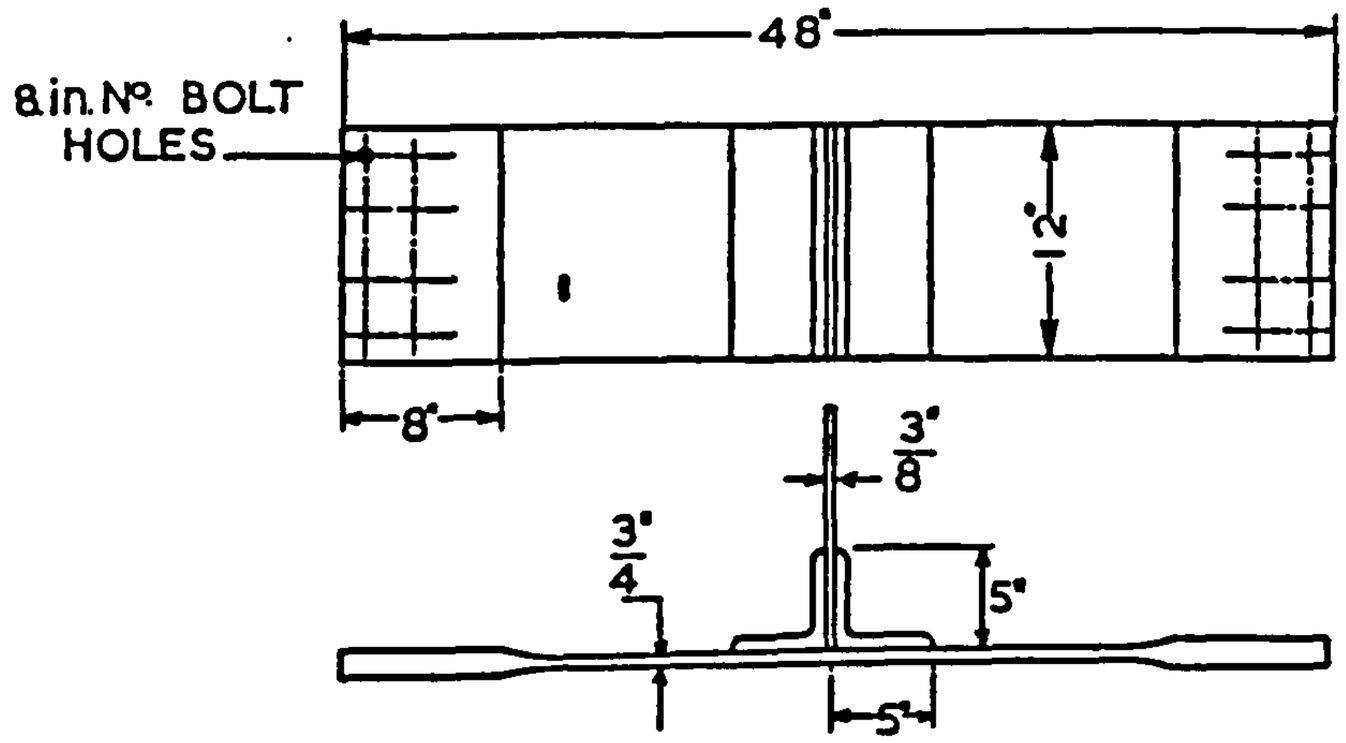

Figure 3.7 Bulkhead to Shell Tee Joint Test Specimen. (Usher et al. (1972))

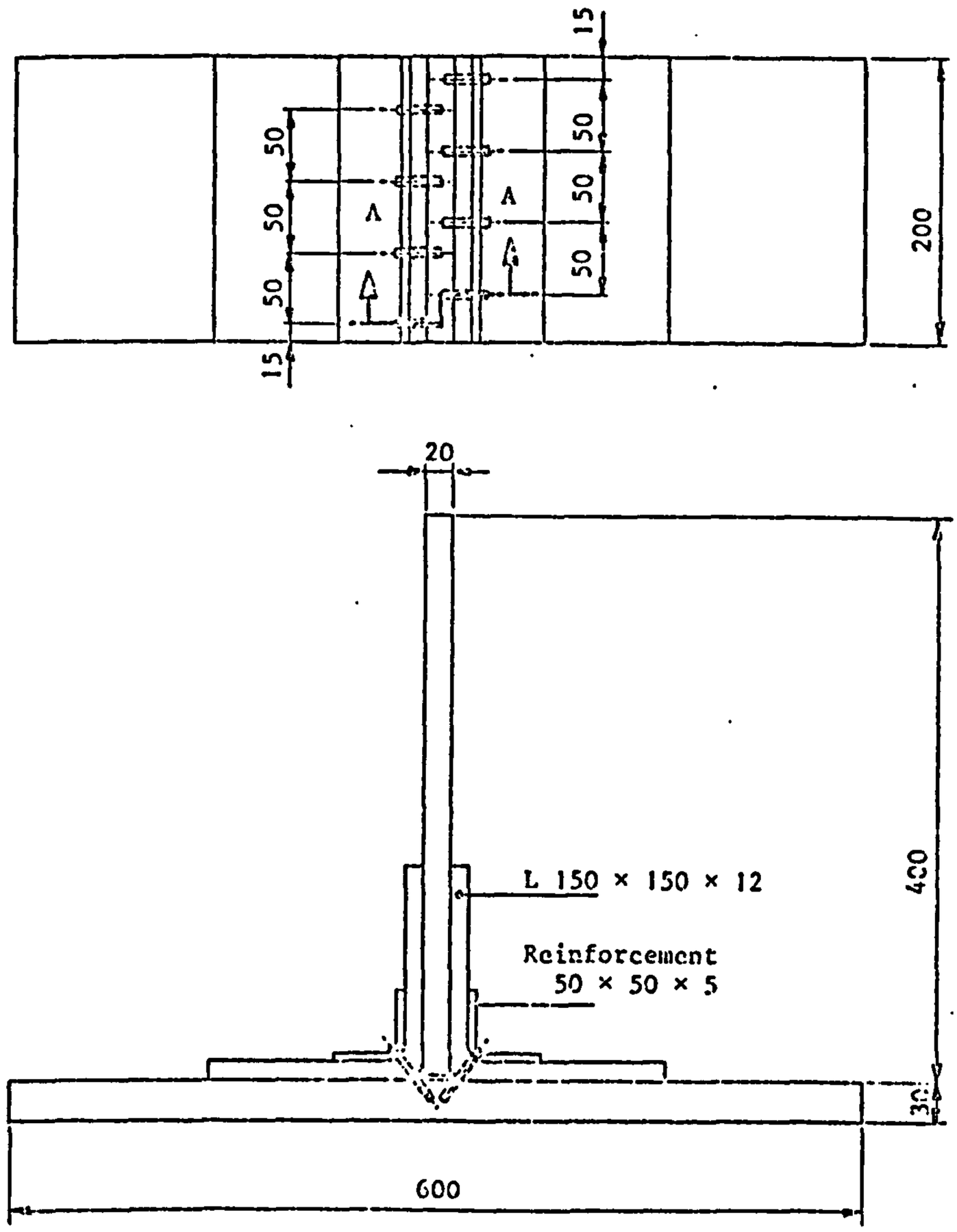

Figure 3.8 Tee Joint Test Specimen. (Scholte (1977))

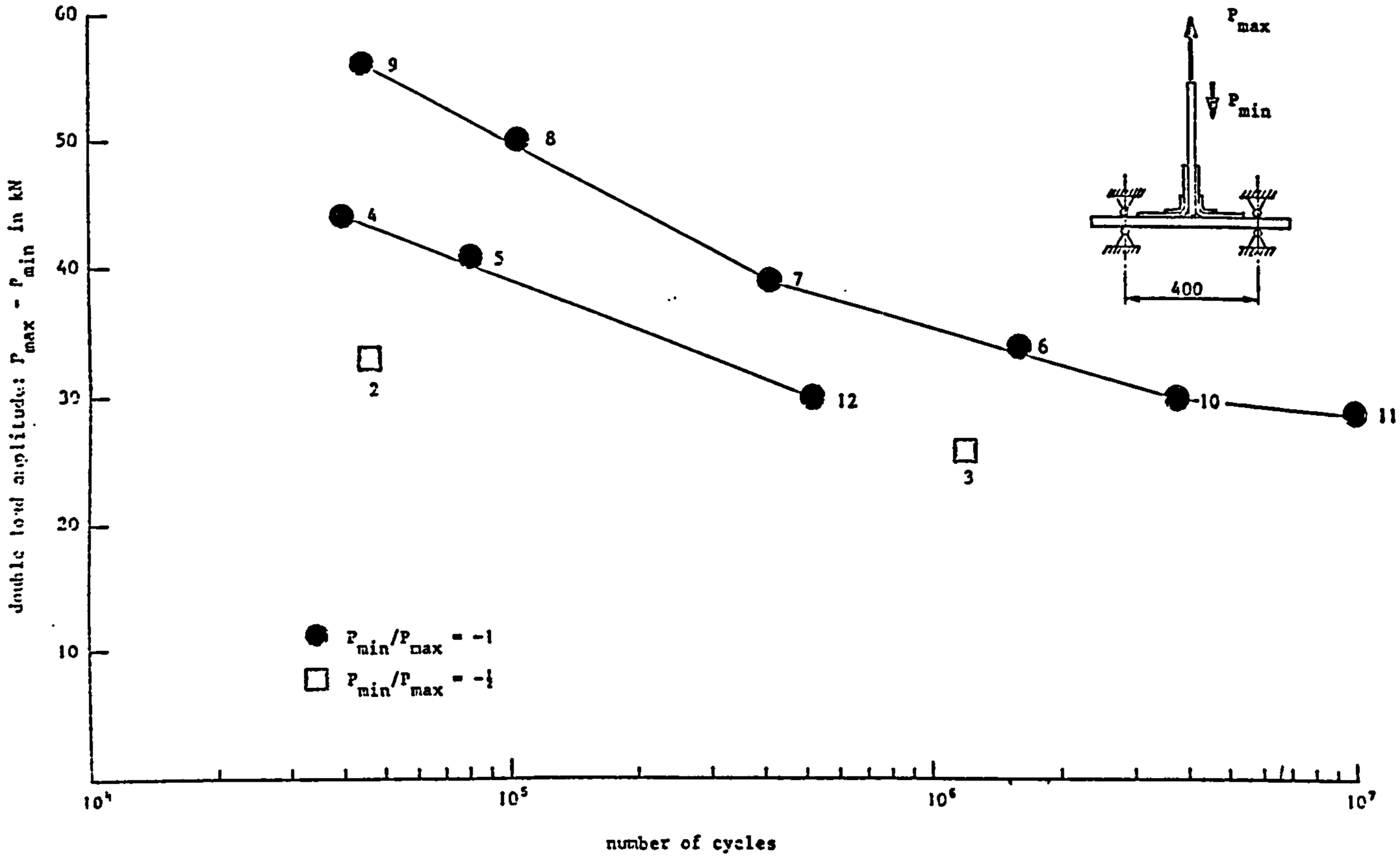

Figure 3.9 Double Amplitude Load - Life Data for a Bulkhead to Shell Tee Joint. (Scholte (1977))

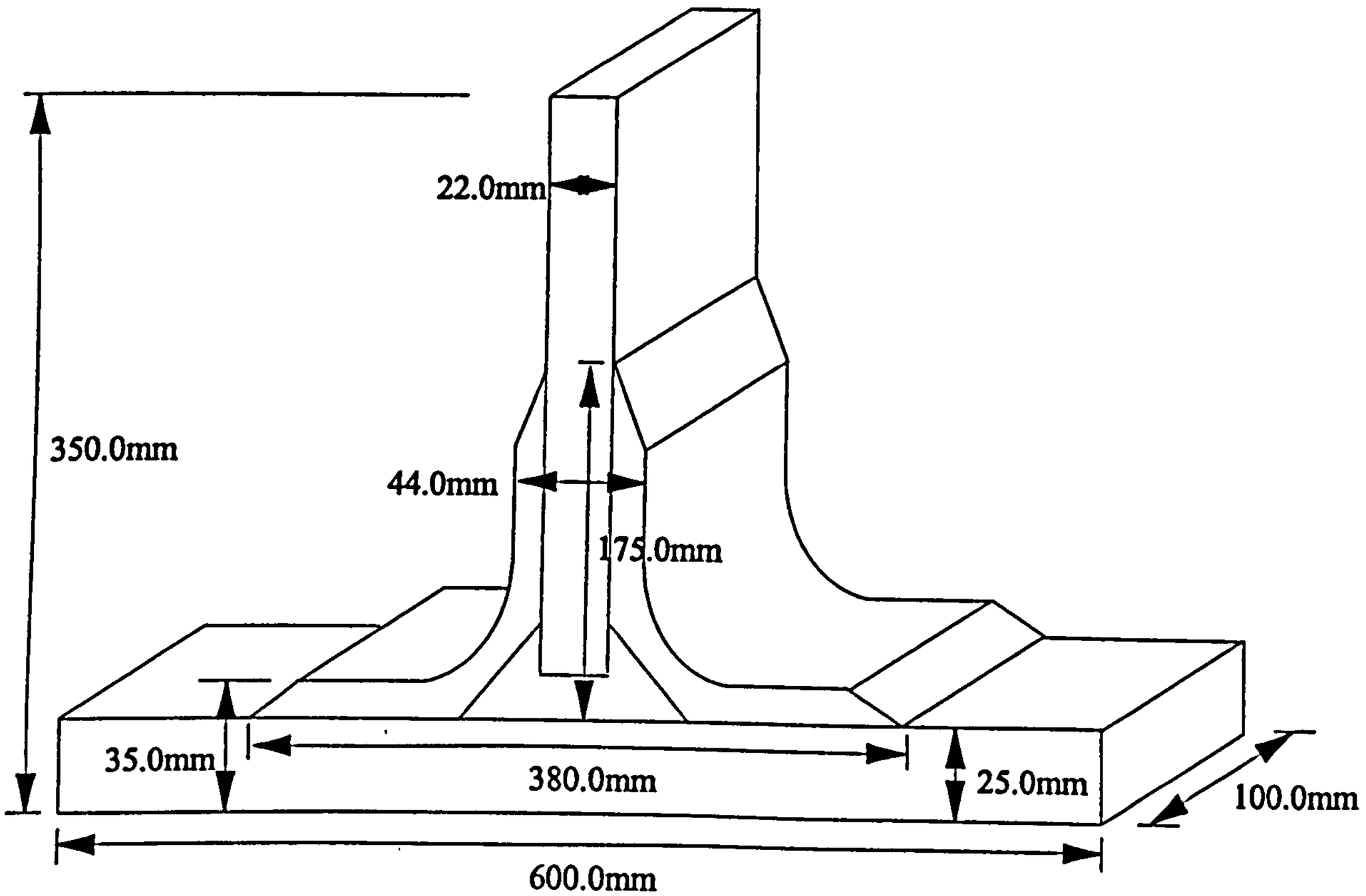

Figure 3.10 Tee Joint Test Specimen. (DRA/SMC/TR963012)

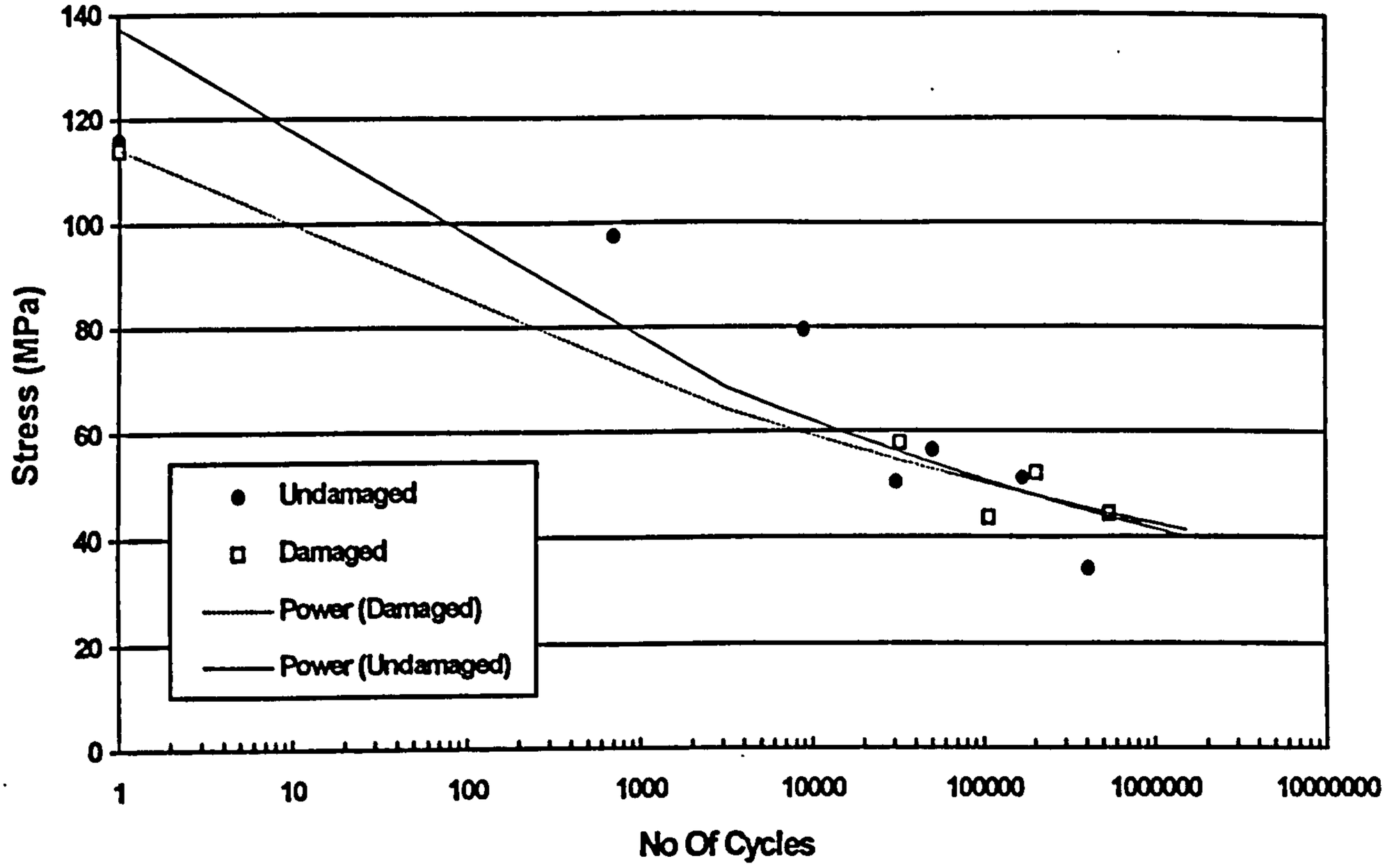

Figure 3.11 S-N Curve for Tee Joint Fatigue Tests. (DRA/SMC/TR963012)

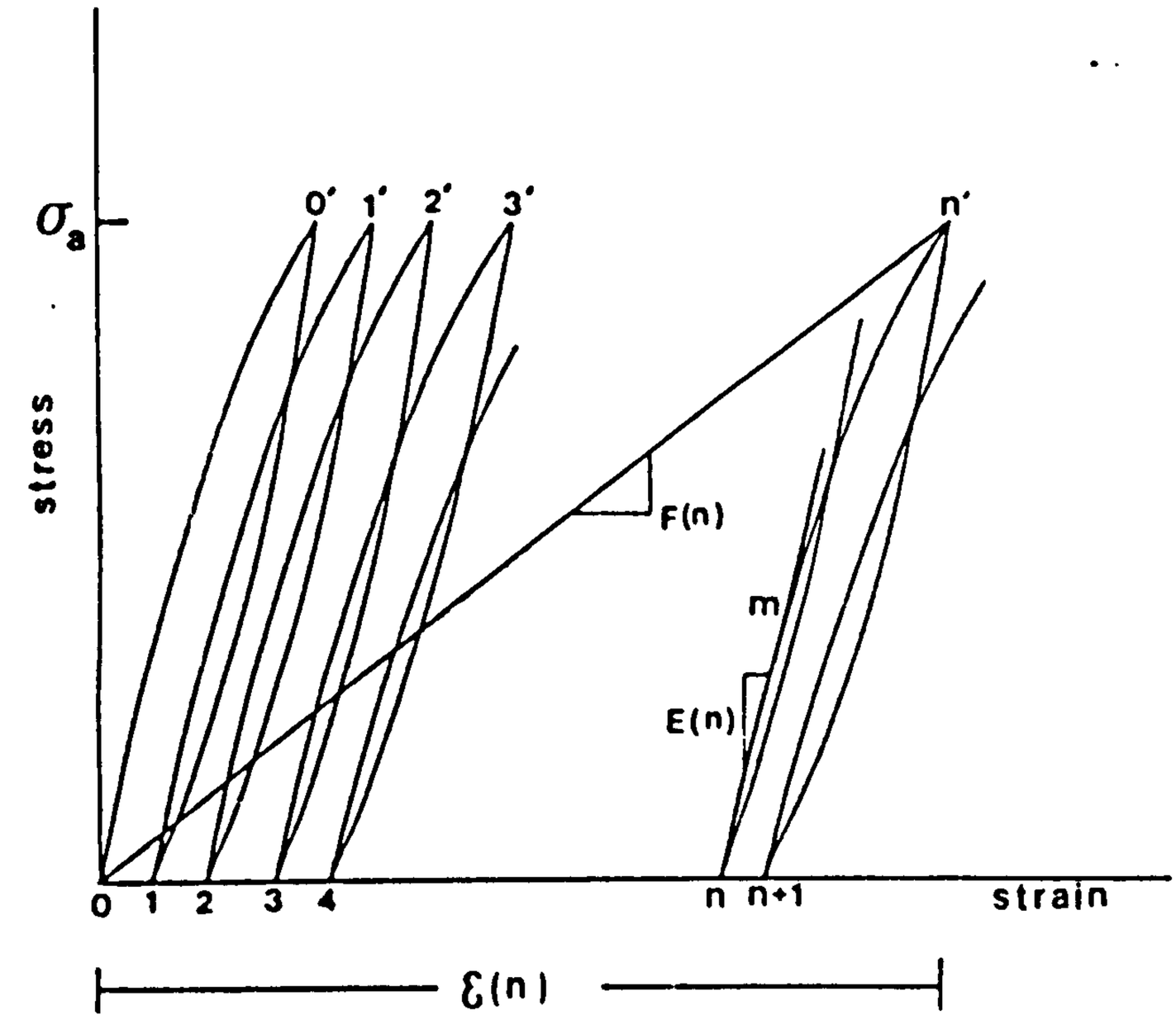

Figure 4.1 Schematic Representation of Fatigue Modulus. (Hwang and Han (1986))

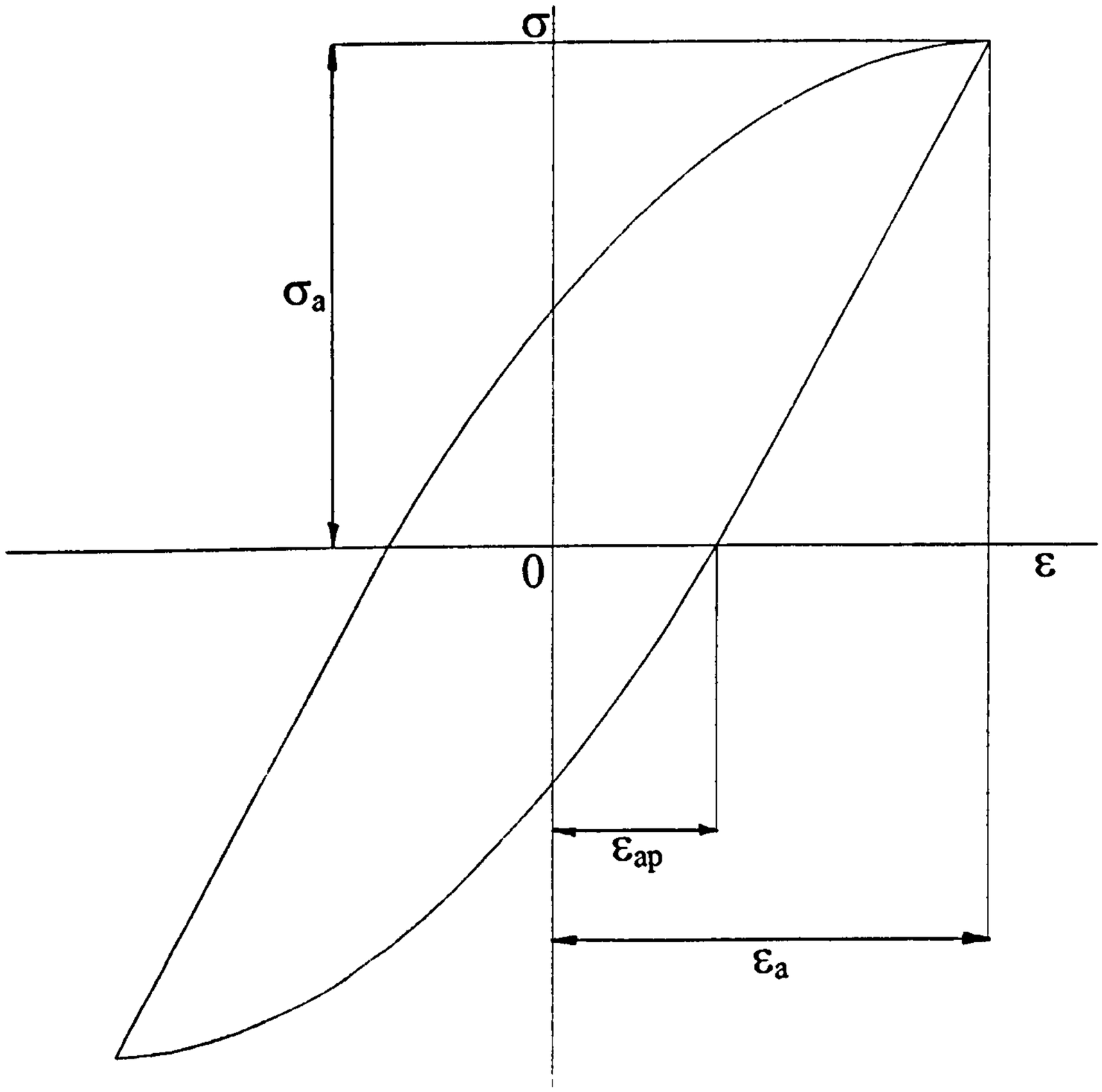

Figure 4.2 Definition of Stress-Strain Hysteresis Loop.

Figure 5.1a Test Rig Set-up for the Tee Joint Experimental Programme.

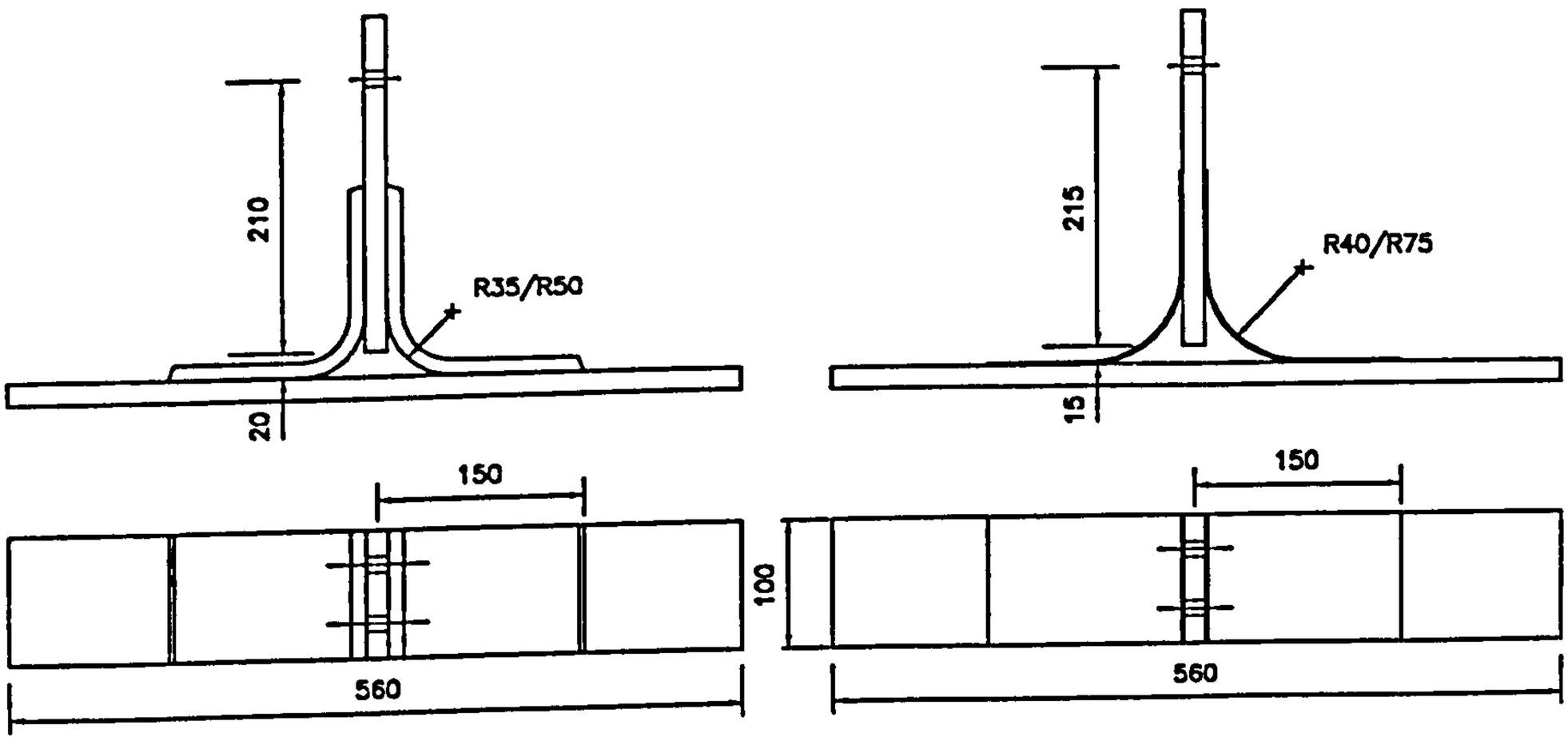

Figure 5.1b Test Specimen Details for the Tee Joint Experimental Programme.

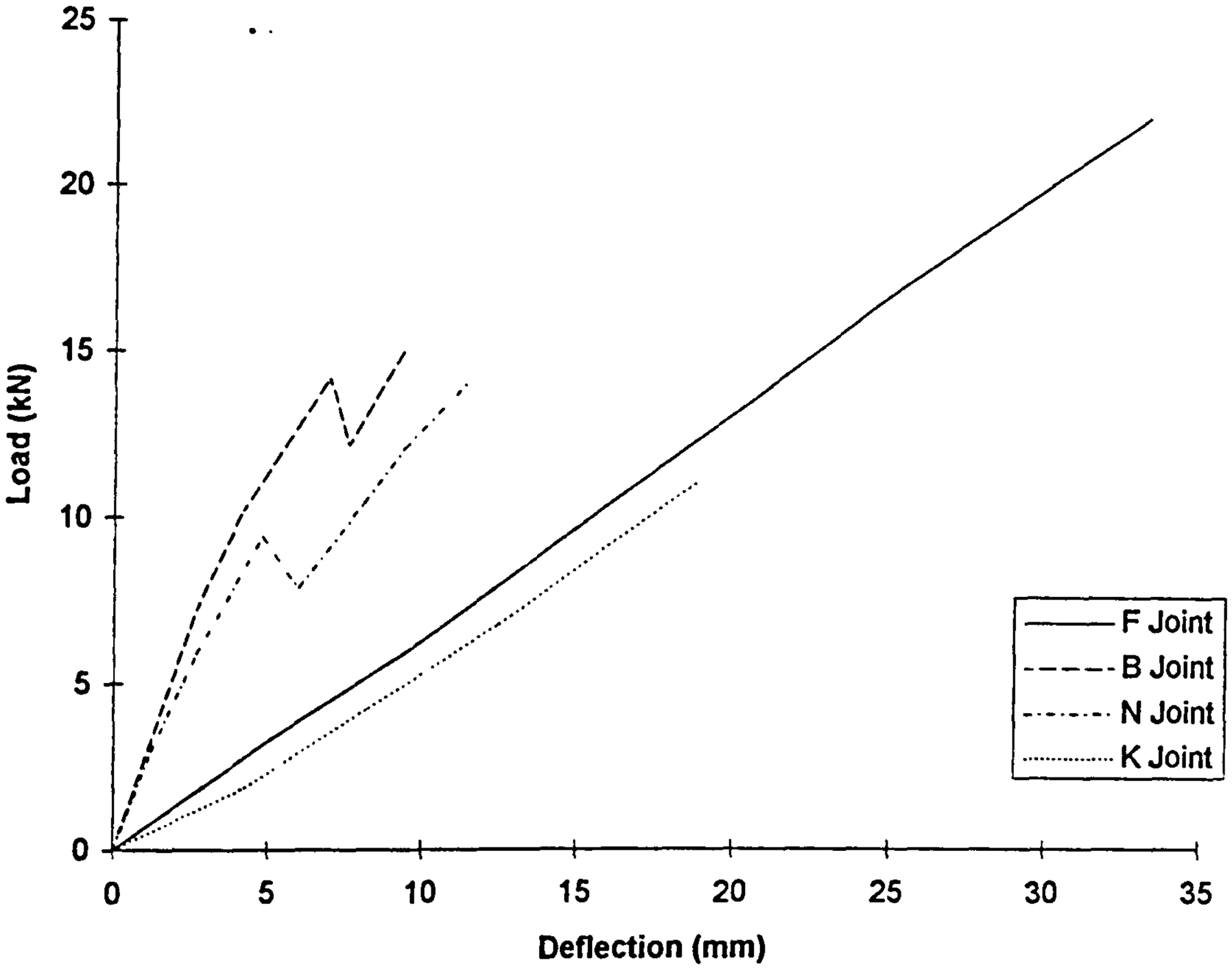

Figure 5.2 Load-Deflection Curves for Each Joint Type.

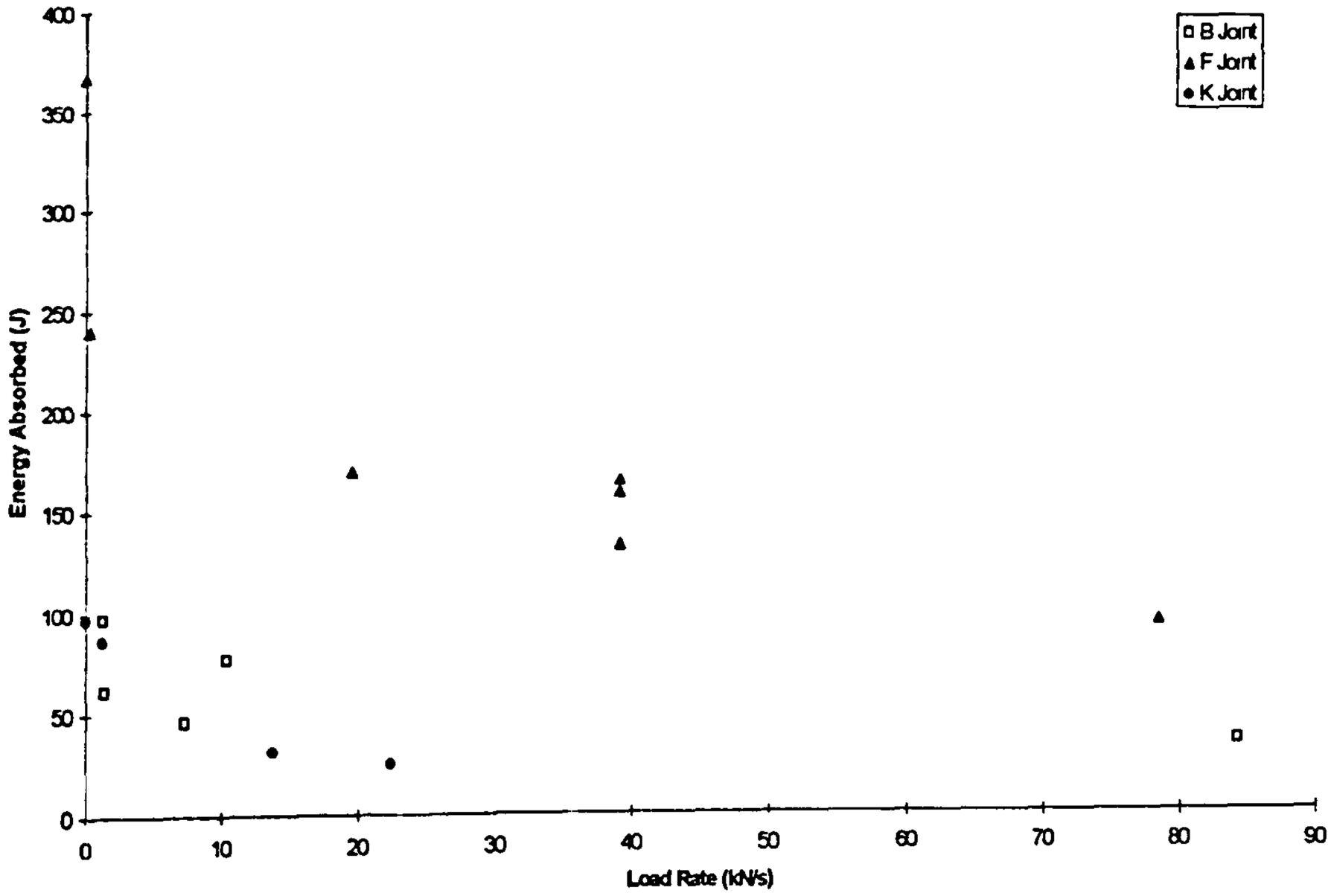

Figure 5.3 Energy Absorbed Data from Load Rate Sensitivity Tests.

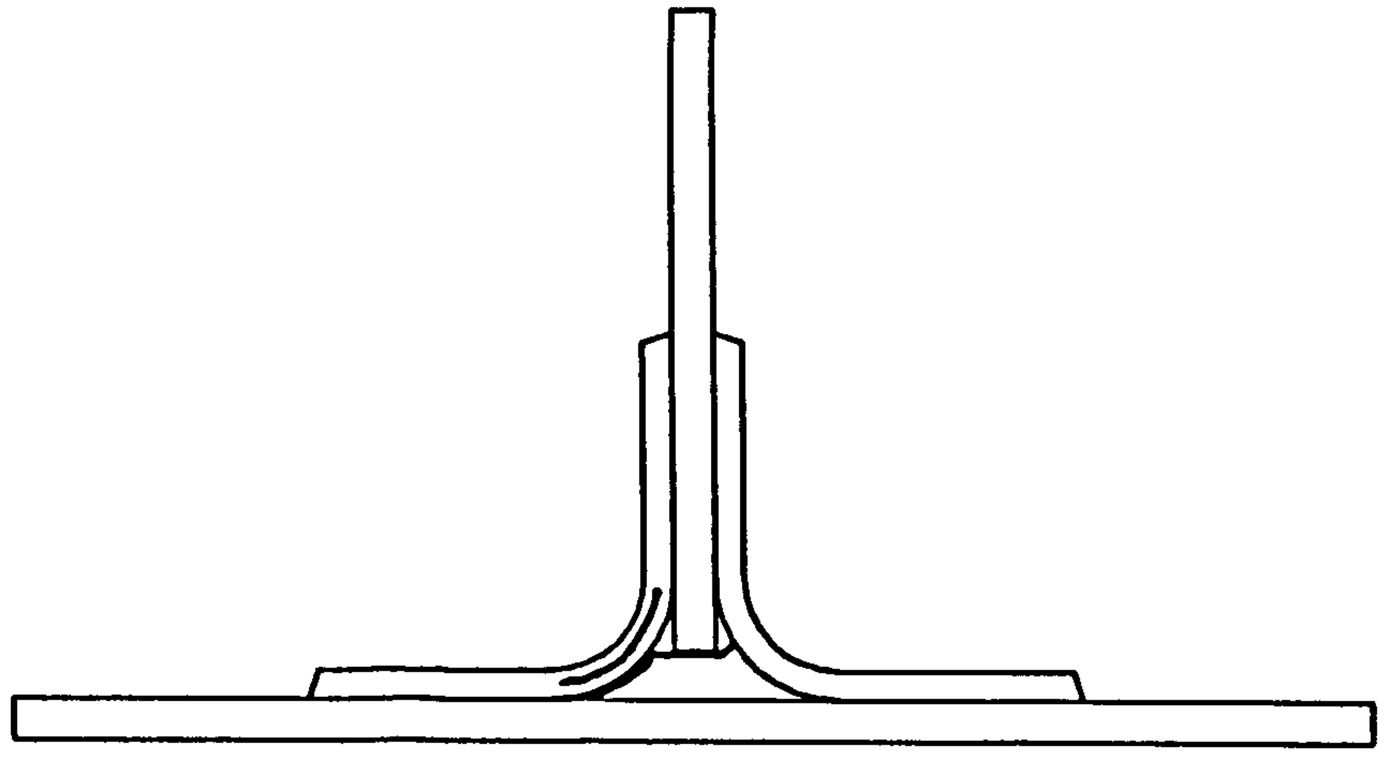

(a)

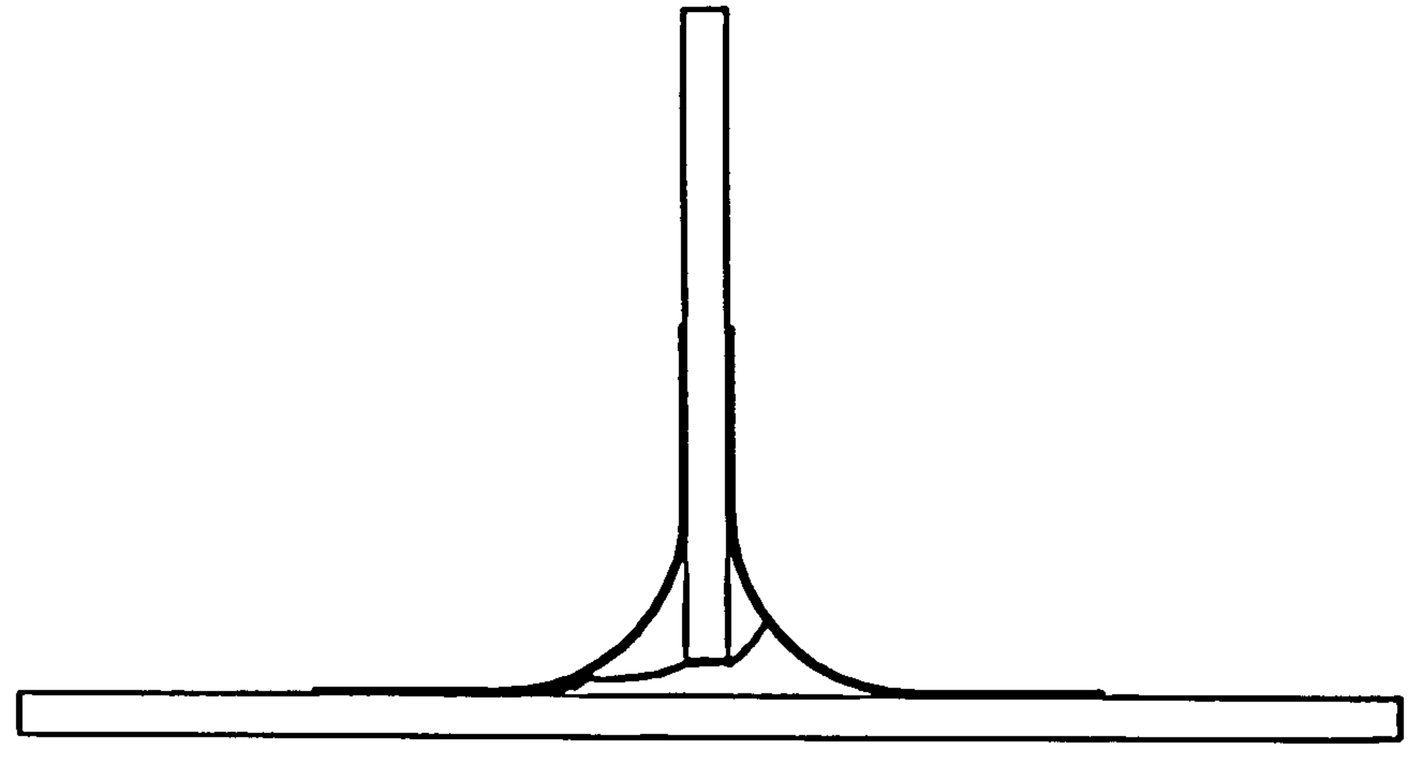

(b)

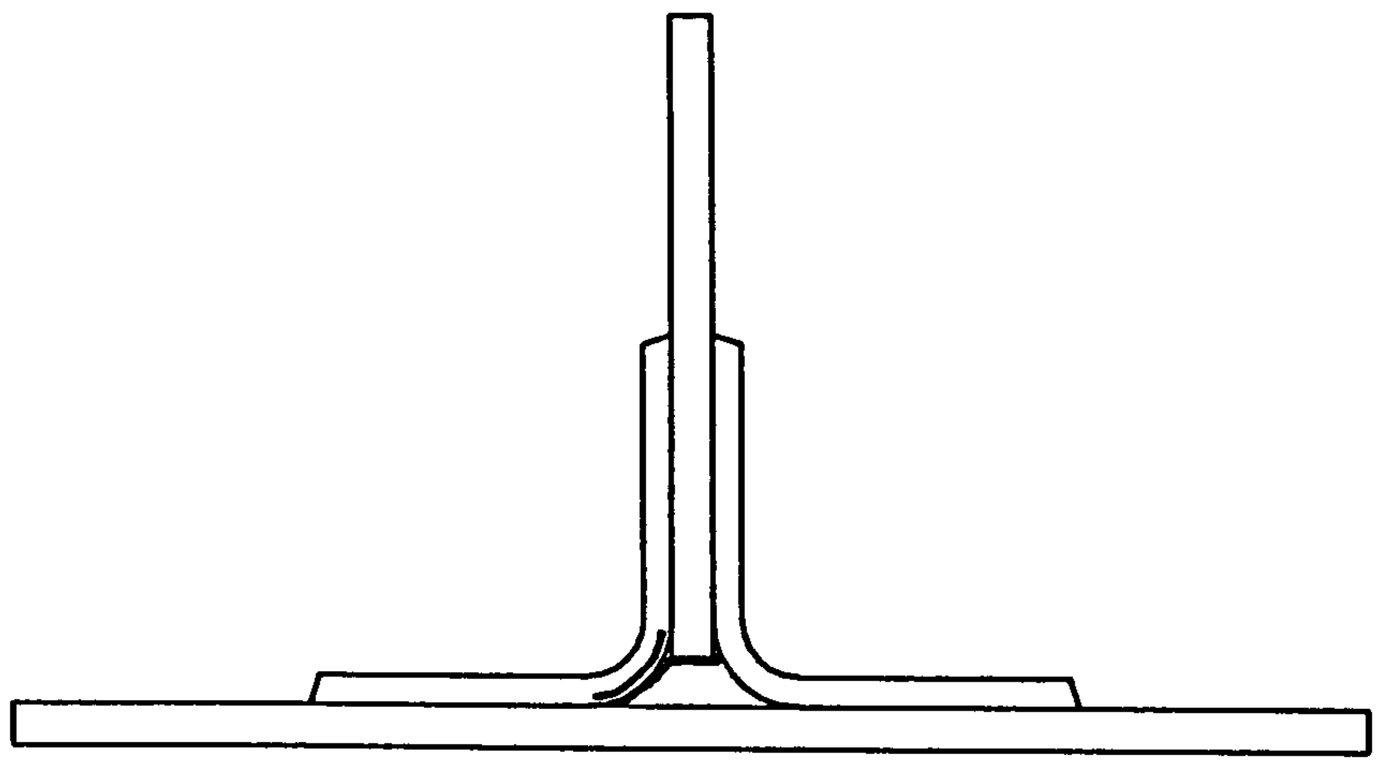

(c)

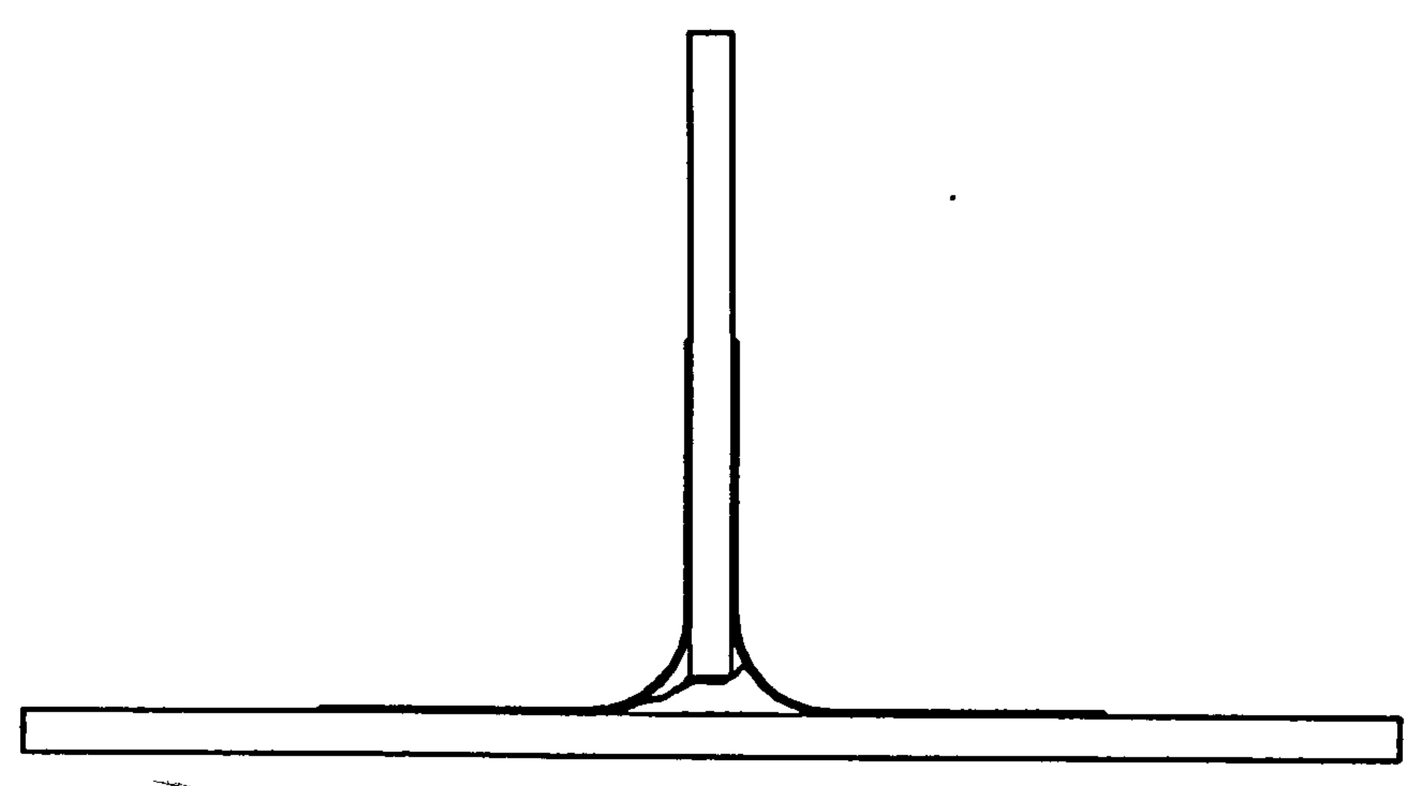

(d)

Figure 5.4 Failure Mechanisms for Each joint Type; (a) Joint Type B; (b) Joint Type F; (c) Joint Type N; (d) Joint Type K.

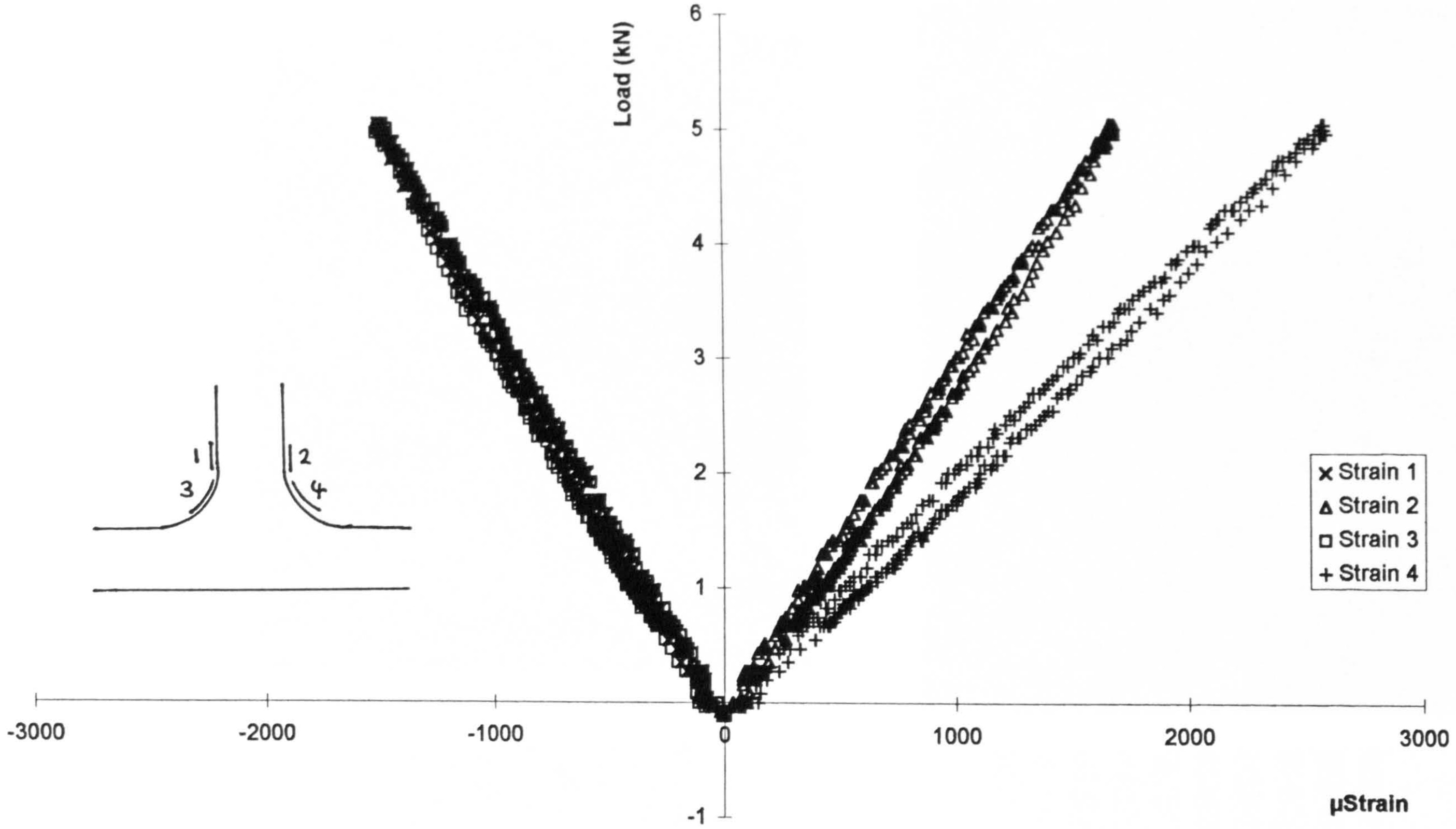

Figure 5.5 Load vs Strain Results for the B Type Joint.

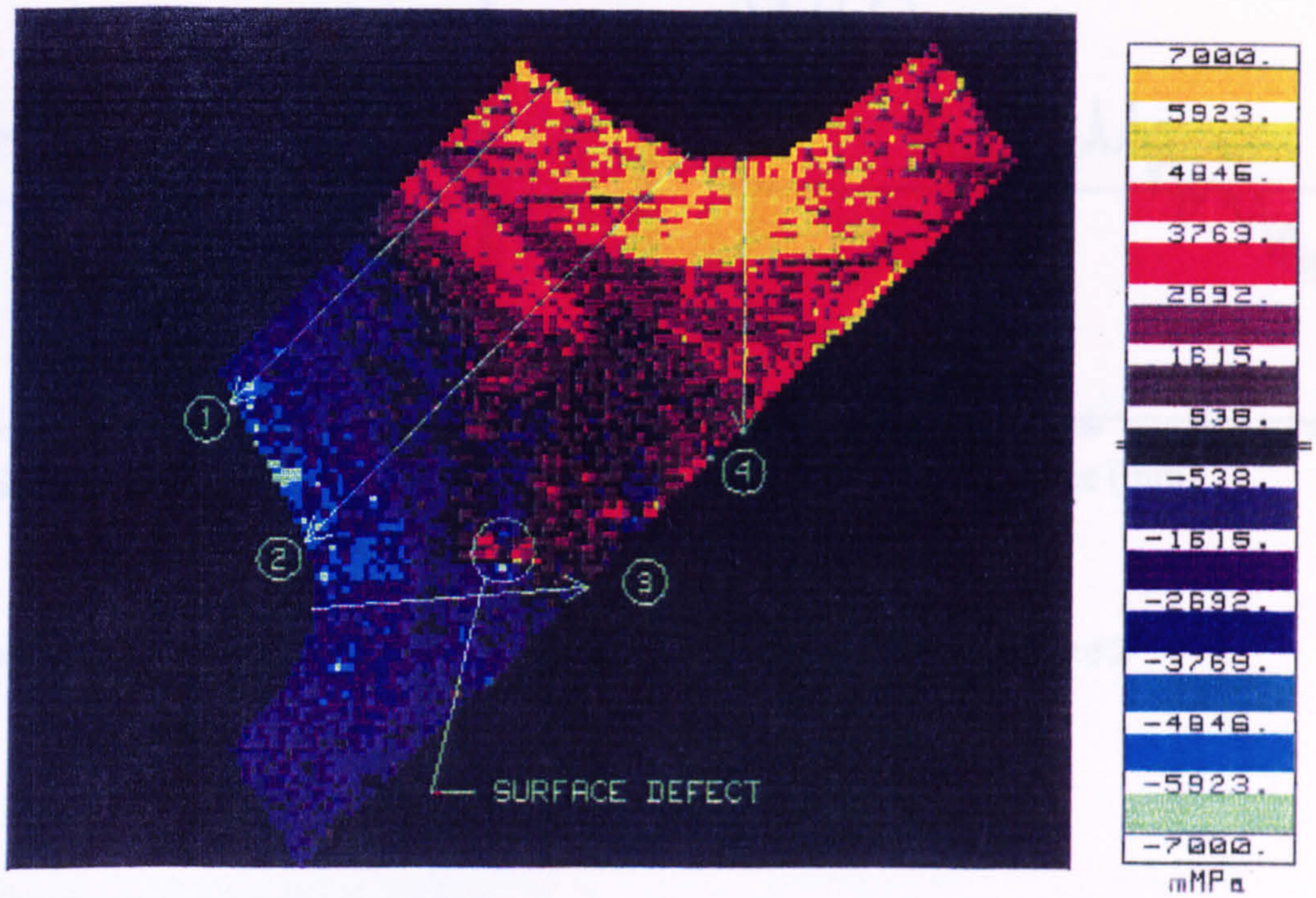

(a)

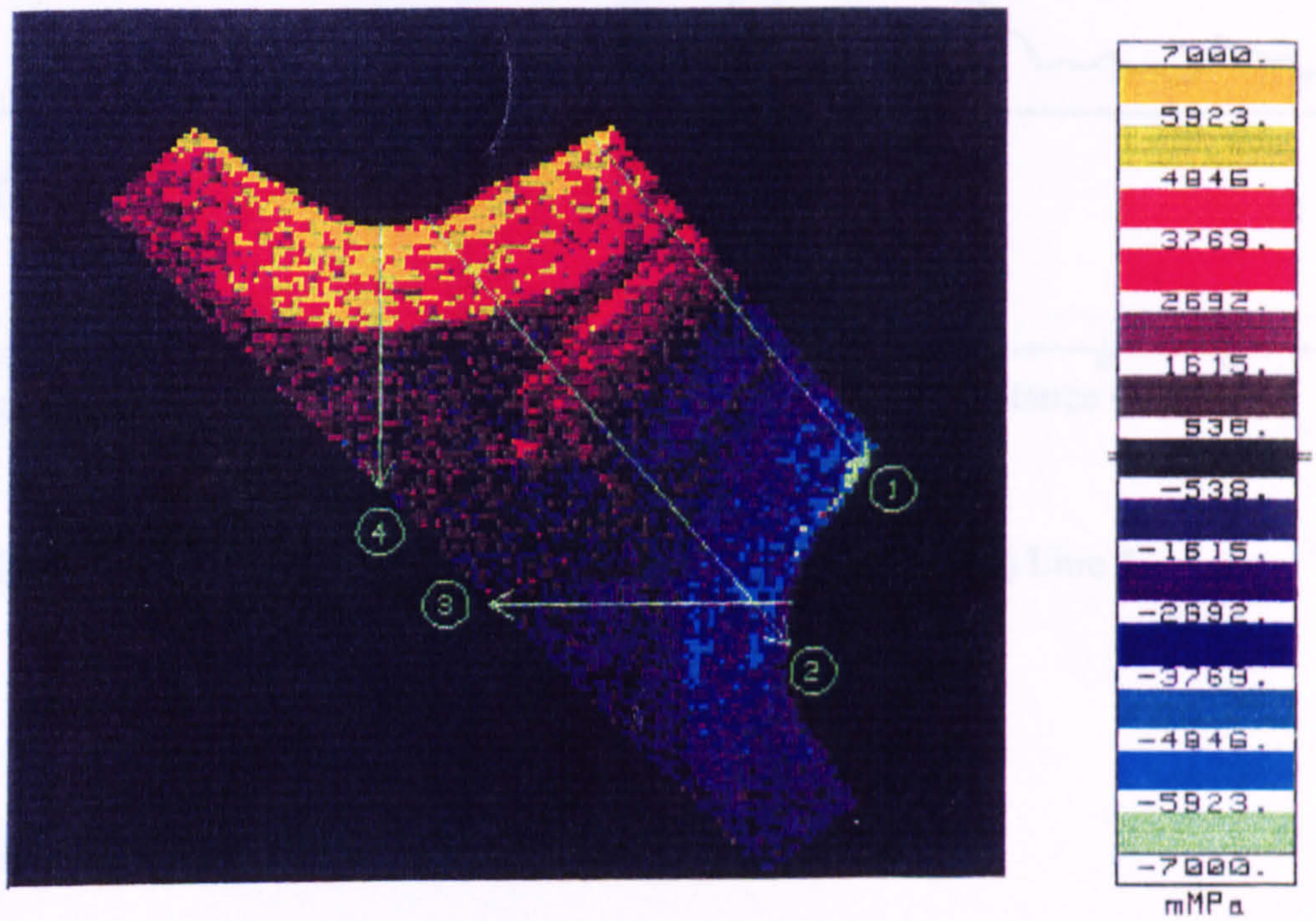

(b)

Figure 5.6 SPATE Contour Plots for Both Faces of the B Type Joint; (a) Face 1; (b) Face 2.

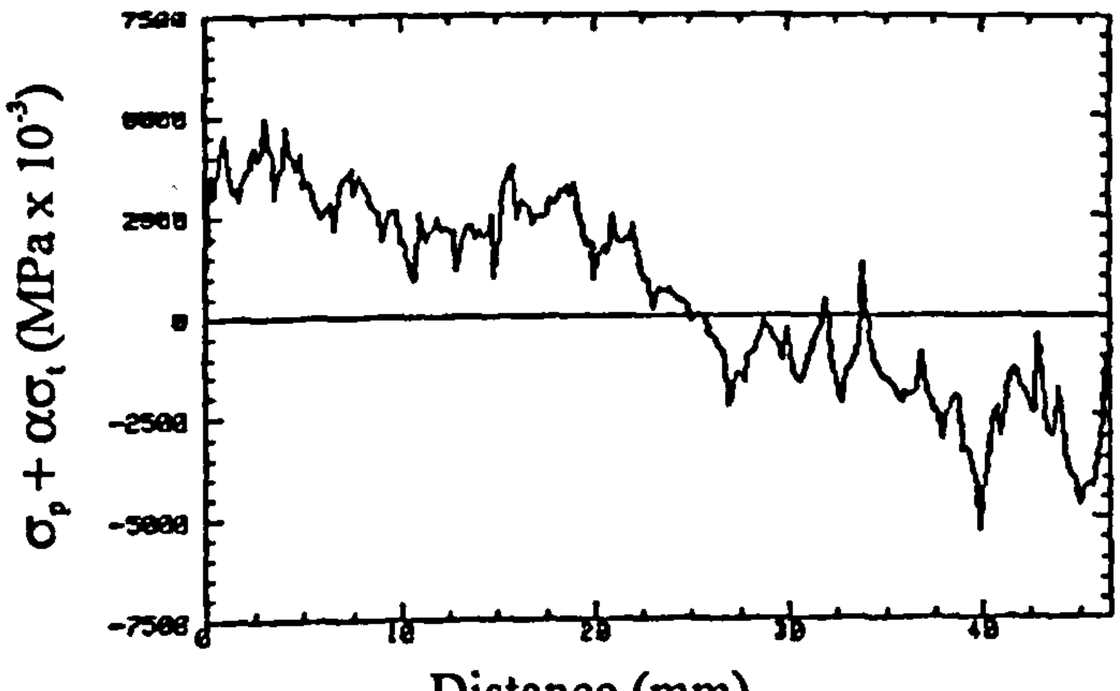

(a) Line 1

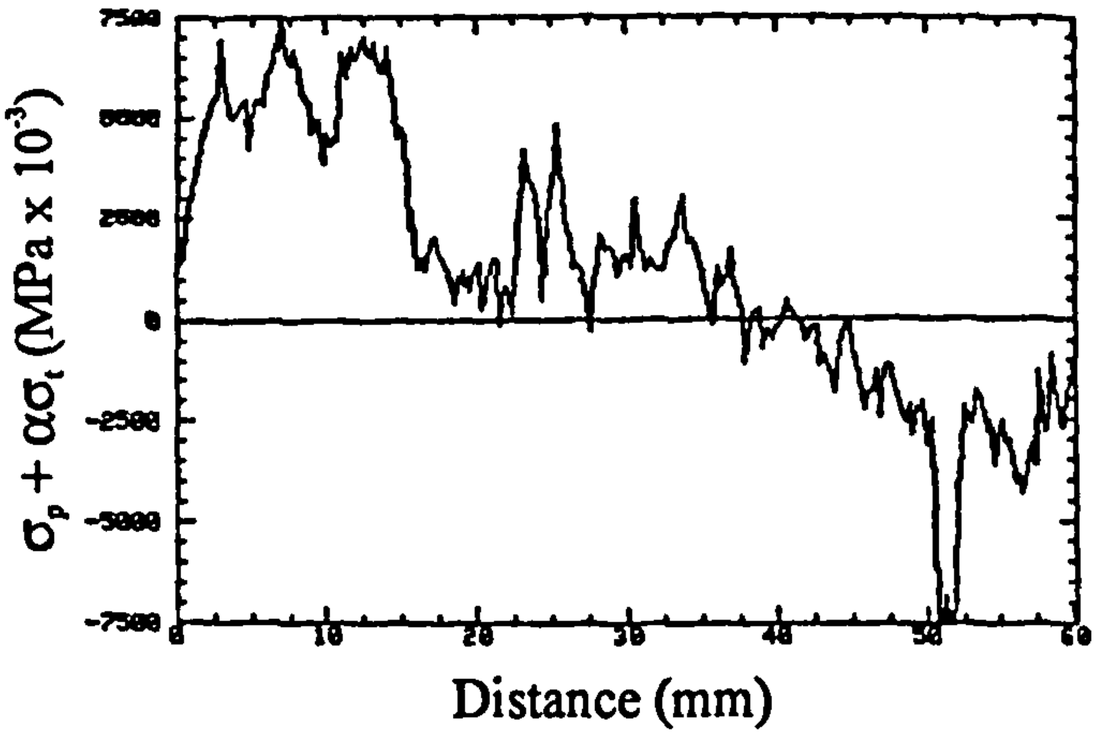

(b) Line 2

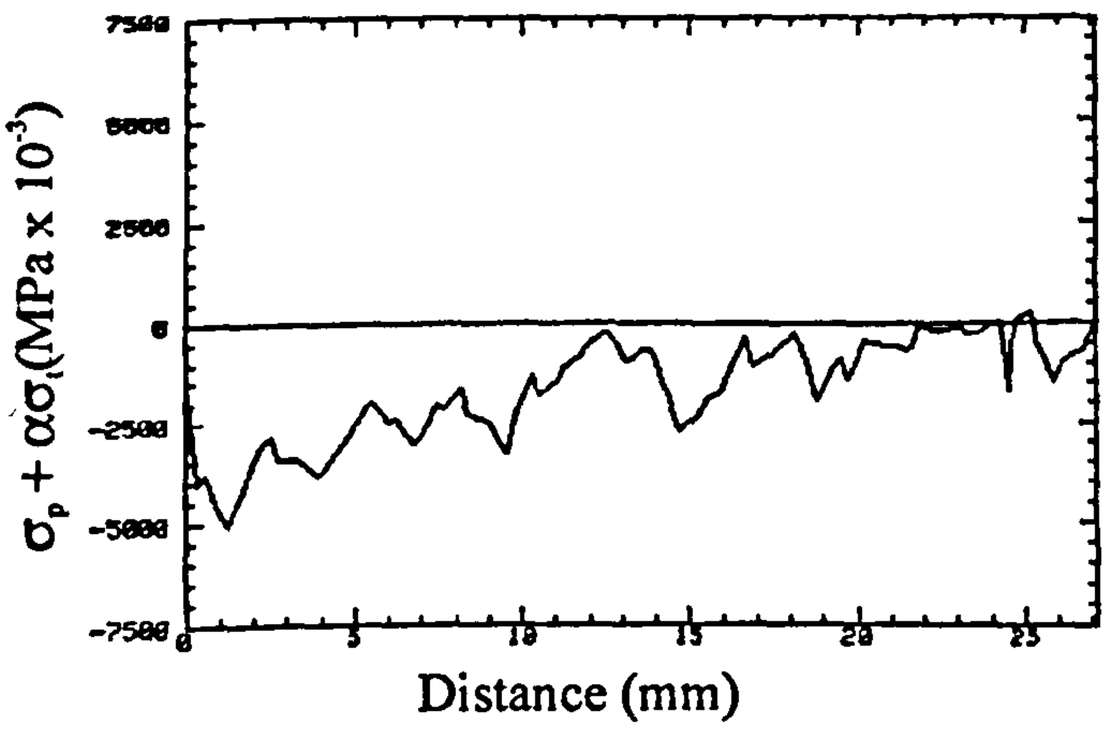

(c) Line 3

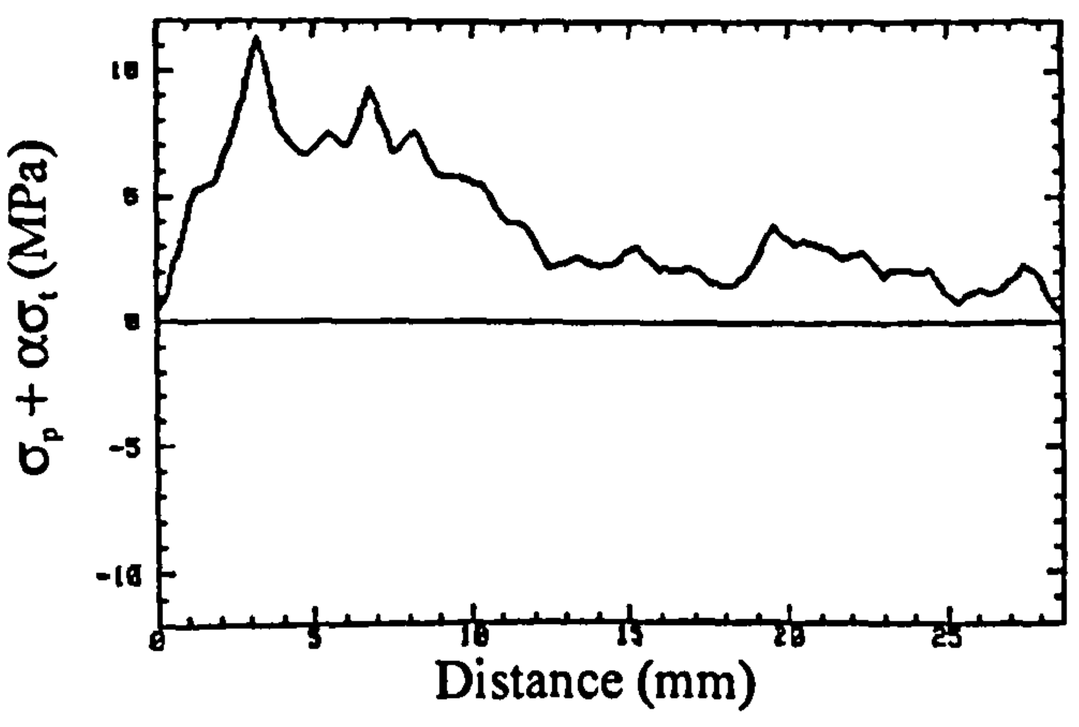

(d) Line 4

Figure 5.7 SPATE Line Plots along Lines 1 to 4 for Face 1.

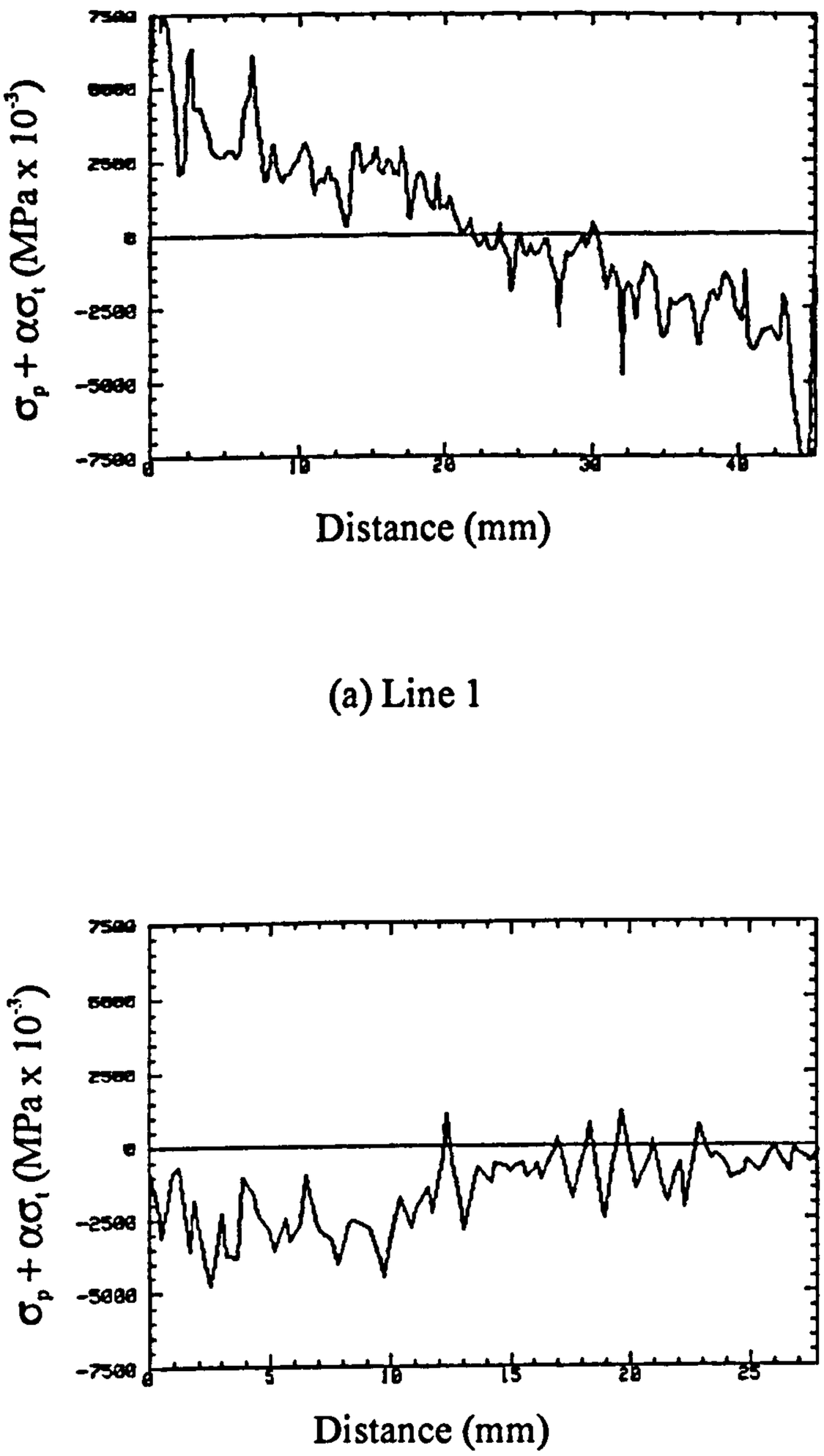

Figure 5.8 SPATE Line Plots along Lines 1 to 4 for Face 2.

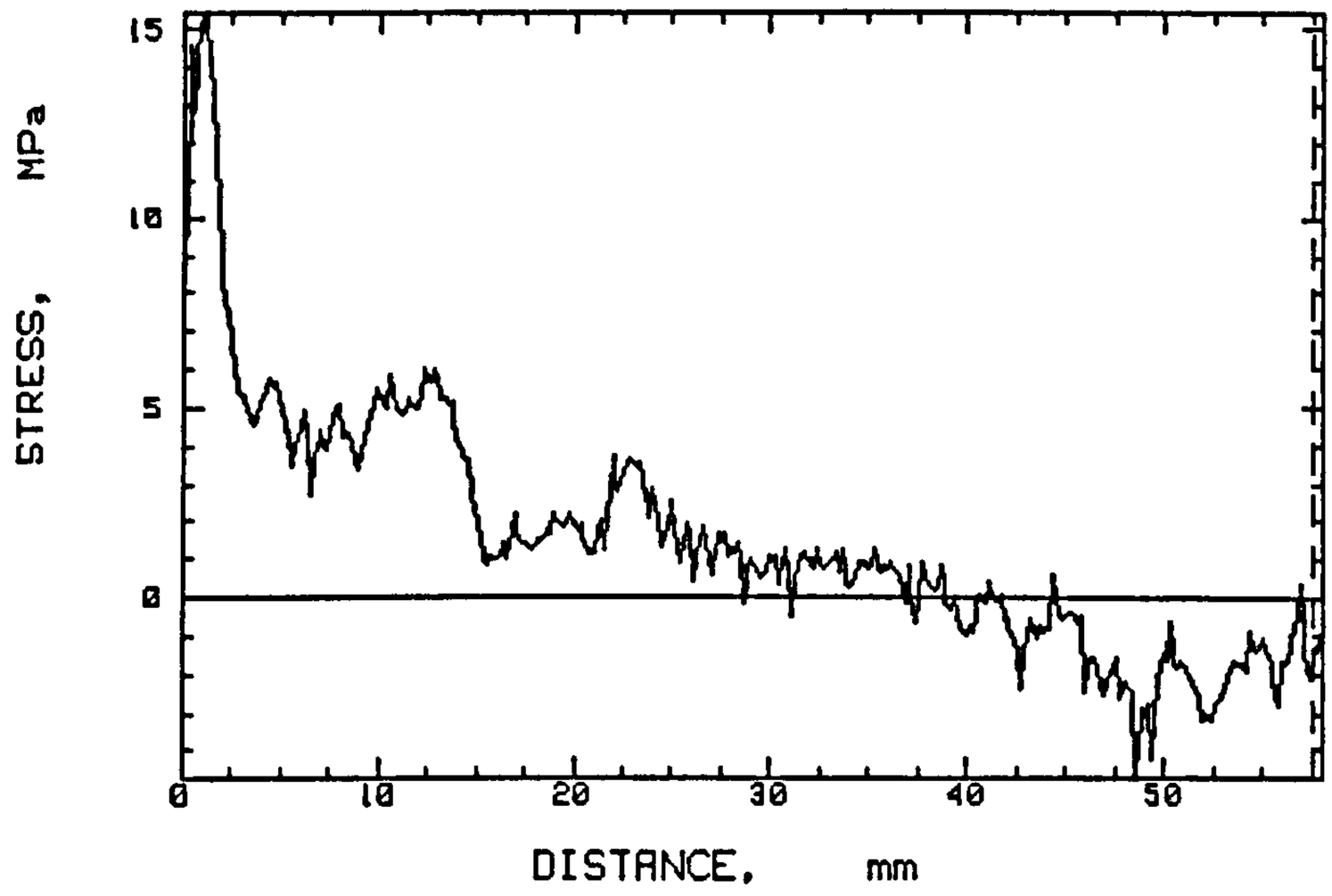

Figure 5.9 SPATE Line Plot along Line 2, Face 1 with a Photoelastic Coating Bonded in Place.

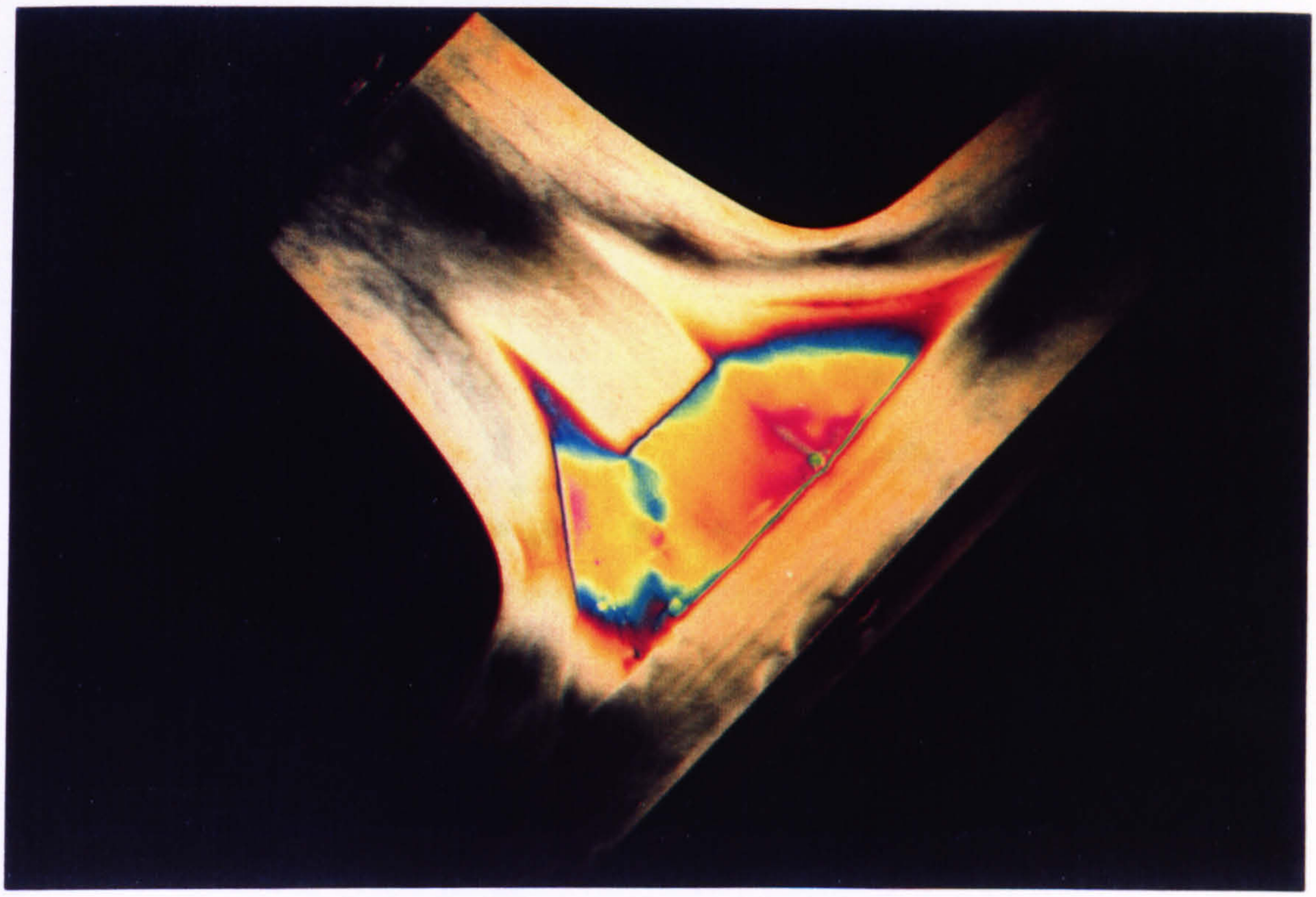

Figure 5.10 Photoelastic Fringe Pattern for Face 2 of the B Type Joint at 5 kN.

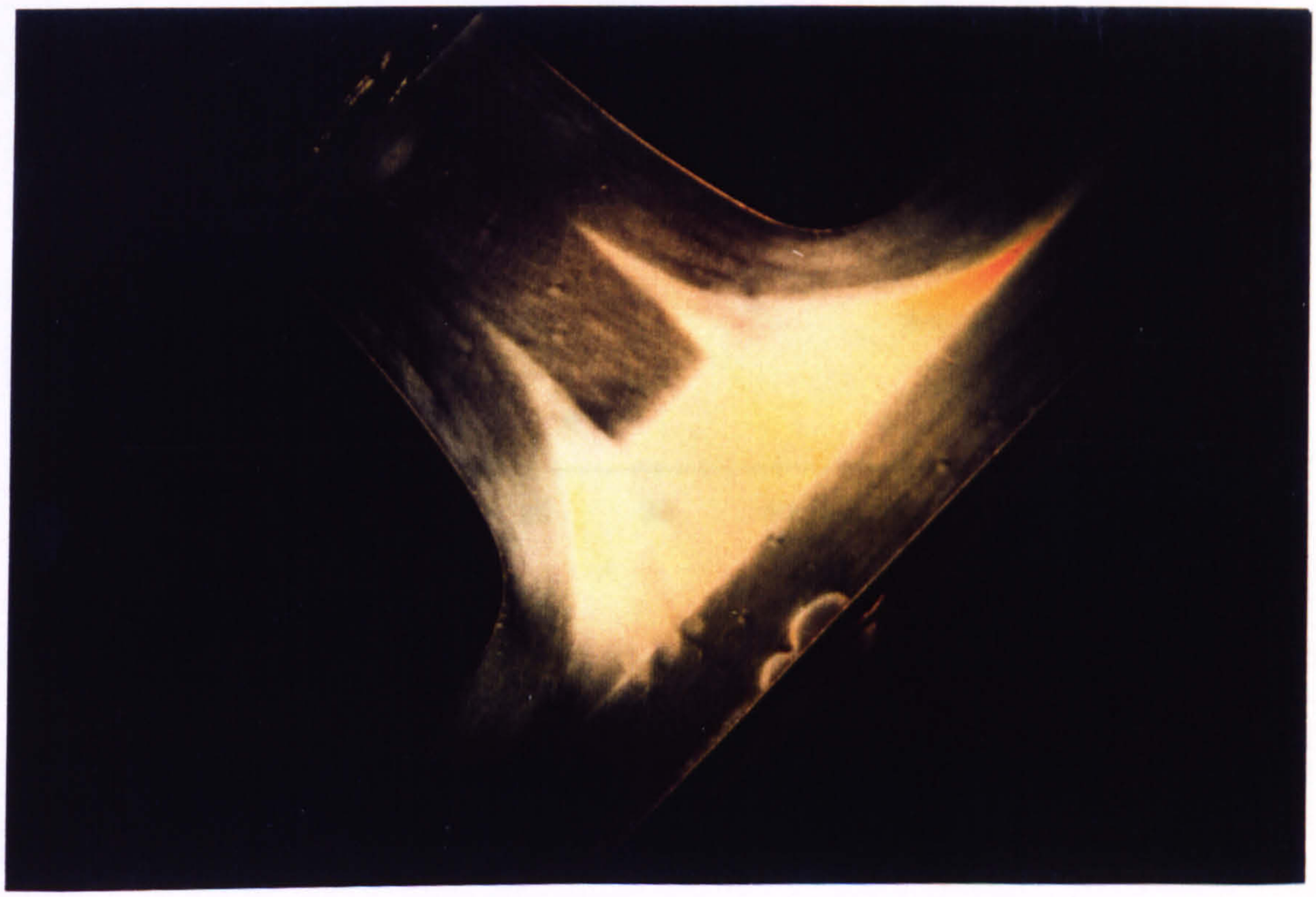

Figure 5.11 Photoelastic Fringe Pattern for Face 2 of the B Type Joint at 0 kN.

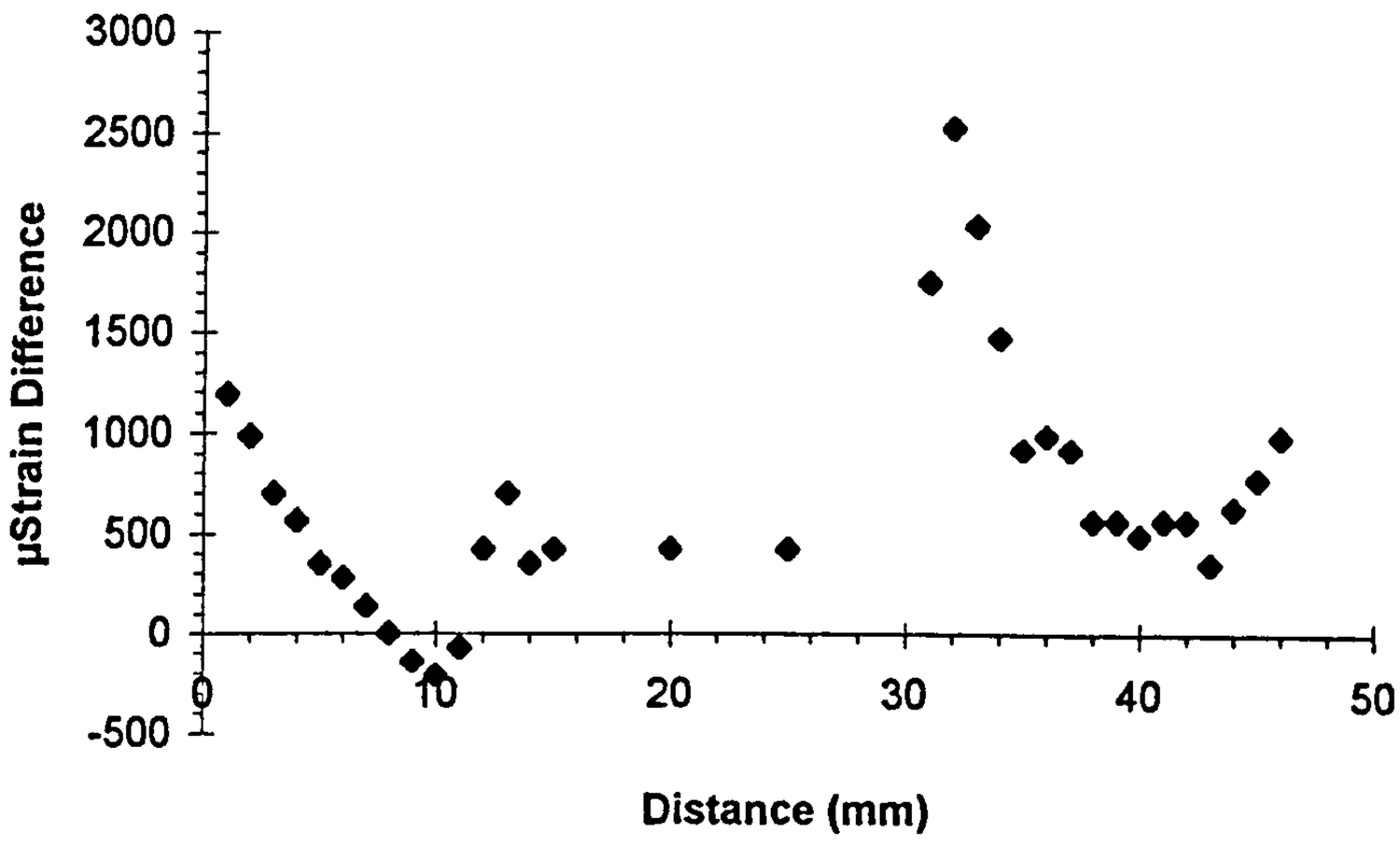

Figure 5.12a Photoelastic Line Plot along Line 1 for Face 2.

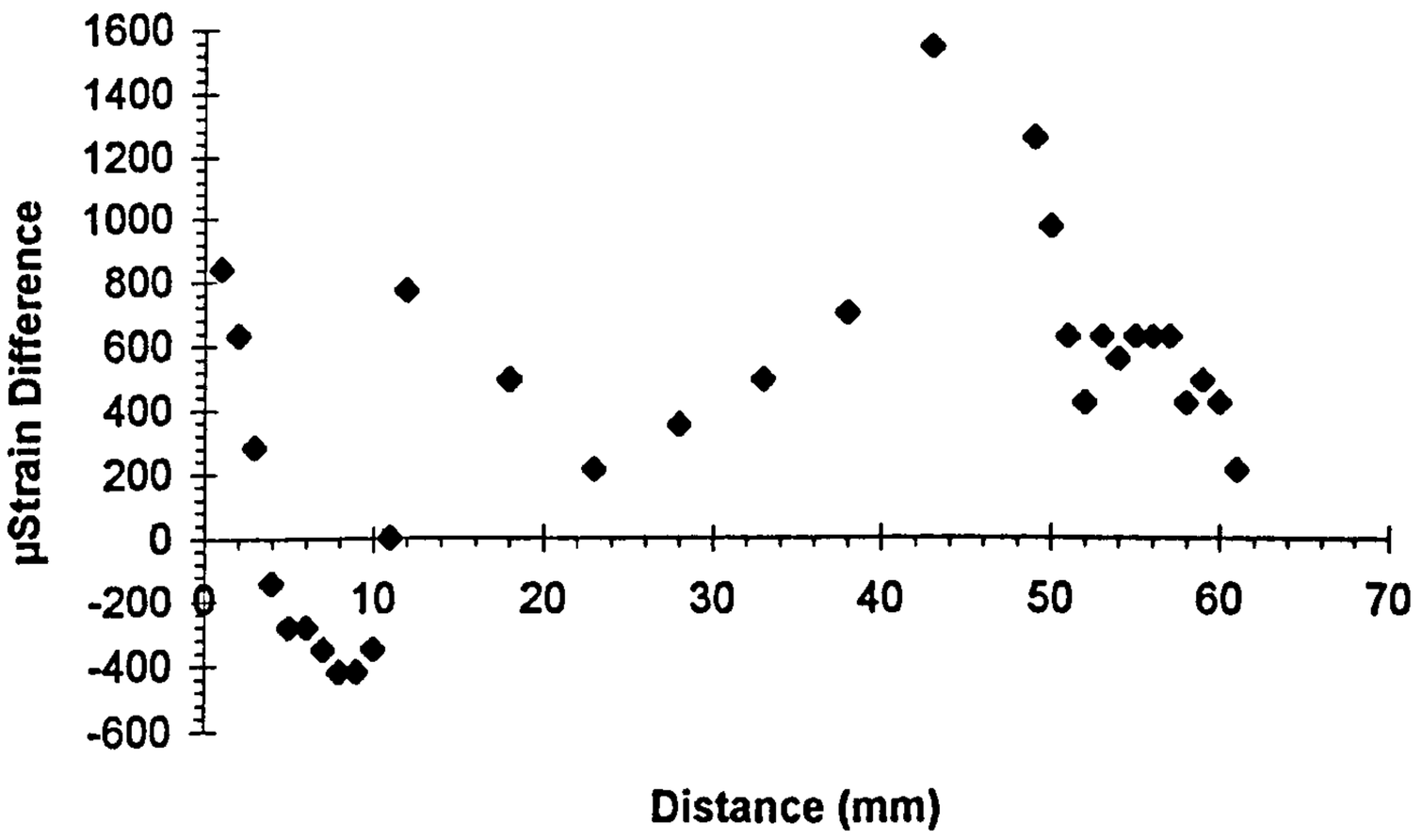

Figure 5.12b Photoelastic Line Plot along Line 2 for Face 2.

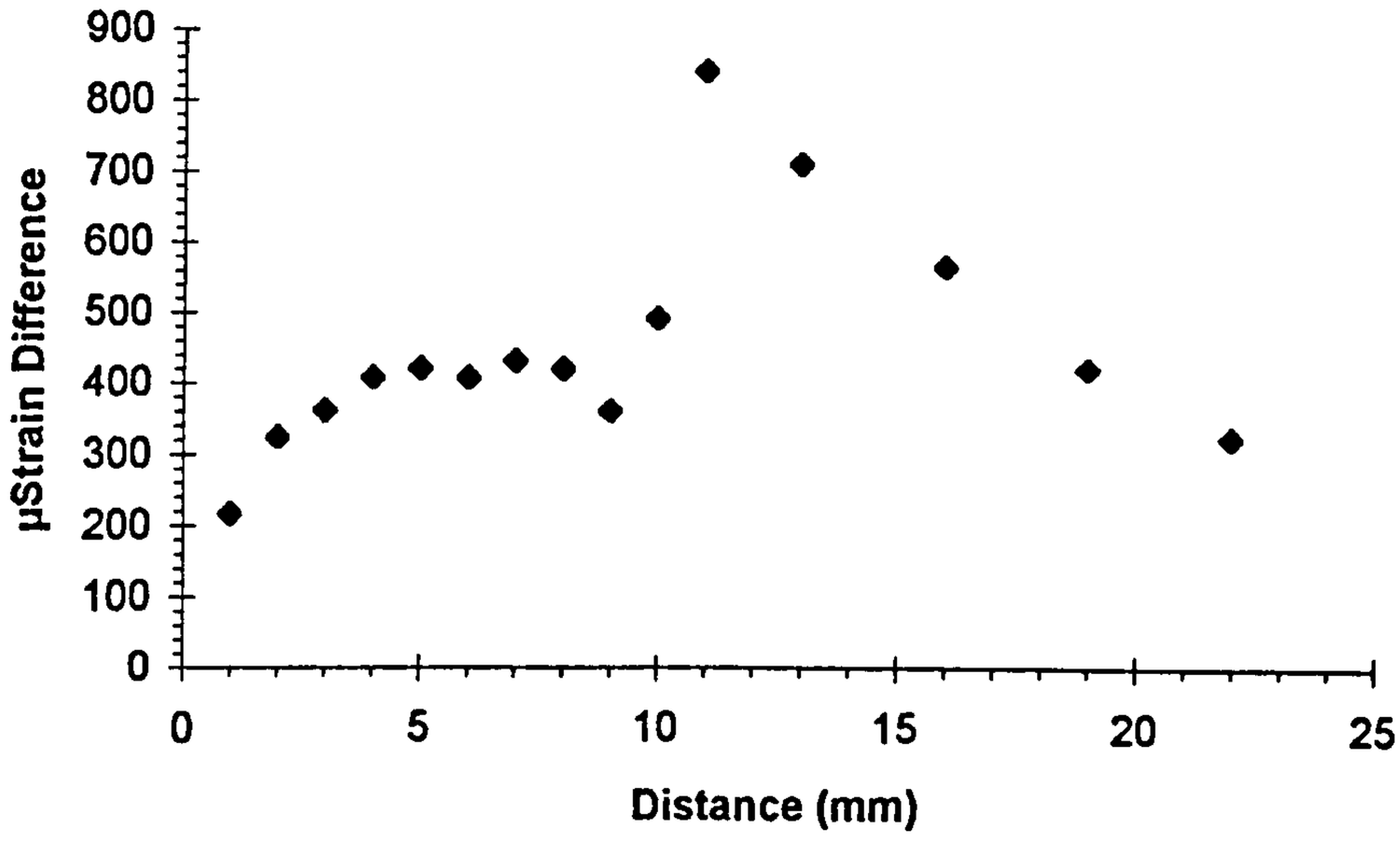

Figure 5.12c Photoelastic Line Plot along Line 3 for Face 2.

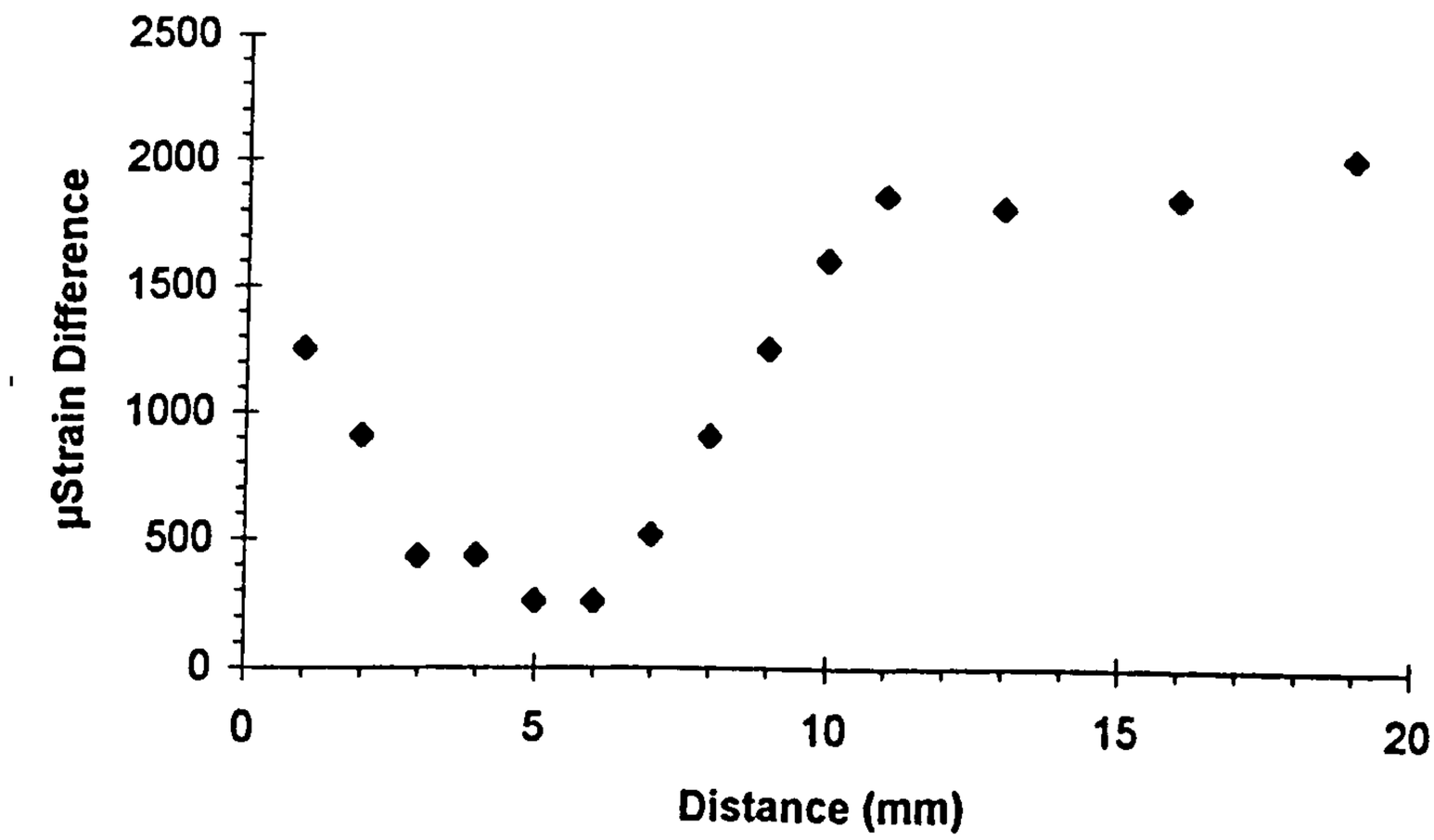

Figure 5.12d Photoelastic Line Plot along Line 4 for Face 2.

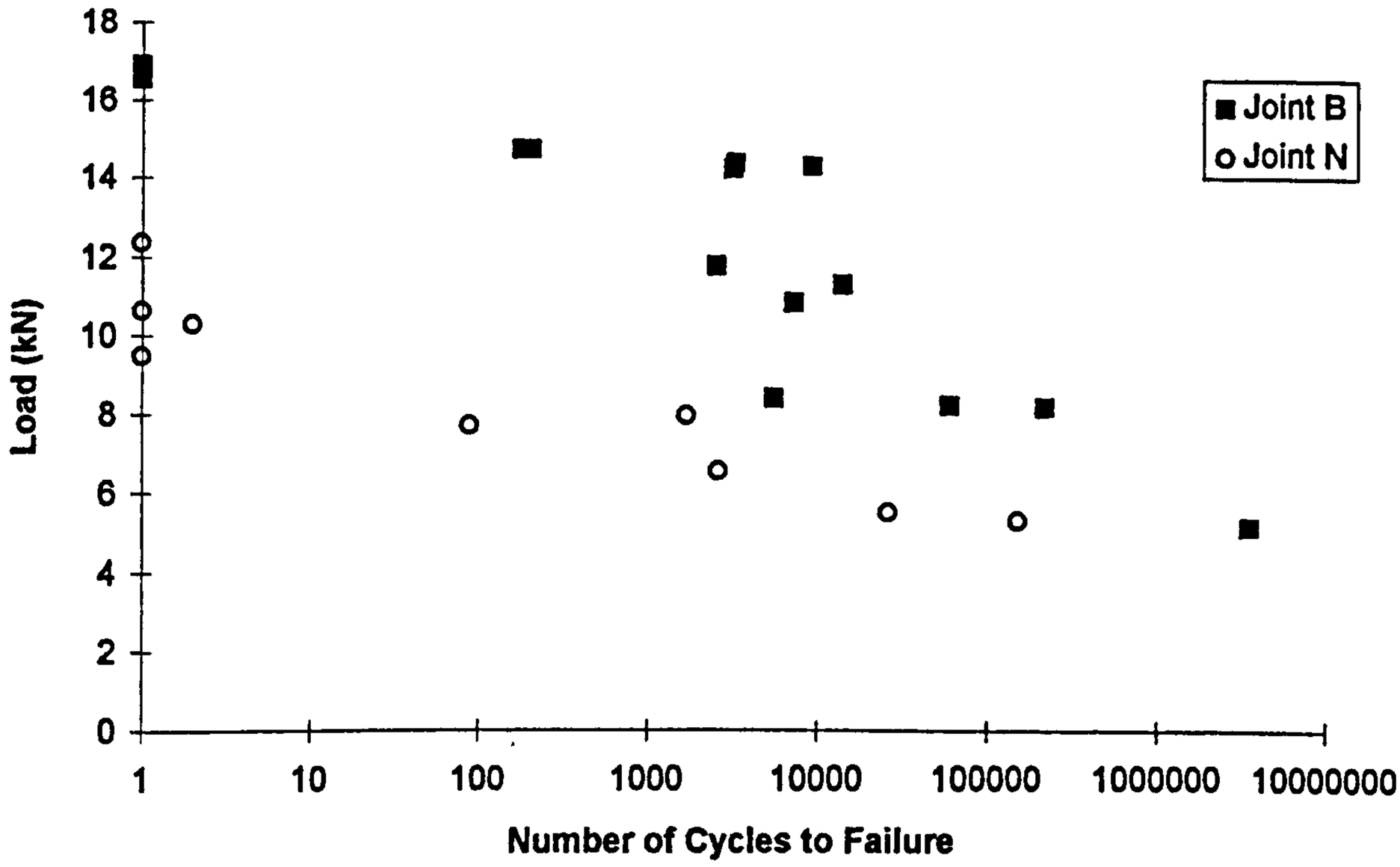

(a)

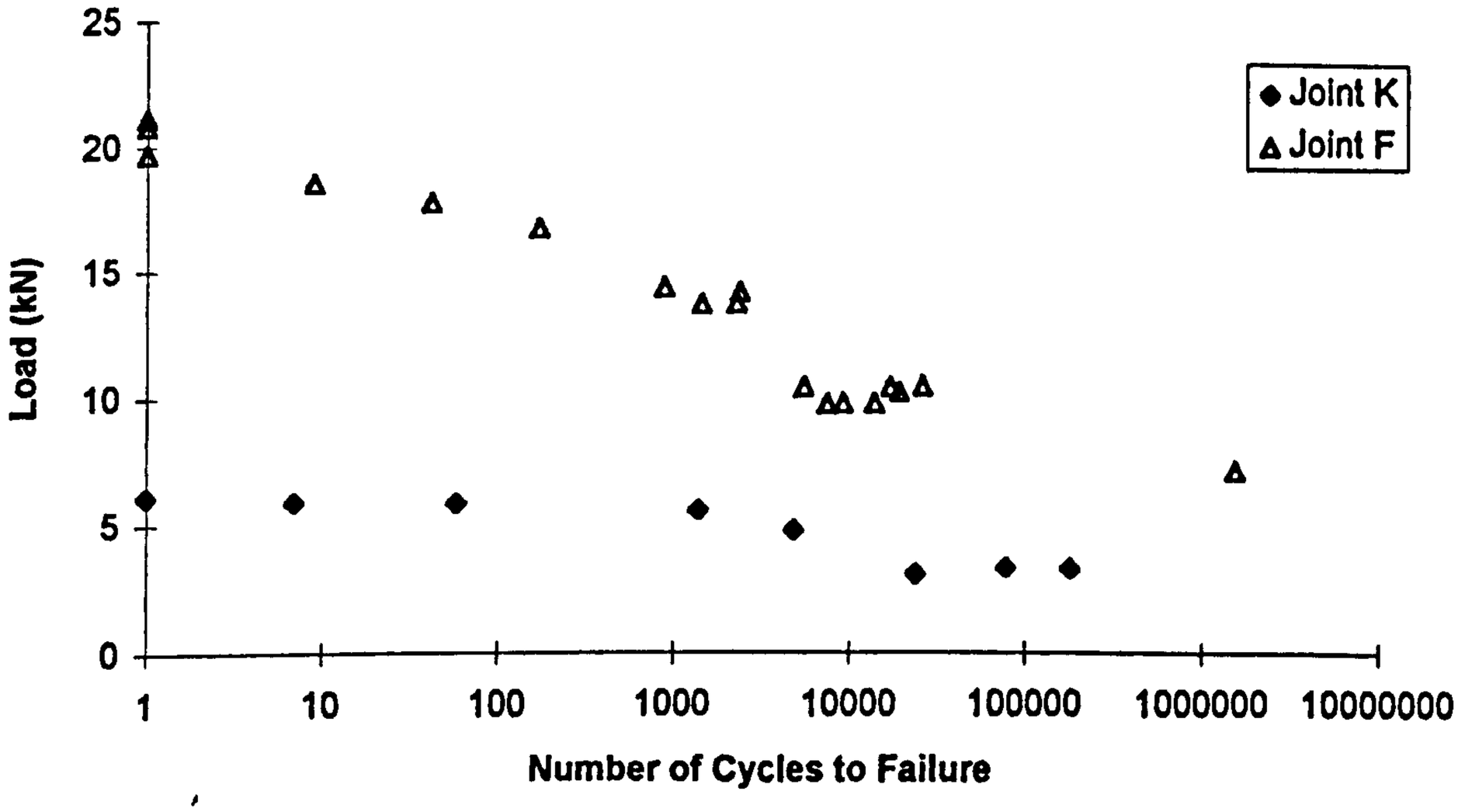

(b)

Figure 6.1 Tee Joint Load - Life Results, Comparison of Radii for; (a) Joint Types B and N; (b) Joint Types K and F.

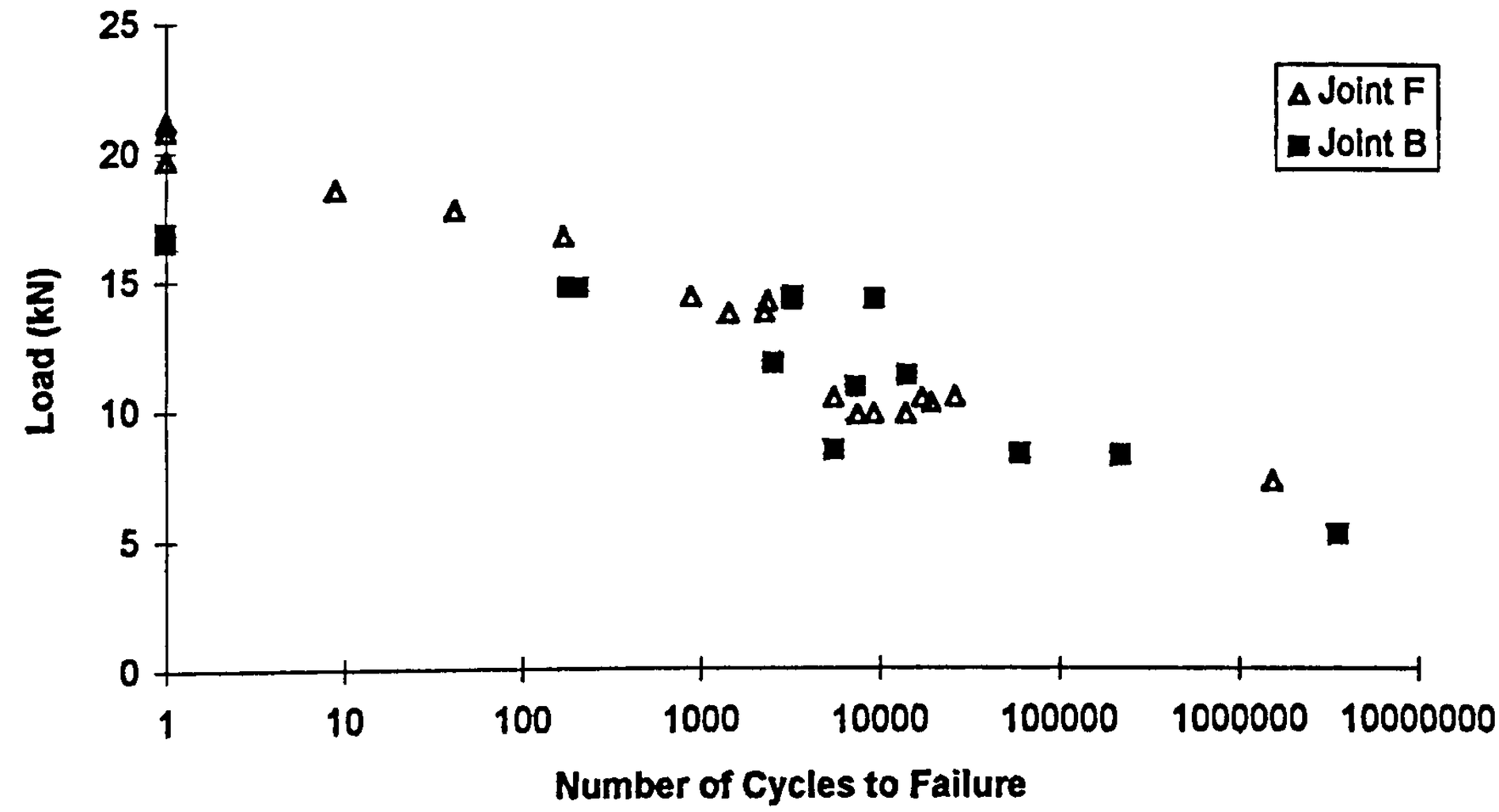

(a)

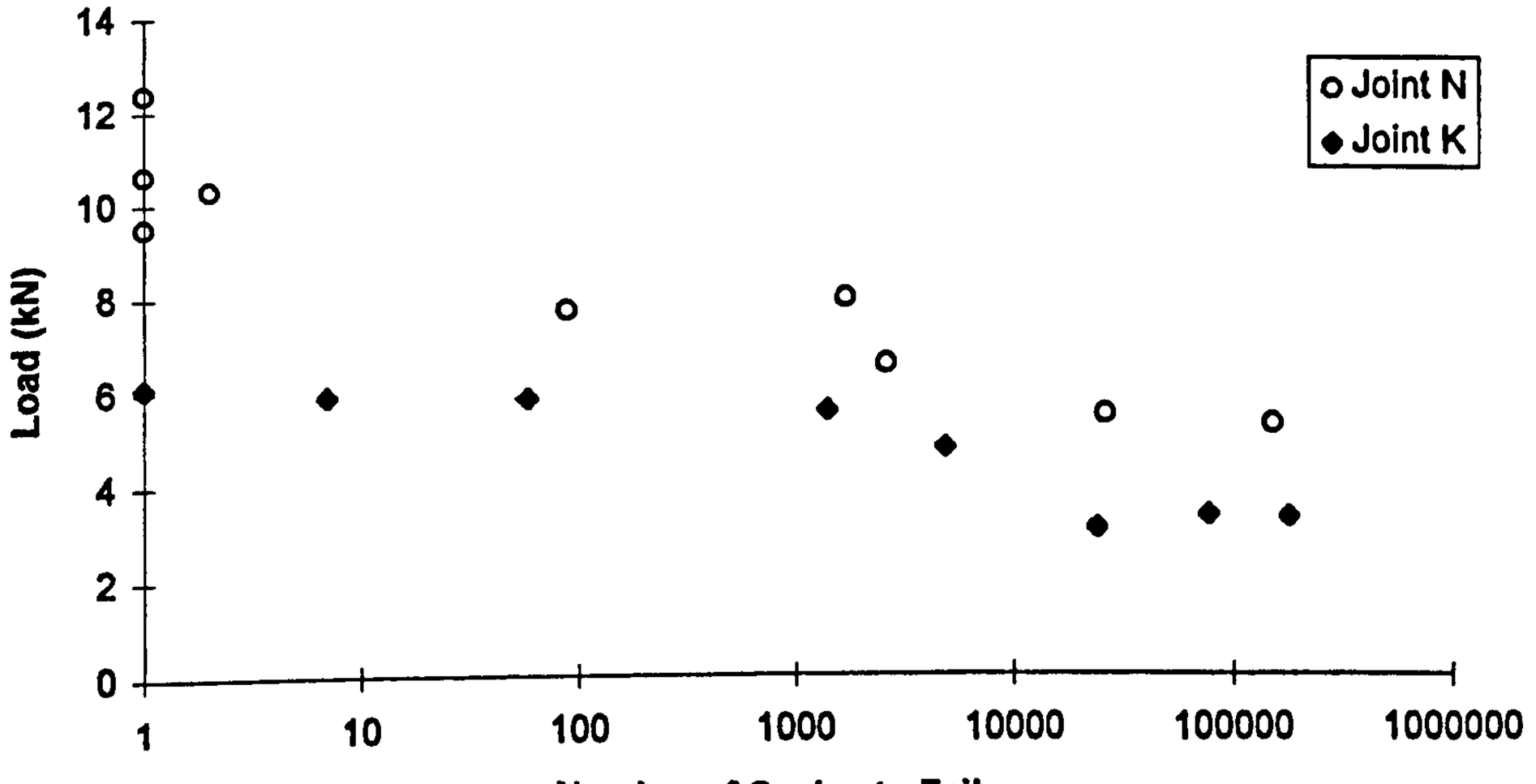

(b)

Figure 6.2 Tee Joint Load - Life Results, Comparison of Number of Plies for; (a) Joint Types B and F; (b) Joint Types K and N.

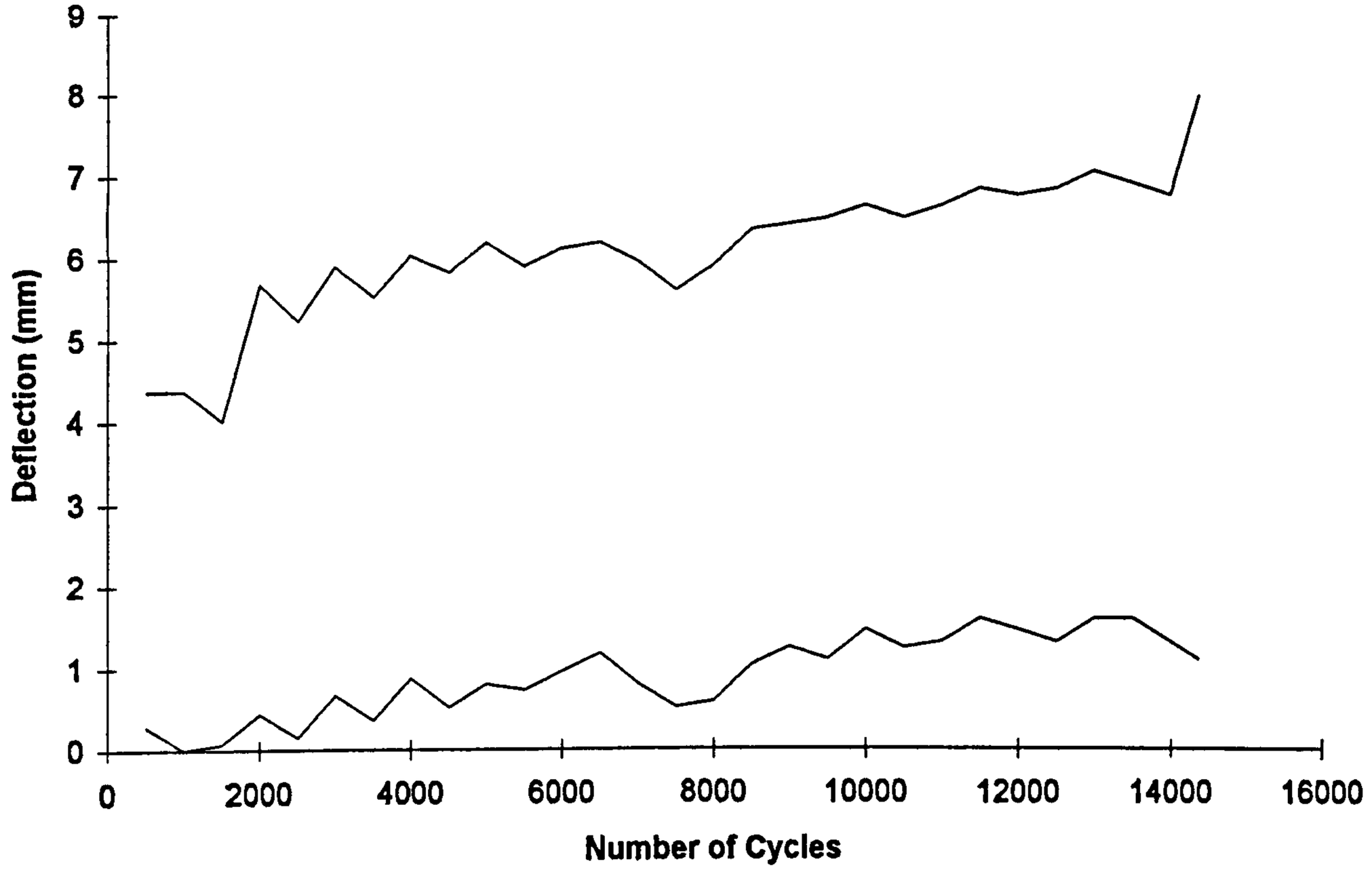

Figure 6.3a Deflection vs Number of Cycles for Joint Type B.

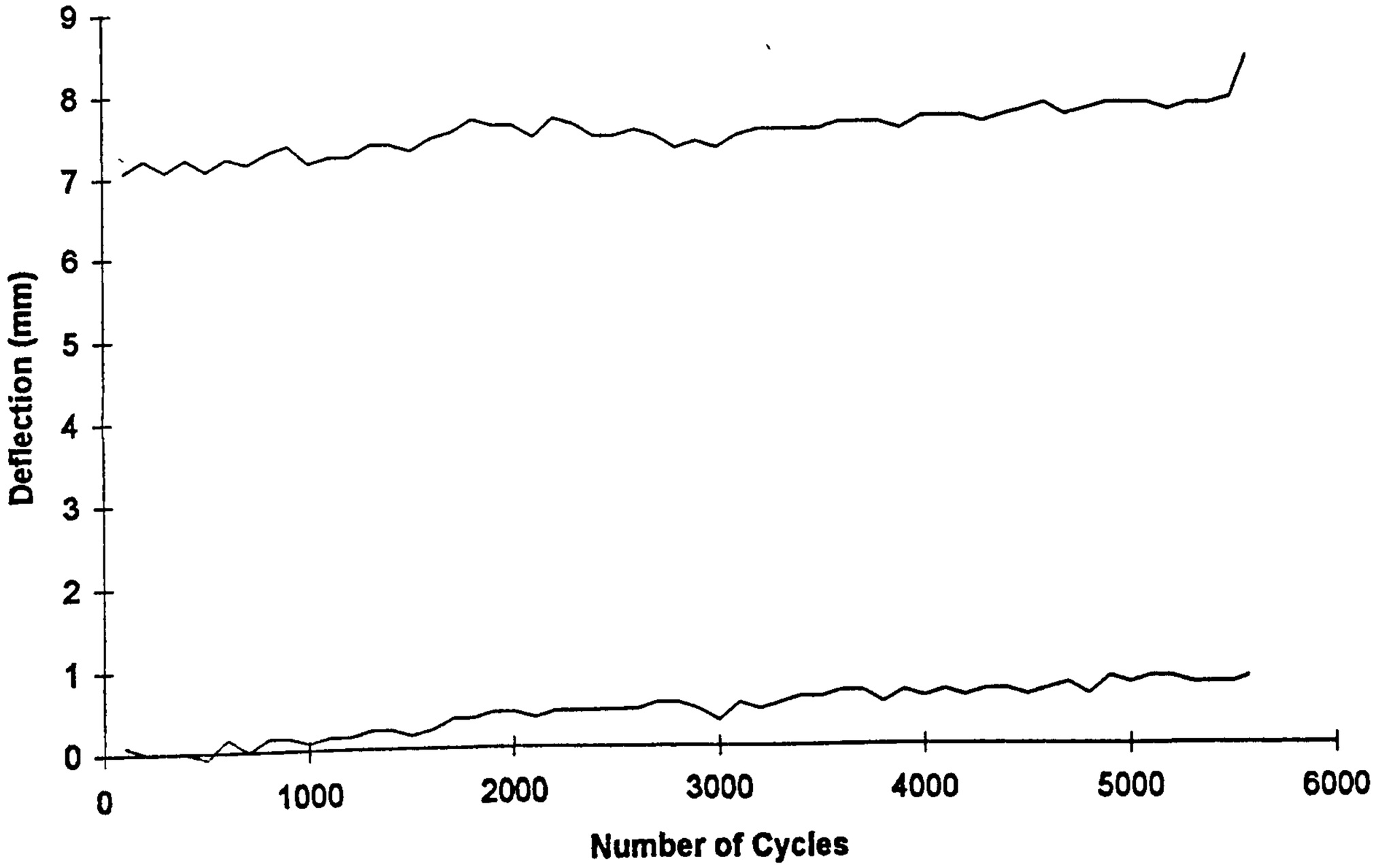

Figure 6.3b Deflection vs Number of Cycles for Joint Type F.

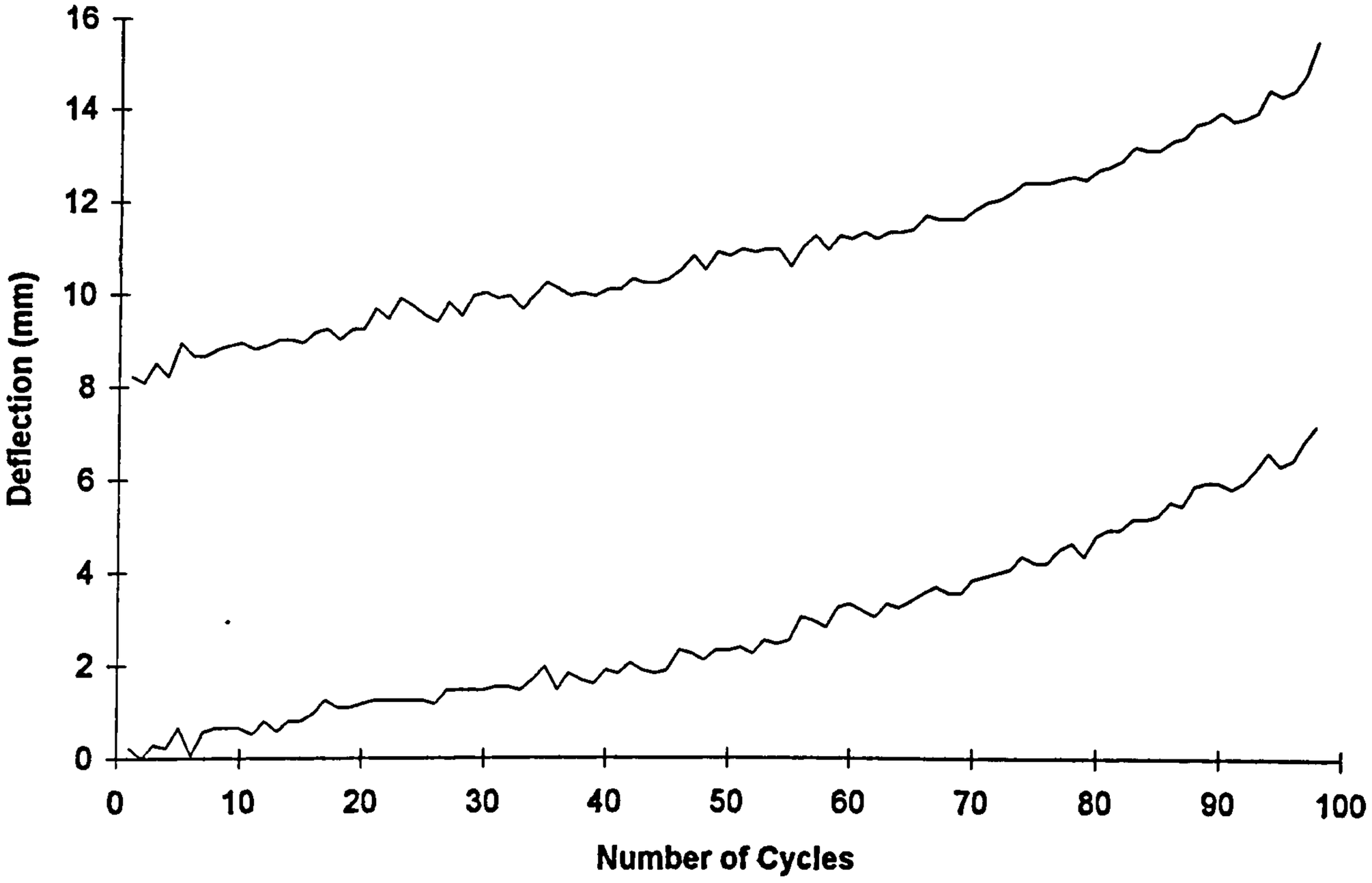

Figure 6.3c Deflection vs Number of Cycles for Joint Type K.

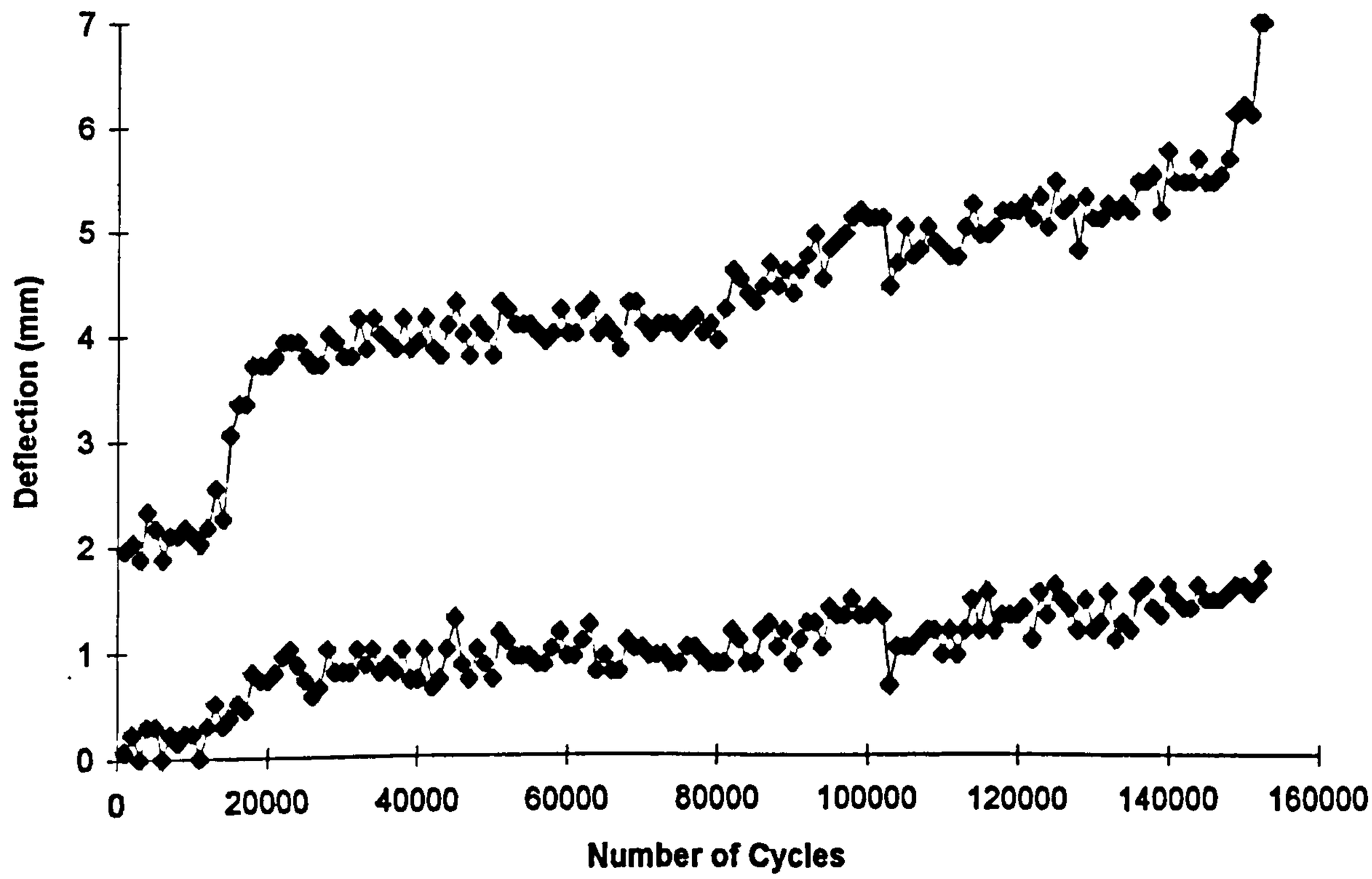

Figure 6.3d Deflection vs Number of Cycles for Joint Type N.

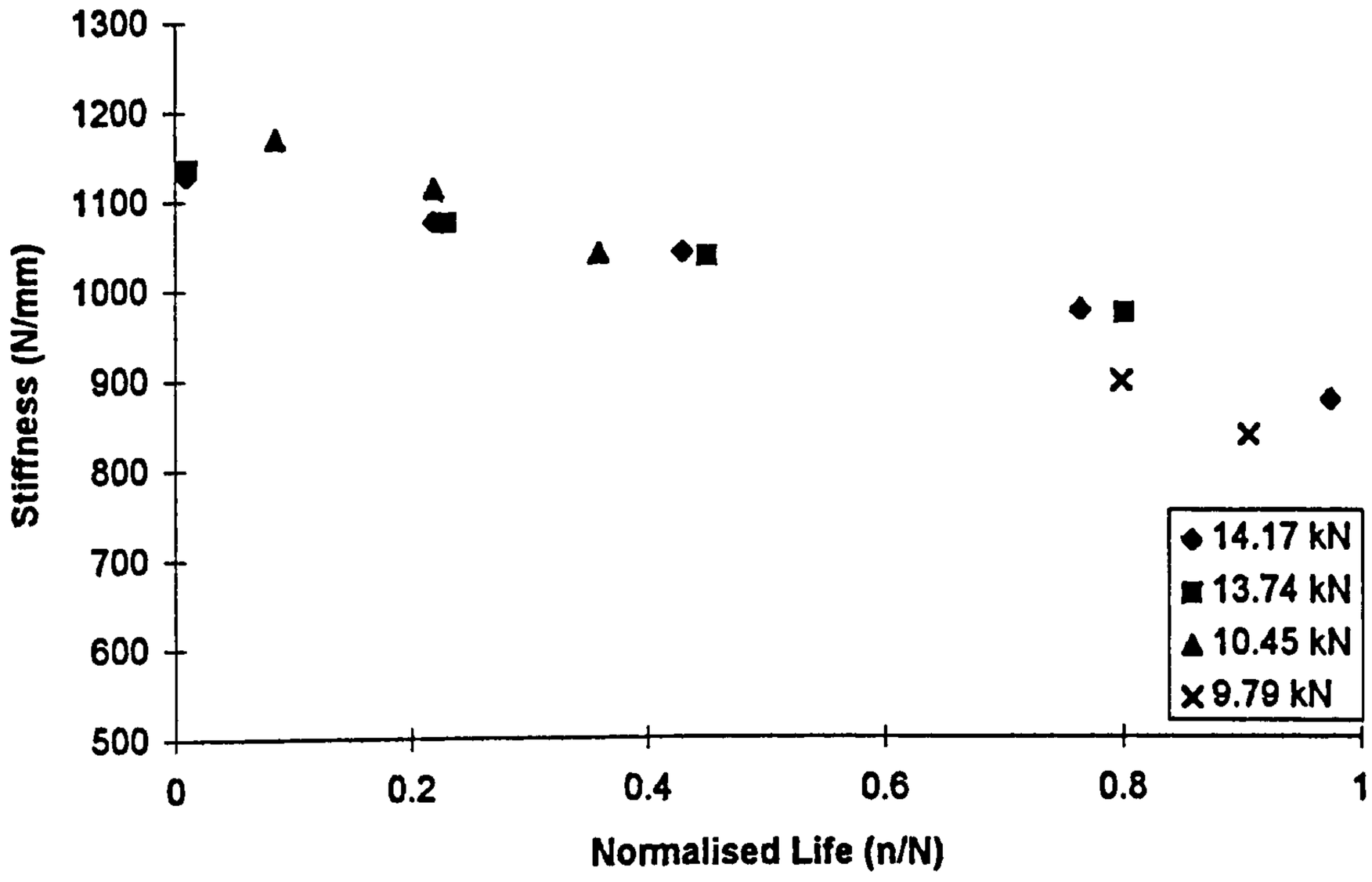

(a)

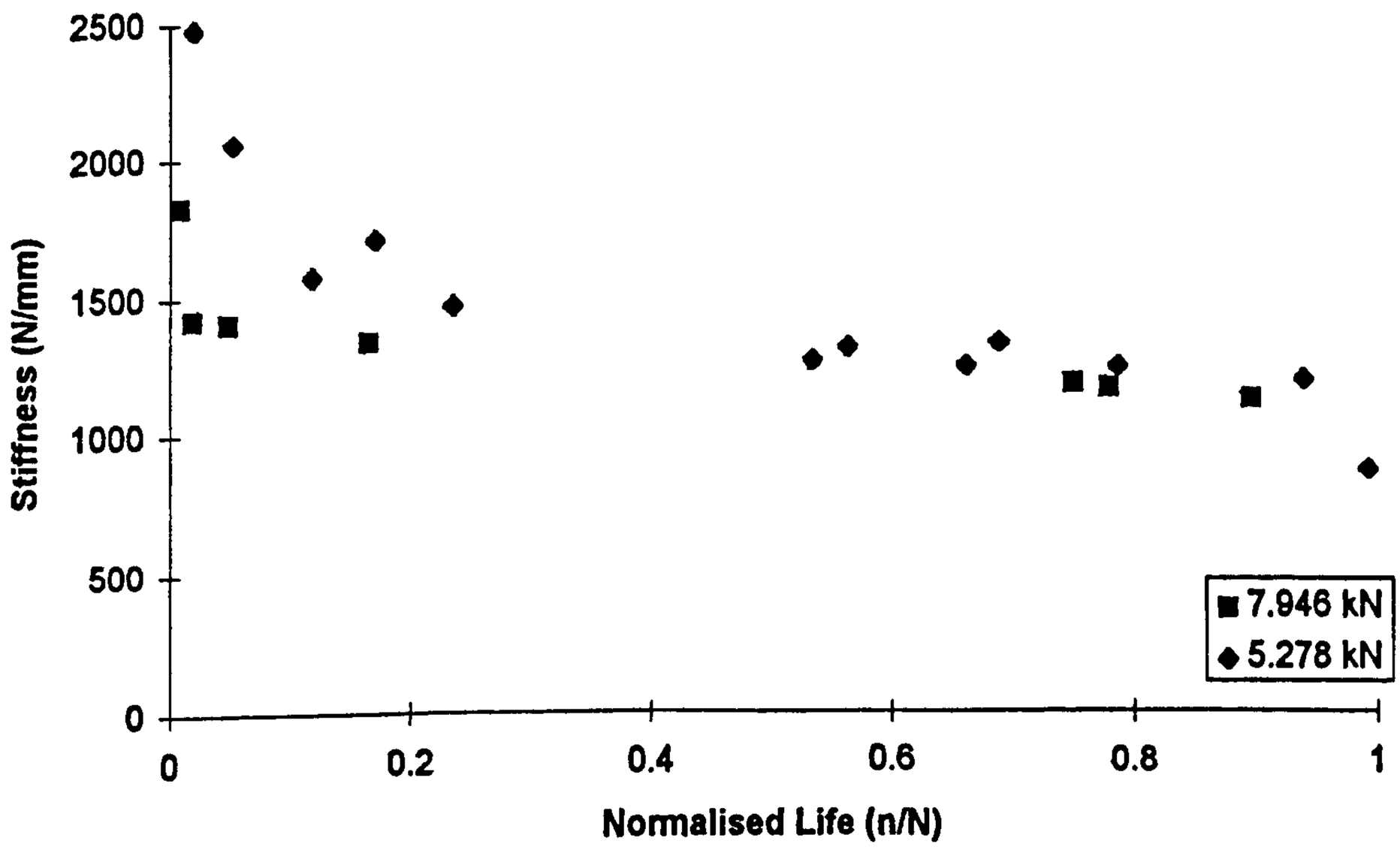

(b)

Figure 6.4 Stiffness Degradation Characteristics for; (a) Joint Type F; (b) Joint Type N.

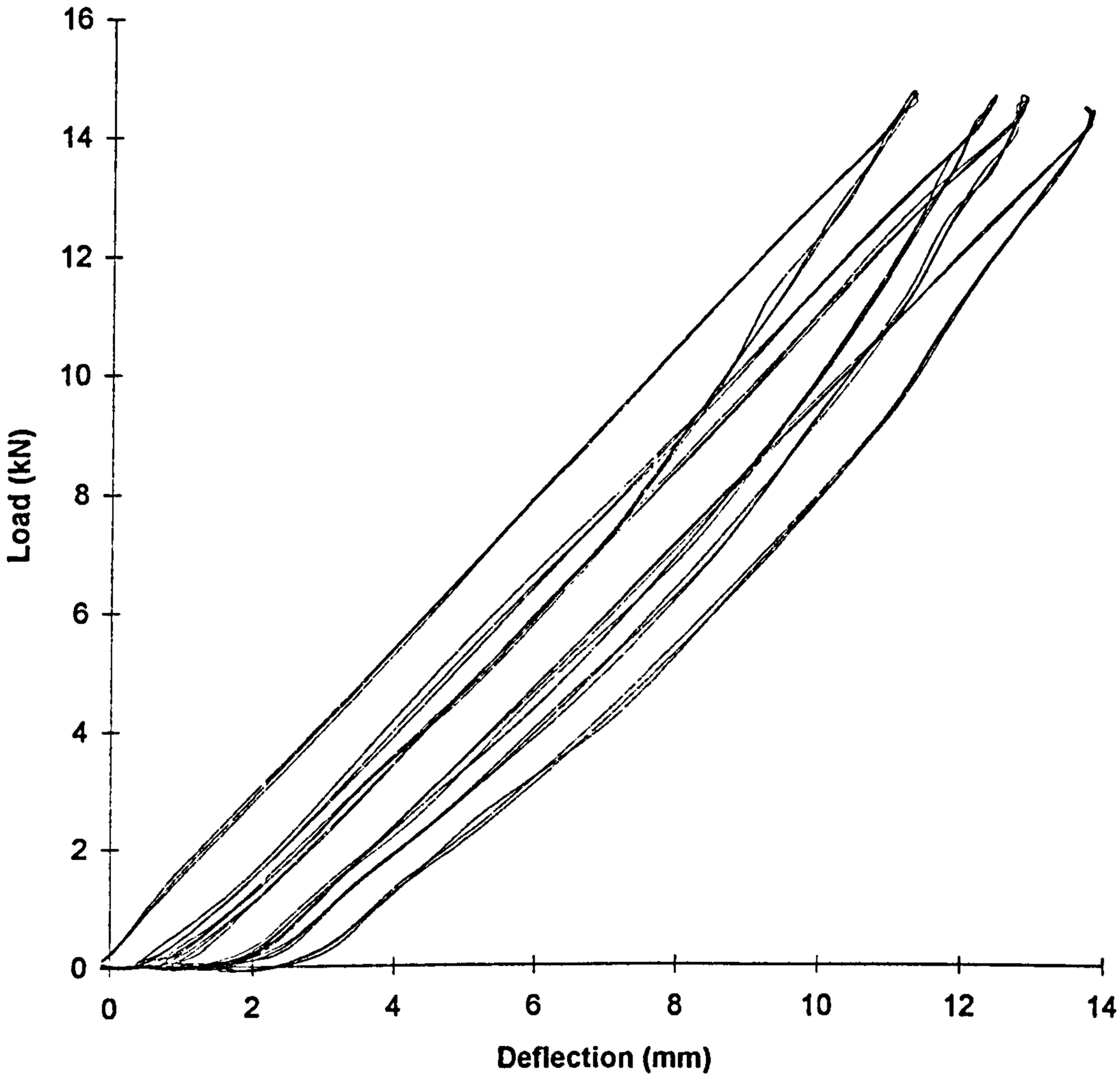

Figure 6.5 Typical Hysterisis Loops for Joint Type F at 70% USS.

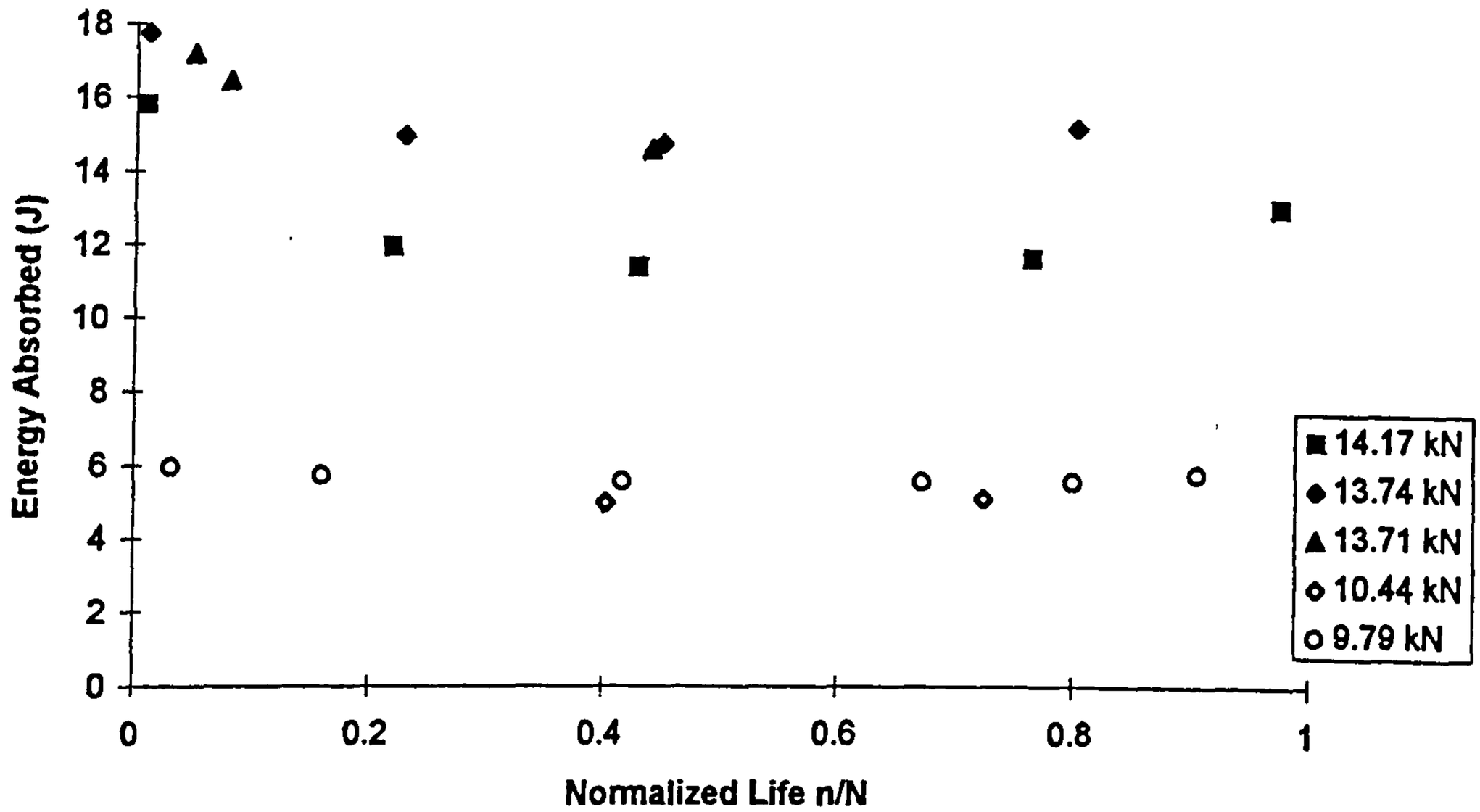

(a)

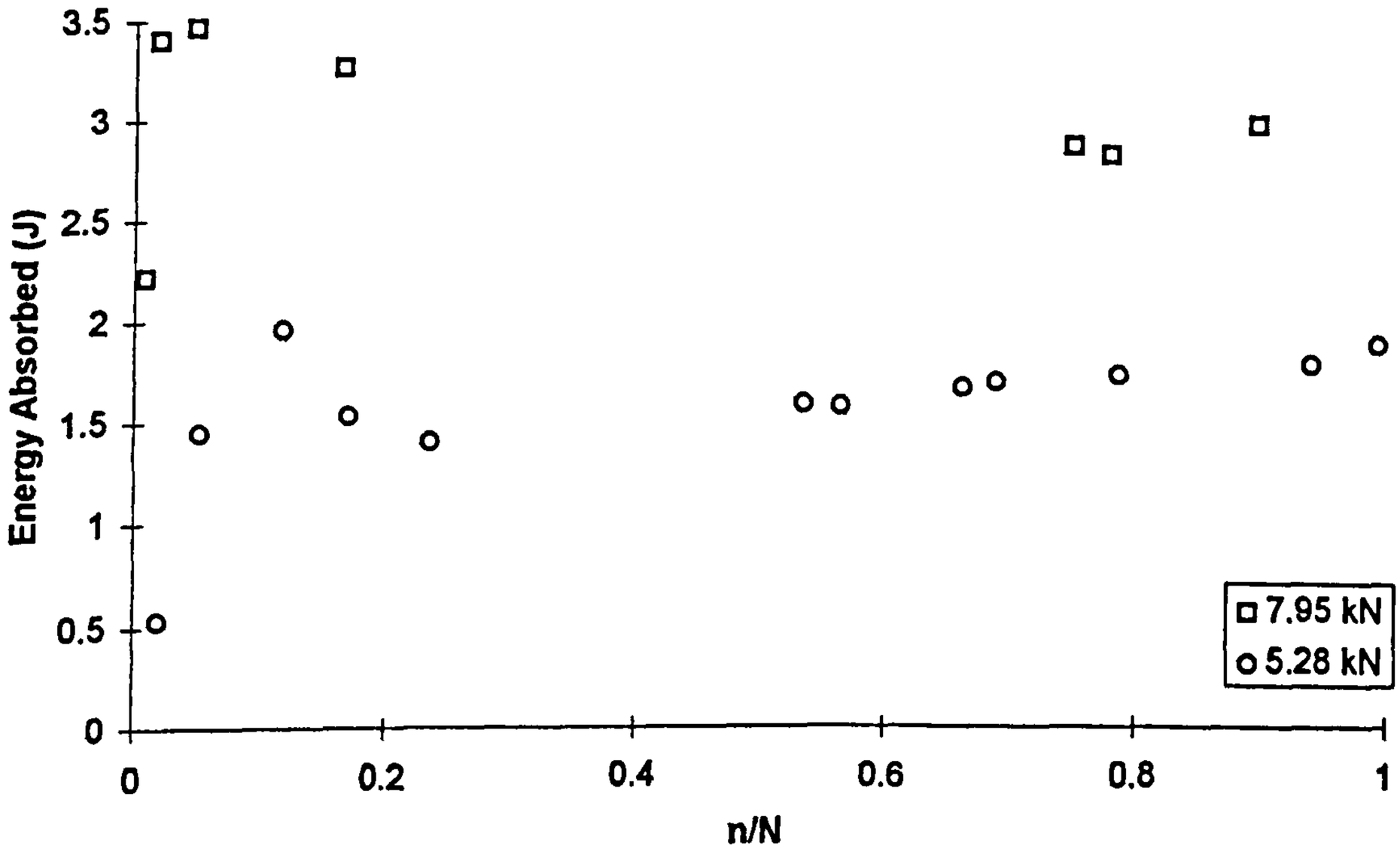

(b)

Figure 6.6 Energy Dissipation Characteristics for; (a) Joint Type F; (b) Joint Type N.

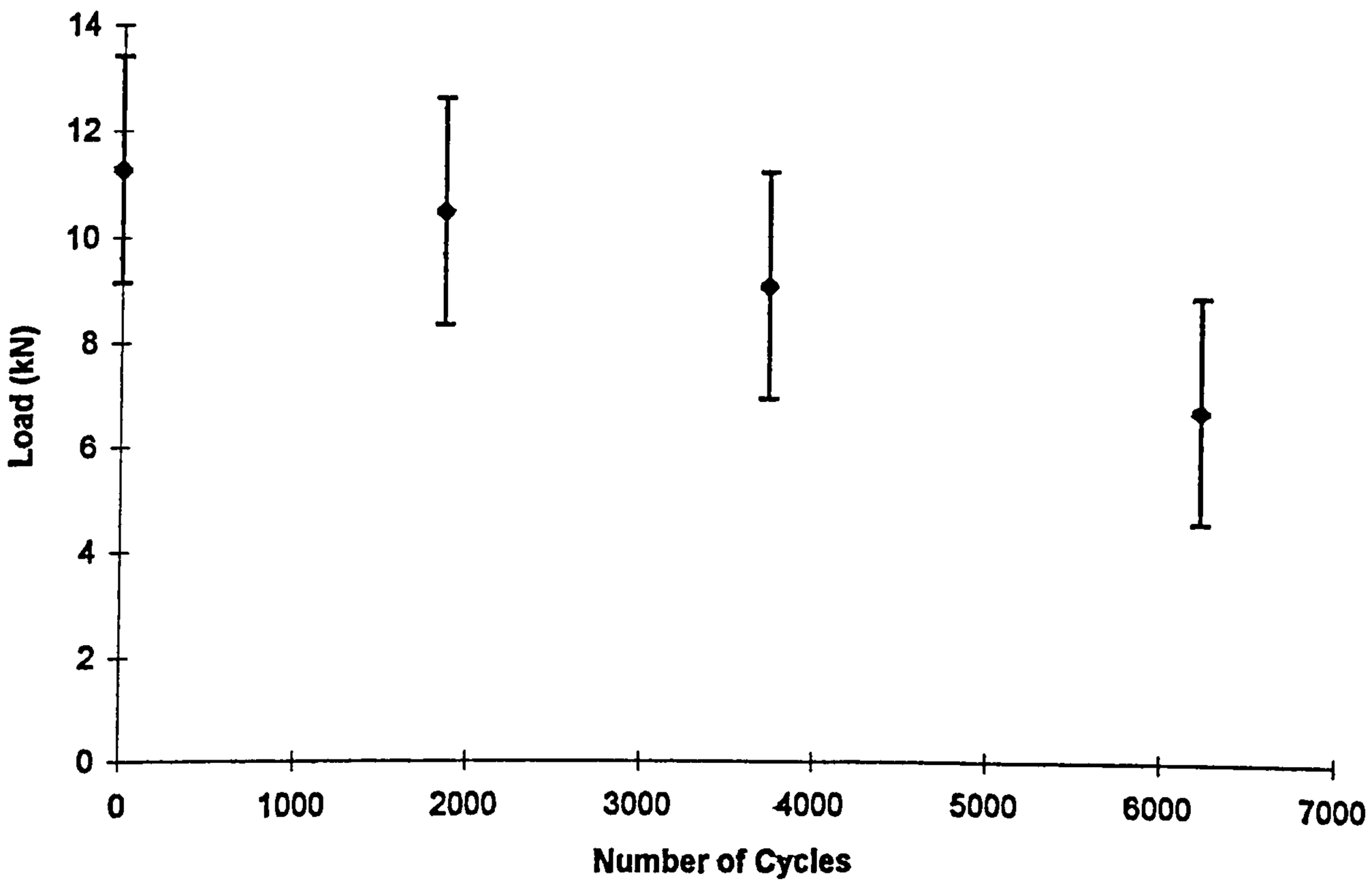

Figure 6.7 Residual Strength Degradation Characteristics for Joint Type N at 60% USS.

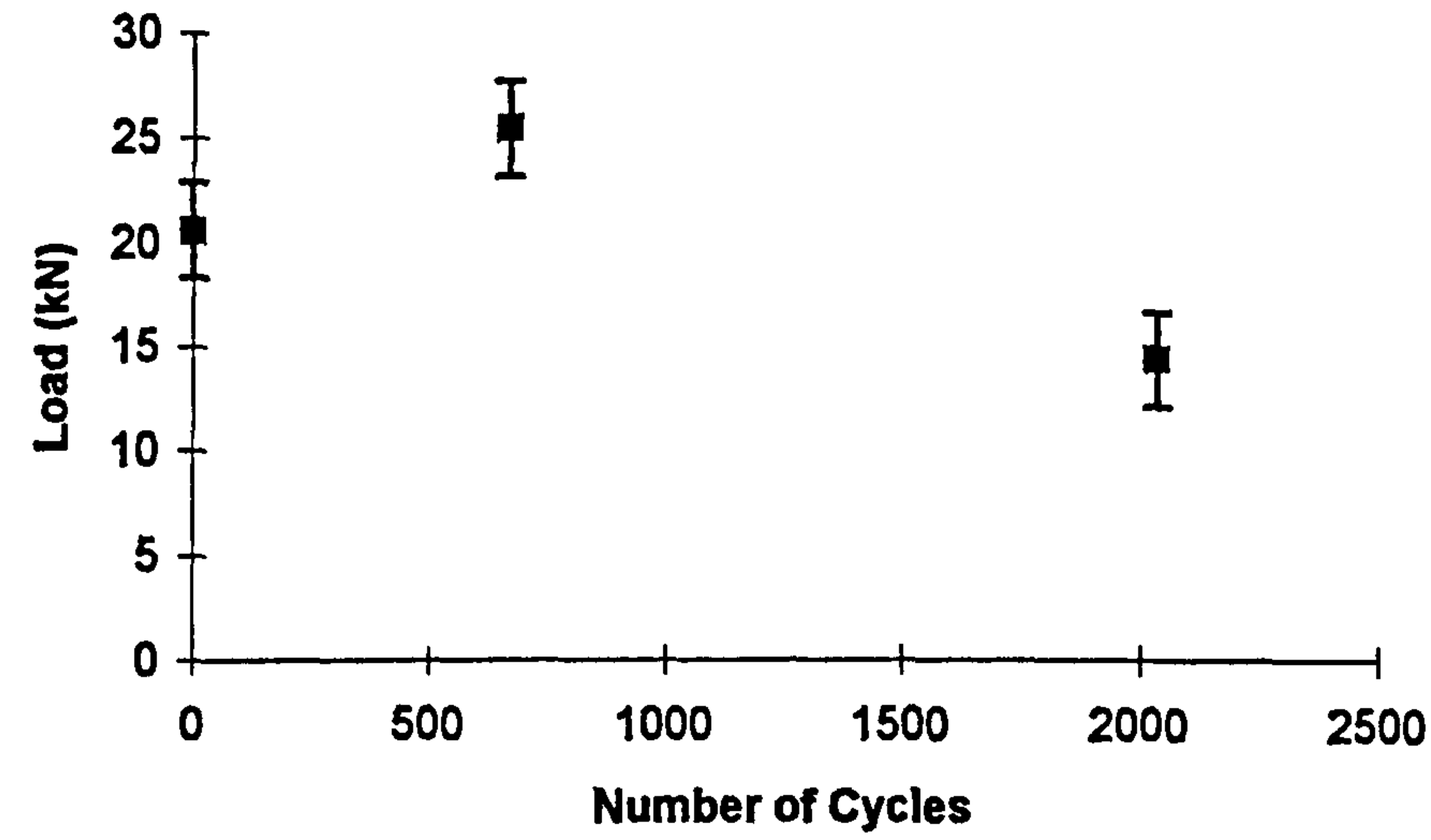

(a)

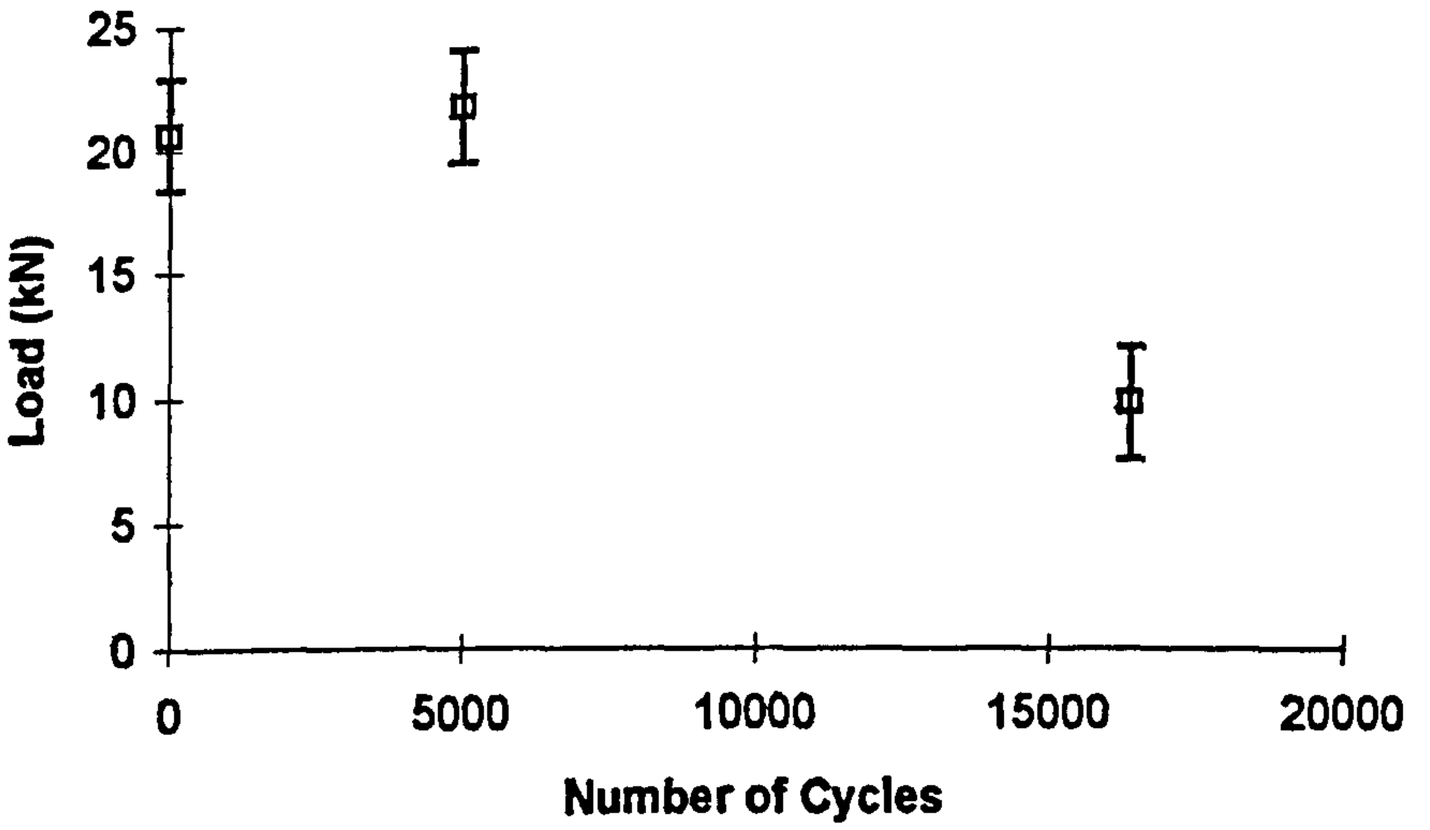

(b)

Figure 6.8 Residual Strength Degradation Characteristics for Joint Type F at; (a) 70% USS; (b) 50% USS.

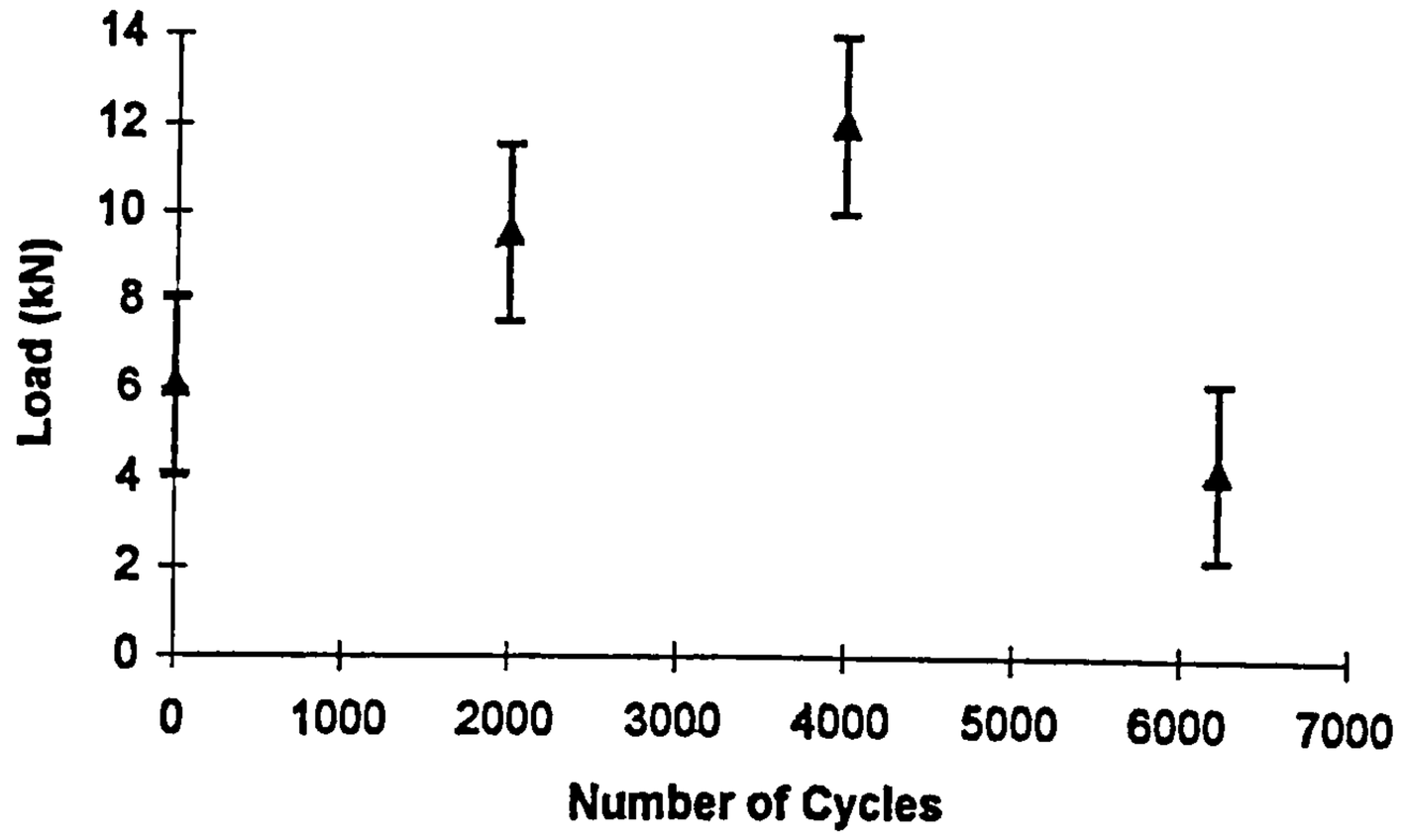

(a)

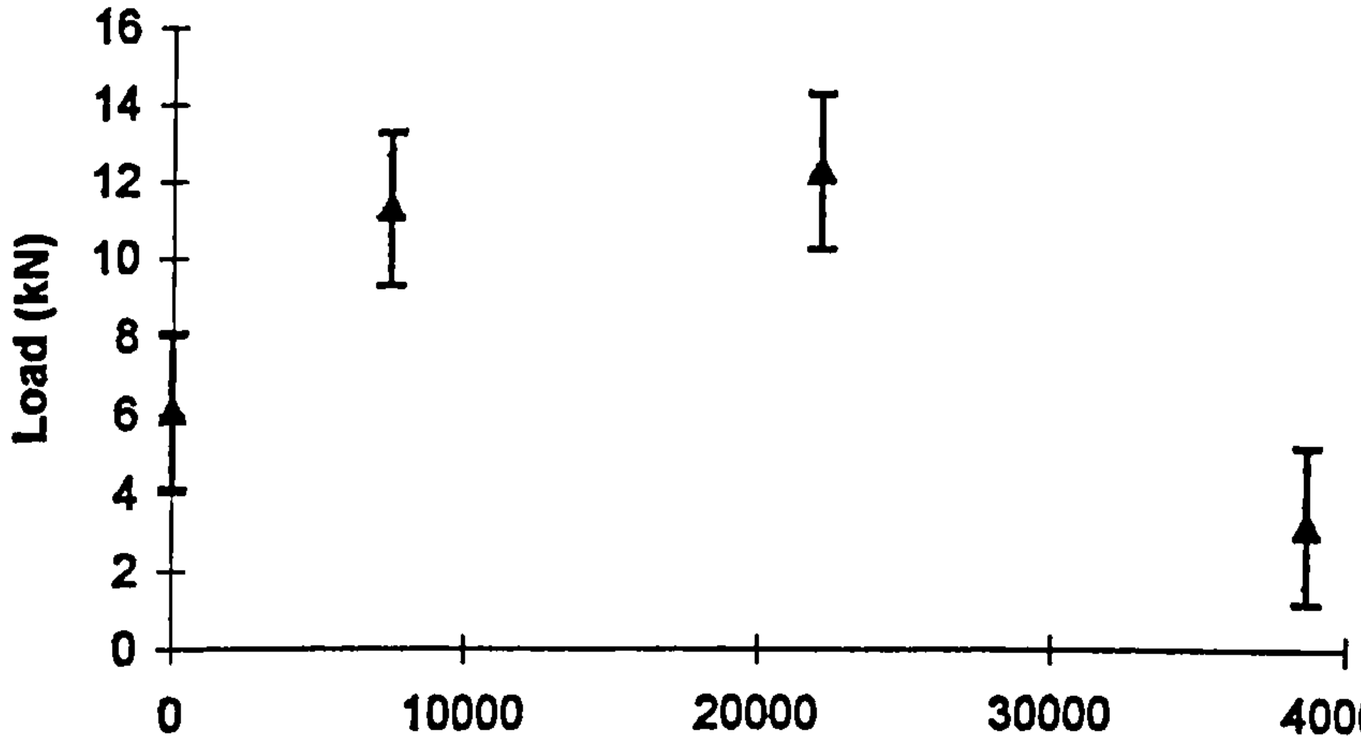

(b)

Figure 6.9 Residual Strength Degradation Characteristics for Joint Type K at; (a) 70% USS; (b) 50% USS.

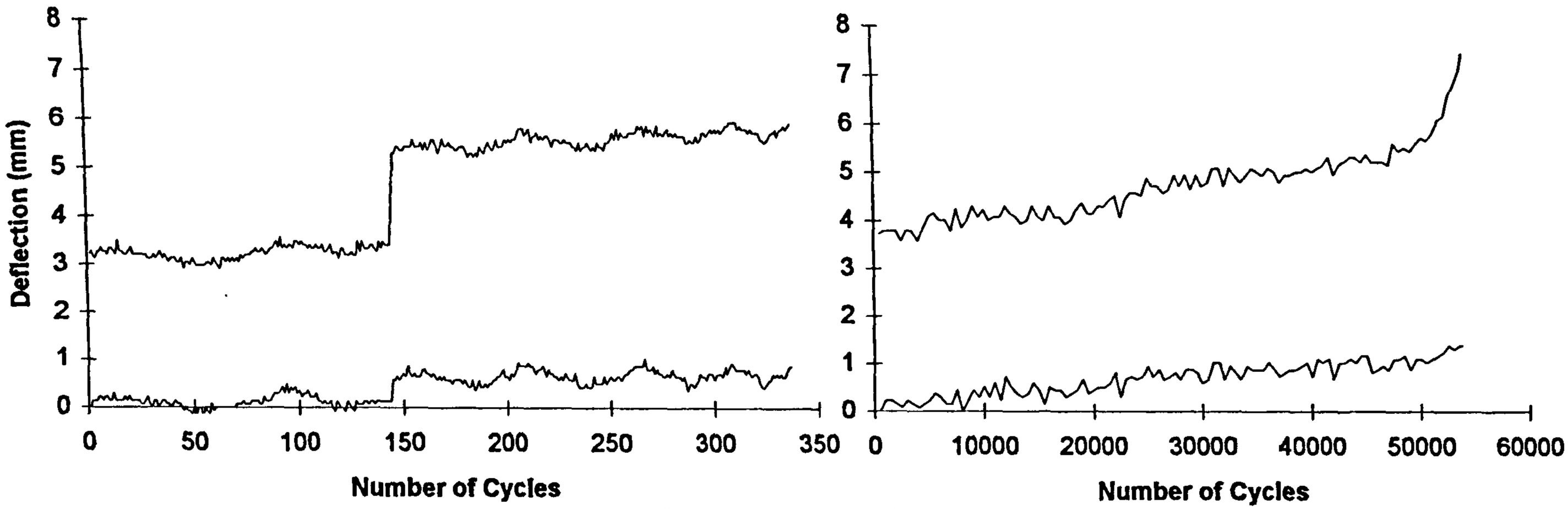

Figure 6.10 Deflection vs Number of Cycle for Joint type N subjected to Two-Stage Loading.

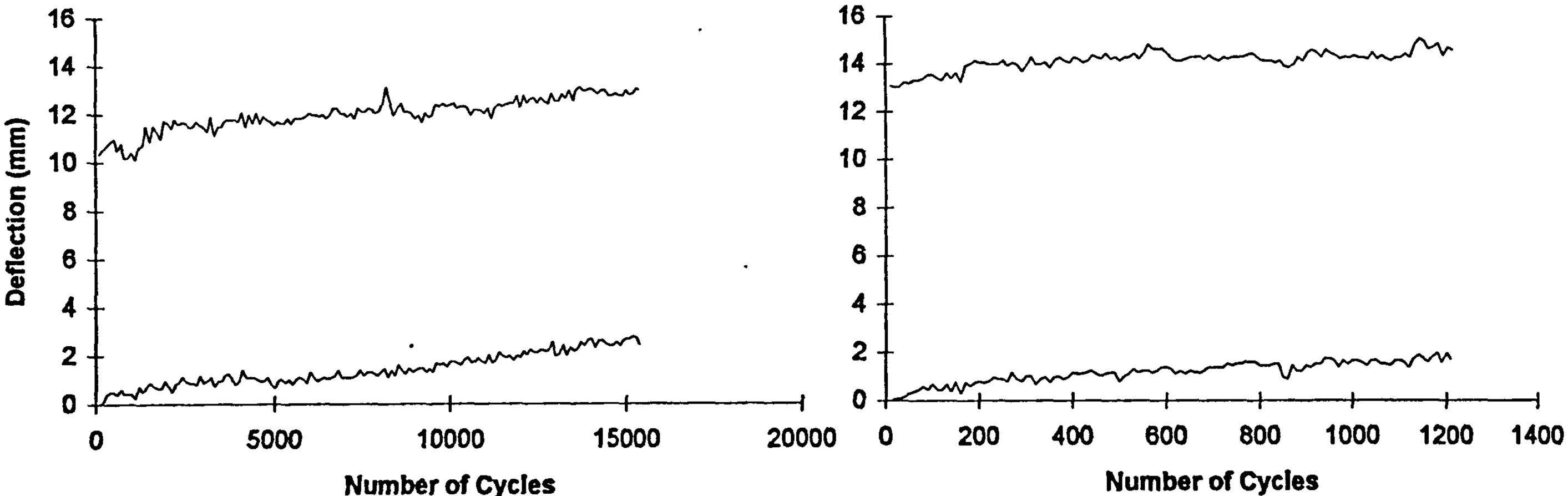

Figure 6.11 Deflection vs Number of Cycle for Joint type F subjected to Two-Stage Loading.

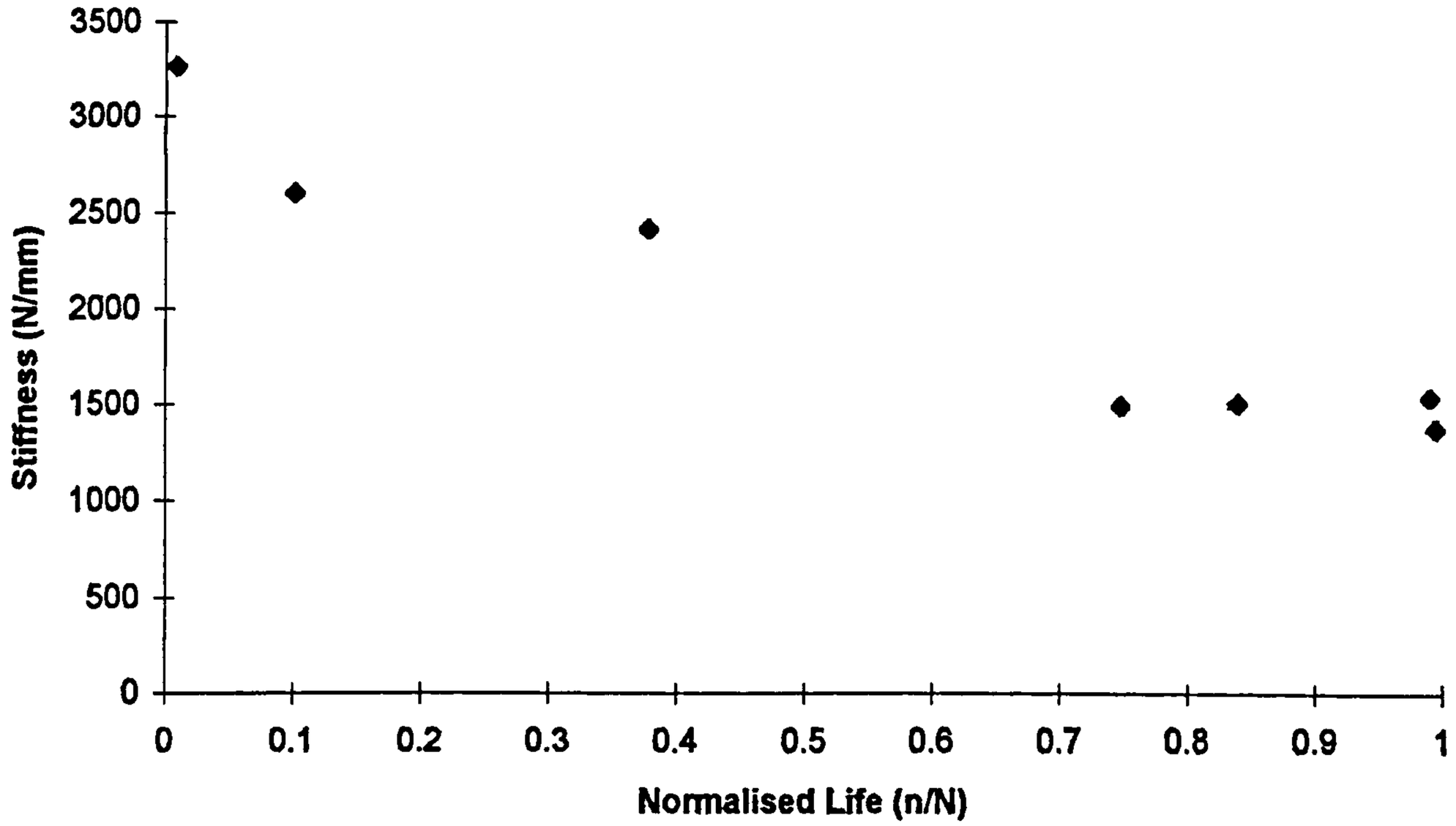

Figure 6.12 Stiffness Degradation Characteristics for Joint Type N subjected to Two-Stage Loading.

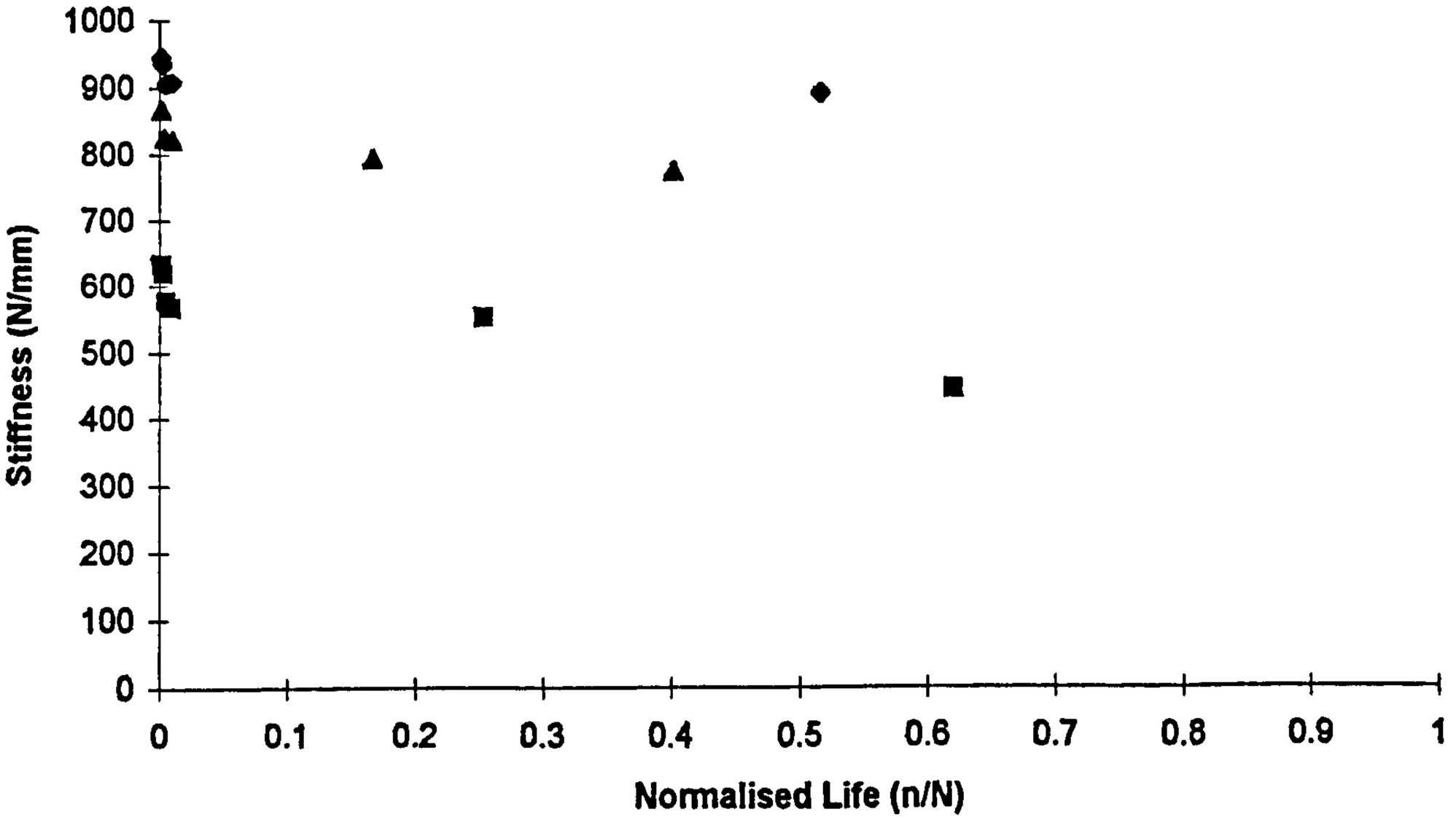

Figure 6.13a Stiffness Degradation Characteristics for Joint Type F subjected to Two-Stage High-Low Loading.

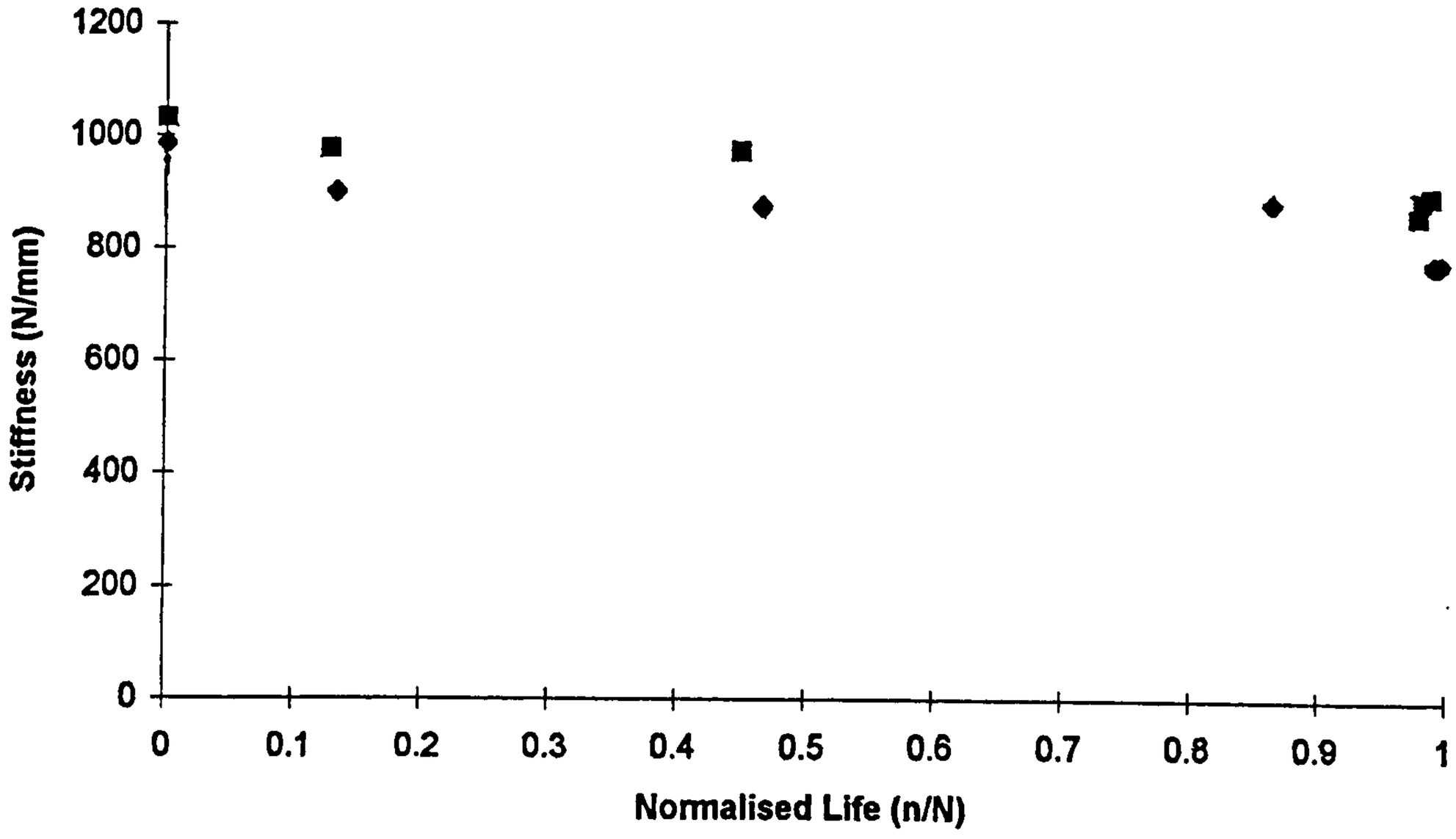

Figure 6.13b Stiffness Degradation Characteristics for Joint Type F subjected to Two-Stage Low-High Loading.

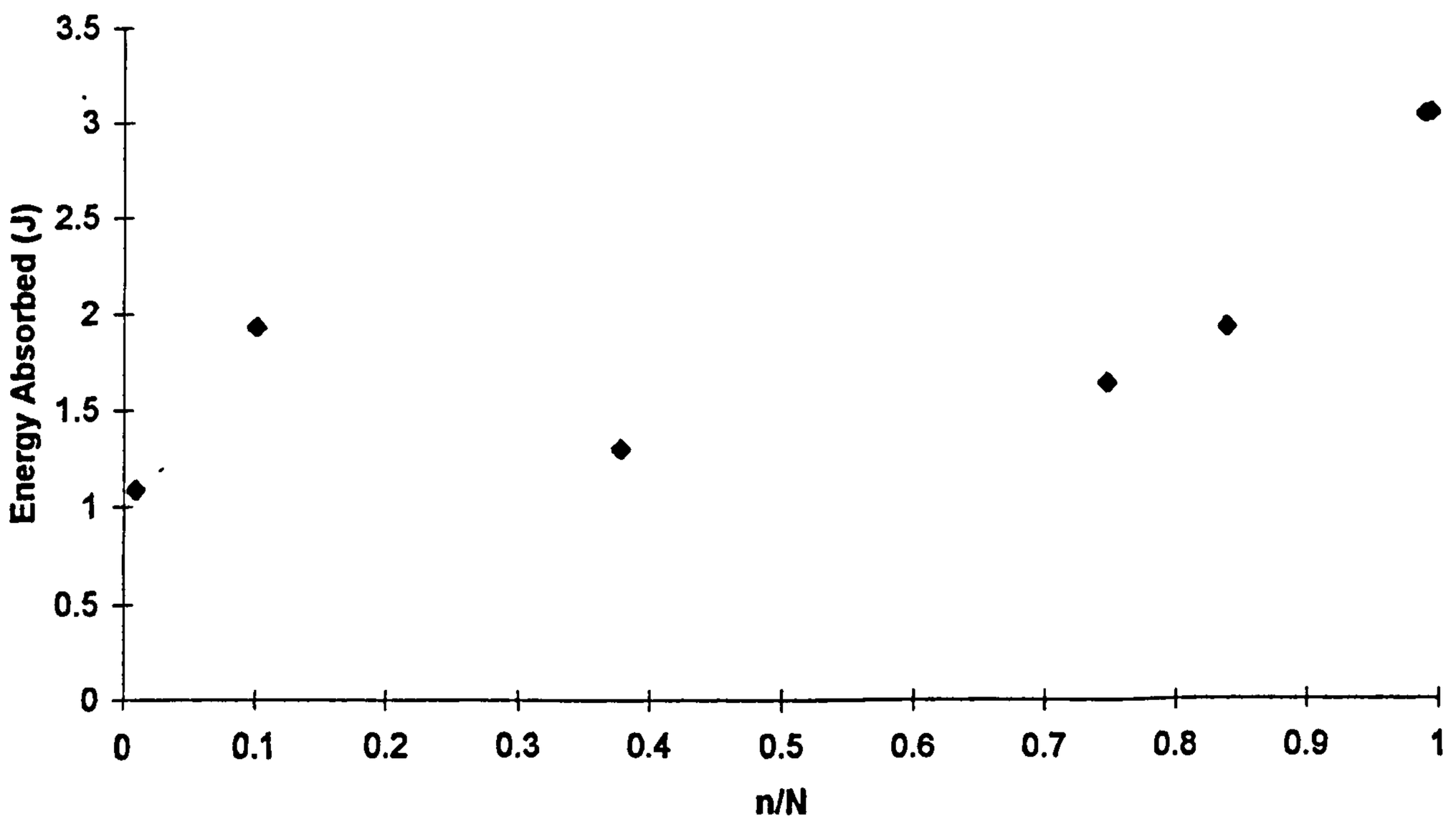

Figure 6.14 Energy Dissipation Characteristics for Joint Type N subjected to Two-Stage Loading.

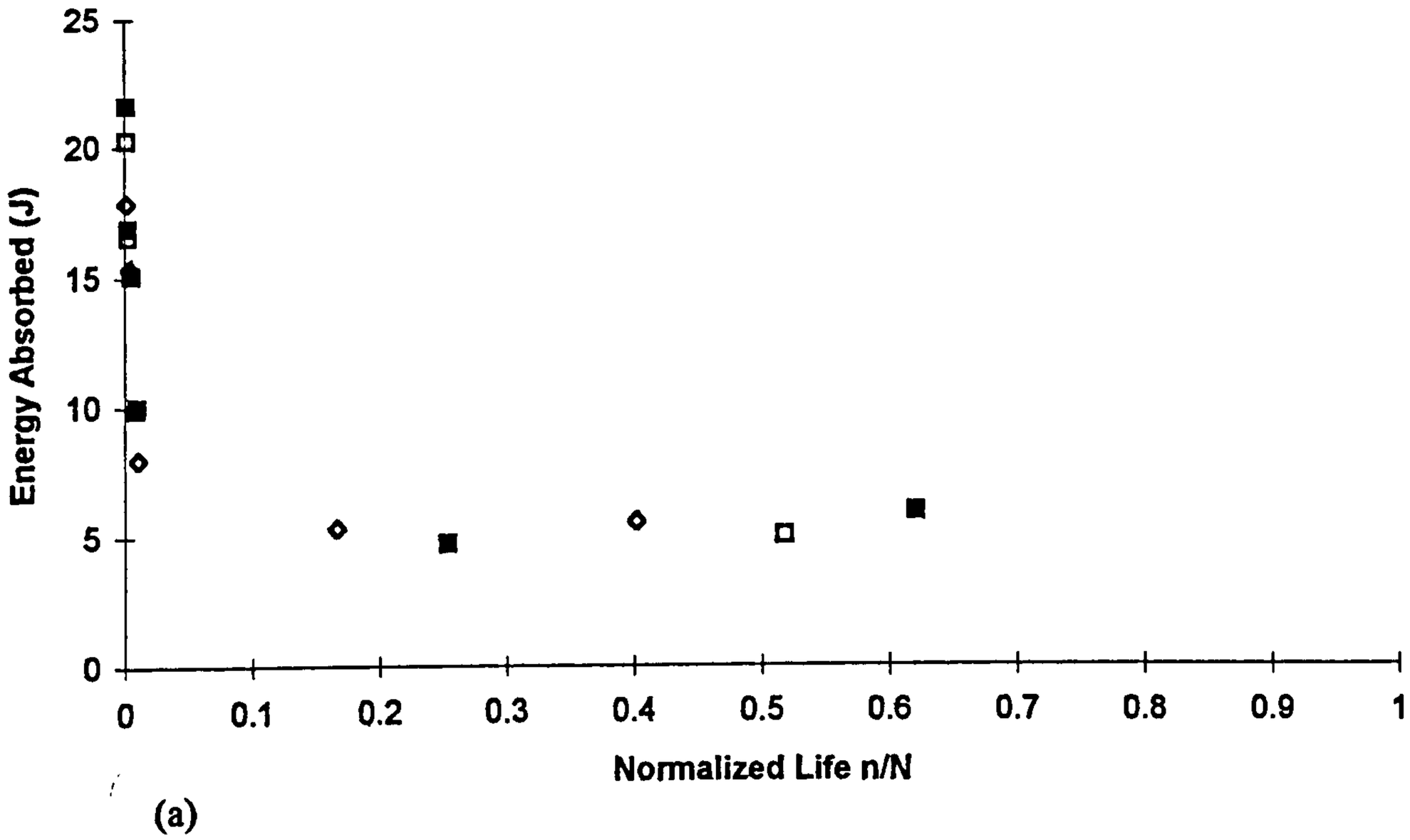

Figure 6.15 Energy Dissipation Characteristics for Joint Type F subjected to Two-Stage Loading; (a) High-Low; (b) Low-High.

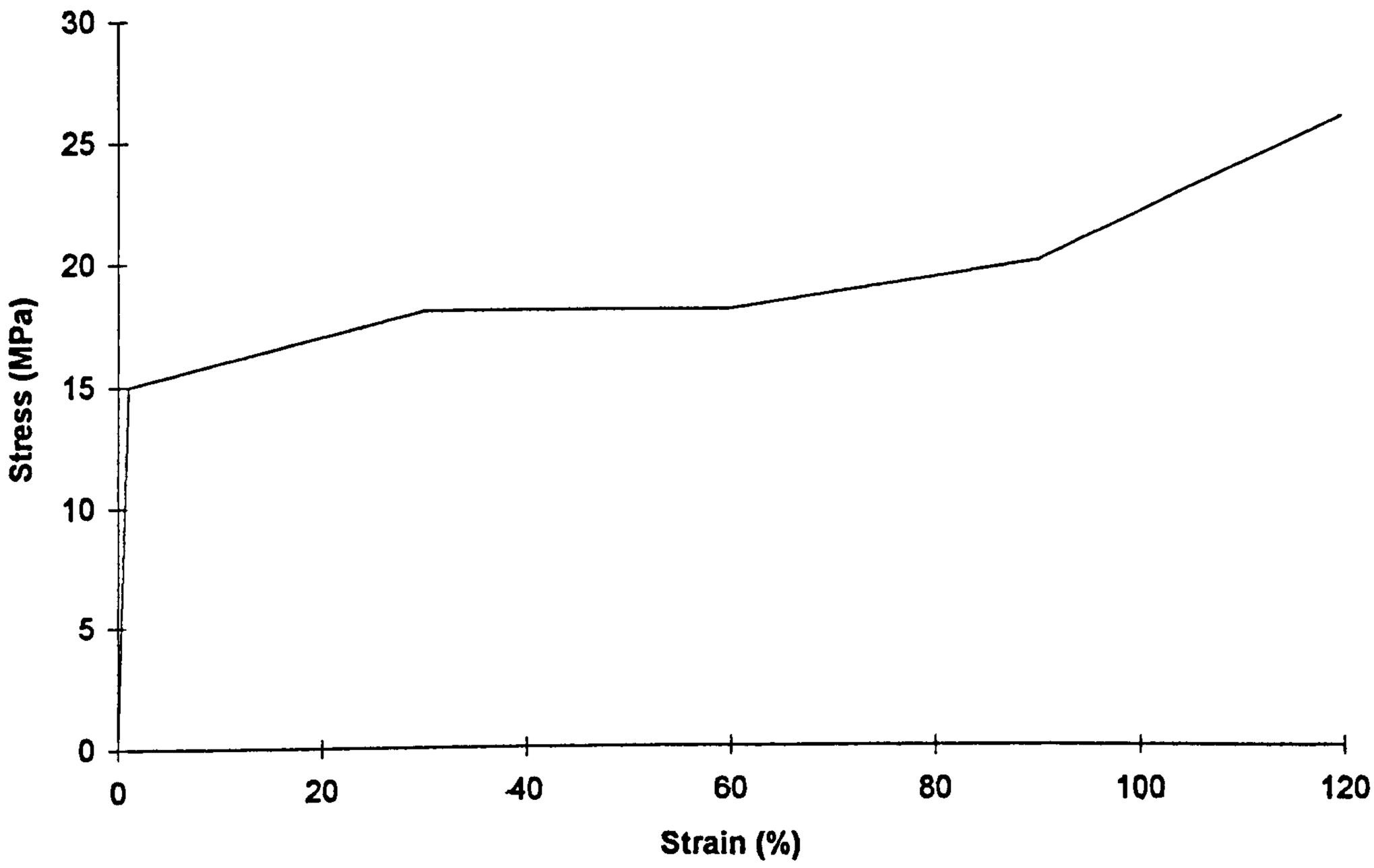

Figure 7.1 Stress-Strain Characteristics of the Fillet Resin.

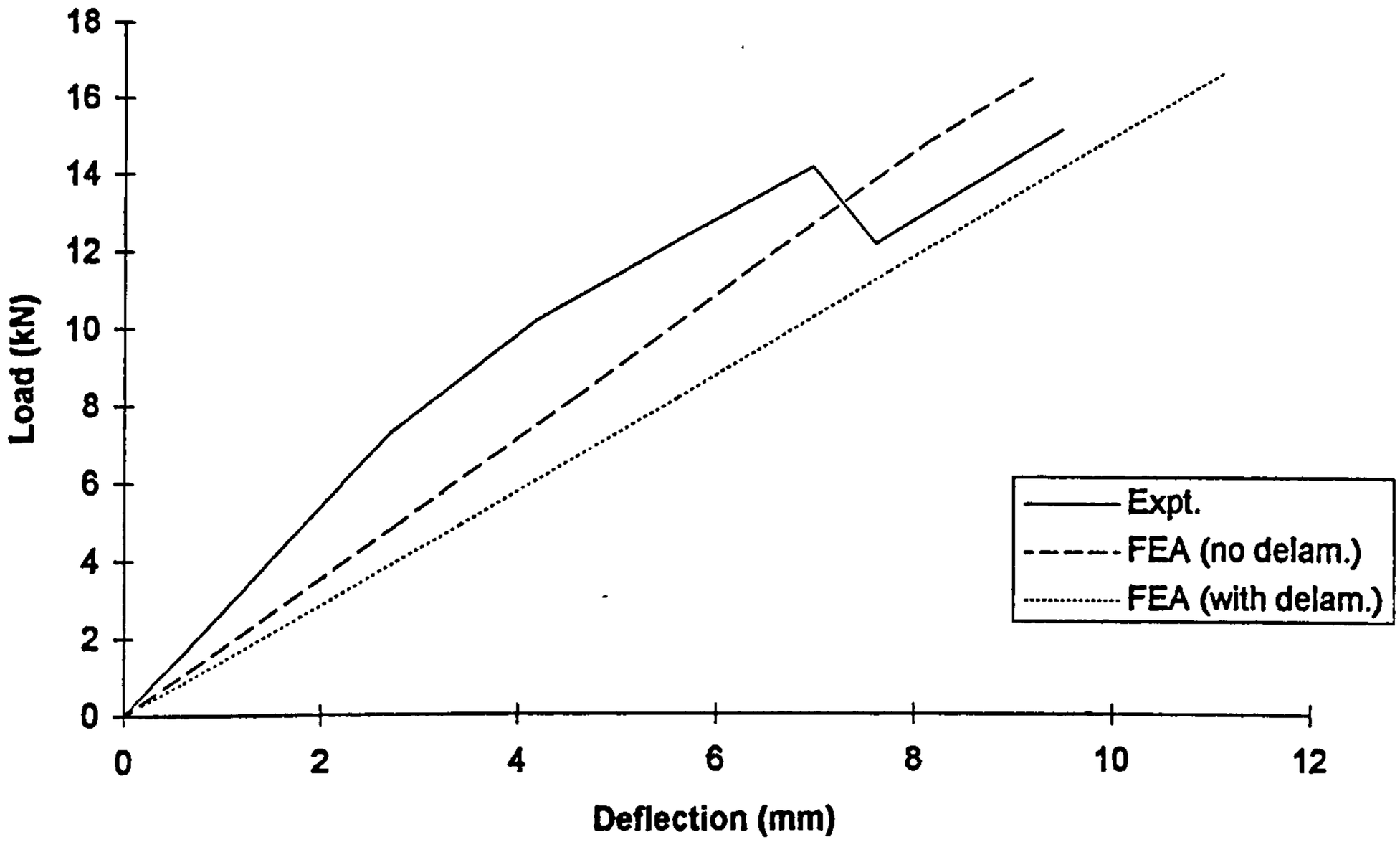

Figure 7.2a Experimental and FEA Load - Deflection Results for Joint Type B.

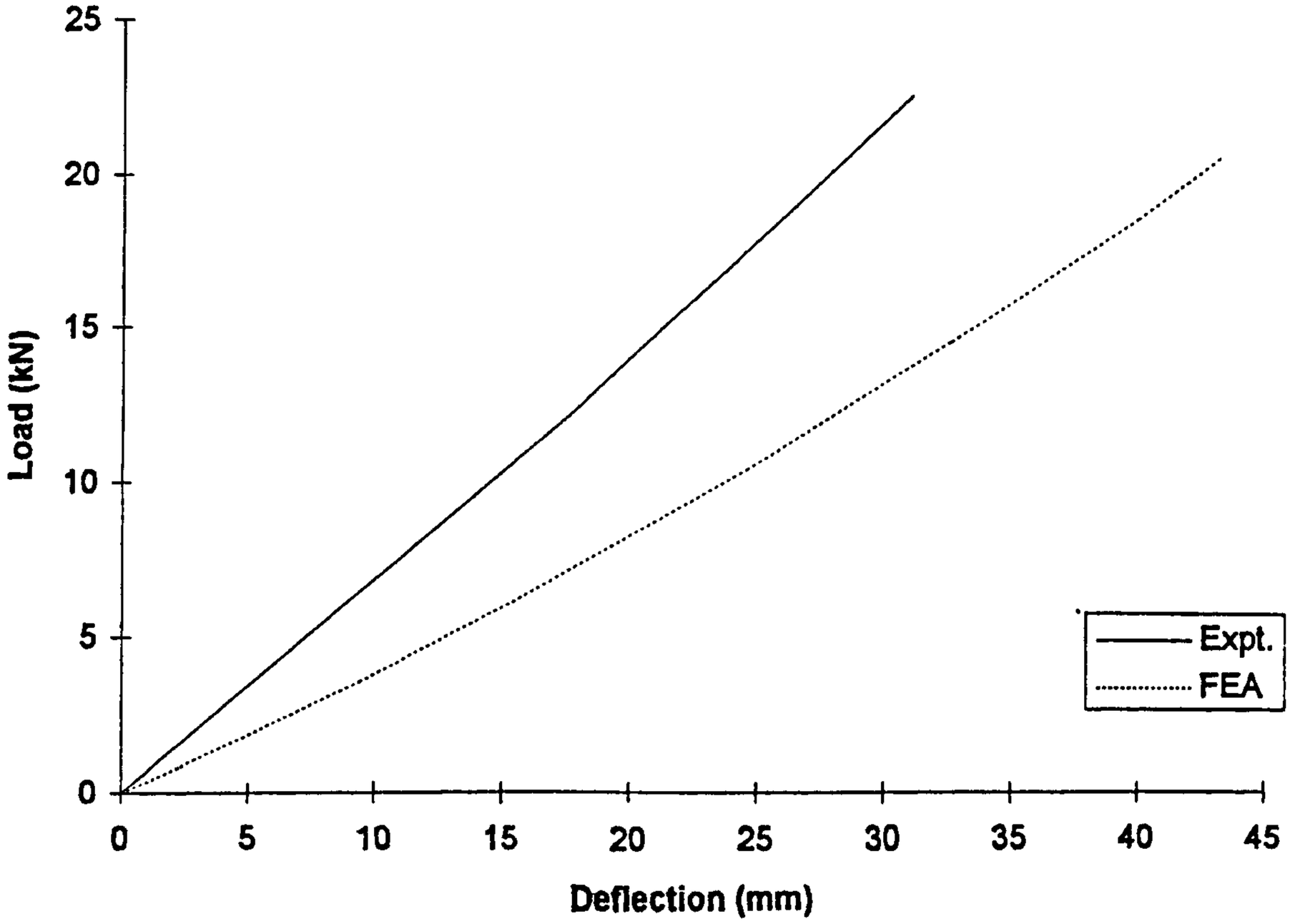

Figure 7.2b Experimental and FEA Load - Deflection Results for Joint Type F.

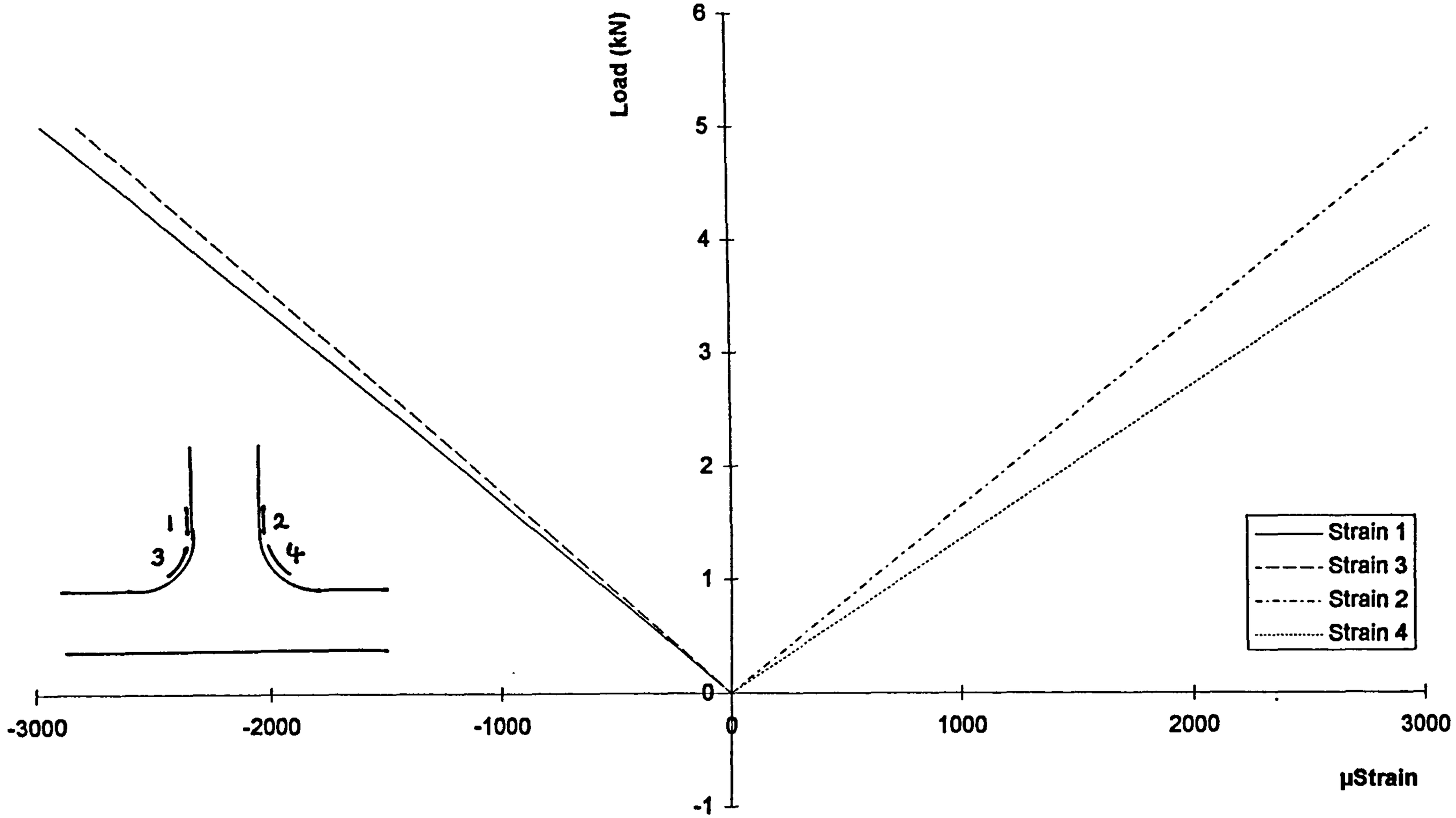

Figure 7.3 FEA Load-Strain Results for Joint Type B.

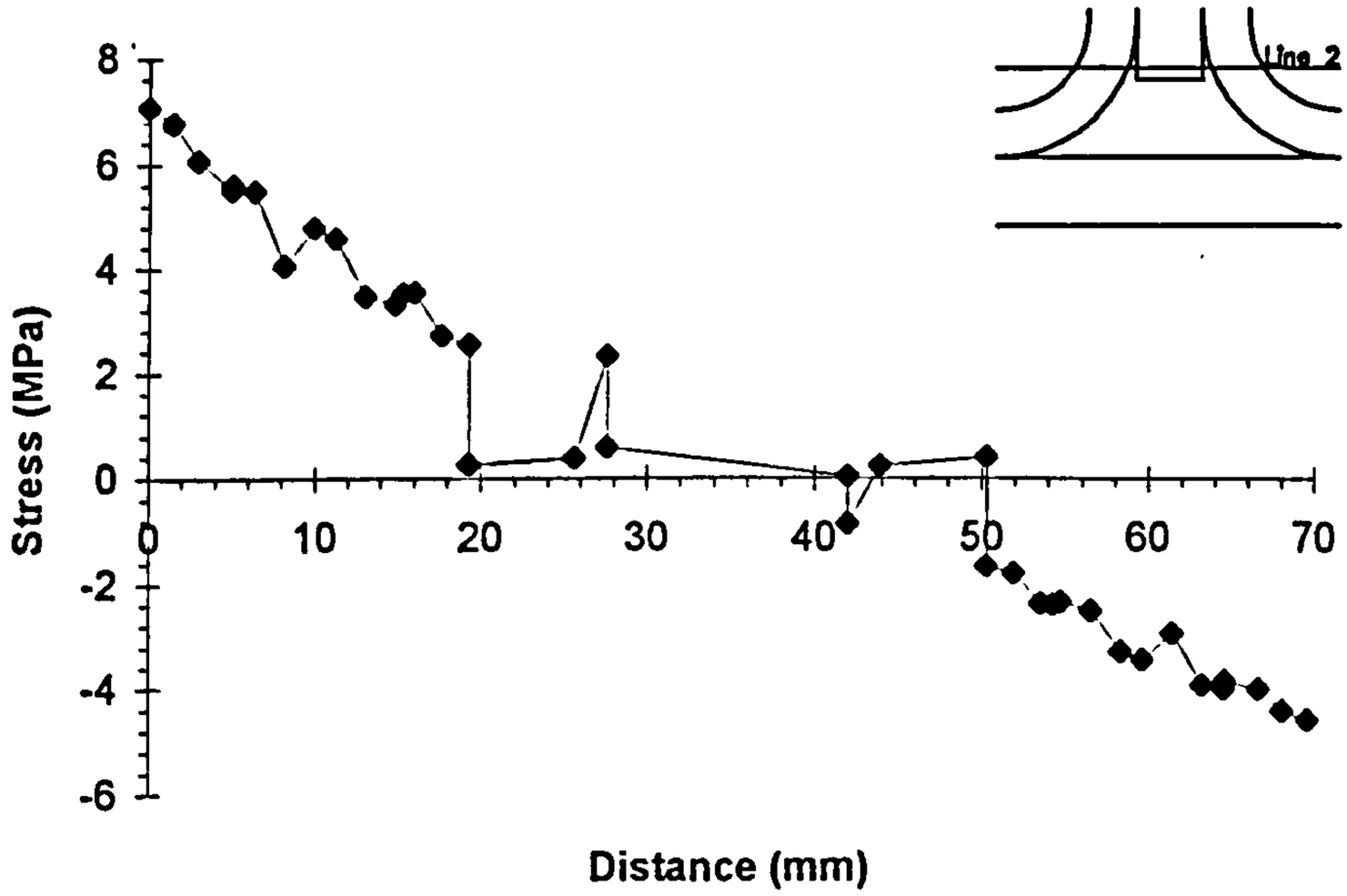

Figure 7.4 FEA Stress Line Plot along Line 2 for Joint Type B.

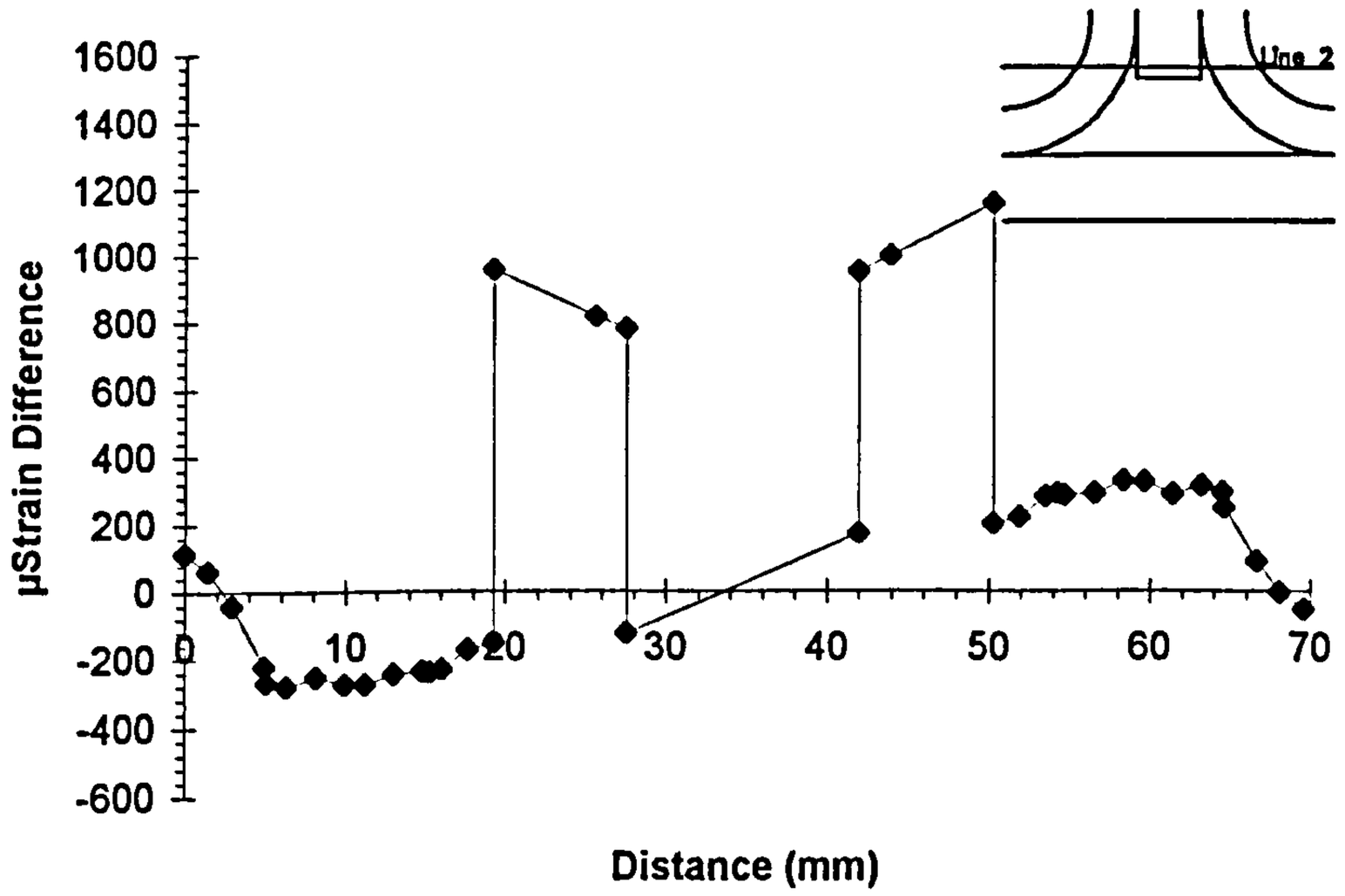

Figure 7.5 FEA Strain Line Plot along Line 2 for Joint Type B.

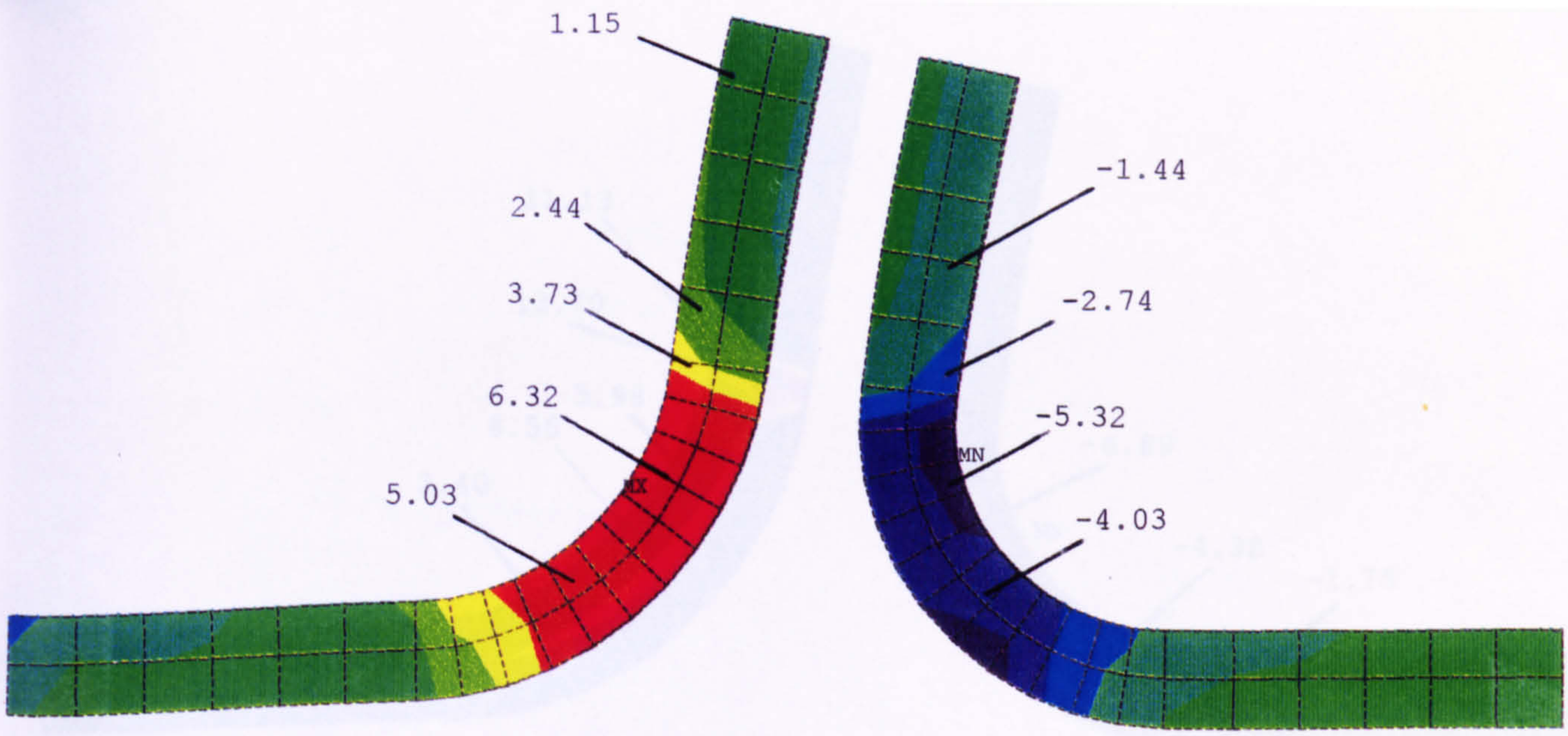

(a) Normal Interlaminar Stresses in the Overlaminates.

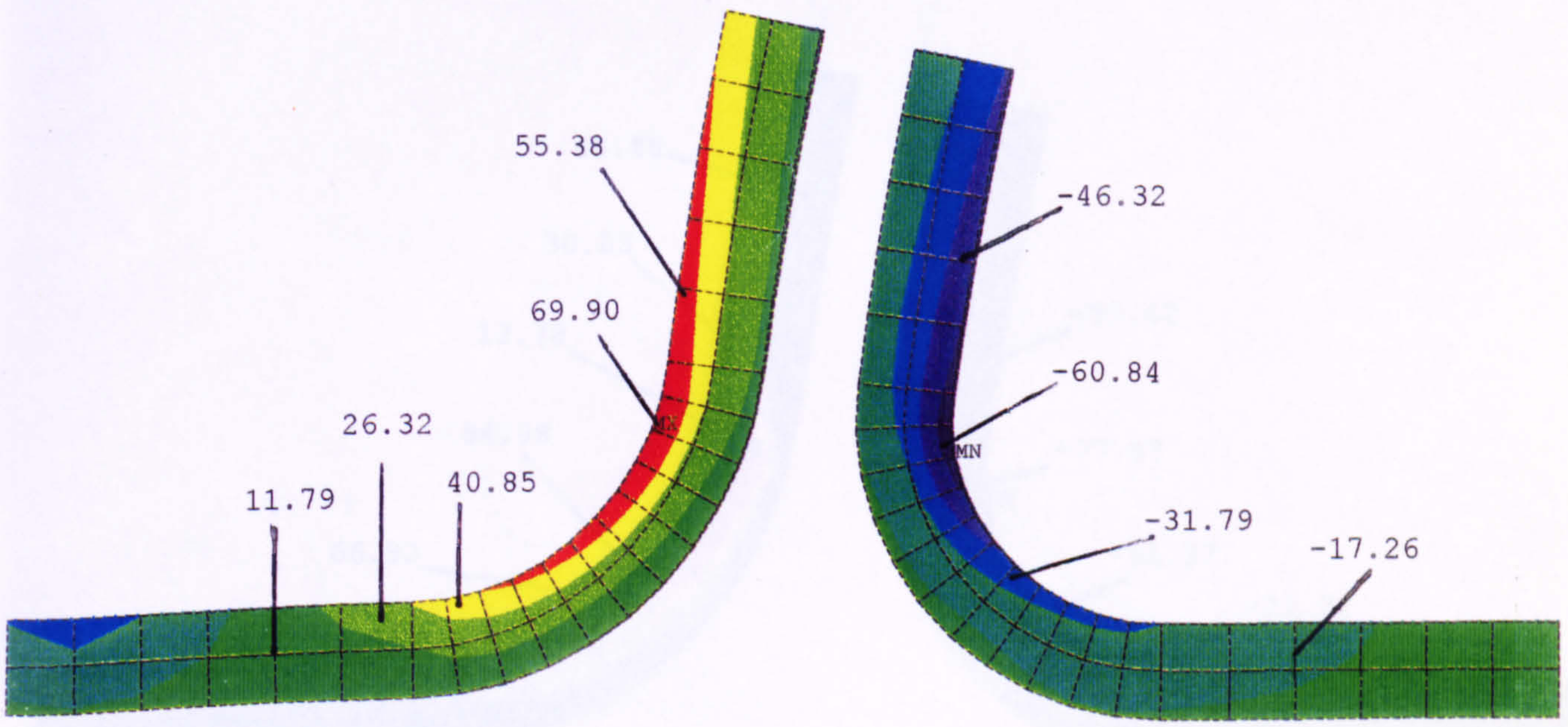

(b) In-plane Stresses in the Overlaminates.

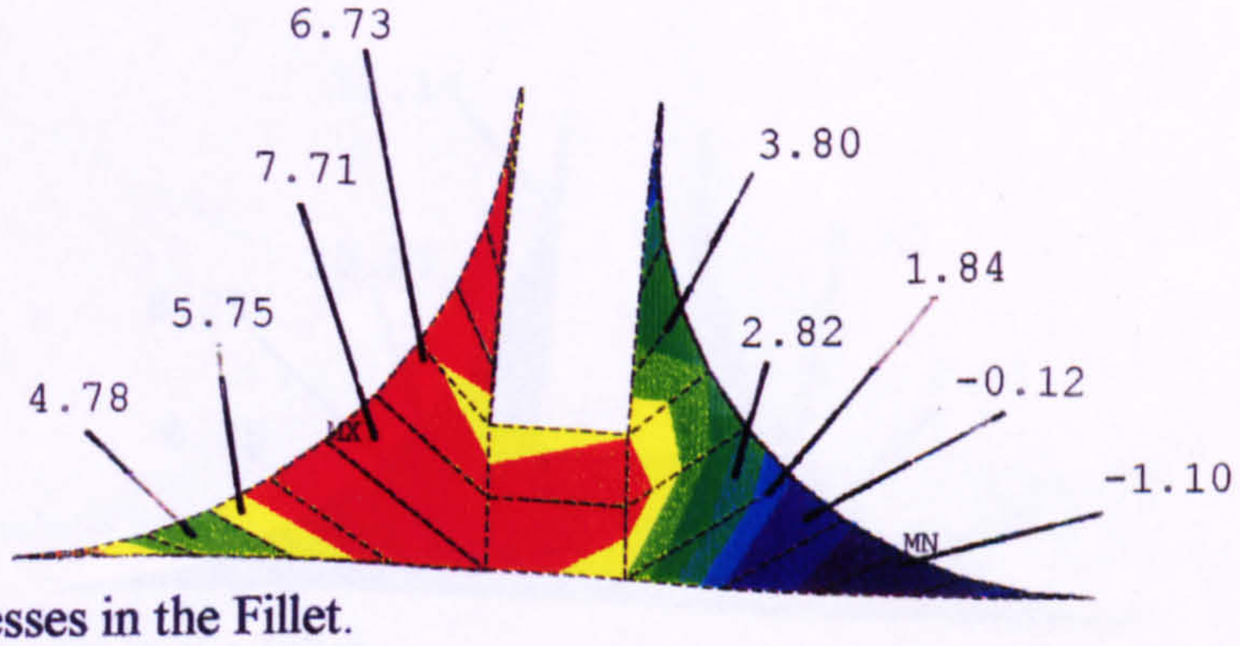

(c) Principal Stresses in the Fillet.

Figure 7.6 FEA Stress Distributions for Joint Type B.

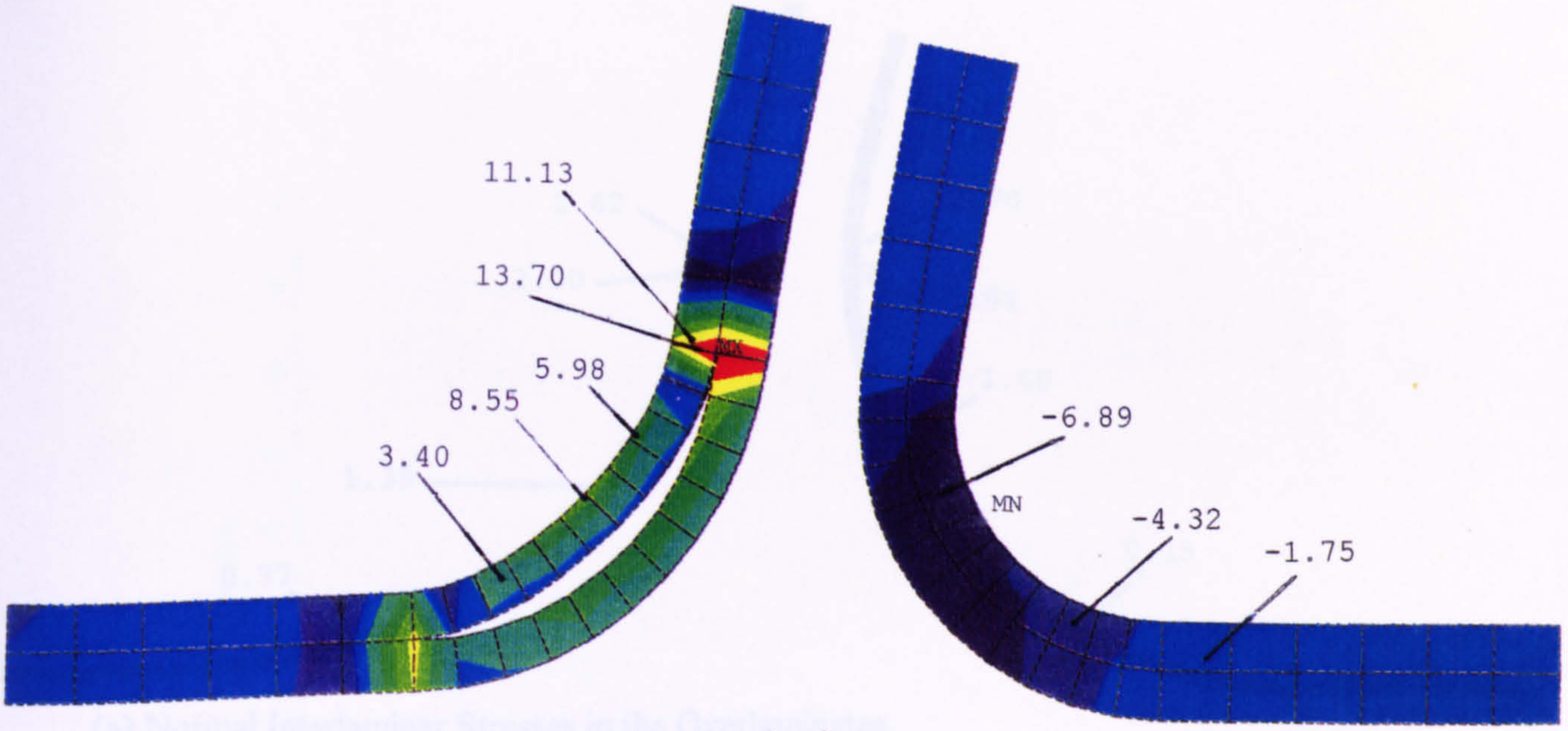

(a) Normal Interlaminar Stresses in the Overlaminates.

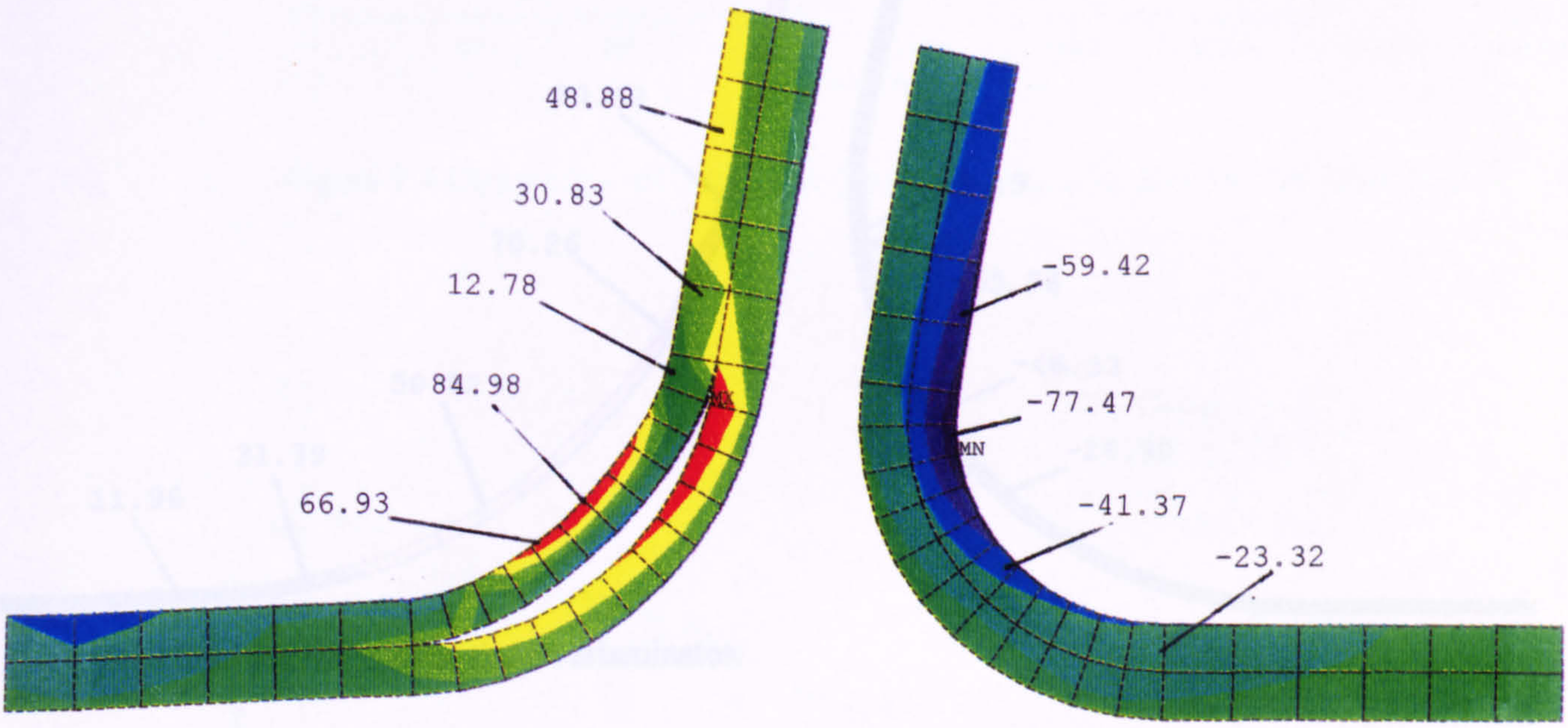

(b) In-plane Stresses in the Overlaminates.

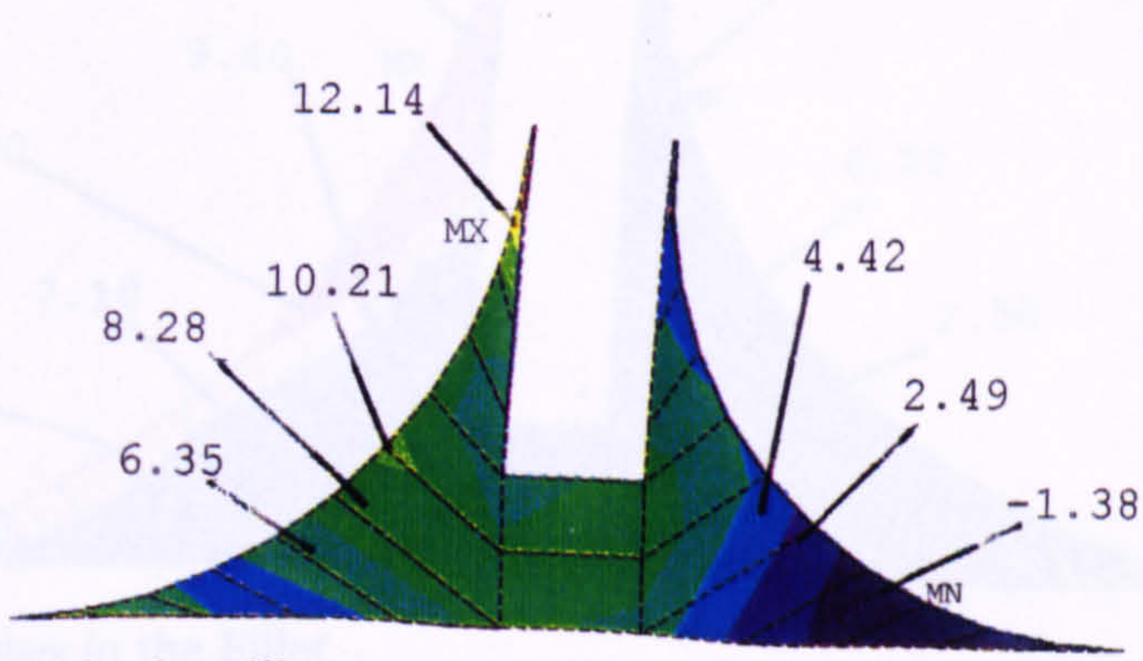

(c) Principal Stresses in the Fillet.

Figure 7.7 FEA Stress Distributions for Joint Type B with an Initial Delamination.

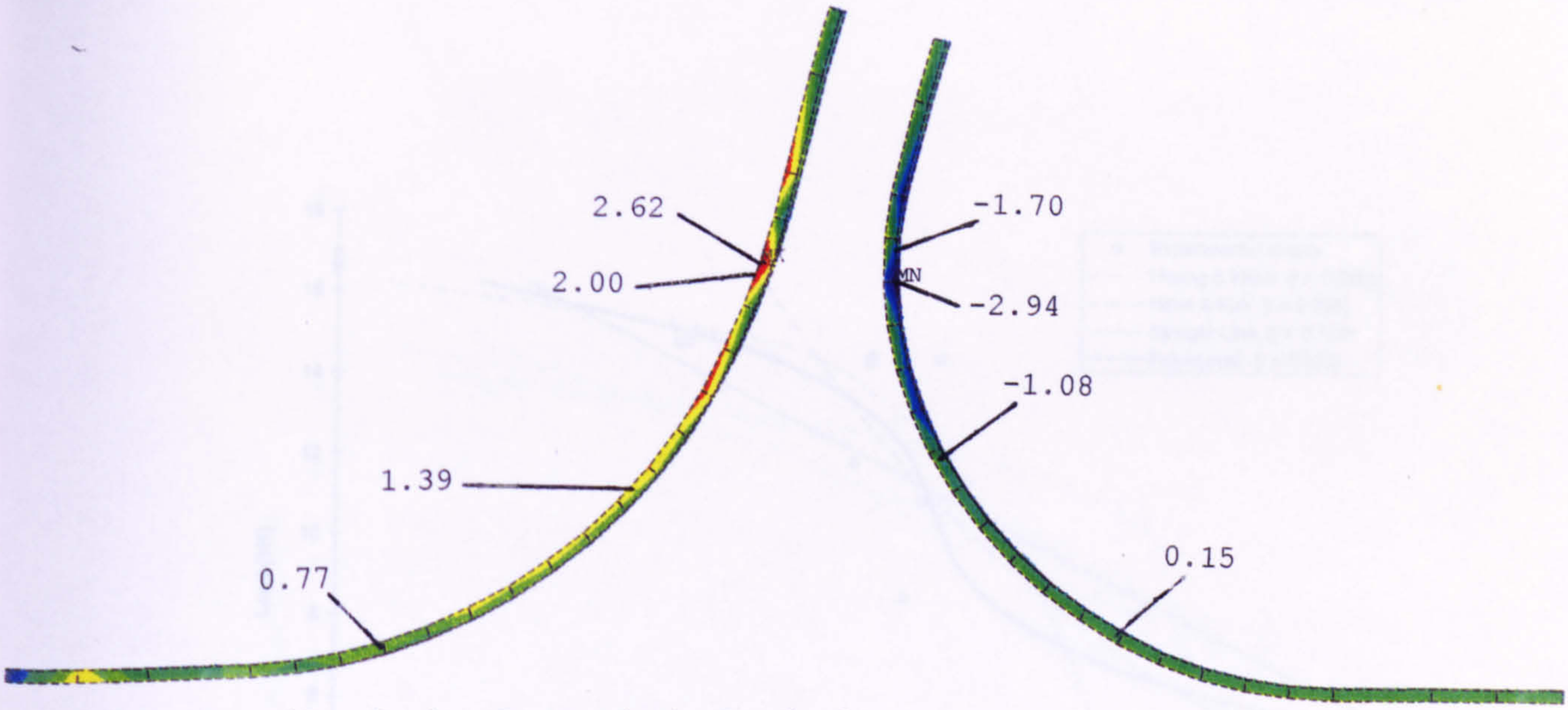

(a) Normal Interlaminar Stresses in the Overlaminates.

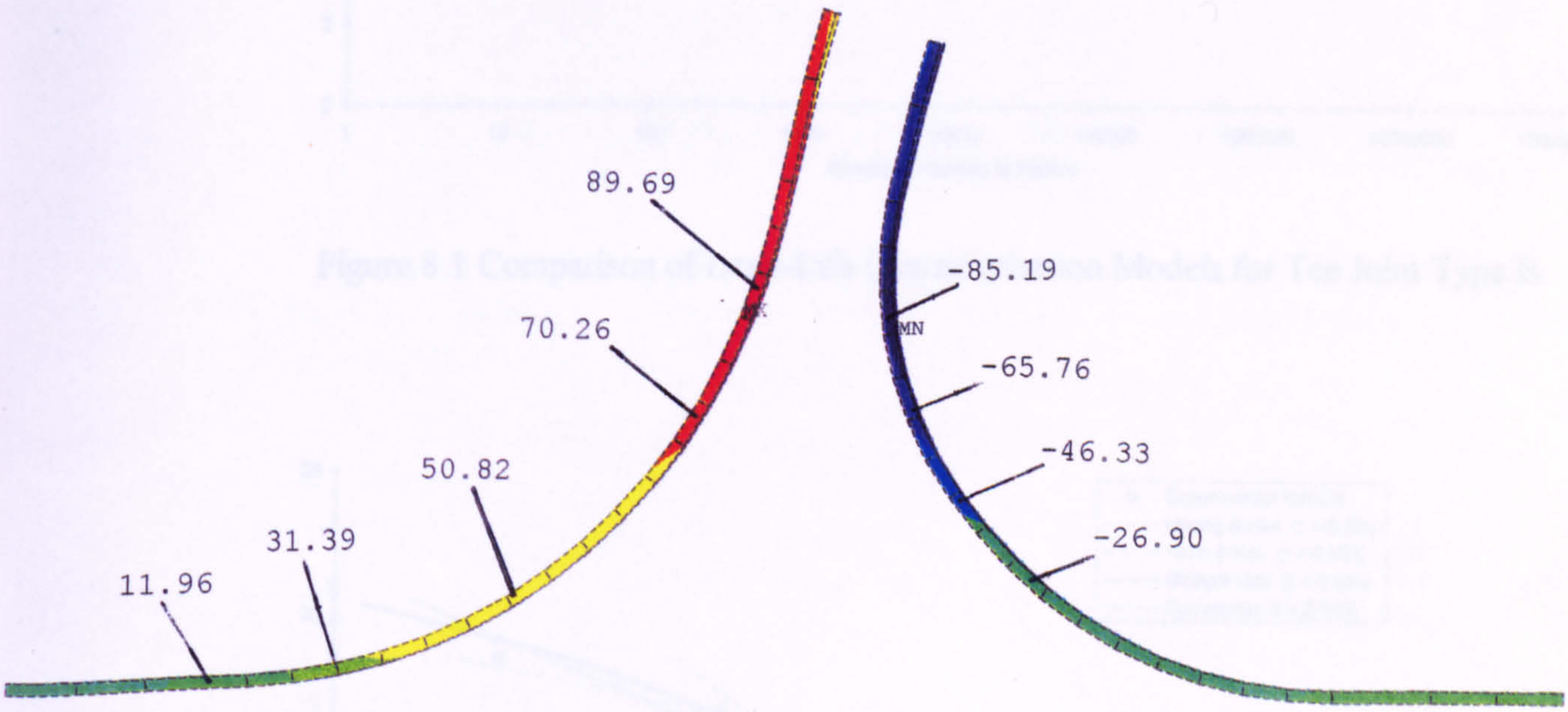

(b) In-plane Stresses in the Overlaminates.

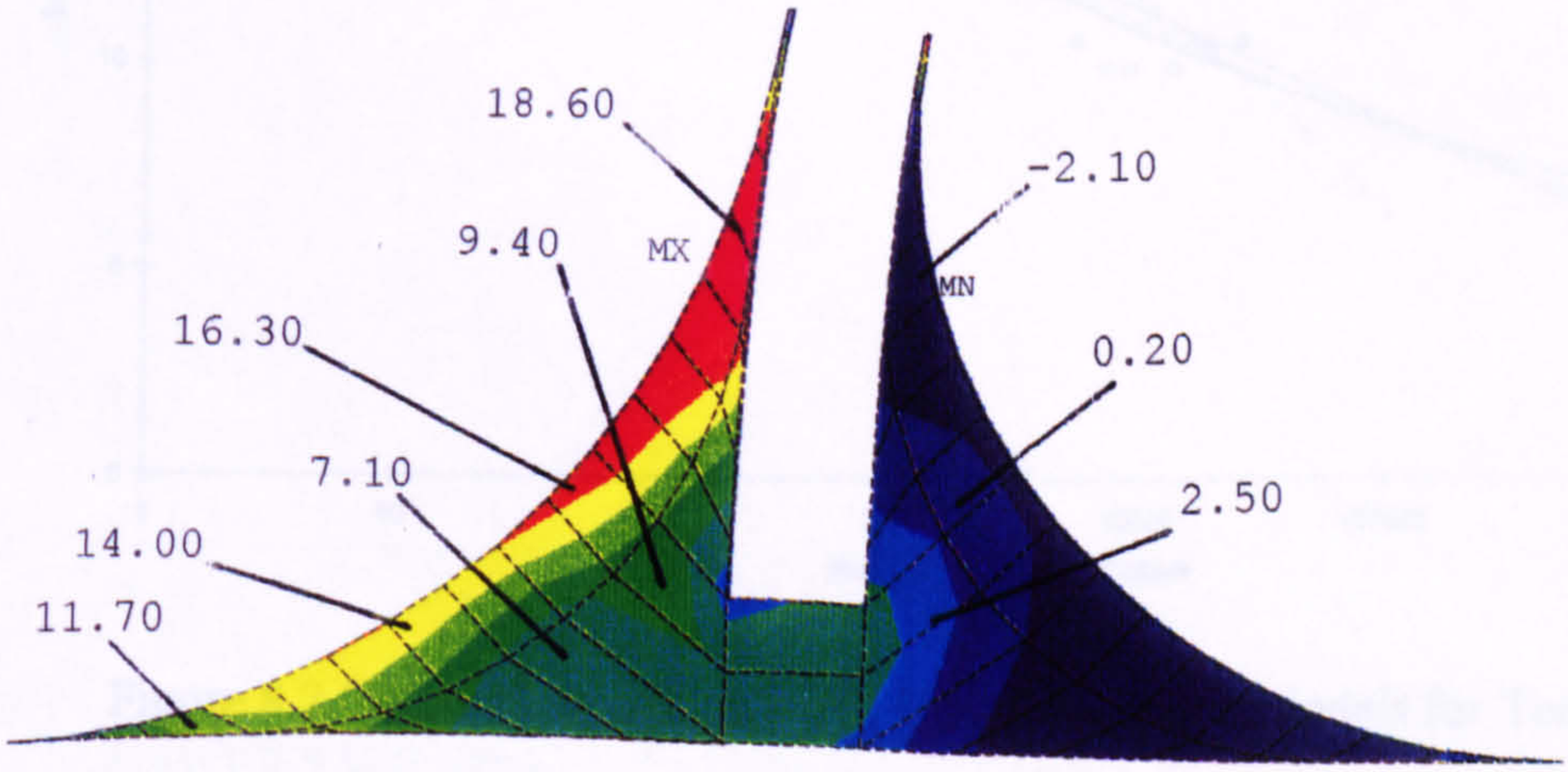

(c) Principal Stresses in the Fillet.

Figure 7.8 FEA Stress Distributions for Joint Type F.

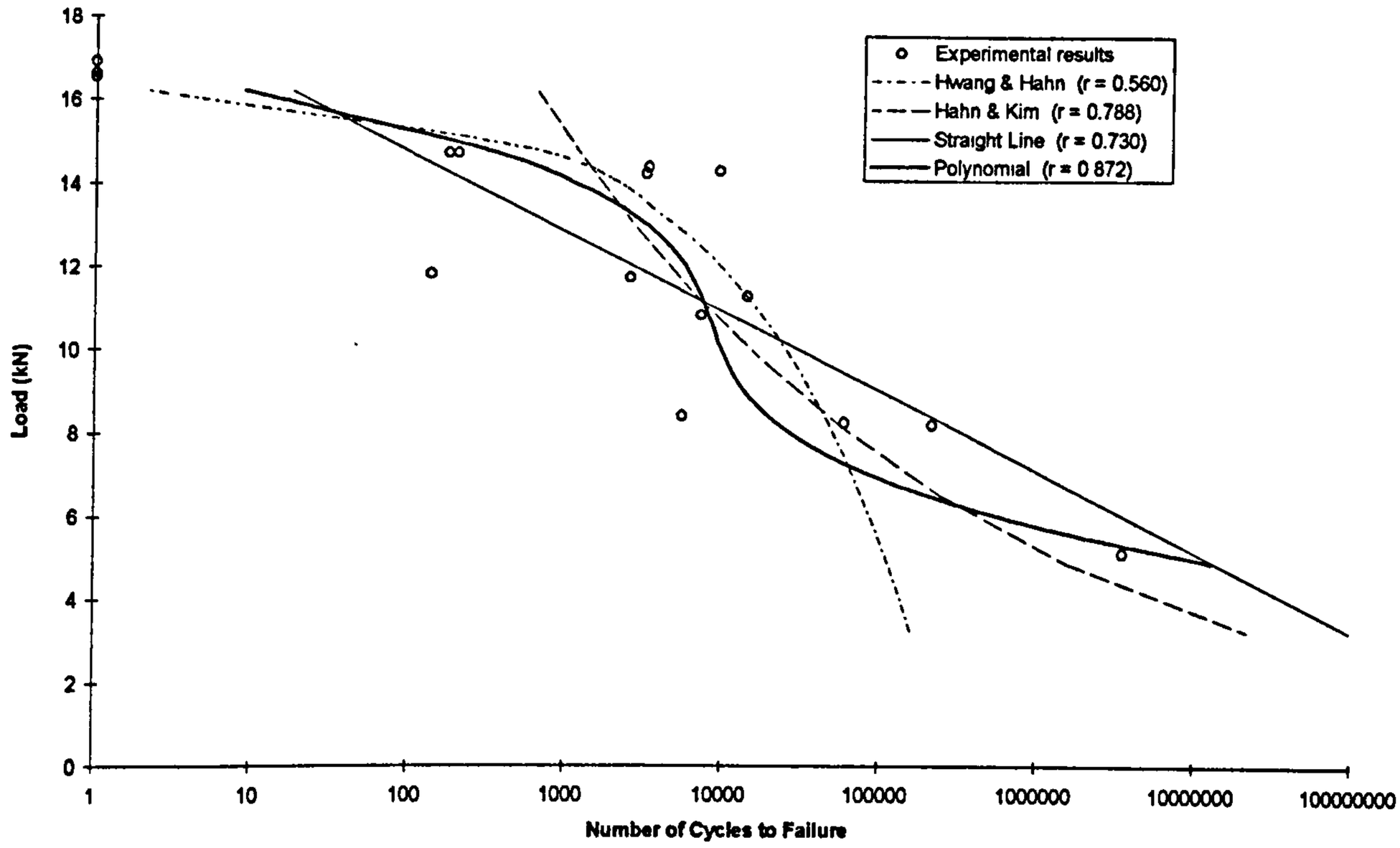

Figure 8.1 Comparison of Load-Life Characterisation Models for Tee Joint Type B.

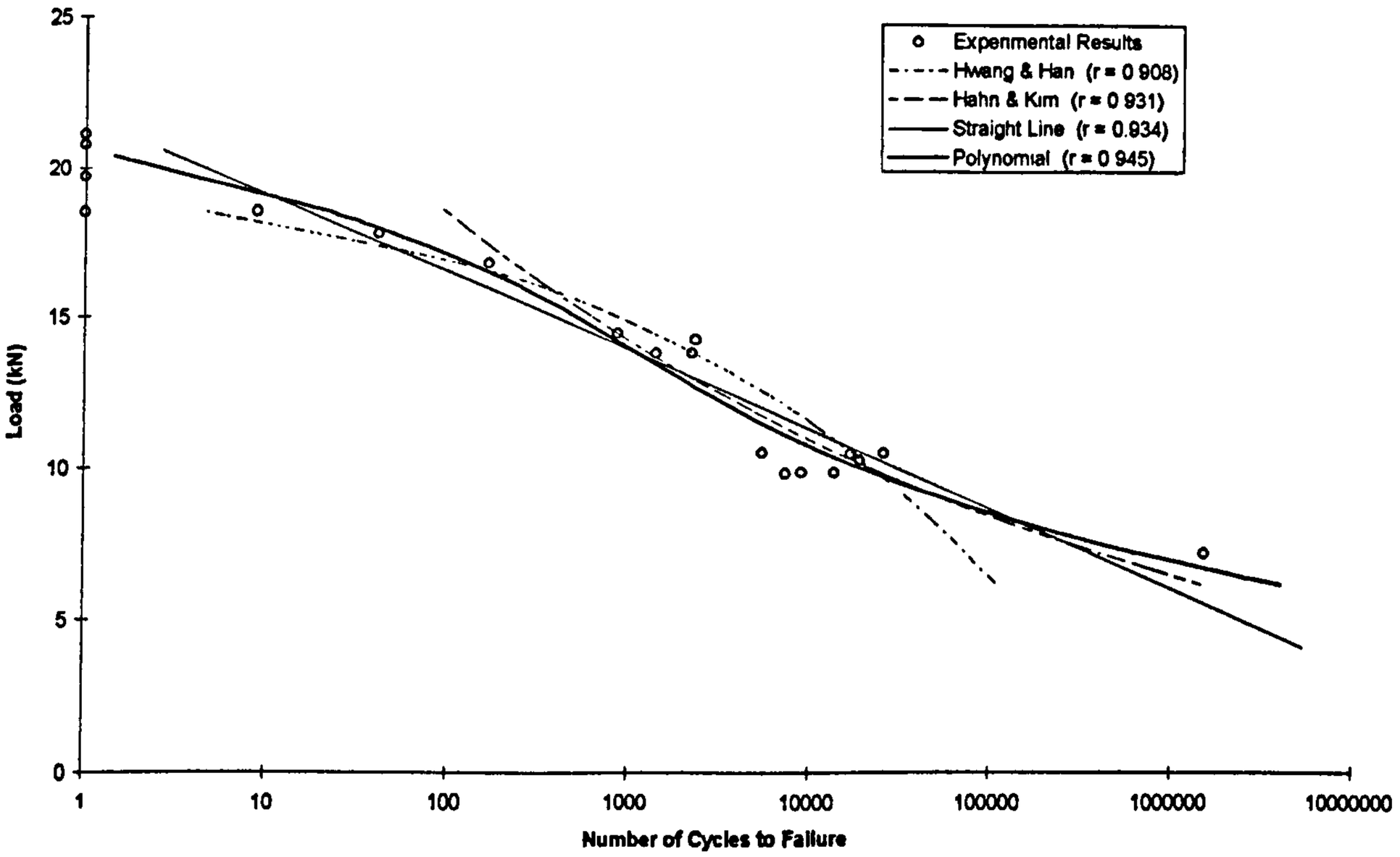

Figure 8.2 Comparison of Load-Life Characterisation Models for Tee Joint Type F.

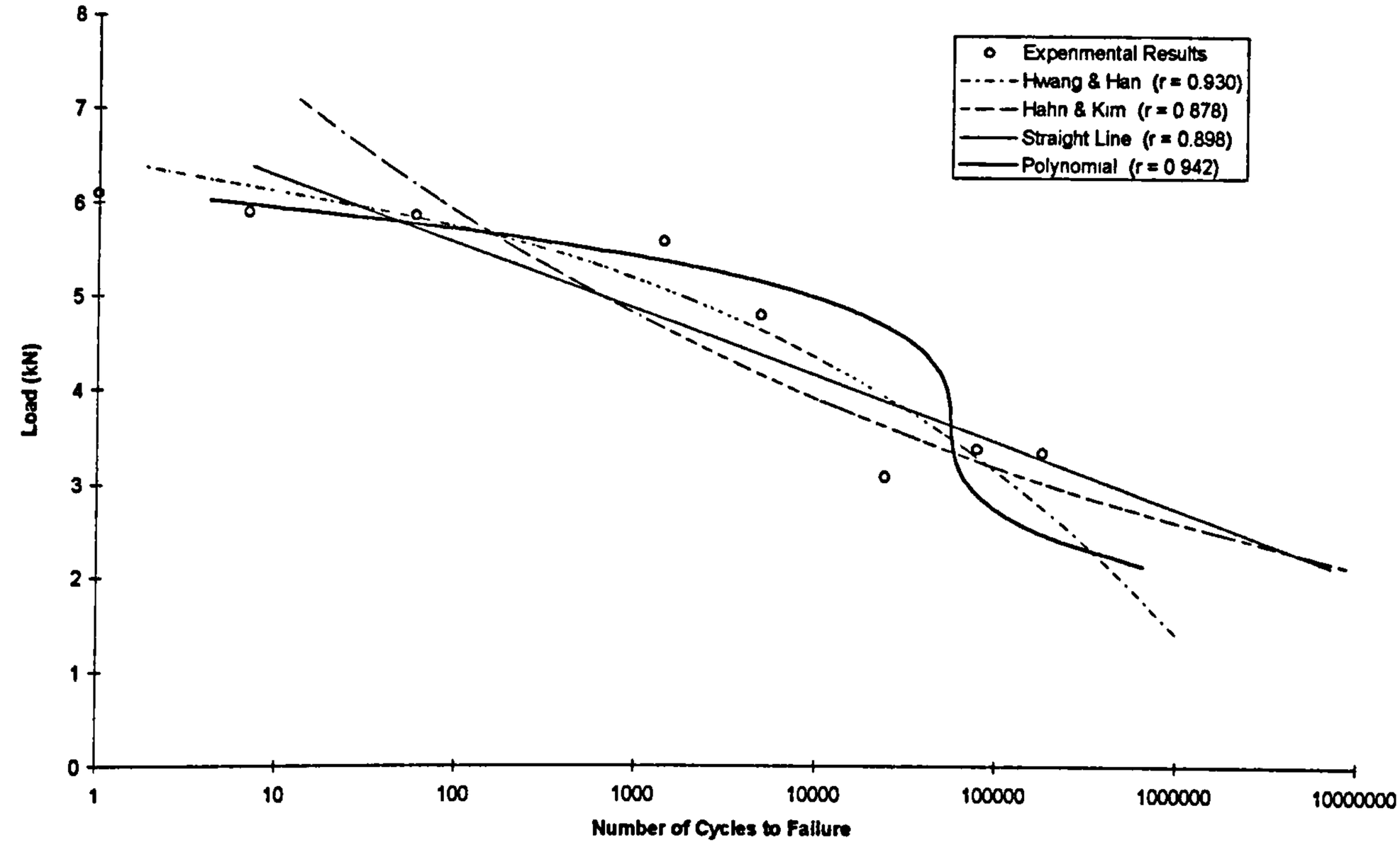

Figure 8.3 Comparison of Load-Life Characterisation Models for Tee Joint Type K.

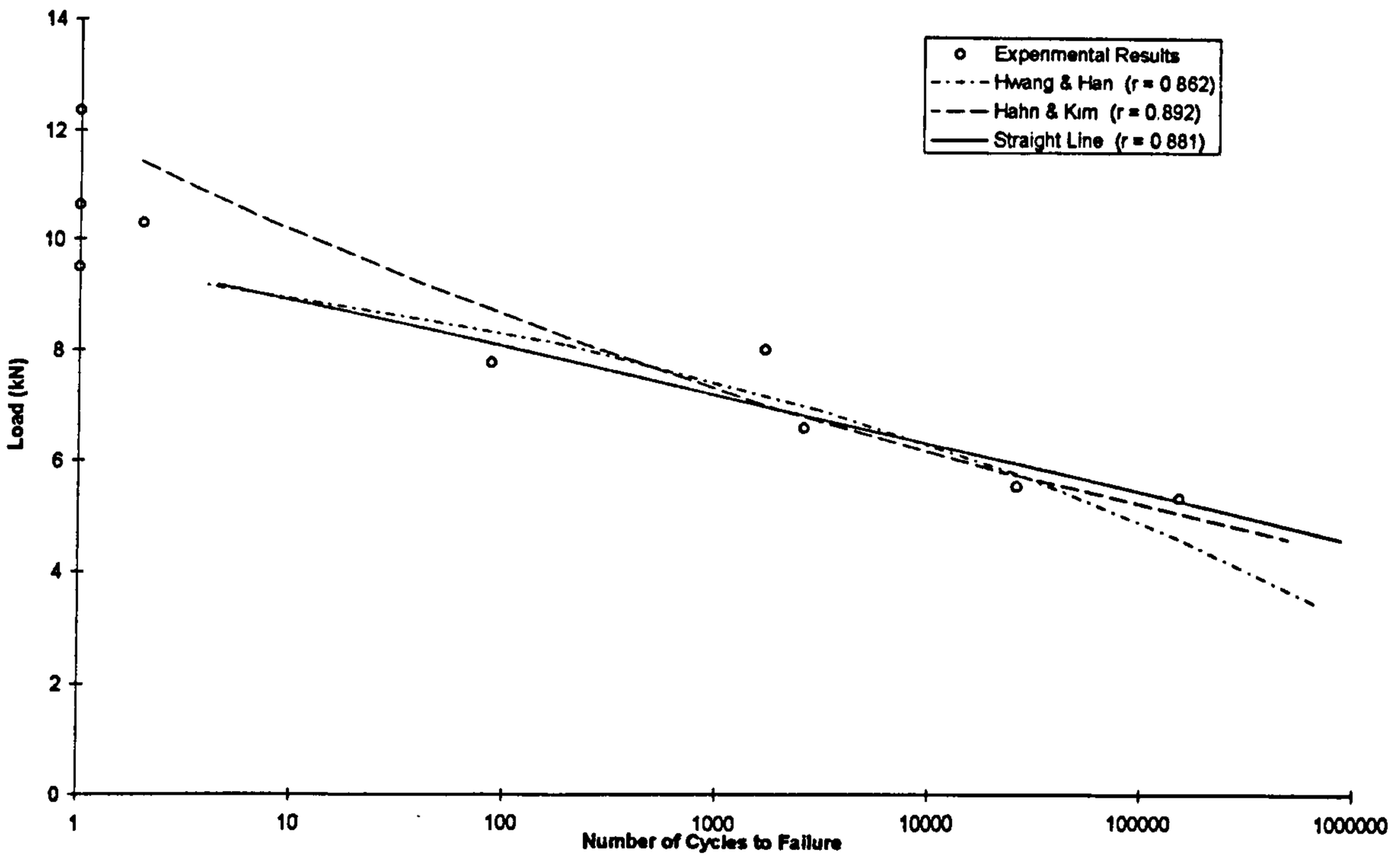

Figure 8.4 Comparison of Load-Life Characterisation Models for Tee Joint Type N.

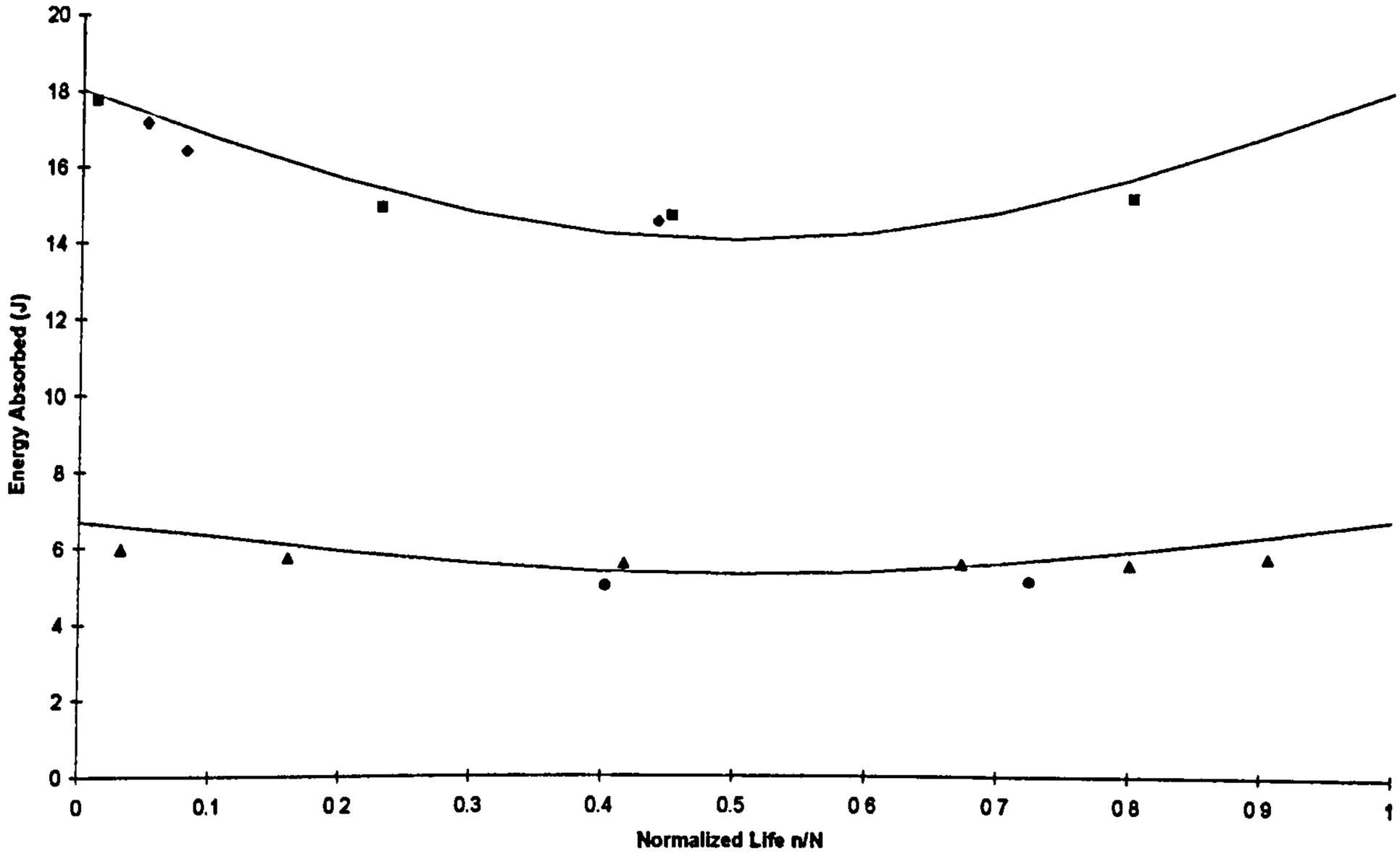

Figure 8.5 Theoretical Prediction of Energy Dissipation vs Experimental Results for Joint Type F.

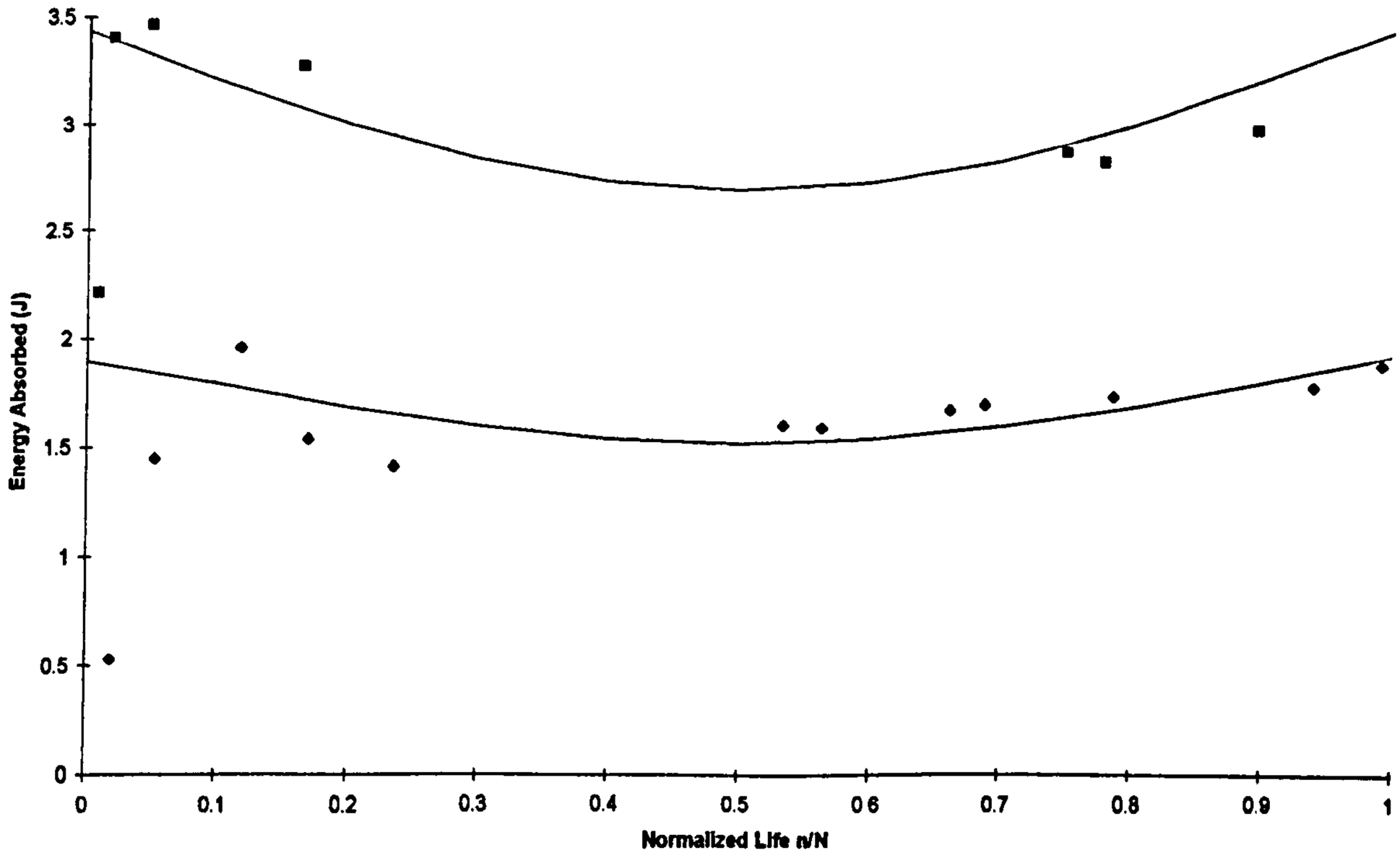

Figure 8.6 Theoretical Prediction of Energy Dissipation vs Experimental Results for Joint Type N.

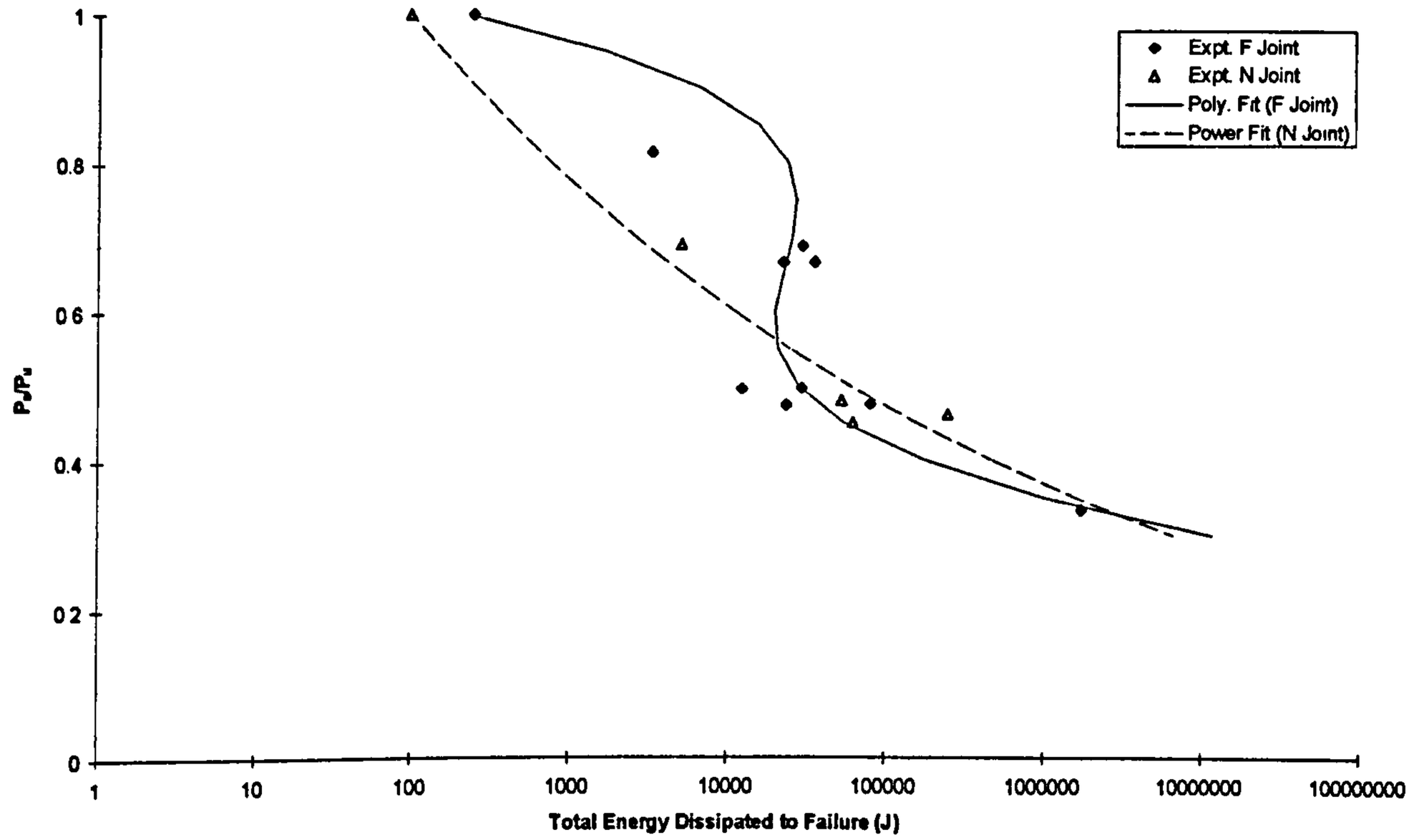

Figure 8.7 Theoretical Prediction of Total Energy Dissipated to Failure vs Experimental Results for Joint Types F and N.

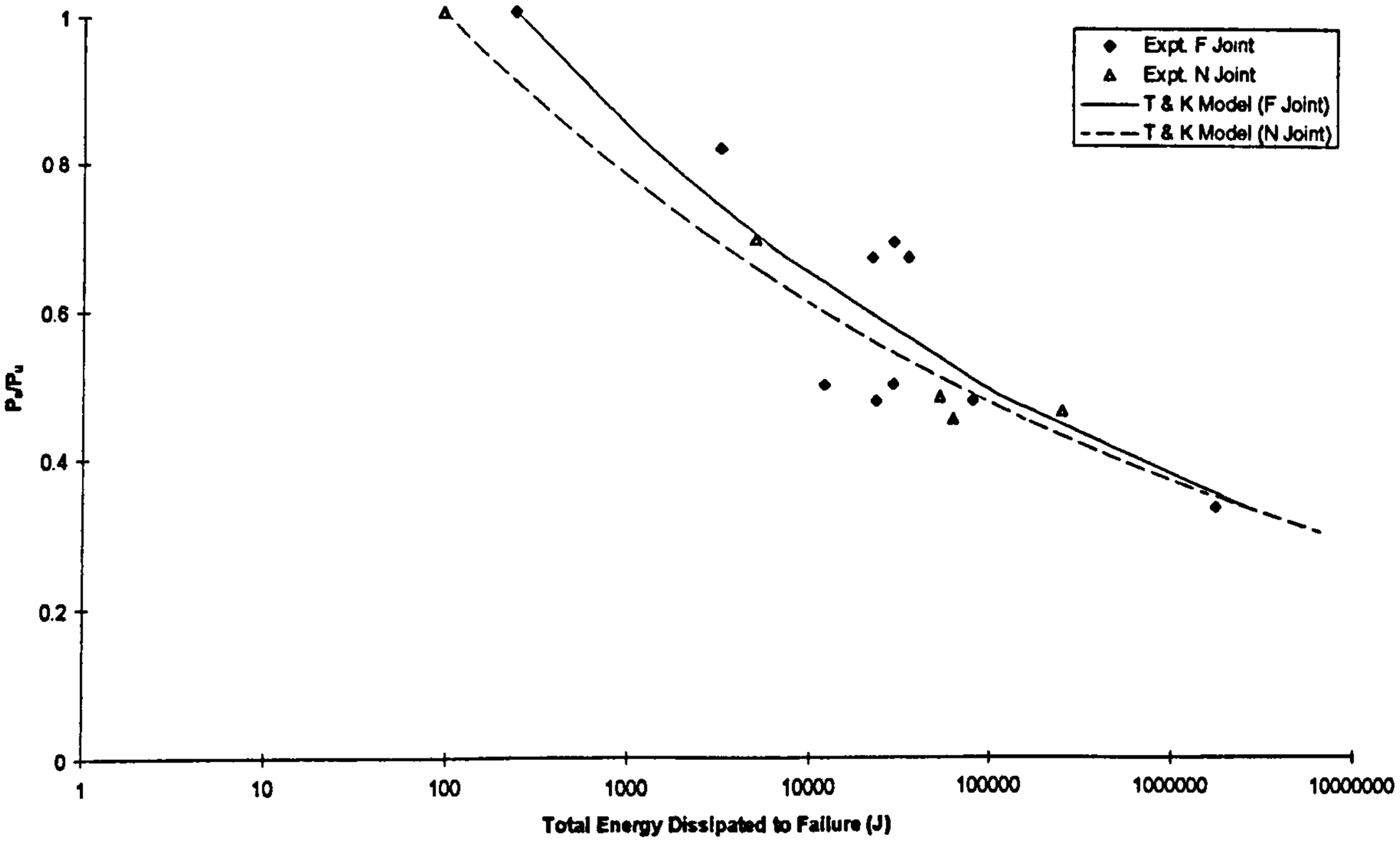

Figure 8.8 Treshenko and Khamaza Prediction of Total Energy Dissipated to Failure vs Experimental Results for Joint Types F and N.

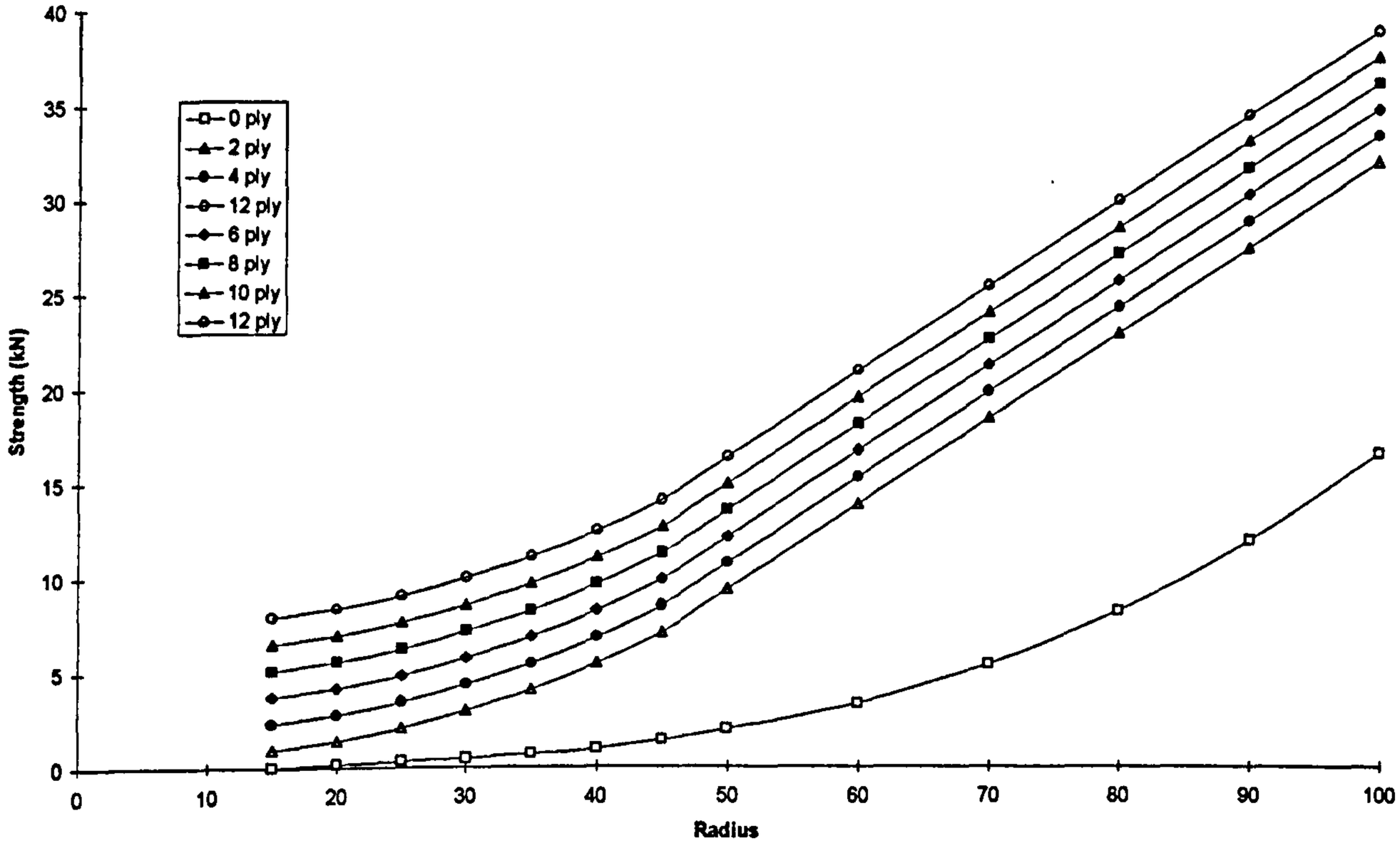

Figure 8.9 Design Curves of Tee Joint Static Strength.

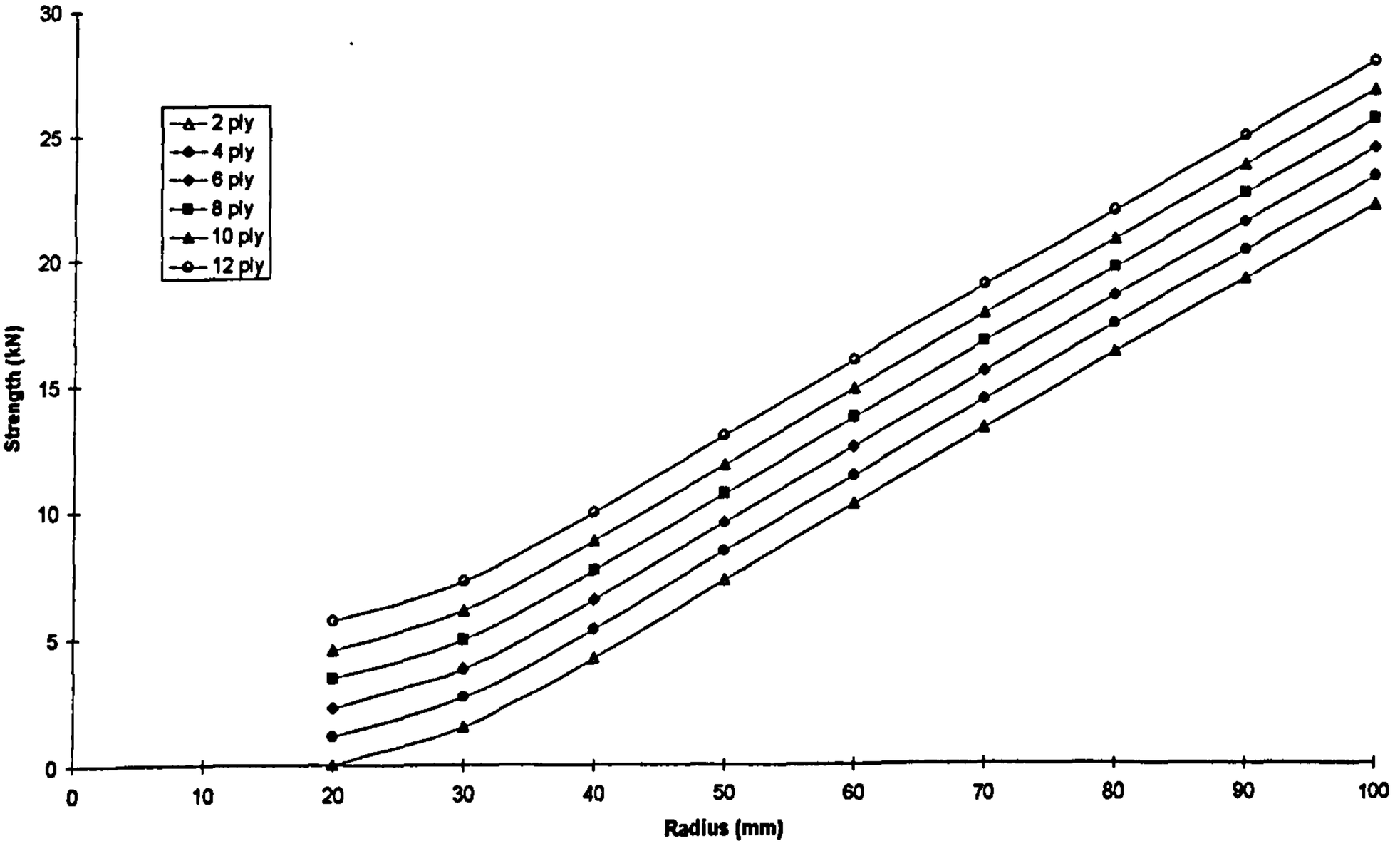

Figure 8.10 Design Curves of Tee Joint Fatigue Strength @ 10^3 Cycles.

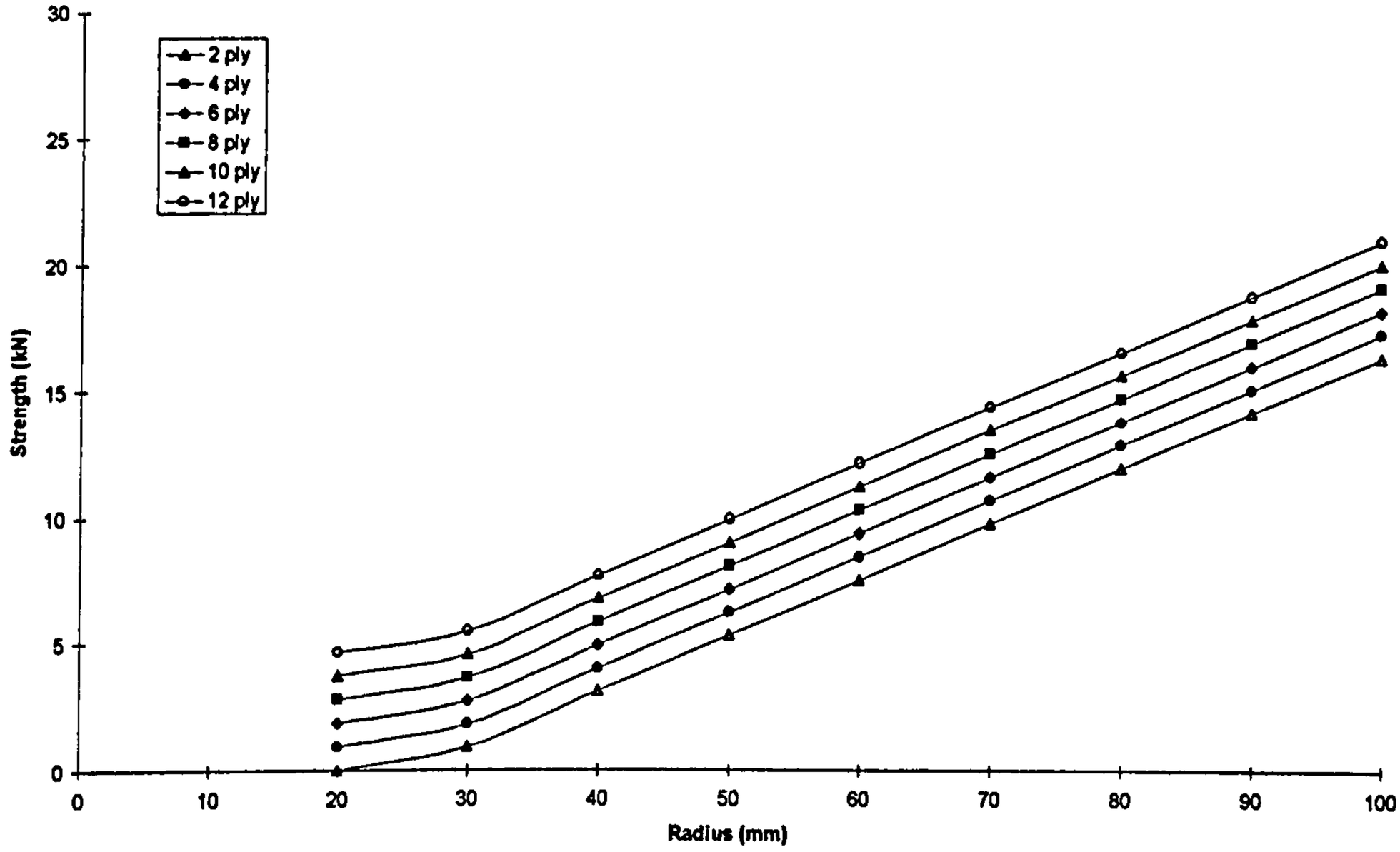

Figure 8.11 Design Curves of Tee Joint Fatigue Strength @ 10^4 Cycles.

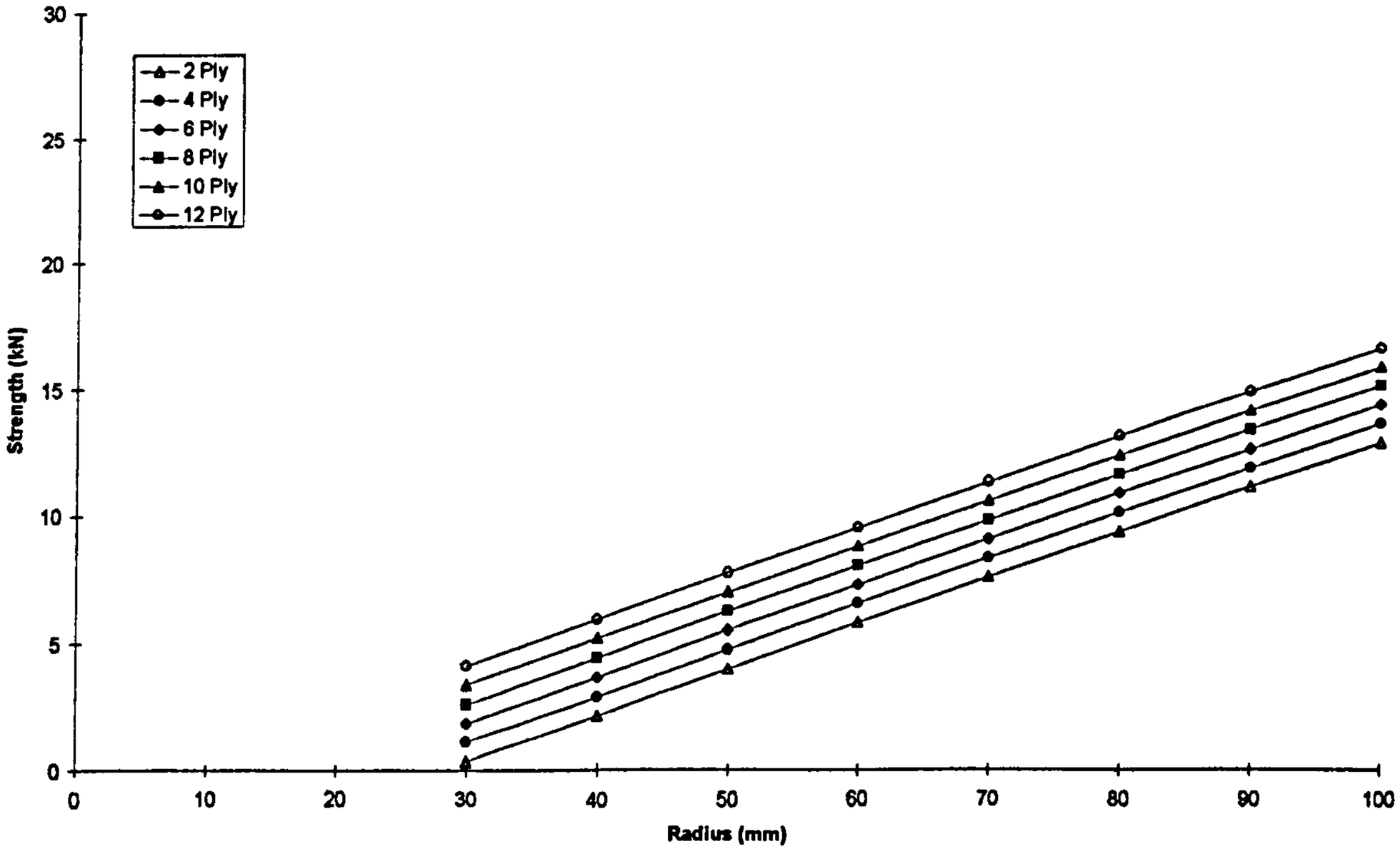

Figure 8.12 Design Curves of Tee Joint Fatigue Strength @ 10^5 Cycles.

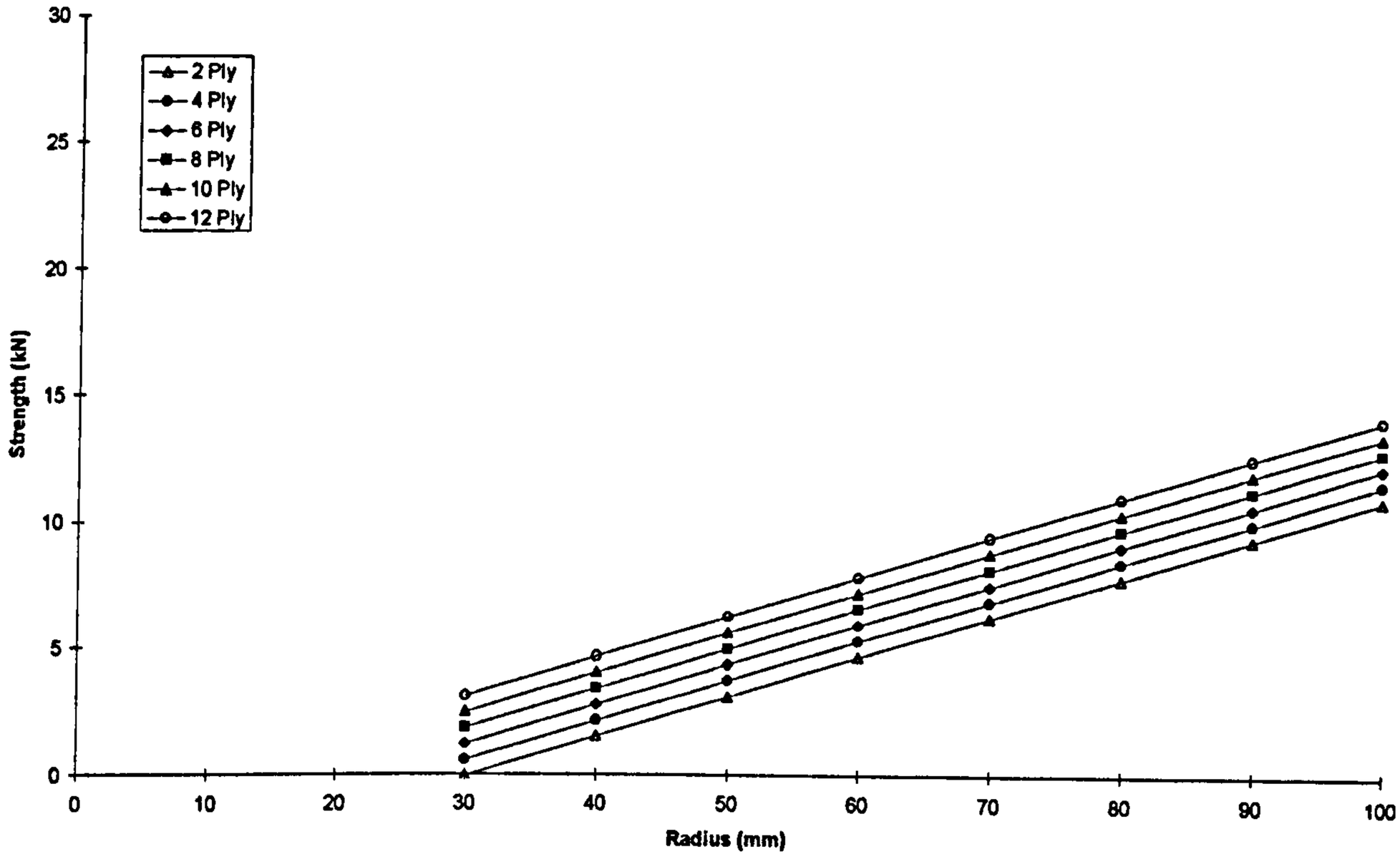

Figure 8.13 Design Curves of Tee Joint Fatigue Strength @ 10^6 Cycles.

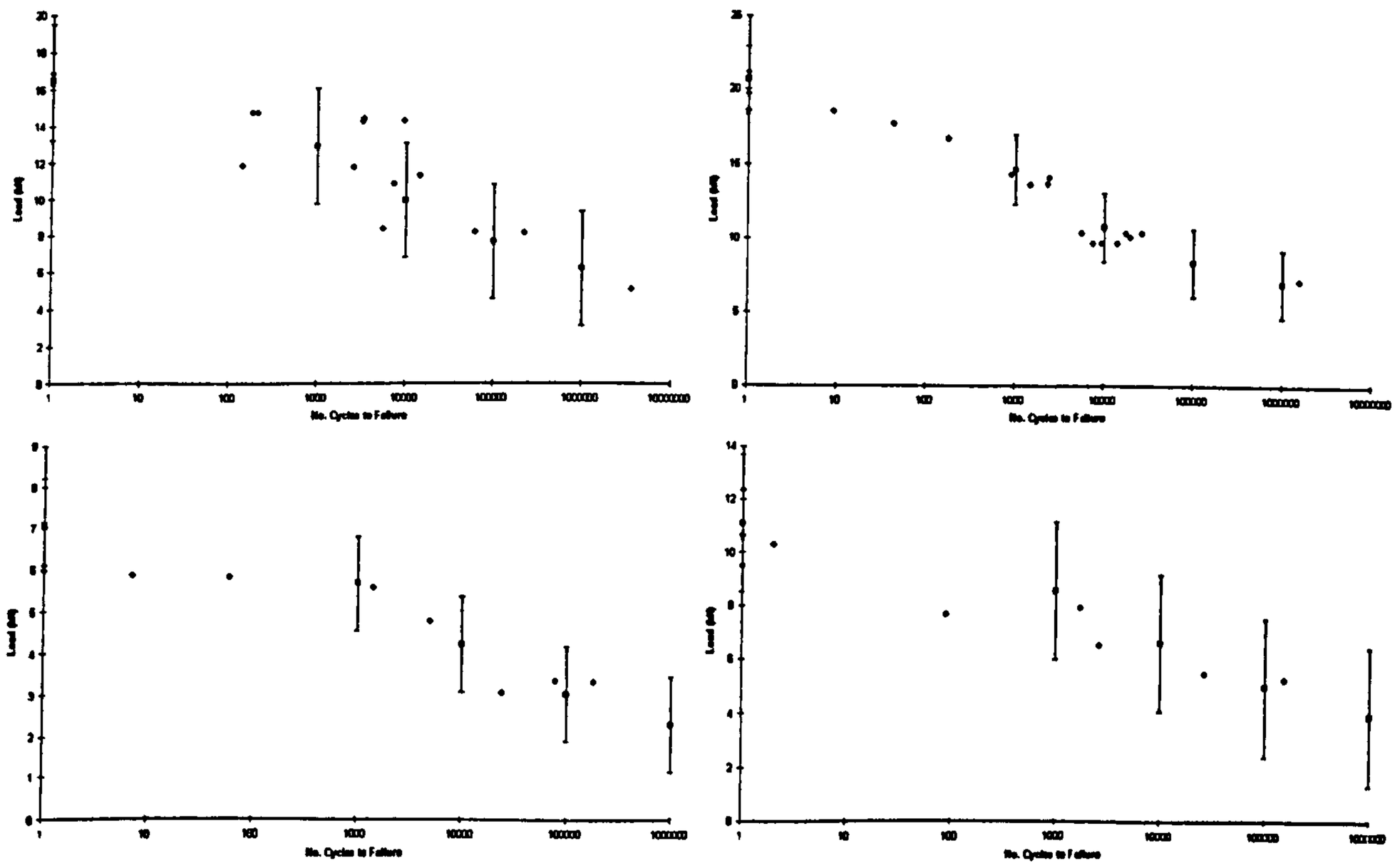

Figure 8.14 Design Curve Predictions of Fatigue Life vs Experimental Results for Joints B, F, K and N (working from top left).

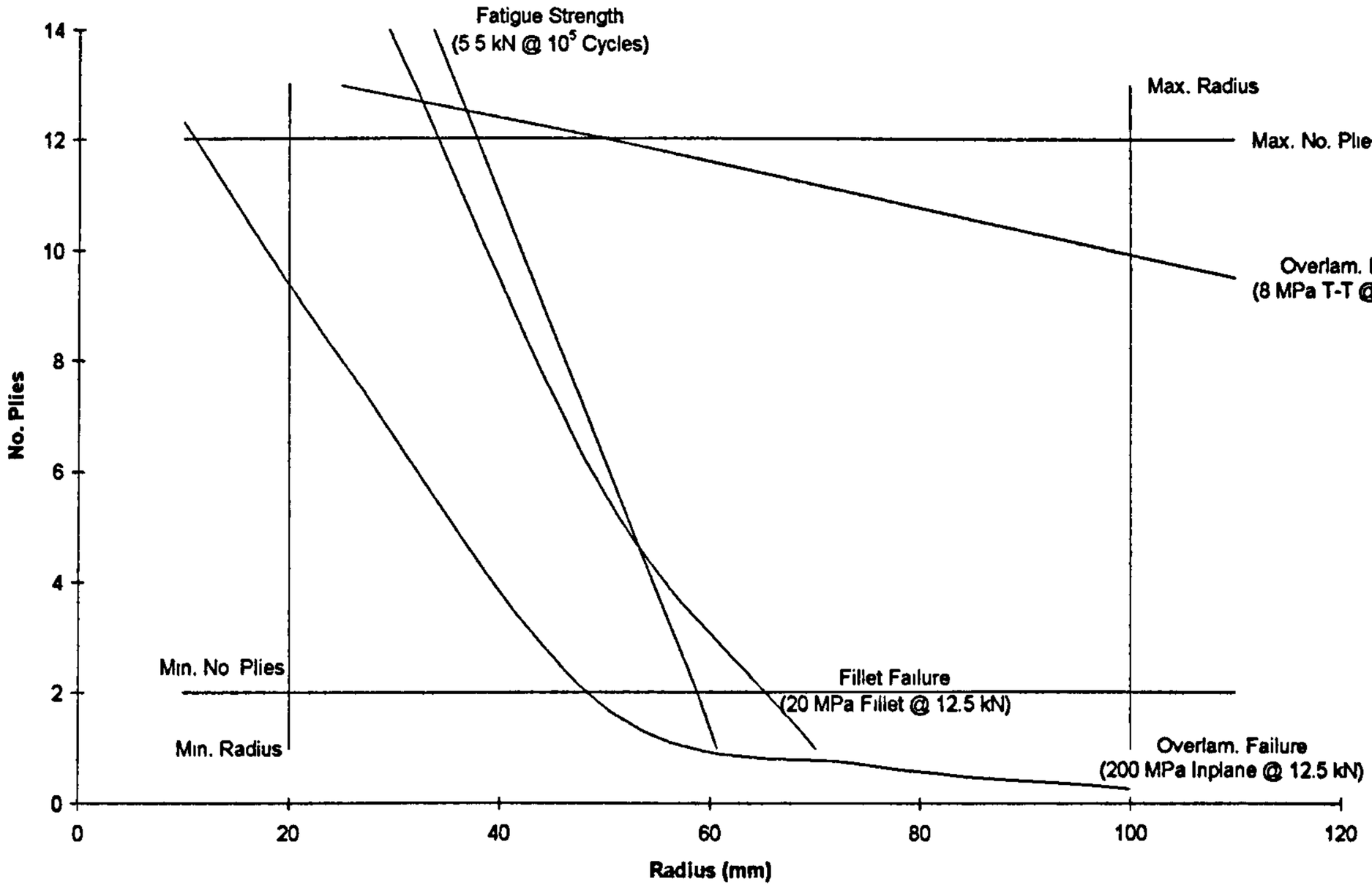

Figure 8.15 A Possible Design Envelope Arrangement.

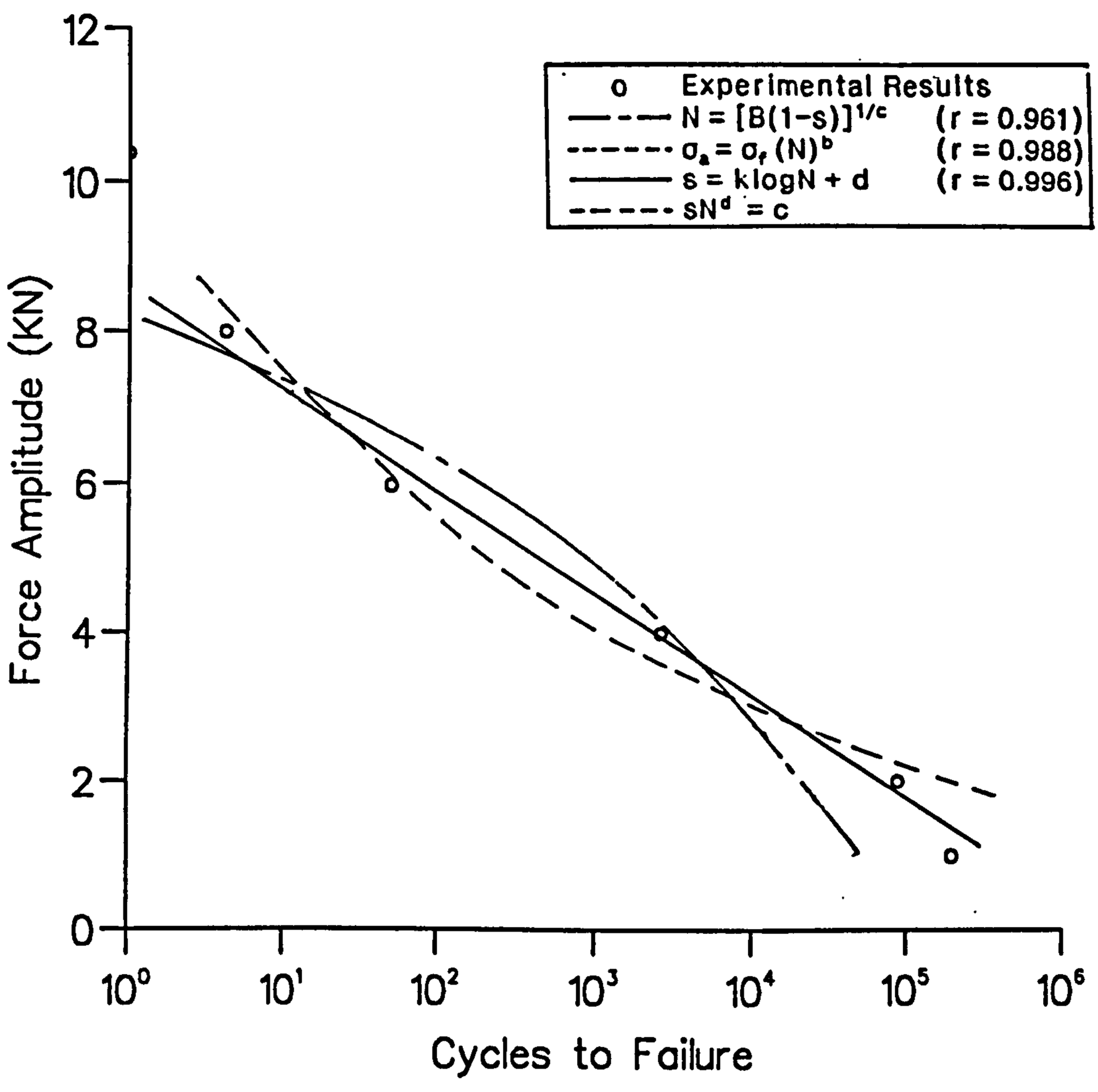

Figure A.1a Application of S-N Models to a Woven Glass Cloth / Polyester Laminate Designated Rovimat. (Howsen et al. (1992))

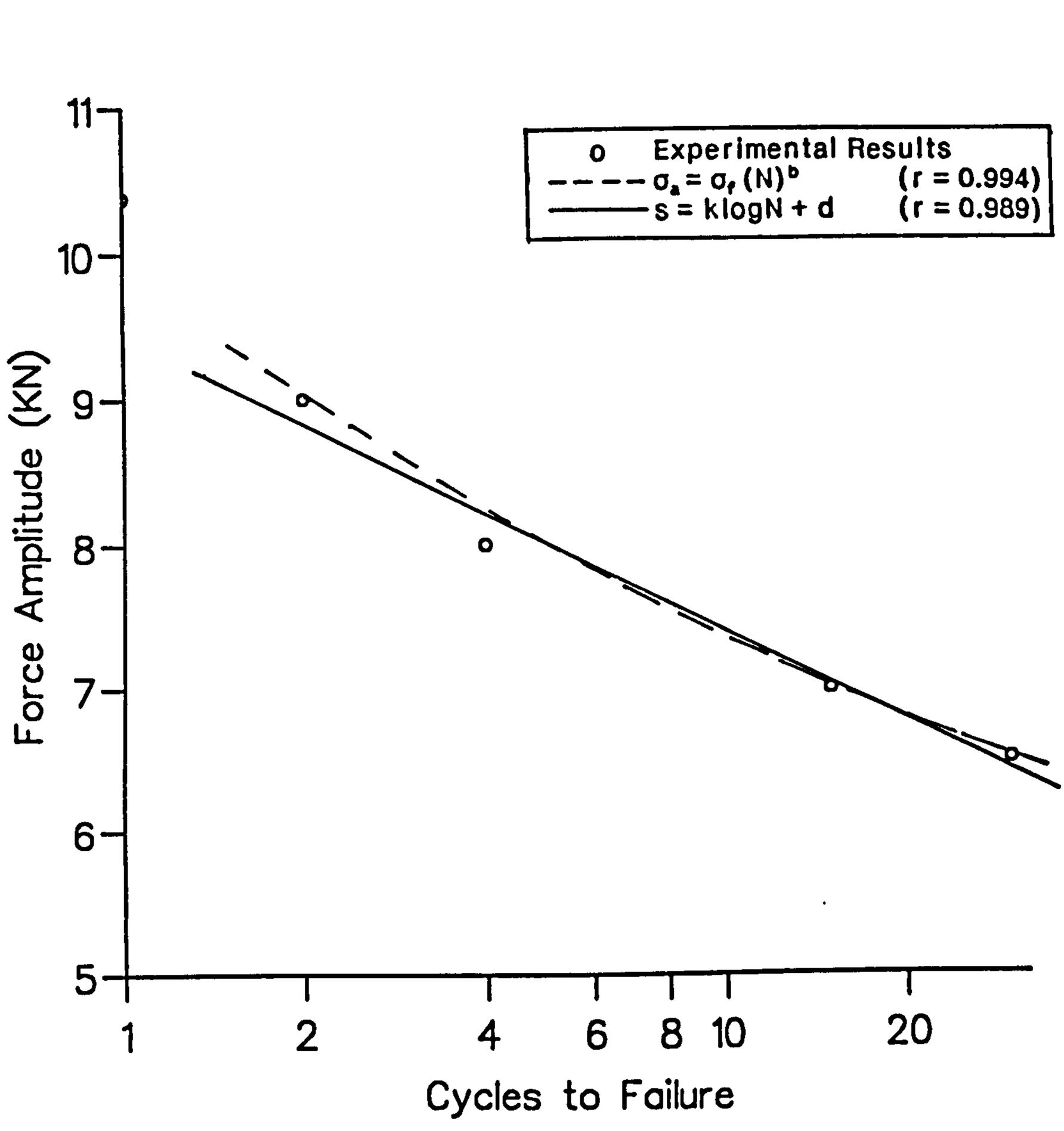

Figure A.1b Application of S-N Models to the Low-Cycle Part of a Woven Glass Cloth / Polyester Laminate Designated Rovimat. (Howsen et al. (1992))

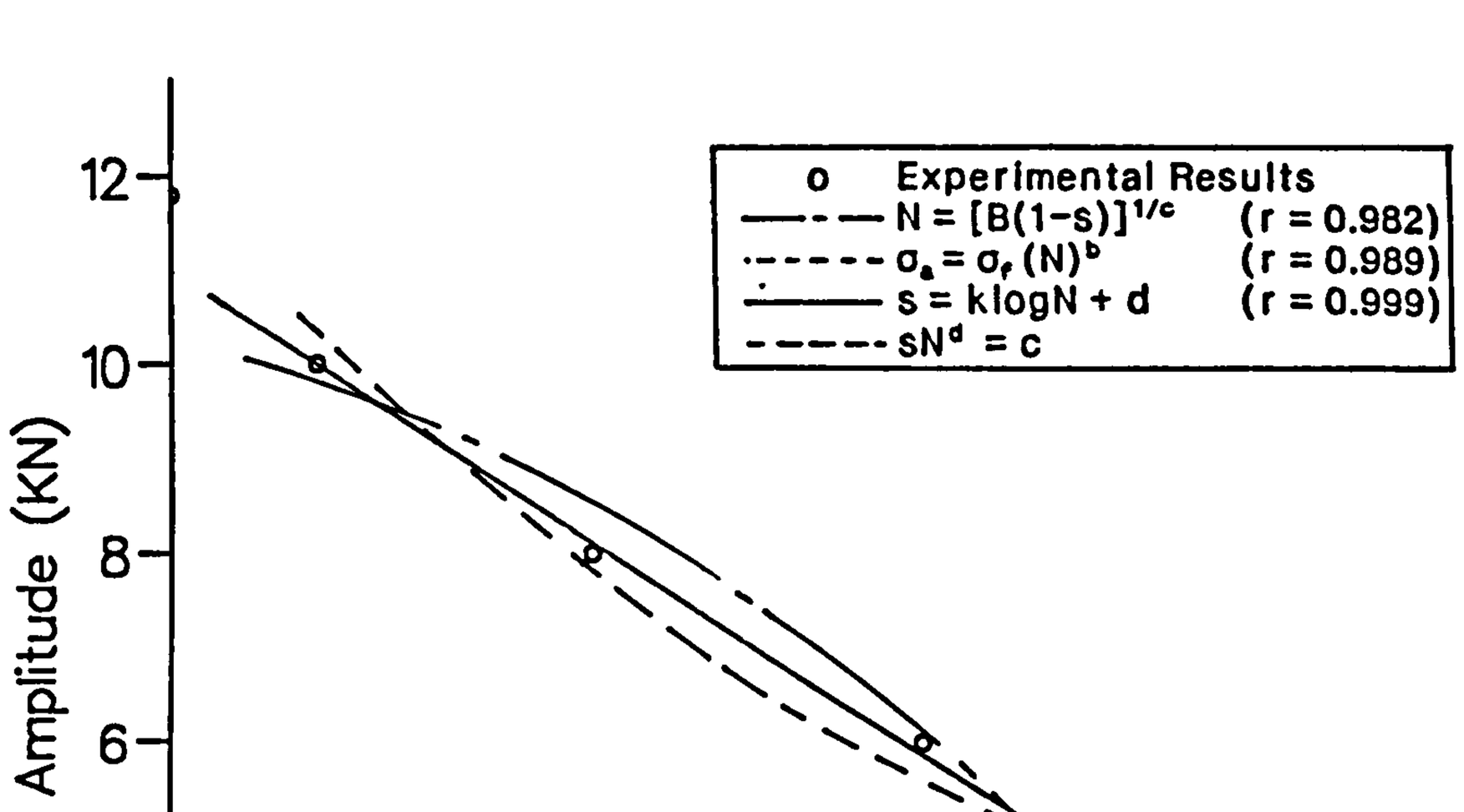

Figure A.2 Application of S-N Models to a Woven Glass and Kevlar Hybrid Cloth / Polyester Laminate Designated Aramat. (Howsen et al. (1992))

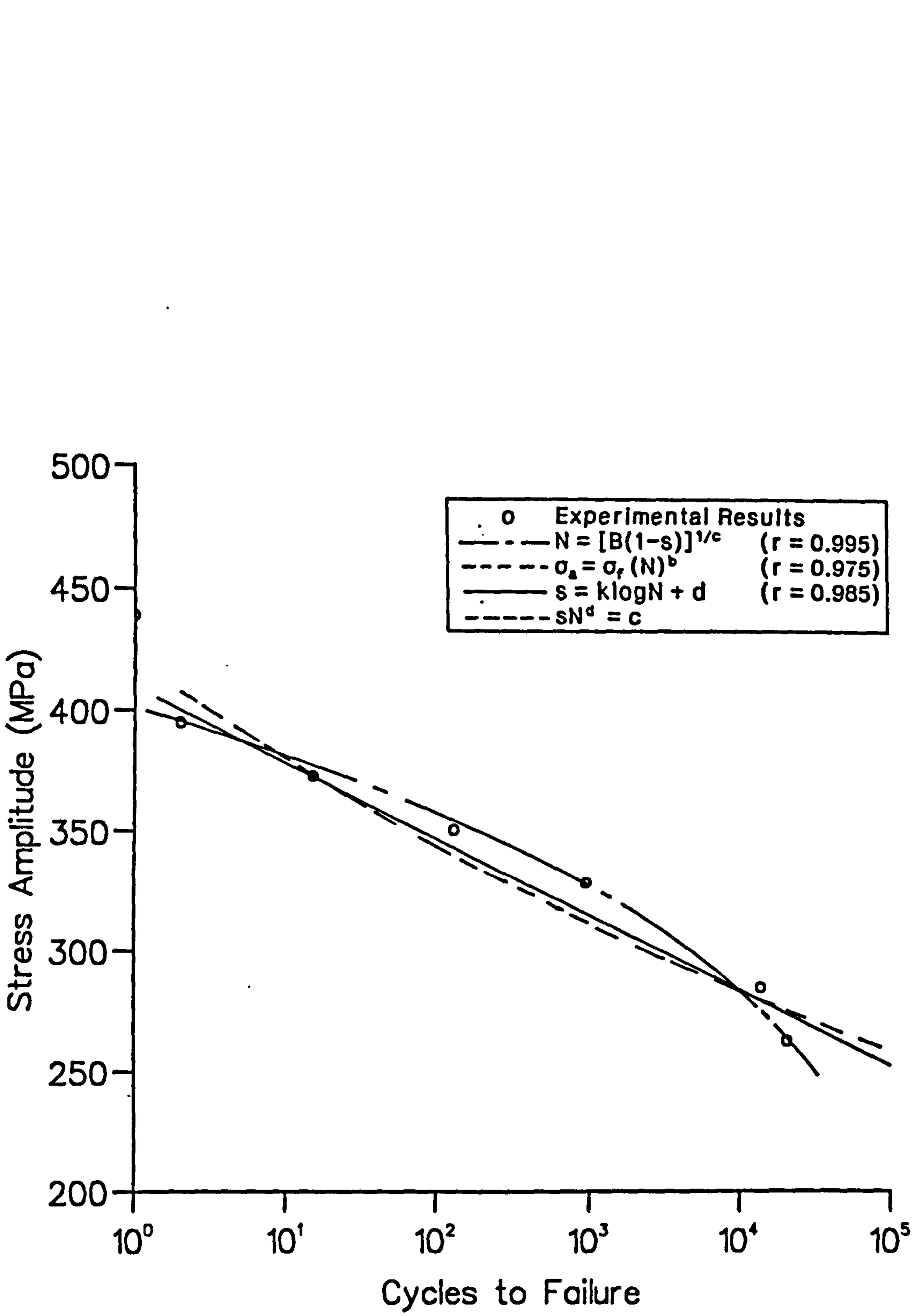

Figure A.3 Application of S-N Models to a Woven Glass Cloth / Epoxy Laminate. (Hwang and Han (1986))

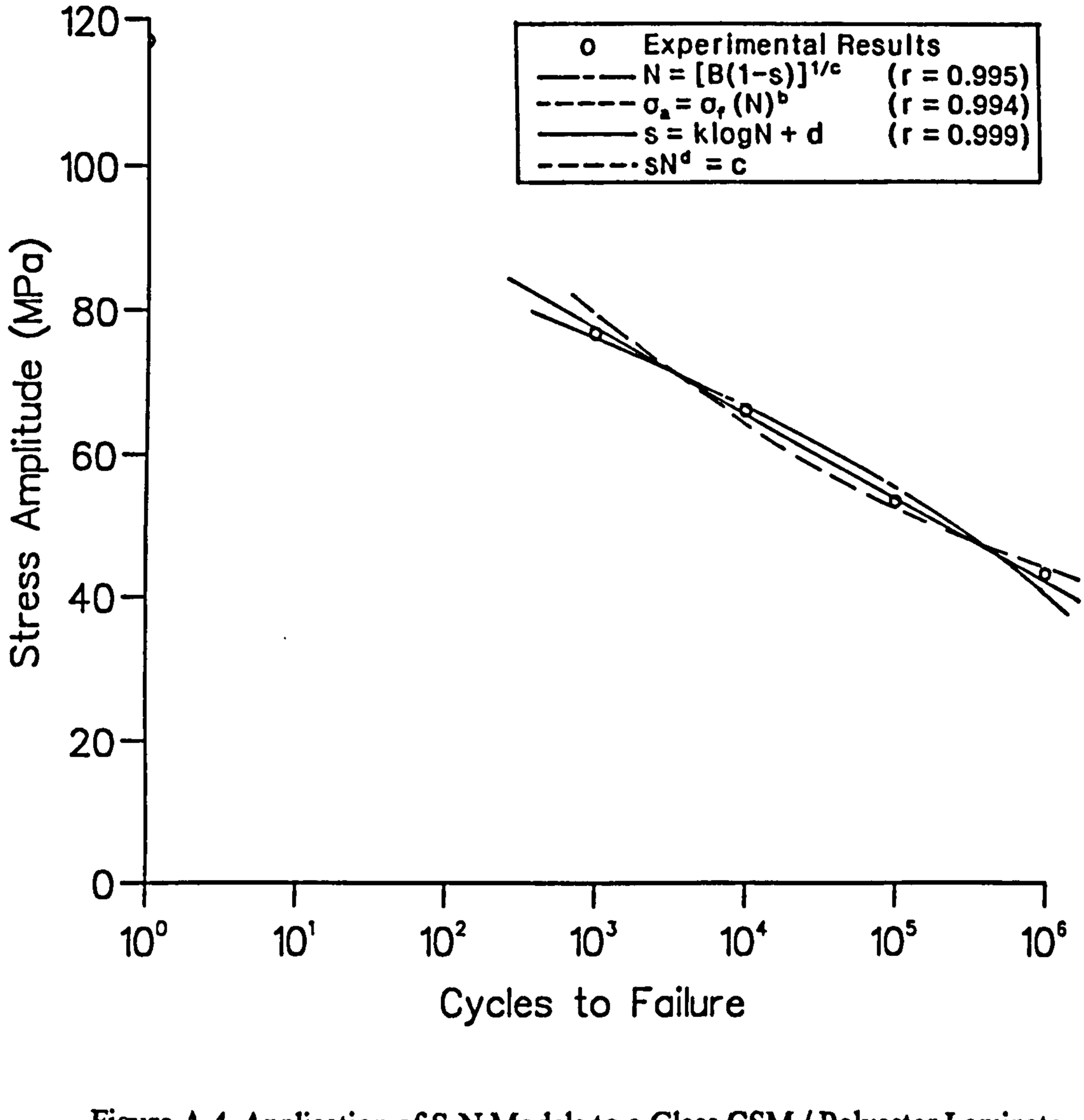

Figure A.4 Application of S-N Models to a Glass CSM / Polyester Laminate.
(Owen and Smith (1968))

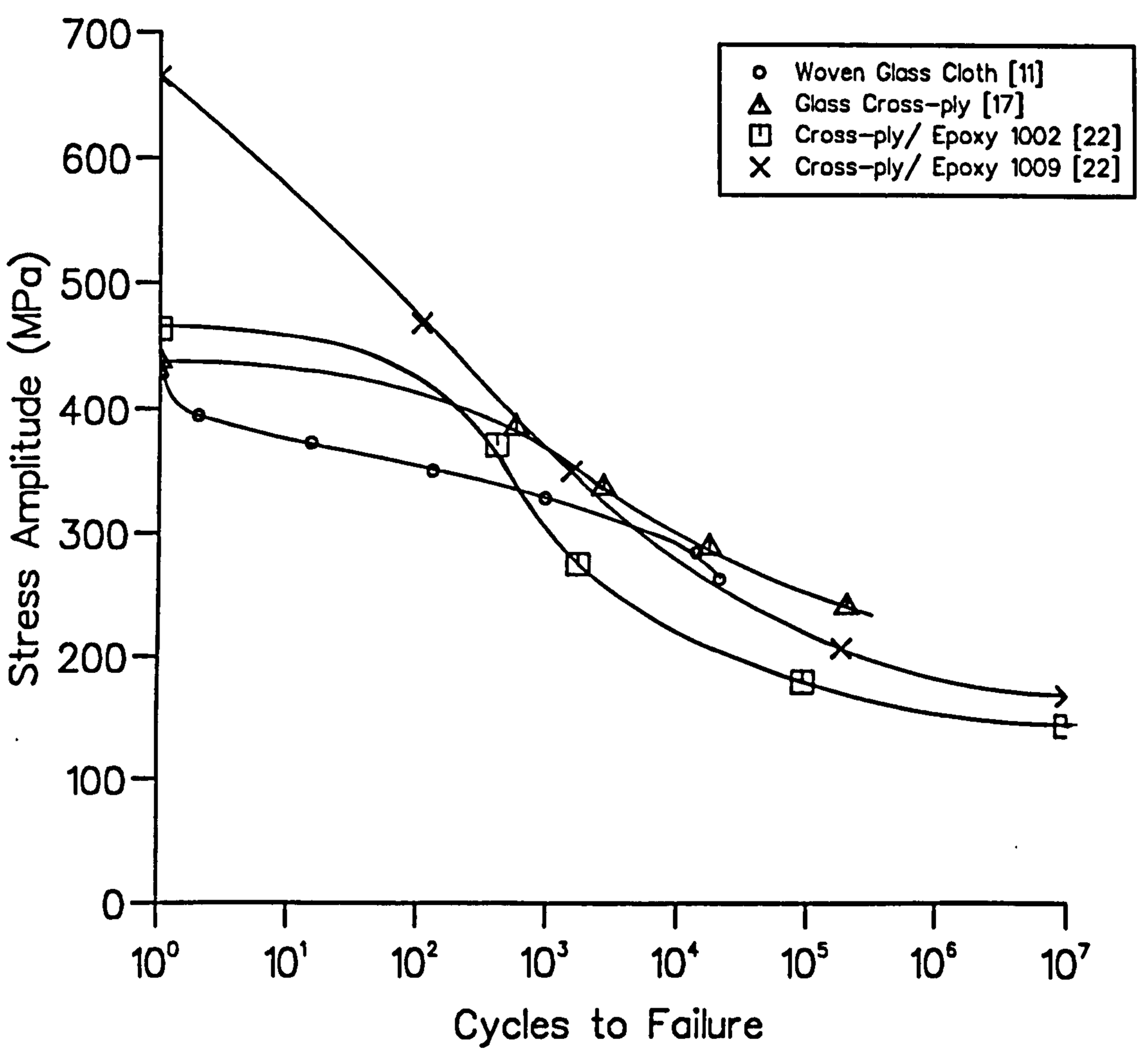

Figure A.5 S-N Curves for Four Glass Reinforced Epoxy Laminates.

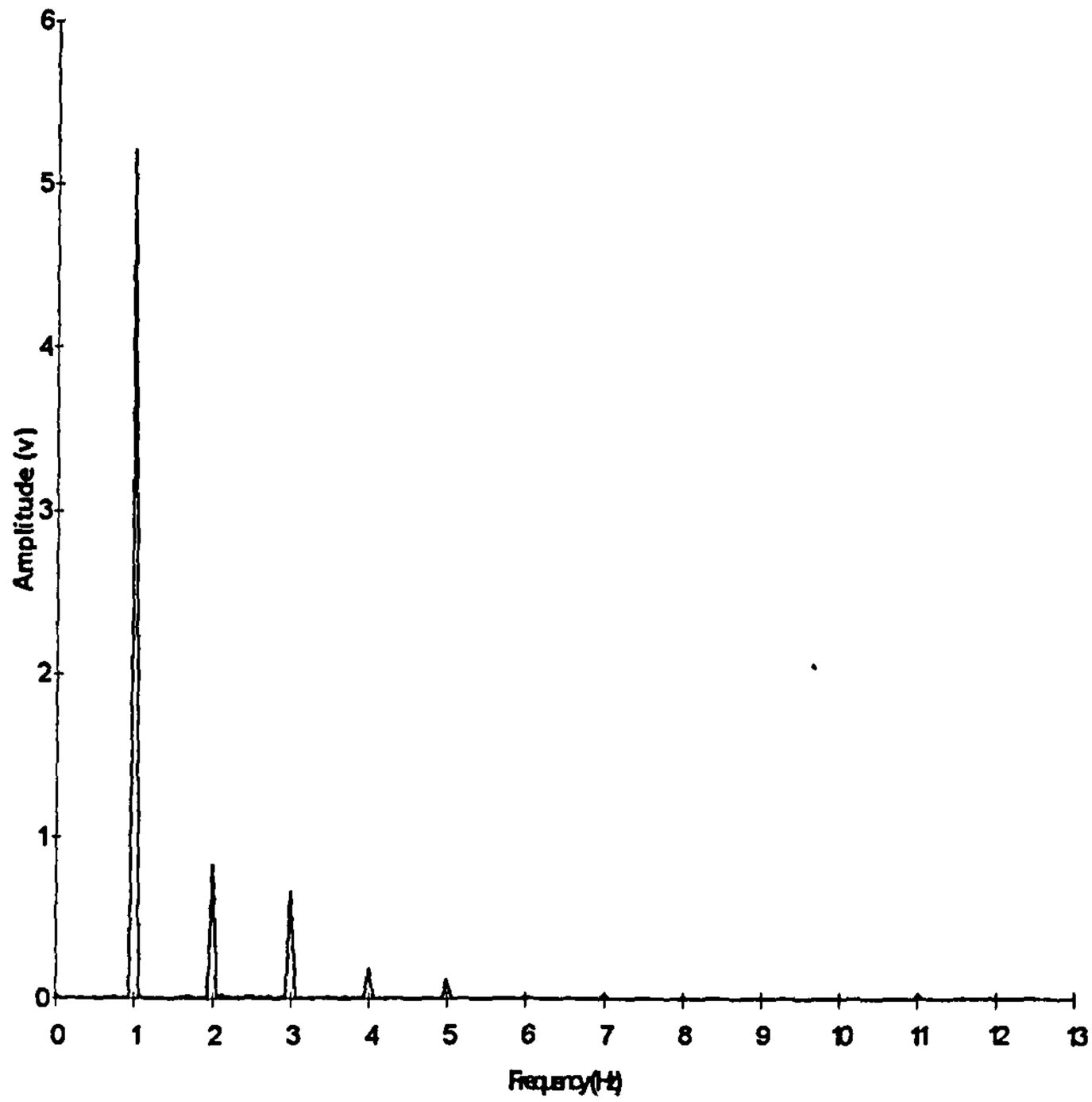

Figure B.1 Spectral Analysis Sample at an Applied Fatigue Load of 0.4kN

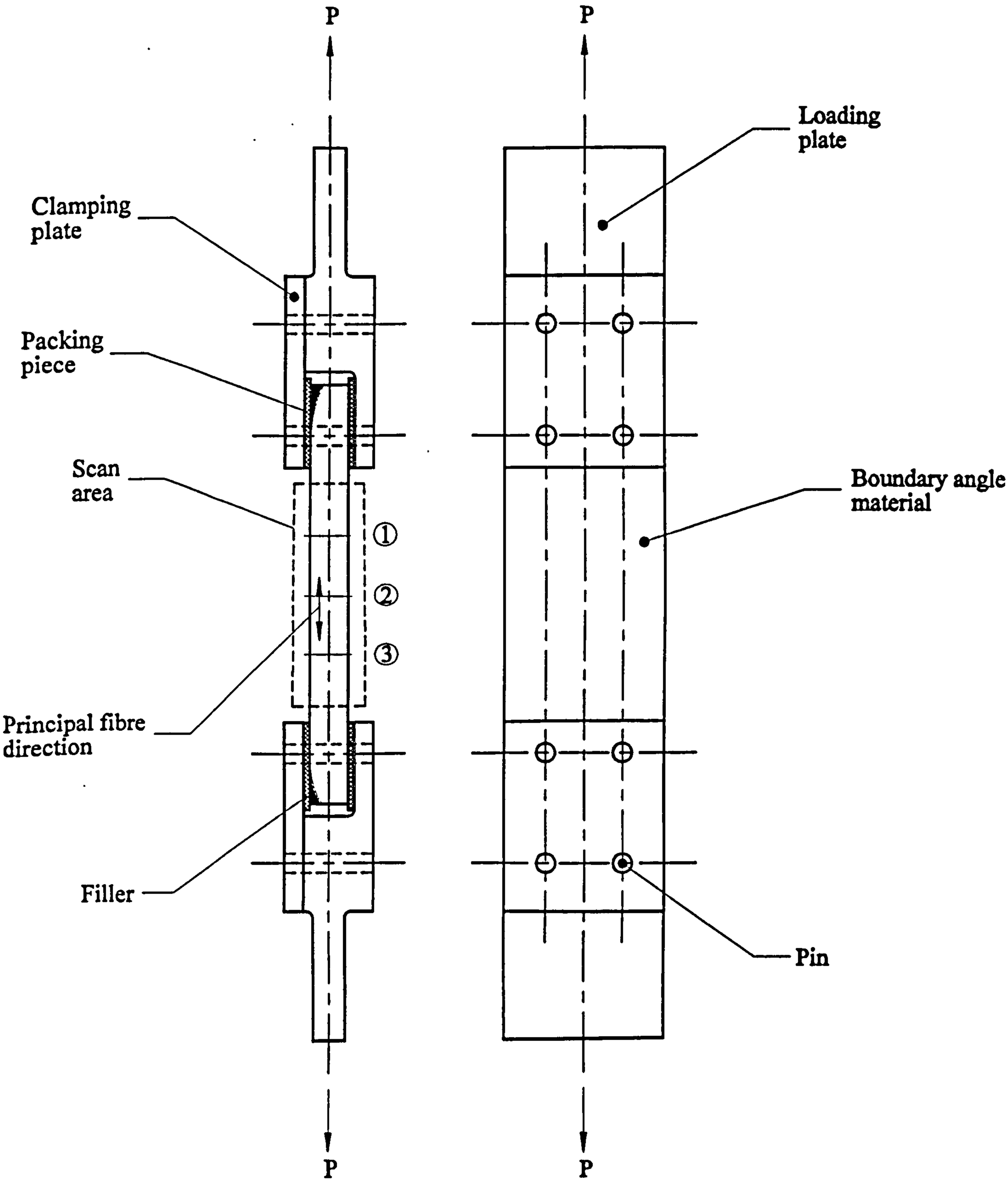

Figure D.1 Tensile Test Specimens for Calibration of SPATE Constants.

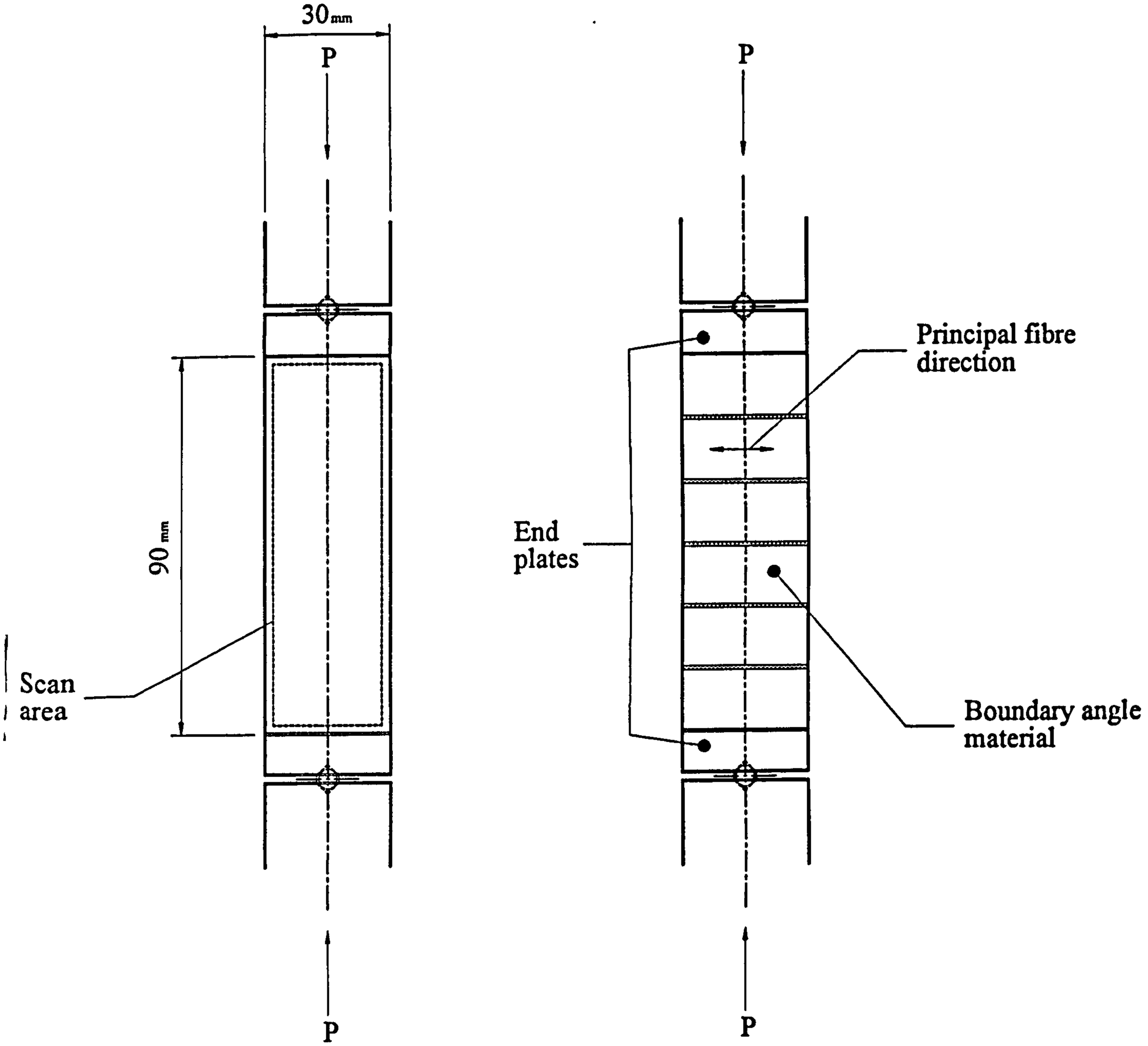

Figure D.2 Compressive Test Specimens for Calibration of SPATE Constants.